

Universiteit
Leiden
The Netherlands

The role of quiescent and cycling stem cells in the development of skin cancer

Glind, G.C. van de

Citation
Glind, G. C. van de. (2018, April 18). *The role of quiescent and cycling stem cells in the development of skin cancer*. Retrieved from https://hdl.handle.net/1887/61622

Version:	Not Applicable (or Unknown)
License:	Licence agreement concerning inclusion of doctoral thesis in the Institutional Repository of the University of Leiden
Downloaded from:	https://hdl.handle.net/1887/61622

Note: To cite this publication please use the final published version (if applicable).

Cover Page



Universiteit Leiden



The handle http://hdl.handle.net/1887/61622 holds various files of this Leiden University dissertation.

Author: Glind, G.C. van de
Title: The role of quiescent and cycling stem cells in the development of skin cancer
Issue Date: 2018-04-18

The Role of Quiescent and Cycling Stem Cells in the Development of Skin Cancer

Gerline van de Glind

THE ROLE OF QUIESCENT AND CYCLING STEM CELLS IN THE DEVELOPMENT OF SKIN CANCER

GERLINE VAN DE GLIND

The role of quiescent and cycling stem cells in the development of skin cancer
PhD thesis, Leiden University, The Netherlands

Copyright © G.C. van de Glind, Utrecht, 2018
All rights reserved. No part of this publication may be reproduced or transmitted in any form or by any means without prior permission of the author.

ISBN: 978-94-6299-877-3
Lay-out and cover photo: G.C. van de Glind
Cover lay-out: F. van der Spek, Ridderprint B.V.
Printing by: Ridderprint B.V.

This research project was funded by the Dutch Cancer Society (UL 2010-4812).
Financial support for printing of this thesis was kindly provided by the Dutch Cancer Society.

THE ROLE OF QUIESCENT AND CYCLING STEM CELLS IN THE DEVELOPMENT OF SKIN CANCER

PROEFSCHRIFT

ter verkrijging van
de graad van Doctor aan de Universiteit Leiden,
op gezag van Rector Magnificus, prof. mr. C.J.J.M. Stolker,
volgens besluit van het College voor Promoties
te verdedigen op woensdag 18 april 2018
klokke 16.15 uur

door

GERRITJE CORNELIA VAN DE GLIND

geboren te Amersfoort in 1986

Promotor	Prof. Dr. R. Willemse
Co-promotoren	Dr. F.R. de Gruijl Dr. C.P. Tensen
Leden Promotiecommissie	Prof. Dr. M.H. Vermeer
	Prof. Dr. S. Gibbs *VU University Medical Centre, Amsterdam*
	Prof. Dr. M. Garmyn *University Hospital, Leuven*

CONTENTS

	List of abbreviations	7
Chapter 1	General Introduction	9
Chapter 2	UV-induced ablation of the epidermal basal layer including p53-mutant clones resets UV carcinogenesis showing squamous cell carcinomas to originate from interfollicular epidermis.	23
Chapter 3	Fractionation of a tumor-initiating UV dose introduces DNA damage-retaining cells in hairless mouse skin and renders subsequent TPA-promoted tumors non-regressing	47
Chapter 4	$Lgr5^+$ stem cells and their progeny in mouse epidermis under regimens of exogenous skin carcinogenesis, and their absence in ensuing skin tumors	75
Chapter 5	$Lgr6^+$ stem cells and their progeny in mouse epidermis under regimens of exogenous skin carcinogenesis, and their absence in ensuing skin tumors	101
Chapter 6	RNA-seq analysis of $Lgr6^+$ stem cells and identification of an Lgr6 isoform	131
Chapter 7	Summary and General Discussion	157
Chapter 8	Nederlandse samenvatting (Dutch Summary)	167
	List of publications	173
	Curriculum Vitae	175

List of abbreviations

6-4PP 6-4 photoproduct
AEC 3-Amino-9-ethylcarbazole
AK Actinic keratosis
aMED Actual MED
AT Annealing temperature
BCC Basal cell carcinoma
BrdU Bromodeoxyuridine
BSA Bovine serum albumin
cDNA Complementary DNA
CI Confidence intervals
CLSM Confocal laser scanning microscopy
CPD Cyclobutane pyrimidine dimer
CRBCs CPD-retaining basal cells
CSCs Cancer stem cells
DAPI 4',6-diamidino-2-phenylindole
DMBA Dimethylbenz[a]-antracene
DNA Deoxyribonucleic acid
EDTA Ethylenediaminetetra- acetic acid
EGFP Enhanced Green Fluorescent Protein
FDR False discovery rates
HF Hair follicle
IFE Interfollicular epidermis
K1 Keratin 1
K10 Keratin 10
K14 Keratin 14
K5 Keratin 5
Lgr5 Leucine-rich repeat containing G-protein coupled receptor 5
Lgr6 Leucine-rich repeat containing G-protein coupled receptor 6
LncRNA Long non-conding RNA
LogCPM Log count per million bases
LogFC Log Fold change
LOH Loss of heterozygosity
LR Log Ratio
LRCs Label-retaining cells
MED Minimal edema/erythemal dose
mRNA Messenger RNA
MS-MCA Methylation specific melting curve analysis
N.S. Not significant
ncRNA Non-coding RNAs
NGS Normal goat serum
NHS Normal Human Serum
NICD Notch 1 intracellular domain
O/N Overnight
PBS Phosphate buffered saline
PCR Polymerase chain reaction
qPCR Quantitative real-time *PCR*
QSCs Quiescent stem cells
RIN RNA integrity number
RNA Ribonucleic acid
RNA-seq Quantitative RNA deep sequencing
rRNA Ribosomal RNA
RSPO R-spondins
SCC Squamous cell carcinoma
SEM Standard error of the mean
SG Sebaceous gland
SnoRNAs Small nucleolar RNAs
TD Touch down
TICs Tumor-initiating cells
TMM Trimmed Mean of M values
TPA 12-O-etradecanoyl-phorbol-13-acetate
TSS Transcription start site
UV Ultraviolet radiation
UV-A Ultraviolet radiation A (315 – 400 nm)
UV-B Ultraviolet radiation B (280 - 315 nm)
UV-C Ultraviolet radiation C (100 – 280 nm)
WT Wildtype

Chapter 1

General Introduction

1.1. The skin

1.1.1. Function

The skin is the outermost part of our body and therefore the first line of defense against pathogens and other challenges from the external environment such as solar UV radiation. The skin is also actively involved in maintaining body homeostasis: e.g. by thermoregulation, control of water loss, vitamin D production, and as an important frontier of the immune system. Furthermore, the skin contains sensory receptors for touch (pressure) and temperature.

1.1.2. Anatomy

The skin is composed of two main layers: the dermis and the epidermis. The dermis is the innermost layer built up mainly from fibroblasts that form the fibrous dermal matrix (containing collagen and elastin). These fibroblasts do not or rarely replicate in adults. The dermis gives the skin its tensile strength and elasticity, and contains the blood vessels with superficial capillary loops that nourish the skin. These blood vessels together with lymphatic vessels also provide entry and exit ports to immune cells. Furthermore, the dermis supports the overlying outermost viable layer, the epidermis. This is a layer only about 100 microns thick (except for skin on the palms of the hands and soles of the feet where the epidermis is much thicker) and has a much higher cellularity than the dermis. The epidermis consists of contiguous layers of keratinocytes that are renewed by stem cells at the innermost germinative basal cell layer (see Figure 1.1). Cells in this basal layer have keratin 5 (K5) and keratin 14 (K14) in their cytoskeletons. As the cells move outward in epidermal turnover they differentiate and as soon as they are expelled from the basal layer they switch from K5 and K14 to keratin 1 (K1) and keratin 10 (K10) expression. Finally, they die and flatten out into corneocytes that make up the outermost layer, the horny layer or stratum corneum (Figure 1.1). Thus, damaged differentiated cells in the outer layers are continuously replaced by vital “new recruits”. The turnover time is about 7 weeks in human skin (around 20 days for the stratum basale, 12 days for the differentiated layers and 14 – 20 days for the stratum corneum) [1, 2]. The epidermis also forms appendages protruding into the dermis: hair follicles with sebaceous glands and separate sweat glands.

1.1.3. Hair follicles and their cycle

Different structures can be distinguished in the hair follicle (see Figure 1.1). At the base the bulb forms the hair which grows outward. The bulb region encapsulates a dermal papilla which is highly vascularized and nourishes the bulb. The bulge is located higher up at the level of attachment of a small muscle (arrector pili), which when contracted causes a “goose bump” and upstanding hair. The zone from the bulge to the ducts of the sebaceous glands

is the isthmus followed by the infundibulum, the funnel-shaped upper part of the follicle that opens up to the surface.

Hair follicles increase and decrease in length as they go through the hair cycle. In telogen, the resting phase, the hair follicles are shallow, with the bulge as the deepest part and without a bulb. This phase is followed by anagen, the growth phase, with about a 3-fold lengthening of the follicle into the dermis with an active bulb at the base. This growth phase is followed by the catagen phase in which the extended part below the bulge is lost in apoptosis. In the human scalp one cycle takes about 3-6 years, in mice it only takes about 4 weeks. Cell kinetics of the follicle during the hair cycle has been extensively studied in mice. Traditionally this research focuses on the bulge, where stem cells reside that drive the renewal of the hair follicle in the hair cycle.

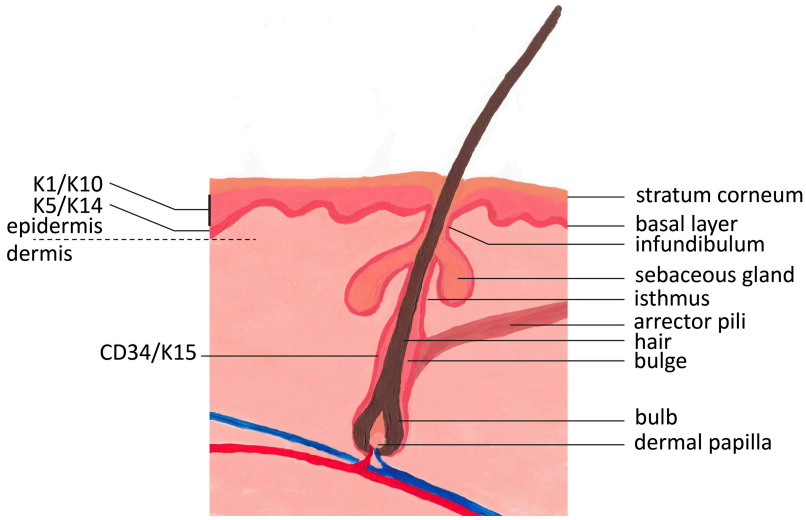


Figure 1.1: The skin and its appendages.

1.2. Stem cells in the skin

The continuous replacement of cells in the epidermis and its appendages, such as hair follicles, obviously requires a lasting reservoir of germinative cells. These must entail ultimate “mother cells” that reside life-long in the skin: the adult stem cells. In this thesis when stem cells are mentioned we refer to these adult stem cells. As already alluded to above, stem cells are present in different designated locations in the skin: besides the bulge and interfollicular (IF) epidermis, they are found in the bulb, isthmus and sebaceous glands.

1.2.1. Classic quiescent stem cells

The classic stem cell candidates are identified as label-retaining cells (LRCs). After loading the neonatal skin of mice with tritiated thymidine or a thymidine analog, bromodeoxyuridine (BrdU), these cells still showed the label in their nuclei months later. Retention of the label implies that these cells hardly divide and remain in a dormant or 'quiescent' state. These quiescent stem cells (QSCs) were located in the basal layer of the epidermis between the hair follicles and in the bulge region of the hair follicle [3]. The bulge cells proved to be positive for the hematopoietic stem and progenitor marker CD34 and were also found to express specifically K15. Experiments with selective ablation of these cells showed that the progeny of the $K15^+$ cells did not contribute to the IF epidermis and remained in the follicles [4]. Evidently, LRCs persisted but their numbers decreased with age: after 14 months they were no longer observed in the interfollicular (IF) epidermis, but some still persisted in the bulge region of hair follicles [3]. Persistence is a characteristic of stem cells, but a complete lack of replication and consequently a permanent retention of BrdU is not. A stem cell necessarily needs to replicate and generate progeny. Therefore, it was thought that these cells divided rarely and that their direct progeny formed a pool of highly proliferating "transit amplifying cells" that really drove the epidermal turnover [3].

1.2.2. Actively proliferating stem cells: $Lgr5^+$ and $Lgr6^+$ stem cells

More recently stem cells have been identified that, in contrast to the quiescent stem cells, actively proliferate. They appear to be the ever active "work horses" in epithelial renewal. These cells were identified by the expression of Lgr5 and Lgr6. These proteins are leucine-rich repeat containing G-protein coupled receptors, of which a prototypic receptor was first identified in snails [5]. $Lgr5^+$ stem cells were first identified in the intestine. Barker et al. showed by long term lineage tracing that the $Lgr5^+$ cells in the crypts of the small intestine and colon were rapidly cycling stem cells, i.e., they were not the LRCs in the crypts [6]. Jaks et al. went on to show that $Lgr5^+$ cells were also cycling stem cells in the bulb and lower bulge of the hair follicles, and consequently these cells did not include the LRCs higher up in the bulge. The $Lgr5^+$ stem cells maintained the follicle throughout the hair cycle but did not produce progeny that moved into the IF epidermis [7]. However, the progeny of $Lgr5^+$ stem cells does migrate into the IF epidermis upon wounding [8]. Subsequently to Lgr5 another receptor family member was identified, Lgr6, which marked a stem cell population higher up in the follicles, in the isthmus [9]. In embryos, $Lgr6^+$ cells form the early follicles (they precede the $Lgr5^+$ population) and in adults they provide progeny to the sebaceous glands, the upper part of the hair follicle and to the IF epidermis. Snippert et al. showed that Lgr6 progeny also contributed to wound repair, and this progeny remained in the healed area (at least up to 106 days) [9].

1.3. UV radiation

1.3.1. Types of UV radiation

Ultraviolet (UV) radiation from the sun plays an important role in the etiology of skin cancer. Invisible UV radiation with wavelengths below 400 nm borders violet light, and can be divided in UV-A (315-400 nm), UV-B (280-315 nm) and UV-C (100-280 nm). The stratospheric ozone layer blocks a part of the solar UV radiation: UV-C completely and UV-B for a large part. Only a fraction of UV-B and most of the UV-A reach the Earth's surface. It is that small fraction (< 5%) of solar UV flux in the UV-B range at ground level that is predominantly responsible (~ 80%) for the harmful effects of UV radiation, such as sunburn. The skin serves as a protective layer against UV radiation by absorbing part of it in the stratum corneum. The remaining UV radiation penetrates into the skin. The different wavelengths of UV radiation penetrate to different depths; UV-A penetrates through the epidermis into the dermis. In humans UV-B hardly penetrates past the epidermis [10], but in mice UV-B penetrates more easily, since the epidermis is much thinner than in humans [11].

1.3.2. Acute and chronic effects of UV radiation on the skin

UV radiation can have far reaching effects if it is absorbed by DNA. Sites of neighboring pyrimidine bases in a DNA strand are preferentially damaged by short-wavelength UV radiation (UV-B), forming dimers between these bases: either a cyclobutane pyrimidine dimer (CPD) or a 6-4 photoproduct (6-4PP) [12, 13]. CPDs, and more so 6-4PPs, cause a distortion of the DNA helix which can be detected and enhances repair of these DNA lesions [14, 15]. The damage renders the base unrecognizable to DNA and RNA polymerases. In replication of DNA such "non-instructive" damaged bases may give rise to UV signature mutations: cytosine (C) to thymidine (T) at sites of adjacent pyrimidines and CC to TT transitions [16, 17]. CPDs can even give rise to double strand breaks by stalling replication forks [18] and thus cause chromosomal aberrations.
Furthermore, CPDs obstructing RNA polymerase may contribute to acute effects in the skin, e.g. sunburn, starting with reddening of the skin (erythema). Erythema arises from an inflammatory reaction in which superficial small capillary vessels widen (causing the reddening), become more permeable (causing edema) and from which immune cells infiltrate the skin [19]. UV sensitivity is determined by the reciprocal of the Minimal Erythemal Dose (MED), which is defined as the threshold dose of UV radiation for a (just perceptible) skin reddening. If the dose of UV radiation is too high, e.g. an overexposure, epidermal cells will undergo apoptosis (programmed cell death). Apoptosis is induced in cells that contain extensive DNA damage and where repair is overwhelmed. Thus, apoptosis can protect against mutations.

The skin defends itself against chronic UV exposure by thickening and pigmentation of the epidermis. The thickening is caused by an increase in cell layers, hyperplasia. This reduces the penetration of UV radiation to the germinative basal layer of the epidermis [10]. Besides this protective effect, hyperplasia may stimulate the outgrowth of early tumor cells. The pigmentation of the skin is the reason why many people sunbath. This tanning is caused by melanocytes in the epidermis that produce more melanin upon UV exposure and pass it on to neighboring epidermal cells (keratinocytes) [20].

1.4. Skin cancer

Non melanoma skin cancer, comprising of basal cell carcinoma (BCC) and squamous cell carcinoma (SCC) (therefore better referred to as keratinocyte carcinoma), is the most common form of cancer affecting white Caucasians [21, 22]. Incidences have steadily increased in the Netherlands to well over 40,000 new cases a year, posing a serious public health problem (KWF site accessed on 3 Dec 2016). This increase in skin cancer incidences may be largely attributable to increases in sunbathing and holidays to the (sub-) tropics, since UV radiation is the main exogenous driver in skin carcinogenesis. More efficient, less invasive and less labor-intensive therapies or preventive interventions are called for in combating this swell in morbidity from skin cancer and corresponding burden on public health care. Such advancements would also benefit the growing cohorts of organ transplantation recipients who run a dramatically increased risk of SCCs. These SCCs often arise in multiples in sun-exposed skin areas littered with precursor lesions (actinic keratoses, AKs); a phenomenon also called “field cancerization”.

1.4.1. The role of UV-induced DNA damage in skin carcinogenesis

In human SCCs and BCCs the *P53* tumor suppressor genes bear predominantly UV signature mutations (see 1.3.2). Mutation analyses on micro-sections from tumors showed that, next to variably present *P53* mutations, a common *P53* mutation was usually present throughout the tumor mass and could therefore be considered a “founding mutation” [23]. Such *P53* mutations are already present in Actinic Keratoses (AK), precursors of SCC [24]. A dysfunctional *P53* pathway is likely to affect protective responses against DNA damage and oncogenic signaling. Hence, the early occurrence of *P53* mutations may cause genomic instability and thus facilitate further carcinogenic progression. BCC and SCC frequently show losses of chromosomal fragments, *i.e.* loss of heterozygosity (LOH) [25]. More recently, regularly sun-exposed skin was shown to bear an extremely high UV-signature mutational load in 74 cancer-related genes, among which *P53*. Correspondingly, skin cancers, particularly BCC and SCC, rank in the absolute top of cancers with highest mutational loads [26].

Next to mutant P53, AKs also carry extensive LOH [27]. As discussed above (1.3.2) UV radiation can cause crude chromosomal aberrations in mammalian cells, even giving rise to micro-nuclei formation, i.e. UV radiation is clastogenic [28, 29]. People who had skin carcinomas removed turned out to display a slower repair of DNA breaks in their UV-exposed lymphocytes than controls [30], and showed significant differences in polymorphisms in genes coding for proteins involved in double strand break repair [31].

1.4.2. Skin cancer experimental models

In experimental skin cancer research two different approaches to induce skin cancer are used: UV irradiation and chemical treatment. The former is physiologically relevant for human skin cancer development, since UV radiation is the prominent exogenous risk factor. The second one is only analytically relevant, because the resulting *Ras* mutations are not very common in human skin carcinomas, specifically in SCCs [32, 33]. In the first approach hairless mice are used that are daily exposed to sub-sunburn dosages of UV radiation. These hairless mice develop SCCs bearing UV-signature mutations in *p53* similar to those observed in humans. At moderately high-dosages (still without sunburns), they develop SCCs in multiples in areas of the skin displaying field cancerization. Berg et al. found that microscopic foci with overexpression of p53 protein in mutant conformation were already present in UV-exposed mice long before the tumors appeared [34]. Two weeks after stopping the daily irradiations some of the p53-mutant foci, 'p53 patches', were found to persist, signifying that these foci could still develop into tumors. Considering that the turn-over time of viable murine epidermis is about a week, the persistence of these foci would indicate that they originate at least from transit amplifying cells and most likely also from stem cells. Such p53 patches have also been found in sun-exposed human skin, which after microdissection were found to harbor UV-related mutations in *P53* genes [35, 36].
The second, and widely employed chemical regimen consists of an initiator and a promotor stage. First, the initiator, a genotoxic agent (e.g. dimethylbenz[a]antracene, DMBA), is applied to "initiate" the tumor. This is followed by repeated applications of a promotor, a phorbolester (most commonly 12-O-tetradecanoylphorbol-13-acetate, TPA), to promote tumor development (outgrowth) [37]. The initial genotoxic action - even from a single application - is sufficient to introduce persistent latent foci for the later development of tumors. The TPA applications may be delayed for weeks or months and still produce tumors. The molecular-genetical changes relevant to tumor formation under this regimen have been studied in depth in mice [38]. The tumors commonly carry mutations in the *H-ras* oncogene, and amplification of the mutated allele and loss of the wild type allele [39]. TPA stimulates epidermal hyperplasia (LRCs get activated and disappear), and appears to evoke chromosomal aberrations. The repeated applications of TPA are found to result mainly in benign papillomas which - besides the *H-ras* mutations - show loss of heterozygosity at various loci [39, 40]. Malignant progression is not very common, but is strongly increased

by further application of DMBA after promotion. Repeated genotoxic challenges with DMBA leads to more effective malignant conversion [41-43].

1.5. Stem cells targeted in skin carcinogenesis?

Over the previous century the theory on carcinogenesis has evolved from conceptual and mathematical models on unspecified "multi-hits" involving genetic material [44, 45] to (experimental) models with series of specific genetic changes [46, 47]. Next to changes in the genetic code (mutations), epigenetic changes are being explored for contributions to carcinogenesis. The essential changes in cell physiology ("Hall Marks") that constitute malignant growth have been defined as self-sufficiency in growth, insensitivity to growth control signals, evasion of programmed cell death, limitless replicative potential, sustained angiogenesis, changing energy metabolism, immune evasion, tissue invasion and metastasis [48, 49]. These traits appear to develop in stages with the molecular changes in the neoplastic cell, and generally take time. Hence, the targeted cell in carcinogenesis needs to reside in the body for a long time in order to acquire a series of alterations resulting in malignant growth. Furthermore, the cell most likely needs to divide to incur mutations (replication of damaged DNA carries a high risk of mutagenesis) and pass these mutations on to daughter cells. These requirements of long term residence combined with cell division point to stem cells as the most evident target cells.

1.6. Aim and outline of this thesis

The aim of the research described in this thesis was to identify the main (stem) cell pool that drives skin carcinogenesis. Selective elimination of these altered tumor stem cells at an early stage would prevent the development of field cancerization and SCCs in high-risk individuals, such as organ transplant recipients. To this end, we investigated different stem cell populations in the skin.

In **Chapter 2** we set out to test whether (stem) cells in the hair follicle or in the IF epidermis are targeted in UV carcinogenesis. We subjected hairless mice to a chronic UV regimen inducing p53 patches. By a single UV overexposure we selectively eradicated the basal cells in the IF epidermis, including the p53 patches. Subsequently, the chronic UV regime was restarted to assess whether this ablative intervention affected early SCC development.

Our group established earlier that QSCs can accumulate and retain UV-induced DNA damage under a regime of very low level UV exposures that do not activate QSCs and do not give rise to hyperplasia. In **Chapter 3** we investigated if these DNA damage-retaining QSCs would be poised to give rise to SCCs or other skin tumors if they were forced to divide by the application of the tumor promoter TPA.

Besides QSCs, we also studied cycling stem cells in the skin: the $Lgr5^+$ and $Lgr6^+$ cells. We investigated their response to carcinogenic stimuli (UV and chemical): i.e. their roles in

replacing basal cells after UV overexposure, in driving (UV/TPA-induced) hyperplasia and in UV- and chemically induced skin carcinogenesis. The results for $Lgr5^+$ stem cells are described in **Chapter 4** and those for $Lgr6^+$ stem cells are described in **Chapter 5**. In **Chapter 6** we use next generation sequencing of RNA to further characterize the $Lgr6^+$ cells in the skin of hairless mice.

The overall results on epidermal stem cells and skin carcinogenesis presented in this thesis are summarized and discussed in **Chapter 7**.

References

1. Iizuka H. Epidermal architecture that depends on turnover time. J Dermatol Sci. 1995; 10(3):220-223.
2. Zhang H, Hou W, Henrot L, Schnebert S, Dumas M, Heusele C and Yang J. Modelling epidermis homoeostasis and psoriasis pathogenesis. Journal of the Royal Society, Interface. 2015; 12(103).
3. Morris RJ and Potten CS. Highly persistent label-retaining cells in the hair follicles of mice and their fate following induction of anagen. J Invest Dermatol. 1999; 112(4):470-475.
4. Ito M, Liu Y, Yang Z, Nguyen J, Liang F, Morris RJ and Cotsarelis G. Stem cells in the hair follicle bulge contribute to wound repair but not to homeostasis of the epidermis. Nat Med. 2005; 11(12):1351-1354.
5. Tensen CP, Van Kesteren ER, Planta RJ, Cox KJ, Burke JF, van Heerikhuizen H and Vreugdenhil E. A G protein-coupled receptor with low density lipoprotein-binding motifs suggests a role for lipoproteins in G-linked signal transduction. Proceedings of the National Academy of Sciences of the United States of America. 1994; 91(11):4816-4820.
6. Barker N, van Es JH, Kuipers J, Kujala P, van den Born M, Cozijnsen M, Haegebarth A, Korving J, Begthel H, Peters PJ and Clevers H. Identification of stem cells in small intestine and colon by marker gene Lgr5. Nature. 2007; 449(7165):1003-1007.
7. Jaks V, Barker N, Kasper M, van Es JH, Snippert HJ, Clevers H and Toftgard R. Lgr5 marks cycling, yet long-lived, hair follicle stem cells. Nat Genet. 2008; 40(11):1291-1299.
8. Kasper M, Jaks V, Are A, Bergstrom A, Schwager A, Svard J, Teglund S, Barker N and Toftgard R. Wounding enhances epidermal tumorigenesis by recruiting hair follicle keratinocytes. Proceedings of the National Academy of Sciences of the United States of America. 2011; 108(10):4099-4104.
9. Snippert HJ, Haegebarth A, Kasper M, Jaks V, van Es JH, Barker N, van de Wetering M, van den Born M, Begthel H, Vries RG, Stange DE, Toftgard R and Clevers H. Lgr6 marks stem cells in the hair follicle that generate all cell lineages of the skin. Science. 2010; 327(5971):1385-1389.
10. Bruls WA, Slaper H, van der Leun JC and Berrens L. Transmission of human epidermis and stratum corneum as a function of thickness in the ultraviolet and visible wavelengths. Photochem Photobiol. 1984; 40(4):485-494.
11. de Gruijl FR and Forbes PD. UV-induced skin cancer in a hairless mouse model. Bioessays. 1995; 17(7):651-660.
12. Setlow RB and Carrier WL. Pyrimidine dimers in ultraviolet-irradiated DNA's. J Mol Biol. 1966; 17(1):237-254.
13. Varghese AJ and Patrick MH. Cytosine derived heteroadduct formation in ultraviolet-irradiated DNA. Nature. 1969; 223(5203):299-300.
14. Jiang N and Taylor JS. In vivo evidence that UV-induced C-->T mutations at dipyrimidine sites could result from the replicative bypass of cis-syn cyclobutane dimers or their deamination products. Biochemistry. 1993; 32(2):472-481.
15. Liu B, Xue Q, Tang Y, Cao J, Guengerich FP and Zhang H. Mechanisms of mutagenesis: DNA replication in the presence of DNA damage. Mutation research Reviews in mutation research. 2016; 768:53-67.
16. Brash DE. UV mutagenic photoproducts in Escherichia coli and human cells: a molecular genetics perspective on human skin cancer. Photochem Photobiol. 1988; 48(1):59-66.
17. Brash DE, Rudolph JA, Simon JA, Lin A, McKenna GJ, Baden HP, Halperin AJ and Ponten J. A role for sunlight in skin cancer: UV-induced p53 mutations in squamous cell carcinoma. Proceedings of the National Academy of Sciences of the United States of America. 1991; 88(22):10124-10128.
18. Garinis GA, Mitchell JR, Moorhouse MJ, Hanada K, de Waard H, Vandeputte D, Jans J, Brand K, Smid M, van der Spek PJ, Hoeijmakers JH, Kanaar R and van der Horst GT. Transcriptome

analysis reveals cyclobutane pyrimidine dimers as a major source of UV-induced DNA breaks. EMBO J. 2005; 24(22):3952-3962.

19. Parrish JA, Jaenicke KF and Anderson RR. Erythema and melanogenesis action spectra of normal human skin. Photochem Photobiol. 1982; 36(2):187-191.
20. Gilchrest BA, Park HY, Eller MS and Yaar M. Mechanisms of ultraviolet light-induced pigmentation. Photochem Photobiol. 1996; 63(1):1-10.
21. Lomas A, Leonardi-Bee J and Bath-Hextall F. A systematic review of worldwide incidence of nonmelanoma skin cancer. Br J Dermatol. 2012; 166(5):1069-1080.
22. Griffin LL, Ali FR and Lear JT. Non-melanoma skin cancer. Clin Med (Lond). 2016; 16(1):62-65.
23. Backvall H, Asplund A, Gustafsson A, Sivertsson A, Lundeberg J and Ponten F. Genetic tumor archeology: microdissection and genetic heterogeneity in squamous and basal cell carcinoma. Mutat Res. 2005; 571(1-2):65-79.
24. Rehman I, Quinn AG, Healy E and Rees JL. High frequency of loss of heterozygosity in actinic keratoses, a usually benign disease. Lancet. 1994; 344(8925):788-789.
25. Quinn AG, Sikkink S and Rees JL. Basal cell carcinomas and squamous cell carcinomas of human skin show distinct patterns of chromosome loss. Cancer Res. 1994; 54(17):4756-4759.
26. Martincorena I, Roshan A, Gerstung M, Ellis P, Van Loo P, McLaren S, Wedge DC, Fullam A, Alexandrov LB, Tubio JM, Stebbings L, Menzies A, Widaa S, Stratton MR, Jones PH and Campbell PJ. Tumor evolution. High burden and pervasive positive selection of somatic mutations in normal human skin. Science. 2015; 348(6237):880-886.
27. Rehman I, Takata M, Wu YY and Rees JL. Genetic change in actinic keratoses. Oncogene. 1996; 12(12):2483-2490.
28. Keulers RA, de Roon AR, de Roode S and Tates AD. The induction and analysis of micronuclei and cell killing by ultraviolet-B radiation in human peripheral blood lymphocytes. Photochem Photobiol. 1998; 67(4):426-432.
29. Emri G, Wenczl E, Van Erp P, Jans J, Roza L, Horkay I and Schothorst AA. Low doses of UVB or UVA induce chromosomal aberrations in cultured human skin cells. J Invest Dermatol. 2000; 115(3):435-440.
30. Wang LE, Xiong P, Strom SS, Goldberg LH, Lee JE, Ross MI, Mansfield PF, Gershenwald JE, Prieto VG, Cormier JN, Duvic M, Clayman GL, Weber RS, Lippman SM, Amos CI, Spitz MR, et al. In vitro sensitivity to ultraviolet B light and skin cancer risk: a case-control analysis. J Natl Cancer Inst. 2005; 97(24):1822-1831.
31. Han J, Colditz GA, Samson LD and Hunter DJ. Polymorphisms in DNA double-strand break repair genes and skin cancer risk. Cancer Res. 2004; 64(9):3009-3013.
32. Spencer JM, Kahn SM, Jiang W, DeLeo VA and Weinstein IB. Activated ras genes occur in human actinic keratoses, premalignant precursors to squamous cell carcinomas. Arch Dermatol. 1995; 131(7):796-800.
33. Fernandez-Medarde A and Santos E. Ras in cancer and developmental diseases. Genes Cancer. 2011; 2(3):344-358.
34. Berg RJ, van Kranen HJ, Rebel HG, de Vries A, van Vloten WA, Van Kreijl CF, van der Leun JC and de Gruijl FR. Early p53 alterations in mouse skin carcinogenesis by UVB radiation: immunohistochemical detection of mutant p53 protein in clusters of preneoplastic epidermal cells. Proc Natl Acad Sci U S A. 1996; 93(1):274-278.
35. Jonason AS, Kunala S, Price GJ, Restifo RJ, Spinelli HM, Persing JA, Leffell DJ, Tarone RE and Brash DE. Frequent clones of p53-mutated keratinocytes in normal human skin. Proc Natl Acad Sci U S A. 1996; 93(24):14025-14029.
36. Ren Z-P, Pontén F, Nistér M and Pontén I. Two distinct p53 immunohistochemical patterns in human squamous-cell skin cancer, precursors and normal epidermis. Int J Cancer. 1996; 69(3):174-179.

37. Reddy AL and Fialkow PJ. Influence of dose of initiator on two-stage skin carcinogenesis in BALB/c mice with cellular mosaicism. Carcinogenesis. 1988; 9(5):751-754.
38. Akhurst RJ and Balmain A. Genetic events and the role of TGF beta in epithelial tumour progression. J Pathol. 1999; 187(1):82-90.
39. Quintanilla M, Brown K, Ramsden M and Balmain A. Carcinogen-specific mutation and amplification of Ha-ras during mouse skin carcinogenesis. Nature. 1986; 322(6074):78-80.
40. Sutter C, Strickland JE, Welty DJ, Yuspa SH, Winter H and Schweizer J. v-Ha-ras-induced mouse skin papillomas exhibit aberrant expression of keratin K13 as do their 7,12-dimethylbenz[a]anthracene/12-O-tetradecanoylphorbol-13-acetate -induced analogues. Mol Carcinog. 1991; 4(6):467-476.
41. Moon DC, Nakayama J, Urabe A, Terao H, Kinoshita N and Hori Y. Immunohistochemical characterization of cellular infiltrates in epidermal tumors induced by two-stage and complete chemical carcinogenesis in mouse skin. J Dermatol. 1992; 19(3):146-152.
42. Iversen OH. A course of very small doses of DMBA, each of them allegedly with no promoting potency, acts with clear synergistic effect as a strong promoter of DMBA-initiated mouse skin carcinogenesis. A comparison of the tumorigenic and carcinogenic effects of DMBA (7,12-dimethylbenz-alpha-anthracene) and TPA (12-O-tetradecanoyl-phorbol-13-acetate) used as initiators and promoters in classical two-stage experimental protocols. APMIS Suppl. 1994; 41:1-38.
43. Thomas G, Tuk B, Song JY, Truong H, Gerritsen HC, de Gruijl FR and Sterenborg HJ. Studying skin tumourigenesis and progression in immunocompetent hairless SKH1-hr mice using chronic 7,12-dimethylbenz(a)anthracene topical applications to develop a useful experimental skin cancer model. Lab Anim. 2016.
44. Muller HJ. Radiation damage to the genetic material. Am Sci. 1950; 38(1):33-59.
45. Nordling CO. A new theory on cancer-inducing mechanism. Br J Cancer. 1953; 7(1):68-72.
46. Vogelstein B and Kinzler KW. The multistep nature of cancer. Trends Genet. 1993; 9(4):138-141.
47. Dlugosz A, Merlino G and Yuspa SH. Progress in cutaneous cancer research. J Investig Dermatol Symp Proc. 2002; 7(1):17-26.
48. Hanahan D and Weinberg RA. The Hallmarks of Cancer. Cell. 2000; 100(1):57-70.
49. Hanahan D and Weinberg Robert A. Hallmarks of Cancer: The Next Generation. Cell. 2011; 144(5):646-674.

Chapter 2

UV-induced ablation of the epidermal basal layer including p53- mutant clones resets UV carcinogenesis showing squamous cell carcinomas to originate from interfollicular epidermis.

H.G. Rebel, C.A. Bodmann, G.C. van de Glind, F.R. de Gruijl
Carcinogenesis. 2012 vol.33 no.3 pp.714–720

Abstract

Chronic ultraviolet (UV) exposure induces clones of cells overexpressing mutant p53 in the interfollicular epidermis (IFE) and subsequently squamous cell carcinomas (SCCs) with similar p53 mutations. Mutated p53 may give cells growth advantage over neighboring cells by impaired apoptosis. We tested this by UV overexposure of skin laden with p53-mutant clones and assessed the impact on subsequent tumor development. P53-mutant clones were induced in two groups of hairless SKH-1 mice by daily exposures (500 J/m^2 UV from TL12 lamps) for 28 days. On day 29, one group was overexposed (to 10 kJ/m^2 UV), whereas the control group received the regular daily dose. After 1 week of recovery, the daily exposures were resumed in both groups to induce SCCs. UV overexposure forced the entire interfollicular basal layer into caspase-3-driven apoptosis while leaving overlying layers with sunburn cells intact. No apparent regions were spared from apoptosis. Pulse-chase BrdU labelling showed the IFE to be repopulated from the hair follicles (remaining p63 positive). One week after overexposure, the p53-mutant clones had virtually disappeared (0.6, 95% confidence interval 0.5–0.8 per mouse versus 102, 59–179, without overexposure). Tumor development was significantly delayed after UV overexposure ($P < 0.0001$) by an average of 27 days (standard error of the mean 3); a period matching that of daily exposures preceding the overexposure. Thus, we found that UV-induced ablation of the interfollicular epidermal basal layer eliminates p53-mutant clones and resets UV carcinogenesis. Furthermore, and in contrast with earlier reports, our data show that UV-induced p53-mutant clones and SCCs originate from the IFE.

2.1. Introduction

Solar ultraviolet (UV) irradiation causes cutaneous basal cell carcinomas (BCCs) and squamous cell carcinomas (SCCs) in exposed skin. The increased incidence over the last decades poses an increasing burden on public health care. Estimated from annual incidences times a lifetime expectancy of 80 years, lifetime risk ranges from 6 to 8% for BCCs and from 1 to 2% for SCCs in Europe in 2004 [1, 2]. The combined BCC and SCC lifetime risk is predicted to rise with an additional 1% per 5 years. In SCCs and in BCCs, UV signature mutations are found in the P53 tumor suppressor gene: cytosine (C) > thymidine (T) and CC > TT transitions at dipyrimidine sites [3, 4]. Such mutations are also present in the benign precursor lesions of SCCs, actinic keratosis [5]. In chronically UV-exposed skin, immunohistochemically detectable epidermal clones of cells overexpressing mutant p53 (p53-mutant clones or p53 patches) occur in the interfollicular epidermis (IFE). These microscopic lesions are considered to be precursors of actinic keratosis and SCCs. Several observations indicate that these p53-mutant clones are causally related to SCCs: (i) similar UV signature mutations and the very same hotspots in the *p53* gene are found in both types of lesions [6-8], (ii) these lesions show comparable UV dose dependencies [7] and (iii) increased incidence of p53 clones in DNA repair-deficient *Xpa-*, *Xpc-* and *Csb* knockout mice correspond with tumor risk [7]. Furthermore, ~70% of SCCs bear p53 mutations which obstruct the tumor-suppressive action through cell cycle arrest, induction of DNA repair and apoptosis [9]. By suppression of apoptosis and cell cycle arrest, *p53* mutations can give an epidermal cell a growth advantage over its wild-type neighbors. Subsequently, clonal expansion creates an enlarged more susceptible target for the acquisition of additional mutations.

Impaired UV-induced apoptotic responses due to defective p53 signaling were found experimentally both in *p53* knockout mice [10] and in cells with mutated *p53* [11]. P53-mutant clones in the epidermis could therefore be relatively resistant to apoptosis compared with surrounding keratinocytes carrying wild-type *p53* and survive higher UV doses. Because this was never verified directly, we set out to investigate this expected contrast in apoptosis by subjecting skin laden with p53-mutant clones to high level UV exposure. Upon strong overexposure (4–6 times the threshold dose for a minimal sunburn reaction [12, 13]), widespread apoptosis occurs and lost cells leave apparent vacancies in the epidermis. Under these conditions, p53-mutated cells may show a better survival than their neighboring wild-type cells. This should then lead to a preferential outgrowth of the mutant clones at the expense of the wild-type keratinocytes and thus enhance subsequent UV carcinogenesis [14]. On the other hand, if the clones become apoptotic and are replaced by wild-type keratinocytes, the number of clones will drop and subsequent UV carcinogenesis should be reduced.

Against experimental evidence that interfollicular p53 clones are precursors of SCCs, Faurschou et al. [15] reported that laser ablation of IFE of hairless SKH-1 mice that were chronically UV exposed did not impair the tumor induction time of SCCs (also discussed in [16]). This would imply that p53 clones should be considered more as epiphenomena than real precursors of SCCs. However, p53 clone densities before and after the laser ablation were not determined in this study, and adequate elimination of the interfollicular p53-mutant clones was therefore not verified. Our study allowed us to investigate this issue more closely and to assess the corresponding effect on UV carcinogenesis.

The epidermis harbors three stem cell niches: the bulge region, the isthmus of the hair follicle and the basal layer of the IFE [17]. Stem cells in these niches have the ability to self-renew and to generate daughter cells that differentiate in the cells populating the hair follicle, sebaceous gland or IFE, respectively. There is growing evidence for the conjecture that BCCs originate from stem cells in the bulge region of hair follicles [18, 19]. Our experiments provide evidence on which stem cell pool is targeted in the UV-driven genesis of SCCs.

In this study, we found that UV overexposure at the dose we used predominantly ablated the entire interfollicular epidermal basal cell layer, including p53-mutant clones, by caspase-3-driven apoptosis, leaving overlying epidermal layers with sunburn cells and hair follicles largely intact. Such eradication of p53-mutant clones resulted in an apparent restart of UV carcinogenesis when the regimen of daily UV exposure by which the p53-mutant clones were induced was continued. Hence, the UV-induced SCCs in hairless mice appear to originate from the interfollicular epidermal basal layer.

2.2. Materials and methods

2.2.1. Mice

Legal approval for the UV experiments with hairless SKH-1 mice was received from the animal ethical commission. Hairless Crl:SKH1-HR mice were obtained from Charles River, France, and maintained in our breeding facility. Mice from the breeding colony entered the experiment at 6-9 weeks of age and were housed at 25 ± 2^0C in macrolon cages with standard mice chow (SDS, Essex, UK) and water *ad libitum*.

2.2.2. UV exposure, BrdU incorporation and tumors

Male and female SKH-1 mice in 1:1 ratio were irradiated daily with 0.75 minimal edema/erythemal dose to naive skin (MED) during the first 3 days and with one MED (500 J/m^2 UV) in the days thereafter. In all experiments, the UV sources were TL-12 fluorescent lamps (54% of output in UV-B, 280–315 nm, and 46% in UV-A, 315–400 nm).

From earlier studies [12, 13], we knew that four to six MEDs induced widespread apoptosis in the epidermis of a naive (unexposed) skin; higher dosages caused wounding and were

not well tolerated by the mice. However, in the present experiment, the skin first needed to be chronically UV exposed to induce p53-mutant clones. Such a skin adapts and becomes less sensitive to UV exposure, i.e. the actual MED (aMED) will be raised several fold over the MED of the naive skin. In a pilot experiment, we verified that 2 kJ/m^2 (about one aMED) induced hardly any apoptosis in the chronically exposed skin and that 10 kJ/m^2 (five aMEDs) induced widespread apoptosis and was well tolerated. In the final experiment, 28 SKH1 mice were irradiated for 28 days after which a single UV overexposure of 10 kJ/m^2 UV was given to 20 mice, whereas 8 control mice received a 29th day regular one MED (500 J/m^2) of UV. In a series of time points (1, 6, 24, 48 h and 7 days), four mice per point were killed by CO_2 inhalation. Skin biopsies were taken and fixed in phosphate-buffered saline (PBS)-buffered 4% formaldehyde for 24 h at 4^{o}C and stored in 70% ethanol. Additionally, biopsies were snap frozen in liquid nitrogen and stored at -80^{o}C till further processing. For incorporation of 5-bromo-2'-deoxyuridine (BrdU) in the DNA of replicating epidermal cells, the mice were intraperitoneally injected with 300 µl PBS containing 5 mg BrdU (Sigma, St Louis, MO). The mice were killed 1 h after injection for immediate BrdU labelling of replicating cells. BrdU is incorporated in epidermal S-phase cells up to 2 h after injection (the pulse). After this initial BrdU labelling, the label is passed on to the daughter cells without any further uptake of BrdU; this is the BrdU chase period in which the progeny of the initially labelled proliferating cells can be traced [20].

For experiments in which p53 clones were scored, 30 SKH1 mice were similarly given the UV regimen of 28 days of one MED/day. After 28 days, six mice were killed for preparation of epidermal sheets. At the 29th day, 12 mice received a five aMED overexposure, whereas the 12 remaining control mice received a 29th regular one MED. After the UV overexposure, all mice were left unexposed for 6 days, after which the regular one MED/day regimen was resumed. At 35 and 42 days, six overexposed mice and six control mice were killed and epidermal sheets were isolated.

To study the effect of UV overexposure on UV carcinogenesis, 52 SKH-1 mice were subjected to the UV regimen of 28 days with one MED/day. At the 29th day, 26 mice received an overexposure of five aMED (10 kJ/m^2 UV), whereas the remaining 26 control mice received a 29th one MED. After 6 days, the daily irradiations of one MED were resumed at day 35 for all 52 mice. Skin tumors were weekly scored blindly by two trained observers; recorded were location on dorsal skin, number, diameter and tumor type (either actinic keratosis, SCC or papilloma: pedunculated protruding tumor with a 'cauliflower-like' surface; [21]). Reaching a total tumor mass of 0.5 cm^3 was one of the preset ethical criteria that determined when a mouse was to be killed.

2.2.3. Preparation of epidermal sheets

Rectangular segments (32 x 20 mm) of the dorsal skin were excised and placed with dermal side down floating on a 100 mg/ml thermolysin solution (P-1512; Sigma) in PBS containing

1 mM $CaCl_2$, pH 7.8. After overnight incubation at 4^{o}C, each epidermis was rolled onto a polyethylene tube to separate it from the dermis.

2.2.4. Immunohistochemistry

Active caspase-3 staining. Cryosections were cut at 5 µm thickness, placed on Superfrost Plus glasses (Thermo Scientific, Braunschweig, Germany) and immediately fixed in acetone. After blocking with 1% bovine serum albumin and 5% normal goat serum, the sections were incubated for 1 h with anti-active caspase-3 (Ab2302; Abcam, Cambridge, UK) at 1:100 dilution. After a triple PBS wash, goat anti-rabbit (IgG) biotin (diluted 1:300, BA-1000; Vector Laboratories, Burlingame, CA) was applied for 1 h and excess was removed by a triple PBS wash. The third step was incubated for 45 min with avidin-biotin-HRP complex (PK-6100; Vector Laboratories). After a triple PBS wash, peroxidase activity was visualized by a 7 min incubation in 100 ml of 0.1 M acetate buffer containing 20 mg of *N,N,*-dimethylformamide-dissolved 3-amino-9-ethylcarbazol (A-5754; Sigma) and 100 µl of H_2O_2, resulting in a red staining.

P63 staining. Formaldehyde-fixed biopsies were processed in a Tissue-tek VIP apparatus (Miles Scientific), in a graded series of ethanol solutions, 100% toluene and subsequently embedded in paraffin. Paraffin sections were cut at 7 µm, placed on Starfrost glasses and deparaffinized in xylene and a graded series of ethanol solutions. Endogenous peroxidase was blocked by 20 min incubation with 1.5% H_2O_2 in methanol. Antigen retrieval was performed in 0.01 M citrate buffer pH 6.0 in an autoclave for 5 min at 110^{0}C. After a triple PBS wash, the slides were preincubated with 2% normal rabbit serum and 1% bovine serum albumin in PBS and subsequently with anti-p63 antibody clone 4A4 (1:50, M7247; DakoCytomation, Glostrup, Denmark) for 1 h. After washing rabbit anti-mouse (IgG2a) biotin (1:200, 61-0240; Zymed, San Fransisco, CA) was incubated for 1 h. The third step was incubation with avidin-biotin-HRP complex (PK-6100; Vector Laboratories) for 45 min. After a triple wash, peroxidase was visualized with 20 mg of 3,3'-diaminobenzidine dissolved in 100 ml of PBS.
Counter staining was performed with haematoxylin (Klinipath, Duiven, The Netherlands) and sections were mounted in Kaisers' glycerine (Merck, Darmstadt, Germany).

Active caspase-3 p63 double staining. It was performed on paraffin sections with similar procedure as for p63 staining as outlined above and with the red chromophore 3-amino-9-ethylcarbazol instead of 3,3'-diaminobenzidine. Anti-active caspase-3 was visualized by a second step goat anti-rabbit IgG fluorescein isothiocyanate (1:100, 65-6111; Zymed), a third step with sheep anti-fluorescein isothiocyanate alkaline phosphatase (1:400, 1426338; Roche, Mannheim, Germany) and finally with Fast blue (F-3378; Sigma) as the chromophore. Fast blue (25 mg) was dissolved in 100 ml of 0.1 M TRIS/0.05 M $MgCl_2$ buffer

containing 12.5 ng naphthol AS-MX phosphate (N-4875; Sigma) and 35 mg levamisol (L-9756; Sigma).

BrdU staining. It was performed on paraffin sections as described [22, 23]: antigen retrieval was performed with 60 mg pepsin/100 ml of 0.1 M HCl during 30min. The subsequent steps for immunostaining were anti-BrdU (1:100,M0744; DakoCytomation), rabbit anti-mouse (IgG1) biotin (1:50, 61-0140; Zymed), avidin-biotin-HRP complex (Vector Laboratories), 3,3'-diaminobenzidine and haematoxylin counter staining. Sections were photographed with a digital camera (Axiocam; Zeiss, Sliedrecht, The Netherlands) mounted on a light microscope (Axioplan 2, Zeiss, equipped with a ×10 objective).

P53-mutant clones. Epidermal sheets were fixed in PBS-buffered 4% formaldehyde and stained with mutant p53-specific antibody basically as described earlier [7, 23], with two modifications: antigen retrieval in 0.01 citrate buffer in an autoclave for 5 min at 110^0C and anti-mutant p53 (1:250, Pab240; Thermo Fisher Scientific, Fremont, CA). Scoring of p53-mutant clones was carried out as described previously [7, 24].

2.2.5. Statistics

The numbers of p53 clones scored per sheet were log transformed and averaged over the mice to estimate the median (geometric mean of log-normal distribution) and 95% confidence intervals (CI) for the median were calculated [median × exp (±2 SEM), where exp stands for 'exponent' of 10, i.e. 10 to the power (+2 SEM) and SEM stands for standard error in the mean log value]. T-tests were performed with the statistical program SPSS, version 17. Tumor data were transferred to Excel 2003 and Kaplan–Meier tumor-free survival curves were generated and analyzed with GraphPad Prism 5.04. Logrank (Mantel Cox) tests were applied to establish significant differences between the Kaplan–Meier curves.

2.3. Results

2.3.1. UV overexposure ablates the basal layer of the IFE

P53-mutant clones could be readily induced by the sub-sunburn regimen of daily UV exposures for 4 weeks (Supplementary Figure S2.1). On day 29, we overexposed a group (n=20) to a UV dose of 10 kJ/m^2 (about five aMEDs to a UV-adapted skin). In the first days after the UV overexposure, the dorsal skins showed edema, erythema, scaling and some microscopic foci of bacterial infection (indicating a compromised barrier function of the stratum corneum) but remained largely intact and recovered almost completely after 1 week (Supplementary Figure S2.2). To examine the precise time course and extent of the apoptotic response, we stained active caspase-3 [25] on skin biopsies that were taken of mice at 6, 24, 48 h and 7 days after UV overexposure (n=4 per time point, representative

sections in Figure 2.1, first column of panels). Control mice received one additional daily UV dose (500 J/m^2) instead of the UV overexposure. Specific cytoplasmatic active caspase-3 staining was found in UV-overexposed mice at 6, 24 and 48 h. The epidermis of control mice showed no staining of active caspase-3 (Figure 2.1, upper left panel).

The caspase-3-positive cells were predominantly located in the basal layer of the IFE at 6 and 24 h, interspersed at 6 h and contiguous at 24 h. At 48 h, positive cells remnants were found in a suprabasal layer halfway up in the epidermis (an apoptotic front). At 24 h, virtually all of the epidermal cells in the differentiated layers above the active caspase-3-positive basal layer had become sunburn cells (first column of panels in Supplementary Figure S2.3). None of the K10-positive differentiated cells showed activation of caspase-3 (Supplementary Figure S2.4). Active caspase-3-positive staining was absent in hair follicles, except for the rim of the infundibula at 6 h where some cells in the outer root sheet could be positive to at most a depth of three cells under the interfollicular basal layer (arrows in second panel of first column of Figure 2.1). At 24 h and later, cells with activated caspase-3 were exclusively found in the IFE. The caspase-positive apoptotic cells apparently migrated from the basal layer outward in a front as a new epidermis grew underneath. The overlying layers remained intact.

Our attempt to visualize apoptosis directly in p53-mutant clones by double staining with anti-mutant p53 (Pab240) and anti-active caspase- 3 at 6 and 24 h failed because Pab240 staining became false positive in most of the overexposed epidermis (Supplementary Figure S2.5). This was probably due to partial degradation of p53 after the applied UV overexposure, whereby the Pab240 epitope became also accessible in wild-type p53 proteins.

P63 is essential for homeostasis of the epidermis; mice knockout or mutant in *p63* are severely compromised in skin development [26, 27]. P63 also relays an anti-apoptotic signal [28]. Earlier reported immunostaining for p63 with antibody 4A4 revealed p63 expression in the basal cells of the epidermis and in the bulge of the hair follicle, which include adult stem cells [29]. Immunostaining with this p63 antibody on sections at different time points after UV overexposure (Figure 2.1, second column) revealed positive nuclear staining throughout the outer root sheet of the hair follicles and the basal layer of the IFE at all time points, except at 24 h after overexposure. At this time point, p63 expression was completely lost in the IFE, whereas the hair follicles remained positive. At 48 h, a renewed p63-positive basal layer was observed underneath the apoptotic caspase-positive 'front'. Double staining with anti-active caspase-3 and anti-p63 showed no double-positive cells (Figure 2.1, third column), except at 6 h where a few double-positive cells were observed, on average 4.0% (SEM 1.2) of basal cells.

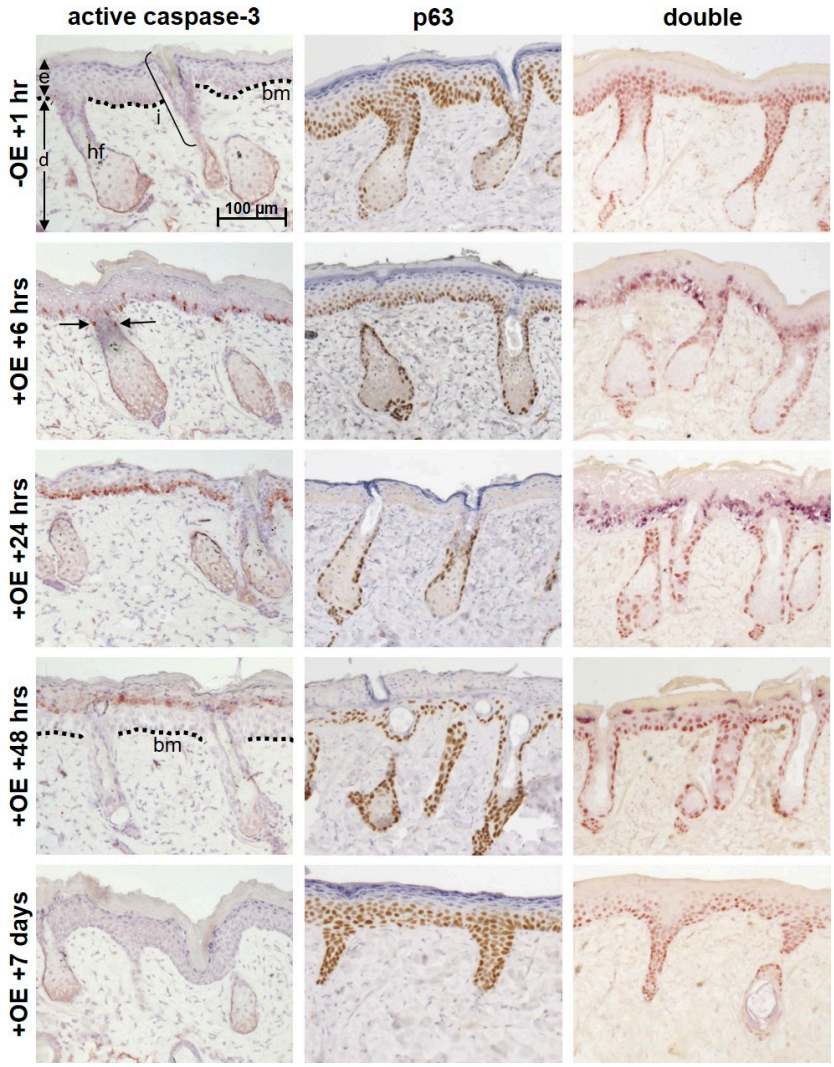


Figure 2.1: Sections of murine skin at several time points after UV overexposure (+OE, 10 kJ/m^2) and control skin at 1 hr after one MED (500 J/m^2, -OE). Preceding the overexposure the mice received 28 days one MED UV/day, resulting in hyperplasia of the IFE. In upper left panel, 'e' denotes epidermis 'd' dermis, 'bm' basal membrane, 'hf' hair follicle and 'i' infundibulum. Left column: active caspase-3 cytoplasmatic staining indicates apoptosis in the basal layer at 6 and 24 h and in a suprabasal layer at 48 h (bm delineated). Virtually no active caspase-3 staining was found in hair follicles. The arrows in the second panel indicate an example of active caspase-3-positive cells at maximum depth in the infundibulum. Middle column: p63 immunostaining absent in the IFE at 24 h and re-appearing in the basal layer at 48 h. Right column: caspase-3 Fast Blue & p63 3-amino-9-ethylcarbazol double staining.

2.3.2. The interfollicular basal layer is repopulated from hair follicles after UV ablation

To study repopulation of the basal cell layer of the IFE after UV ablation, we performed a BrdU pulse-chase experiment in which we injected BrdU at 0, 5, 23 and 167 h after UV overexposure and used chase periods of 17 and 23 h counting from 2 h after injection (Figure 2.2). In skin that was not overexposed, epidermal basal cells showed clear BrdU incorporation, but at 5-6 h after UV overexposure, the BrdU uptake was strongly diminished. No BrdU-positive cells were observed in the IFE after a subsequent chase period up to 24 h after overexposure. At 23-24 h after overexposure, no BrdU uptake was detectable in the IFE, whereas abundant labelling was found in the hair follicles. After a subsequent chase period up to 48 h after the overexposure, BrdU-labelled daughter cells had apparently moved from the hair follicles to the newly formed interfollicular basal cell layer. Seven days after UV overexposure, the BrdU uptake was normal and closely resembled what was observed in skin that had not been overexposed.

Interestingly, p63 staining revealed channels of cells that connected cysts located deep down in the dermis with the rudimentary hair follicle of the hairless mouse (Supplementary Figure S2.6). The channels were only two cells in width and therefore went unnoticed earlier. The dermal cysts remained BrdU positive at all time points (Supplementary Figure S2.7).

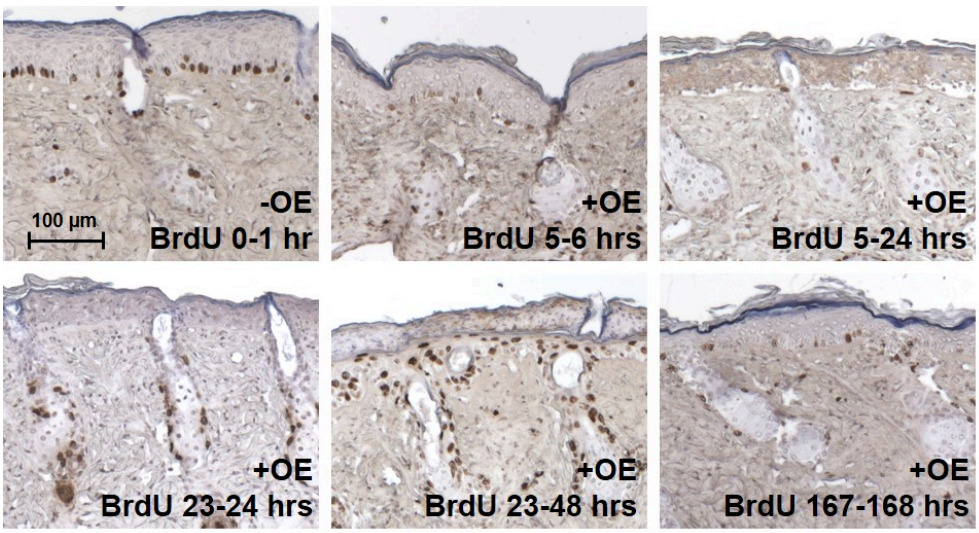


Figure 2.2: BrdU immunostaining of murine skin sections at several time points after UV overexposure (+OE), and control skin (-OE) at 1 h after one MED. The mice were killed 1 h after BrdU injection at 0, 5, 23 and 167 h after overexposure or after a chase period of up to 19 h after injection at 5 h or up to 25 h after injection at 23 h.

2.3.3. P53-Mutant clones eliminated by UV ablation

To study whether p53-mutant clones disappeared after UV ablation of the interfollicular basal cell layer or persisted due to their possible resistance to apoptosis, we first measured the median number of 258 (95% CI 188–354) in dorsal epidermal sheets of six mice killed after the 4 weeks regimen of daily sub-sunburn exposures (i.e. the number just before UV overexposure). The p53-mutant clones appeared to be exclusively located in the IFE (i.e. no staining in hair follicles; Supplementary Figure S2.1). After the UV overexposure, all mice were left unexposed for 1 week for recuperation of the epidermis. At the end of that week, at day 35, the p53 clones in the overexposed group had almost completely disappeared: only 0.6 clones per sheet (95% CI 0.5–0.8) were found, whereas the p53 clones in the control group had dropped in number to 102 per sheet (95% CI 59–179) (Figure 2.3). Compared with these control mice at day 35, 99.5% of the p53 clones were thus eliminated by UV ablation. To ascertain whether the loss of p53-mutant clones was not merely temporary (possibly by survival of stem cells with mutated p53), the UV regimen of daily sub-sunburn exposures was resumed in both groups at day 36 till day 42. In both groups, the p53 clones were found only slightly increased by day 42 [ablated mice: 2.9 per sheet (95% CI 1.4–6.0) and control mice 168 per sheet (95% CI 128–221)]. Hence, the clearance of the p53-mutant clones after UV ablation was virtually complete and permanent.

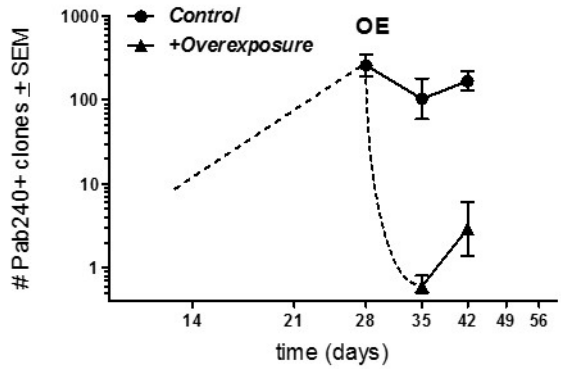


Figure 2.3: Median number of p53-mutant clones and 95% CI in UV-irradiated SKH-1 mice (*n* = 6 per point), clones detected immunohistochemically with anti-mutated p53 antibody (Pab240). One MED (500 J/m^2 UV)/day was given to all mice until day 28. At the 29th day, the test group (triangle) received five aMEDs (10 kJ/m^2), whereas the control group (circles) received another one MED (500 J/m^2). After a recovery period of 1 week, the daily irradiations were resumed at day 36 in both groups. Dashed lines were included to guide the eye, and the one up to 28 days is based on earlier experiments [24]. Highly-significant differences between control and +UV-overexposure group were found at both 35 and 42 days ($p < 0.0005$).

2.3.4. Ablation of basal layer 'resets' UV carcinogenesis

To assess the effect of the ablation of the interfollicular epidermal basal layer, including p53 clones, we performed a UV carcinogenesis experiment by resuming daily sub-sunburn exposures (500 J/m^2 UV/day) 1 week after UV ablation in one group of 26 hairless SKH-1 mice and in a corresponding control group that had not been overexposed (one mouse in the latter group died from unknown cause). The vast majority of the tumors consisted of SCCs and precursor lesions. Very few (<5%) exophytically growing papillomas [30] were observed, which were not included in the analysis. UV carcinogenesis in the UV-ablated group was significantly delayed for all tumor sizes (P<0.0001, Mantel Cox test) (Figure 2.4). The delay was 19, 24, 33 and 31 days for tumors ≥0.5, ≥1, ≥2 and ≥4 mm in diameter, respectively, with an average of 27 (SEM 3) days. Blinded histopathologic analysis showed similar tumor types in both groups, 80% SCCs and 20% Bowenoid tumors, i.e. in situ SCC (samples of n=10). However, two of the eight SCCs from the ablated group showed sarcomatoid morphology with spindle-shaped cells, which lost p63, K5 (data not shown) and pan-keratin staining (Supplementary Figure S2.8).

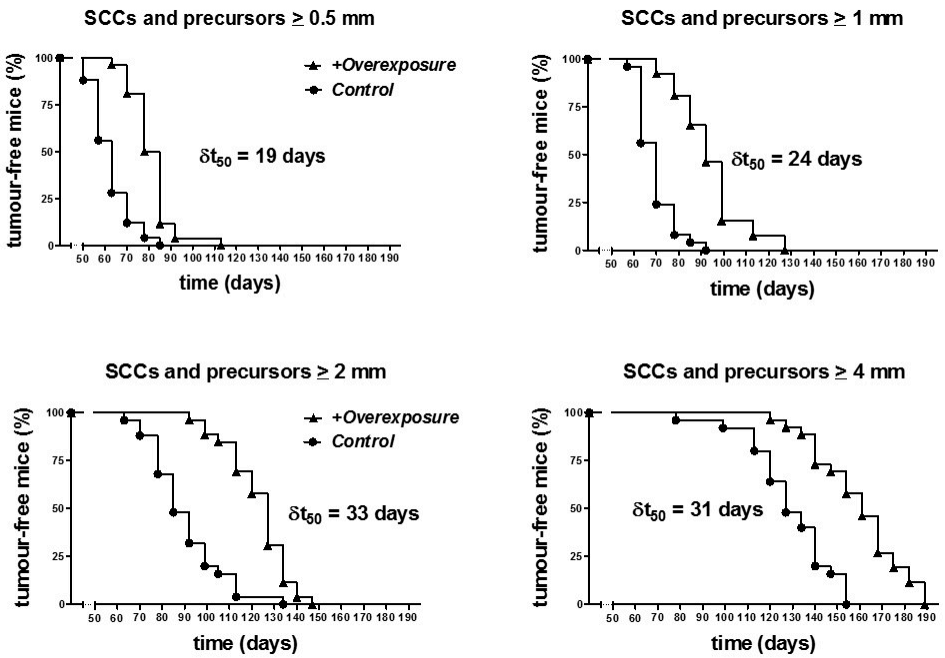


Figure 2.4: Kaplan Meier plots of UV-induced carcinogenesis of successive tumor sizes. SKH1 mice of UV-overexposed group (triangles, *n* = 26) showed increased median tumor induction times ($t_{50}s$) compared with the control group (circles, *n* = 25), for all tumor sizes (*P* < 0.0001, Mantel Cox test). The differences in median tumor induction times ($\delta t_{50}s$) are stated in the successive graphs with an average of 27 (SEM 3) days delay in the overexposed group. The UV overexposure was applied on day 29.

2.4. Discussion

Since UV-induced apoptosis can be impaired after loss of functional p53 [10, 11], one might expect that p53-mutant clones would resist apoptosis after overexposure. However, we found apoptosis, marked by active caspase-3 expression, in the entire basal layer of the IFE laden with p53-mutant clones after strong UV overexposure. We did not see any areas devoid of active caspase-3 staining in the IFE. This indicated that p53-mutant clones were not resistant to apoptosis at the applied overexposure of 10 kJ/m^2 UV (five aMED). Wijnhoven et al. [11] reported impaired UV-induced apoptosis in heterozygous mutant *p53* mice but at the high UV dose we applied, all basal cells became apoptotic.

Apoptosis induced by UV overexposure in the skin of hairless mice was virtually completely restricted to the basal layer of the IFE and was accompanied by a complete loss of p63 protein expression at 24 h after UV ablation. This is in line with the observation that p63 down regulation allows apoptosis induction [28]. Double staining revealed an outward moving active caspase-3-positive and p63-negative apoptotic front of cells and cell remnants at 24 and 48 h, whereas a new layer of p63-positive and active caspase-3-negative cells developed underneath; at these time points, no double-positive cells were found. At 6 h, 96% of the basal cells were either caspase$^+$ or p63$^+$; only a low percentage of 4% double-positive cells was found. In the double-positive cells, p63 might have been already degraded with its remnants still detectable by antibody staining. The reason that p63 expression persisted in hair follicles could be that the UV-B radiation happened to be attenuated below a critical level at these depths or it might be that the follicles were intrinsically less sensitive, perhaps maintaining a pool of (stem) cells for rapid repopulation of the damaged IFE (the latter premise appears to be less likely as a loss of Bcl-2-positive cells after UV overexposure included the hair follicles, only the bulge area and deeper down remained positive; data not shown).

Interestingly, the abundance of sunburn cells in the layers overlying the (active caspase-3 positive) apoptotic basal layer did not show any sign of caspase-3-driven apoptosis or any disassembly and remnants of cells like in the basal layer (Supplementary Figure S2.3). These sunburn cells appear to loose keratins (Supplementary Figures S2.3 and S2.4), become dyskeratotic and their cytoplasm becomes eosinophilic, like the stratum corneum (haematoxylin and eosin staining in Supplementary Figure S2.3) [31]. Hence, these sunburn cells do not appear to be truly apoptotic (although they meet some of the morphological criteria) but they seem to be forced into a premature state of terminal differentiation to speed up their removal from the ranks of functional epidermal cells. Genuine caspase-3-driven apoptosis appears to be limited to cycling cells (in Ki67-positive layers; Supplementary Figure S2.3).

During normal homeostasis, interfollicular stem cells renew the IFE, whereas in wound healing, hair follicle stem cells repopulate the IFE [32]. Our BrdU pulse-chase experiment

showed rapid replacement of the apoptotic IFE from hair follicle keratinocytes with increased proliferation at 24-48 h after UV overexposure. Epidermal repopulation after UV ablation is thus similar to epidermal repopulation from hair follicle cells after abrasion wounding. BrdU labelling was absent in the entire IFE at 5-6 h, which was the prelude to a complete apoptotic response in which neither normal interfollicular epidermal cells nor p53-mutant clone cells survived the applied UV overexposure.

A review report on hairless SKH-1 mice suggested that the rudimentary hair follicles and dermal cysts were not connected [33]. However, our p63 staining revealed narrow channels of keratinocytes connecting dermal cysts and rudimentary hair follicles (Supplementary Figure S2.6). An occasional hair follicle in anagen phase in skin sections from SHK1 mice illustrated that the depth of the cysts in the dermis is indeed comparable with that of the bulbs of normal hair follicles. This revealed a more complete image of the physiology of the remnants of hair follicles in hairless mice; these follicles are seemingly 'frozen' in catagen with bulbs growing into cysts. In line with our findings, an earlier report [34] identified dermal keratinizing cysts as remnants of the external root sheath in which proliferation takes place during UV irradiation. We found that proliferation in the dermal cysts remained unaffected upon UV overexposure.

After UV overexposure, we thus observed two important mechanisms working together to suppress mutagenesis: (i) apoptosis of the most exposed and damaged germinative layer located in the basal layer of the IFE and (ii) replacement of this germinative layer from deep-seated (stem) cells that were more shielded from UV exposure and therefore less damaged. Overly damaged non-proliferating differentiated cells apparently became sunburn cells that showed features of termination in a stage of premature cornification.

The complete elimination of p53 clones at 7 days after UV overexposure confirms the lack of apoptotic-resistant (active caspase-3 negative) cell clusters. This is also in line with the lack of BrdU-positive and the lack of p63-positive cell clusters in the IFE at 24 h after UV overexposure. Apparently, all interfollicular epidermal basal (stem) cells, including the p53-mutant clones, became apoptotic at the high UV dose that we applied.

Our finding that the newly formed epidermis was devoid of p53-mutant clones also indicated that UV-induced p53 clones were not derived from hair follicles. Because, if they were, p53-mutant cells would have proliferated with the hair follicle cells and would have quickly formed new p53 clones in the superficial epidermis.

The fact that the applied UV ablation delays UV carcinogenesis by a period of time (27 (SEM 3) days) comparable with that of daily exposure (28 days) before UV ablation indicates that the onset of tumors was completely nullified by the UV ablation. This 'resetting' of UV carcinogenesis was preceded by elimination of p53-mutant clones.

As in earlier experiments, we found in the present experiment that p53 clones are predictive of tumor risk and may therefore serve as markers of risk of SCCs [35, 36].

A consequence of the fact that ablation of interfollicular epidermal (basal) cells (including p53-clone cells) resulted in a reset of UV carcinogenesis indicates that the origin of UV-induced SCCs is in the IFE and not in the hair follicles (with the possible exception of the shallow outer rim of the infundibulum). The reason that in earlier reported laser-ablation experiments on hairless SKH-1 mice [15, 37], no delay in UV carcinogenesis was found, is most likely attributable to a laser dose that was tuned to naive mice, while the epidermis thickens after weeks of UV exposure [38]. The applied laser dose was probably not high enough to assure ablation of the deeper located cells of the basal layer in chronically exposed skin (this was apparently not checked). We found that after 4 weeks of daily UV exposure, four MED for a naive skin was not enough to induce a clear sunburn reaction or apoptosis in the UV-adapted skin. We raised the UV dose five times more to induce similar levels of apoptosis as in a naive skin after four to six MEDs. Our data are also in contrast with earlier experiments where skin abrasion showed that SCCs induced by two-stage chemical carcinogenesis originated from hair follicles [39]. This may be attributable to storage of solvent in the follicle and possible preferential exposure [40].

Although the interfollicular ablation by a single overexposure suppresses UV carcinogenesis and gives a good cosmetic result, 20% of the SCCs in the ablated group showed features of the more aggressive spindle cell SCCs (Supplementary Figure S2.8 indicating epidermal–mesynchemal transition). Moreover, episodes of severe sunburn are known to increase the risk of BCCs and melanoma in humans [41, 42]. Therefore, it is rather unlikely that genotoxic ablation can be used as a therapeutic treatment. This investigation indicates however that treatments for SCC prevention should be targeted at the IFE rather than the hair follicles.

In conclusion, UV overexposure in hairless mice induces caspase-3-driven apoptosis which is virtually completely restricted to the basal layer of the IFE (not including sunburn cells in overlying spinous layers). BrdU pulse-chase experiments revealed that after this ablation, the IFE is repopulated by outgrowth of hair follicle keratinocytes. Selective UV-induced ablation of the IFE eliminates UV-induced p53-mutant clones and resets UV carcinogenesis. This implies that UV-induced SCCs in SKH-1 mice originate from the IFE.

Acknowledgements

We thank Daniela Salvatori for histopathological analyses of the skin tumors and Peter de Jong for animal care. One of the reviewers is thanked for the query about haematoxylin and eosin stains to verify in detail the ablative effect on the basal layer, which led us to identify the sunburn cells in overlying layers devoid of caspase-3-activated apoptosis.

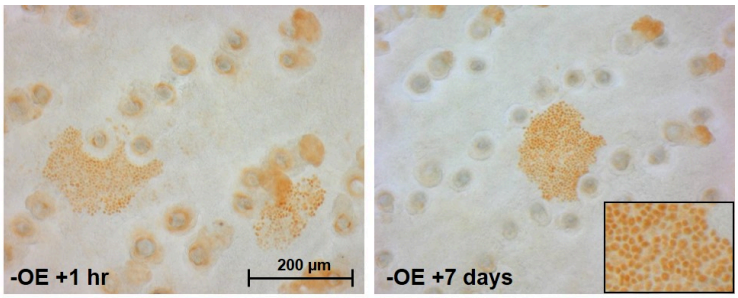
References

1. de Vries E, van de Poll-Franse LV, Louwman WJ, de Gruijl FR and Coebergh JW. Predictions of skin cancer incidence in the Netherlands up to 2015. Br J Dermatol. 2005; 152(3):481-488.
2. Madan V, Lear JT and Szeimies RM. Non-melanoma skin cancer. Lancet. 2010; 375(9715):673-685.
3. Brash DE, Rudolph JA, Simon JA, Lin A, McKenna GJ, Baden HP, Halperin AJ and Ponten J. A role for sunlight in skin cancer: UV-induced p53 mutations in squamous cell carcinoma. Proceedings of the National Academy of Sciences of the United States of America. 1991; 88(22):10124-10128.
4. Bolshakov S, Walker CM, Strom SS, Selvan MS, Clayman GL, El-Naggar A, Lippman SM, Kripke ML and Ananthaswamy HN. p53 mutations in human aggressive and nonaggressive basal and squamous cell carcinomas. Clin Cancer Res. 2003; 9(1):228-234.
5. Backvall H, Asplund A, Gustafsson A, Sivertsson A, Lundeberg J and Ponten F. Genetic tumor archeology: microdissection and genetic heterogeneity in squamous and basal cell carcinoma. Mutat Res. 2005; 571(1-2):65-79.
6. Backvall H, Stromberg S, Gustafsson A, Asplund A, Sivertsson A, Lundeberg J and Ponten F. Mutation spectra of epidermal p53 clones adjacent to basal cell carcinoma and squamous cell carcinoma. Exp Dermatol. 2004; 13(10):643-650.
7. Rebel H, Kram N, Westerman A, Banus S, van Kranen HJ and de Gruijl FR. Relationship between UV-induced mutant p53 patches and skin tumours, analysed by mutation spectra and by induction kinetics in various DNA-repair-deficient mice. Carcinogenesis. 2005; 26(12):2123-2130.
8. Kramata P, Lu YP, Lou YR, Singh RN, Kwon SM and Conney AH. Patches of mutant p53-immunoreactive epidermal cells induced by chronic UVB Irradiation harbor the same p53 mutations as squamous cell carcinomas in the skin of hairless SKH-1 mice. Cancer Res. 2005; 65(9):3577-3585.
9. Brash DE. Roles of the transcription factor p53 in keratinocyte carcinomas. Br J Dermatol. 2006; 154 Suppl 1:8-10.
10. Ziegler A, Jonason AS, Leffell DJ, Simon JA, Sharma HW, Kimmelman J, Remington L, Jacks T and Brash DE. Sunburn and p53 in the onset of skin cancer. Nature. 1994; 372(6508):773-776.
11. Wijnhoven SW, Speksnijder EN, Liu X, Zwart E, vanOostrom CT, Beems RB, Hoogervorst EM, Schaap MM, Attardi LD, Jacks T, van Steeg H, Jonkers J and de Vries A. Dominant-negative but not gain-of-function effects of a p53.R270H mutation in mouse epithelium tissue after DNA damage. Cancer Res. 2007; 67(10):4648-4656.
12. van Schanke A, Jongsma MJ, Bisschop R, van Venrooij GM, Rebel H and de Gruijl FR. Single UVB overexposure stimulates melanocyte proliferation in murine skin, in contrast to fractionated or UVA-1 exposure. J Invest Dermatol. 2005; 124(1):241-247.
13. Kolgen W, Van Weelden H, Den Hengst S, Guikers KL, Kiekens RC, Knol EF, Bruijnzeel-Koomen CA, Van Vloten WA and de Gruijl FR. CD11b+ cells and ultraviolet-B-resistant CD1a+ cells in skin of patients with polymorphous light eruption. J Invest Dermatol. 1999; 113(1):4-10.
14. Zhang W, Hanks AN, Boucher K, Florell SR, Allen SM, Alexander A, Brash DE and Grossman D. UVB-induced apoptosis drives clonal expansion during skin tumor development. Carcinogenesis. 2005; 26(1):249-257.
15. Faurschou A, Haedersdal M, Poulsen T and Wulf HC. Squamous cell carcinoma induced by ultraviolet radiation originates from cells of the hair follicle in mice. Exp Dermatol. 2007; 16(6):485-489.
16. De Gruijl FR and Rebel H. Early Events in UV Carcinogenesis—DNA Damage, Target Cells and Mutant p53 Foci†. Photochem Photobiol. 2008; 84(2):382-387.

17. Haegebarth A and Clevers H. Wnt signaling, lgr5, and stem cells in the intestine and skin. Am J Pathol. 2009; 174(3):715-721.
18. Kruger K, Blume-Peytavi U and Orfanos CE. Basal cell carcinoma possibly originates from the outer root sheath and/or the bulge region of the vellus hair follicle. Arch Dermatol Res. 1999; 291(5):253-259.
19. Wang GY, Wang J, Mancianti ML and Epstein EH, Jr. Basal cell carcinomas arise from hair follicle stem cells in Ptch1(+/-) mice. Cancer Cell. 2011; 19(1):114-124.
20. Stout GJ, Westdijk D, Calkhoven DM, Pijper O, Backendorf CM, Willemze R, Mullenders LH and de Gruijl FR. Epidermal transit of replication-arrested, undifferentiated keratinocytes in UV-exposed XPC mice: an alternative to in situ apoptosis. Proceedings of the National Academy of Sciences of the United States of America. 2005; 102(52):18980-18985.
21. Berg RJ, de Vries A, van Steeg H and de Gruijl FR. Relative susceptibilities of XPA knockout mice and their heterozygous and wild-type littermates to UVB-induced skin cancer. Cancer Res. 1997; 57(4):581-584.
22. Schutte B, Reynders MM, Bosman FT and Blijham GH. Effect of tissue fixation on anti-bromodeoxyuridine immunohistochemistry. J Histochem Cytochem. 1987; 35(11):1343-1345.
23. Berg RJ, van Kranen HJ, Rebel HG, de Vries A, van Vloten WA, Van Kreijl CF, van der Leun JC and de Gruijl FR. Early p53 alterations in mouse skin carcinogenesis by UVB radiation: immunohistochemical detection of mutant p53 protein in clusters of preneoplastic epidermal cells. Proc Natl Acad Sci U S A. 1996; 93(1):274-278.
24. Rebel H, Mosnier LO, Berg RJW, Vries AW-d, van Steeg H, van Kranen HJ and de Gruijl FR. Early p53-positive Foci as Indicators of Tumor Risk in Ultraviolet-exposed Hairless Mice: Kinetics of Induction, Effects of DNA Repair Deficiency, and p53 Heterozygosity. Cancer Res. 2001; 61(3):977-983.
25. Thornberry NA. Caspases: key mediators of apoptosis. Chem Biol. 1998; 5(5):R97-103.
26. Koster MI, Kim S, Mills AA, DeMayo FJ and Roop DR. p63 is the molecular switch for initiation of an epithelial stratification program. Genes Dev. 2004; 18(2):126-131.
27. Yang A, Schweitzer R, Sun D, Kaghad M, Walker N, Bronson RT, Tabin C, Sharpe A, Caput D, Crum C and McKeon F. p63 is essential for regenerative proliferation in limb, craniofacial and epithelial development. Nature. 1999; 398(6729):714-718.
28. Borrelli S, Candi E, Alotto D, Castagnoli C, Melino G, Vigano MA and Mantovani R. p63 regulates the caspase-8-FLIP apoptotic pathway in epidermis. Cell Death Differ. 2009; 16(2):253-263.
29. Senoo M, Pinto F, Crum CP and McKeon F. p63 Is essential for the proliferative potential of stem cells in stratified epithelia. Cell. 2007; 129(3):523-536.
30. de Laat A, van der Leun JC and de Gruijl FR. Carcinogenesis induced by UVA (365-nm) radiation: the dose-time dependence of tumor formation in hairless mice. Carcinogenesis. 1997; 18(5):1013-1020.
31. Olson RL, Gaylor J and Everett MA. Ultraviolet-induced individual cell keratinization. J Cutan Pathol. 1974; 1(3):120-125.
32. Ito M, Liu Y, Yang Z, Nguyen J, Liang F, Morris RJ and Cotsarelis G. Stem cells in the hair follicle bulge contribute to wound repair but not to homeostasis of the epidermis. Nat Med. 2005; 11(12):1351-1354.
33. Benavides F, Oberyszyn TM, VanBuskirk AM, Reeve VE and Kusewitt DF. The hairless mouse in skin research. J Dermatol Sci. 2009; 53(1):10-18.
34. Kligman LH, Akin FJ and Kligman AM. Prevention of ultraviolet damage to the dermis of hairless mice by sunscreens. J Invest Dermatol. 1982; 78(2):181-189.
35. Jans J, Schul W, Sert YG, Rijksen Y, Rebel H, Eker AP, Nakajima S, van Steeg H, de Gruijl FR, Yasui A, Hoeijmakers JH and van der Horst GT. Powerful skin cancer protection by a CPD-photolyase transgene. Curr Biol. 2005; 15(2):105-115.

36. Cozzi SJ, Ogbourne SM, James C, Rebel HG, de Gruijl FR, Ferguson B, Gardner J, Lee TT, Larcher T and Suhrbier A. Ingenol mebutate field-directed treatment of UVB-damaged skin reduces lesion formation and removes mutant p53 patches. J Invest Dermatol. 2012; 132(4):1263-1271.
37. Hedelund L, Lerche C, Wulf HC and Haedersdal M. Carcinogenesis related to intense pulsed light and UV exposure: an experimental animal study. Lasers Med Sci. 2006; 21(4):198-201.
38. de Gruijl FR and Berg RJ. In situ molecular dosimetry and tumor risk: UV-induced DNA damage and tumor latency time. Photochem Photobiol. 1998; 68(4):555-560.
39. Morris RJ, Tryson KA and Wu KQ. Evidence that the epidermal targets of carcinogen action are found in the interfollicular epidermis of infundibulum as well as in the hair follicles. Cancer Res. 2000; 60(2):226-229.
40. Lademann J, Knorr F, Richter H, Blume-Peytavi U, Vogt A, Antoniou C, Sterry W and Patzelt A. Hair follicles--an efficient storage and penetration pathway for topically applied substances. Summary of recent results obtained at the Center of Experimental and Applied Cutaneous Physiology, Charite -Universitatsmedizin Berlin, Germany. Skin Pharmacol Physiol. 2008; 21(3):150-155.
41. Dessinioti C, Tzannis K, Sypsa V, Nikolaou V, Kypreou K, Antoniou C, Katsambas A and Stratigos AJ. Epidemiologic risk factors of basal cell carcinoma development and age at onset in a Southern European population from Greece. Exp Dermatol. 2011; 20(8):622-626.
42. Newton-Bishop JA, Chang YM, Elliott F, Chan M, Leake S, Karpavicius B, Haynes S, Fitzgibbon E, Kukalizch K, Randerson-Moor J, Elder DE, Bishop DT and Barrett JH. Relationship between sun exposure and melanoma risk for tumours in different body sites in a large case-control study in a temperate climate. Eur J Cancer. 2011; 47(5):732-741.

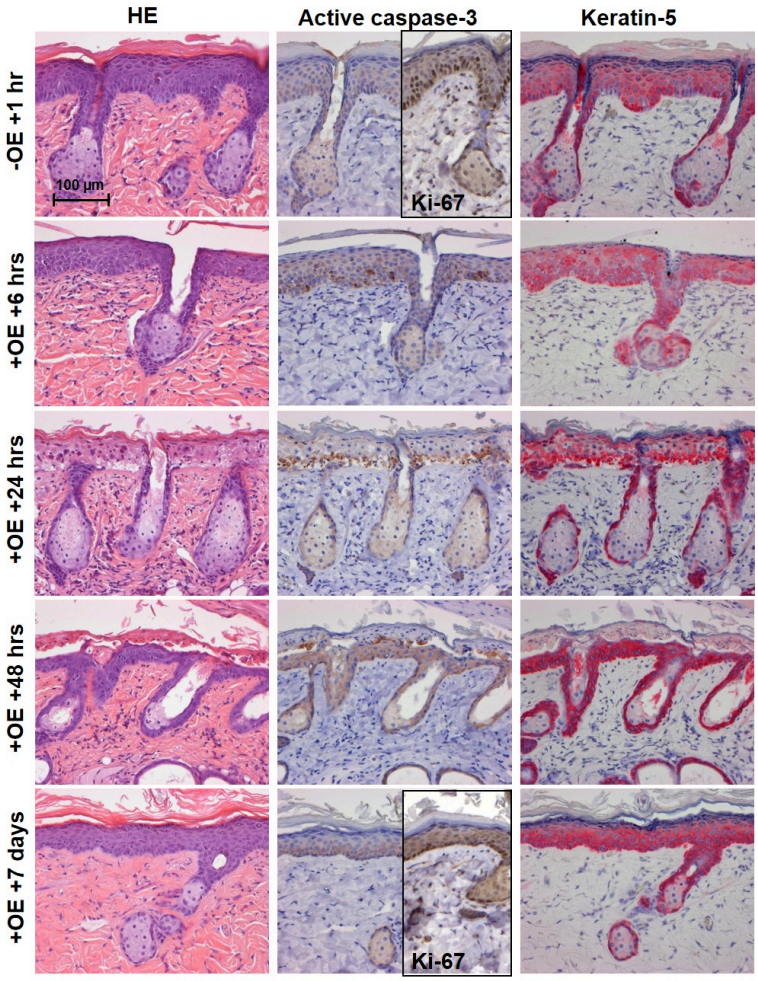
Supplementary Material



Supplementary Figure S2.1: Pab240-positive immunohistochemical stained p53-mutant clones in epidermal sheets of hairless SKH-1 mice that received 1 MED UV/day for 28 days. Left panel: 2 p53-mutant clones in epidermal sheet of control group without UV overexposure at day 28. Right panel: 1 p53-mutant clone in control group without UV overexposure + 7 days without UV. The insert shows specific nuclear staining at higher magnification. Note that the background in hair follicles is not nuclear specific. 10x objective.



Supplementary Figure S2.2: SKH-1 mice had recovered almost completely from sunburn reaction (erythema/edema) and scaling 1 week after UV overexposure. Note variable erythema at the edges of the UV-exposed skin areas where the overexposure was milder and the UV-adapted epidermis was presumably not fully renewed, leaving a longer lasting inflammatory reaction.



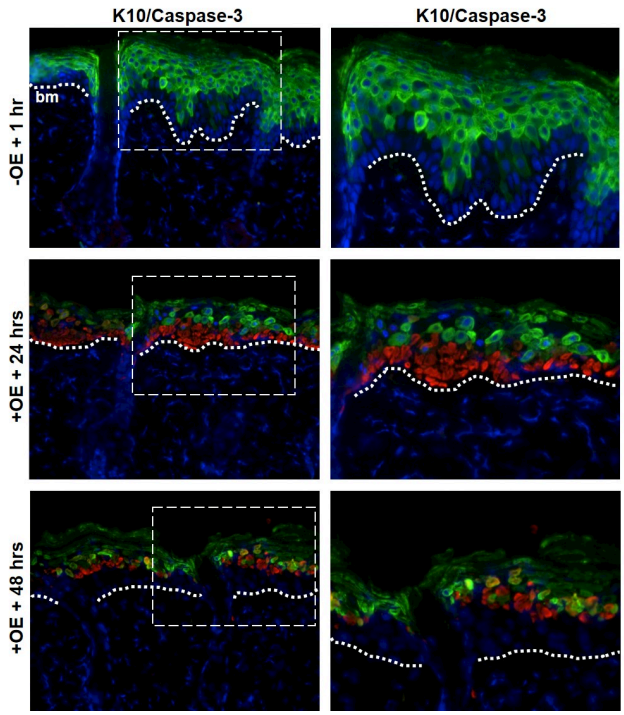
Supplementary Figure S2.3: Immunohistochemistry on sequential dorsal skin sections of mice that received 1 MED UV/day for 28 days, without a subsequent UV overexposure (-OE) or with a subsequent single UV overexposure (+OE) of 10 kJ/m^2 (5 aMED). Skin biopsies were harvested at several time points after overexposure as indicated on the left, and stained for H&E (Haematoxylin & Eosin), anti-active caspase-3 and keratin 5 (K5) shown in the respective columns of panels (annotated at the top). Ki67-stained inserts in top and bottom panels of middle column.

The H&E series of panels in the left column clearly shows increased eosin staining in the epidermis at 24 hrs after UV overexposure, demonstrating that virtually all cells in the layers above the apoptotic basal layer (see staining for active caspase-3 in the neighbouring panel in the middle column) have become "sunburn cells" (with compacted nuclei). As these layers with sunburn cells show no activation of caspase-3 or any loss/vacancies of cells (like in the basal layer) these cells do not appear to be in apoptosis. However, their dyskeratosis reflected by the loss of cytokeratin staining (+OE at 24 hrs in the right column) and strong eosin staining, like in the stratum corneum, indicates a premature stage of terminal differentiation/cornification.

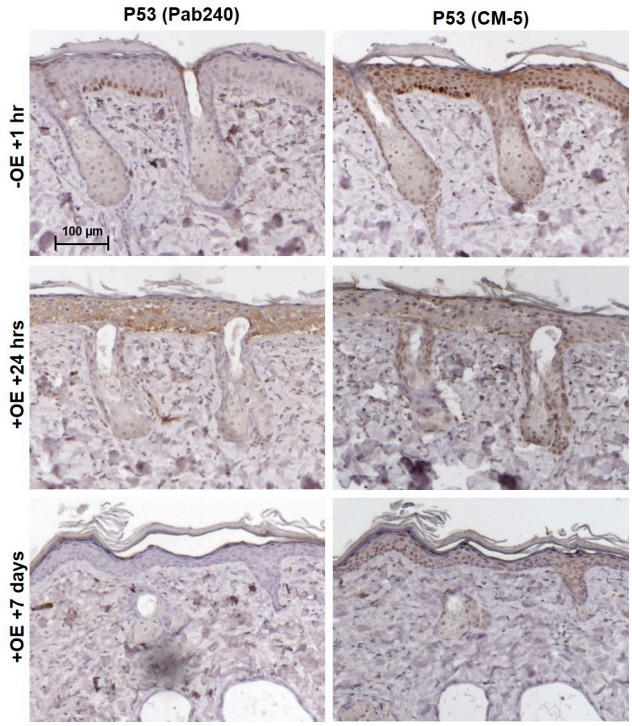
The middle column shows the time sequence of cells becoming positive for active caspase-3, and in the top and bottom panels inserts with Ki67 staining are included to show which layers contain cycling

cells. Ki67 staining is normally limited to the basal layer, as 7 days after overexposure, but also shows up in the cell layer directly overlying the basal layer in the chronically exposed epidermis (top panel). The caspase-3-driven apoptosis appears to be limited to the layers with cycling cells, mainly the basal layer. Upon digitally enlarging the +OE panels at 24 h, the reader will see remnant cell bodies in the apoptotic layer which probably maintain a certain level of adherence (no blister formation). But at 48 hrs the epidermis appears to be fragile at the level of the outward moving "apoptotic front", judged by the cleft introduced by cutting the sections (again no apparent blister formation in the mice at that time, or any other time after overexposure).

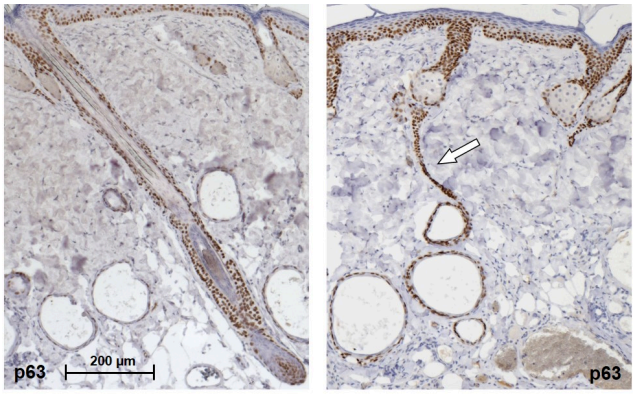
The K5 staining (right column) was performed on paraffin sections with the anti-cytokeratine-5 antibody (Covance, PRB-160P) which is suitable for both humans and mice. The antibody should label the proliferative basal cells in a naive epidermis. Although the antibody indeed shows the strongest staining in the basal layers of epidermis, the layers higher up are also positive. This may either be a feature of the chronically exposed epidermis or it may be due to a possible cross-reactivity with an other type II cytokeratin (e.g. K6, not present in unirradiated skin). Note that the dermis is completely negative, i.e. no aspecific staining outside the epidermis. Also note that the "K5"-staining in the differentiated layers (see K10 staining in Supplementary Figure S2.4) of the epidermis becomes weaker and more mottled at 24 hrs after UV exposure, indicating a loss of keratin in sunburn cells; the keratin expression in these layers is virtually lost at 48 hrs.



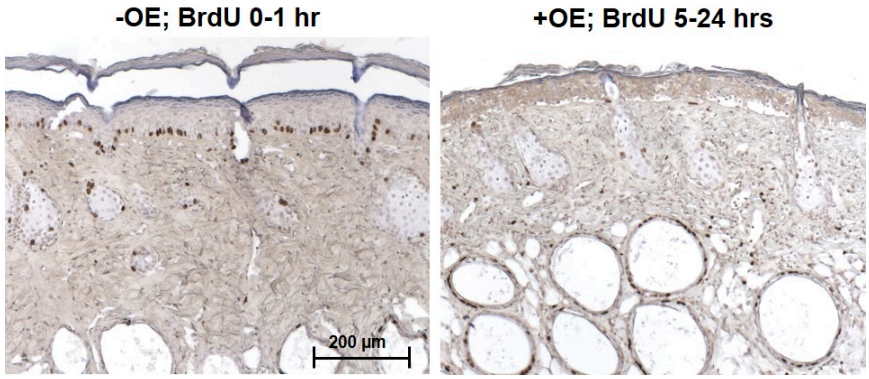
Supplementary Figure S2.4: Double staining of K10 (green fluorescence, primary antibody clone DE-K10, Thermo Scientific, Fremont, USA) and active caspase-3 (red fluorescence) without overexposure (-OE 1 hr) and at 24 and 48 hrs after overexposure (+OE 24 hrs and 48 hrs, resp.). No active caspase-3 in non-overexposed skin, and no double stained cells at 24 hrs after overexposure were observed, i.e. no caspase-3-driven apoptosis was found in differentiated $K10^+$ cells. K10 expression has apparently faded in many suprabasal cells after overexposure.



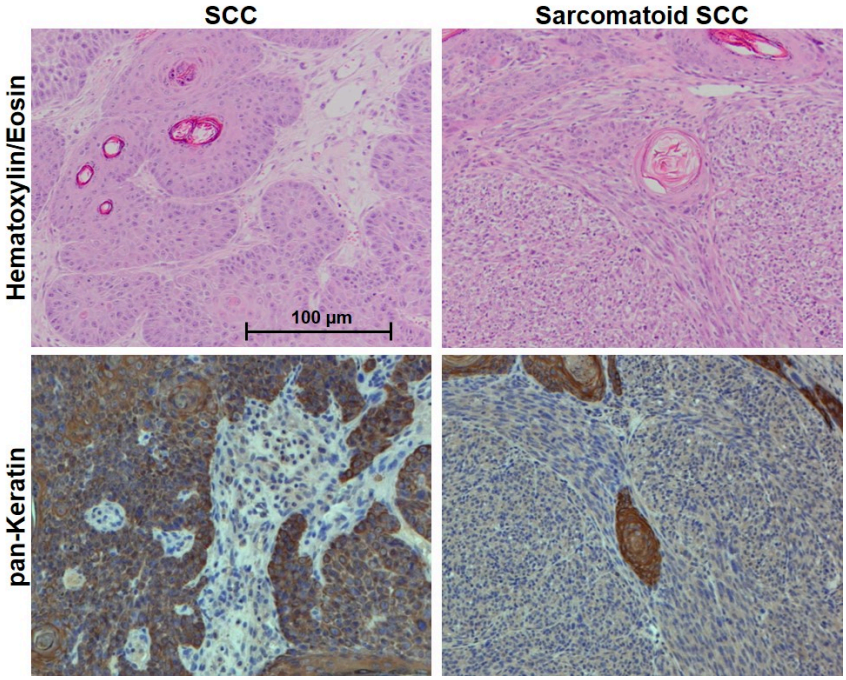
Supplementary Figure S2.5: P53 immunohistochemistry on dorsal sequential skin sections. Left panels: p53-mutant staining with Pab240 antibody. Right panels: wild-type & mutant-p53 staining with CM-5. Top row: mice that received 1 MED UV/day for 28 days (note a p53-mutant clone in between the two follicles). Mid and bottom row: mice at 24 hrs and 7 days after UV overexposure (note aspecific PAb240 staining at 24 hrs).



Supplementary Figure S2.6: Hair follicles in hairless mouse skin stained with anti-p63. Left panel: An occasional normal hair follicle in anagen phase in hairless SKH-1 mouse skin. Right panel: One rudimentary hair follicle shows a connective channel (arrow) from the bulge (stained cells just below the sebaceous glands containing large cells with p63-negative nuclei and clear cytoplasm) to a dermal cyst.



Supplementary Figure S2.7: Bromodeoxyuridine staining on dorsal skin sections of mice that received 1 MED UV/day for 28 days. View included deep-seated cysts. Left panel: BrdU labeling 0 - 1 hr after the last sub-sunburn irradiation. Right panel: BrdU injection at 5 hrs and mouse sacrificed at 24 hrs after UV overexposure. (10x objective)



Supplementary Figure S2.8: Haematoxylin-eosin and pan-keratin staining of squamous cell carcinomas (SCCs). Upper panels: H&E staining. Bottom panels: pan-keratin staining (antibody clone AE1/AE3, Abcam, Ab80826). Left column: SCC from control group without UV overexposure. Right column: sarcomatoid compartment in SCC from overexposed mouse (20x objective).

Chapter 3

Fractionation of a tumor-initiating UV dose introduces DNA damage-retaining cells in hairless mouse skin and renders subsequent TPA-promoted tumors non-regressing

G.C. van de Glind, H.G. Rebel, M.J. van Kempen, C.P. Tensen, F.R. de Gruijl

Oncotarget. 2016 Feb 16;7(7):8067-77

Abstract

Sunburns and especially sub-sunburn chronic UV exposure are associated with increased risk of squamous cell carcinomas (SCCs). Here we focus on a possible difference in tumor initiation from a single severe-sunburn dose (on day 1, 21 hairless mice) and from an equal dose fractionated into very low sub-sunburn doses not causing any (growth-promoting) epidermal hyperplasia (40 days daily exposure, n=20). From day 47 all mice received 12-O-Tetradecanoylphorbol-13-acetate (TPA) applications (2x/wk) for 20 weeks to promote tumor development within the lifetime of the animals. After the sub-sunburn regimen sparse DNA damage-retaining basal cells (quiescent stem cells, QSCs) remained in the non-hyperplastic epidermis. These cells were forced to divide by TPA. After discontinuation of TPA tumors regressed and disappeared in the 'sunburn group' but persisted and grew in the 'sub-sunburn group' (0.06 vs 2.50 SCCs and precursors ≥ 4 mm/mouse after 280 days, p=0.03). As the tumors carried no mutations in *p53*, *H/K/N-Ras* and *Notch1/2,* these 'usual suspects' were not involved in the UV-driven tumor initiation. Although we could not selectively eliminate QSCs (unknown phenotype) to establish causality, our data suggest that forcing specifically DNA damage-retaining QSCs to divide – with high mutagenic risk - gives rise to persisting (mainly 'in situ') skin carcinomas.

3.1. Introduction

The incidence of skin carcinomas has strongly increased since the 1970-s by an average of about 4% per year in NW Europe, to a staggering 100 to 200 new cases per 10^5 persons per year, despite the temperate climate [1-3]. UV radiation plays an important role in the etiology of skin carcinomas, both basal cell carcinomas (BCCs) and squamous cell carcinomas (SCCs) [4, 5]. Kennedy et al. [6] showed that sunburns as well as chronic sun exposure are associated with an increased risk of developing SCCs.

UV radiation preferentially damages sites of neighboring pyrimidine bases in a DNA strand, forming dimers between these bases: either cyclobutane pyrimidine dimers (CPDs) or 6-4 photoproducts (6-4PPs) [7, 8]. These photo lesions cause a distortion of the DNA helix, rendering DNA polymerase unable to read the DNA template, which may result in cytosine (C) → thymidine (T) at sites of adjacent pyrimidines and CC→ TT transitions. These specific transitions are considered UV signature mutations [9, 10]. In SCCs and BCCs the *P53* tumor suppressor genes bear these UV signature mutations [10, 11]. A suitable experimental model for SCCs has been established by chronic (daily) exposure of hairless mice to UV radiation [12]; here the *p53* gene is targeted leading to the UV signature mutations [13], in line with human SCCs. In contrast to two-stage chemical skin carcinogenesis [14], the UV tumors bear no *H-Ras* mutations [15]. Our group found that microscopic foci with overexpression of p53 protein in mutant conformation (detected with antibody PAb240) were already present in UV-exposed mice long before the tumors appeared [16-18]. Such 'p53 patches' have also been found in sun-exposed human skin, which after micro-dissection were found to harbor UV-signature mutations in *P53* genes [19, 20].

The essential cancer traits appear to develop in stages in the neoplastic cell [21], which takes time: cancer is therefore predominantly a disease of the elderly. Hence, the targeted cell in carcinogenesis needs to reside in the body for a long time in order to acquire a series of alterations (gene mutations) resulting in malignant growth. Furthermore, the cell probably needs to divide for fixation of mutations (most likely to arise in replication of damaged DNA) and to pass on the mutations to daughter cells. These requirements of long term residence combined with cell division point at stem cells as likely targeted candidates [22, 23].

Mitchell et al. [24] found that CPDs accumulated in some cells located in the basal layer of the epidermis in the course of chronic low level UV radiation and these cells retained CPDs long after discontinuation of UV exposures (> 50 days). Such cells were found to occur in human skin too [25]. If UV exposure caused significant epidermal hyperplasia (e.g. after a sunburn dose), the CPD-retaining epidermal cells were no longer observed [25]. Our group confirmed that at low level chronic UV exposure (1/7 of the threshold dose for a sunburn/day for 40 days) in absence of hyperplasia CPDs accumulated in long-residing non-dividing skin cells, i.e. in some basal cells and in fibroblasts in the upper dermis. And we

went on to show that persistent quiescent (BrdU-retaining) epidermal stem cells in the basal layer accumulated and retained UV-induced CPDs while neighboring cells did not (because of cell division and epidermal turnover) [26]. The CPD-retaining basal cells (CRBCs) were found to be repair proficient, since 6-4PPs did not accumulate [26]. CRBCs could be forced to proliferate by application of 12-*O*-Tetradecanoylphorbol-13-acetate (TPA) while the CPD-retaining fibroblasts showed no apparent reaction [25, 27]. With repeated TPA applications the accumulated DNA damage in CRBCs was gradually dispersed over daughter cells, and the CRBCs disappeared.

As mentioned above, both sunburns and chronic (sub-sunburn) UV exposure play a role in SCC development in humans [6] but the life-long accumulated UV dose as from chronic (sub-sunburn) exposure appears to be the major exogenous risk factor [28]. Considering also that a severe sunburn exposure induces hyperplasia and no CRBCs (> 4 days after exposure [25]) whereas the same dose fractionated in daily exposures of 1/7 of the sunburn threshold dose does induce CRBC and no hyperplasia, we set out to investigate the effect of non-hyperplastigenic sub-sunburn dose fractionation on skin carcinogenesis. To this end, one group of hairless mice (sunburn group n=21) received a single severe sunburn dose on day 1 while another group (sub-sunburn group) received the same total dose in 40 daily fractions (each 1/7 of the sunburn threshold dose) to induce CPD-retaining cells. After one week pause both groups were subsequently treated with TPA for 20 weeks to raise skin tumors within the lifetime of the mice (either a single high UV exposure or tumor promotion alone does not give rise to tumors in hairless mice [29]; further information in Materials and Methods); the time line of the experimental protocol for both groups is given in Supplementary Figure S3.1.

The tumors were scrutinized for (dis-)similarities with tumors induced by two-stage chemocarcinogenesis (mostly papillomas with *H-Ras* mutations instead of SCCs) and skin carcinogenesis by chronic UV exposure (i.e. life-long daily sub-sunburn exposure resulting in SCCs and actinic keratosis as benign precursors, both types of lesions with UV-signature mutations in *p53)*.

3.2. Materials and methods

3.2.1. Mice

As legally required, the experiments were performed with the approval of the Leiden University Medical Centers' ethics committee for animal experiments (DEC10229) and executed according to EU regulations on animal experiments (Directive 2010/63/EU).

Male and female albino Crl:SKH1-HR hairless mice (breeding pairs from Charles River, Sulzfeld, Germany) entered the experiment at 6-9 weeks of age. The mice were kept individually in Macrolon type 1 cages with standard chow and tap water *ad libitum*, in a

room at 25 ±2^{o}C, 50% humidity and illuminated by yellow fluorescent tubes (no UV radiation) in a 12 h-on-12 h-off cycle.

3.2.2. UV radiation

For the fractionated UV dose we used the protocol used previously by our group [26, 27]; this regimen yielded CPD-retaining skin cells. In short, Philips TL-12/40W tubes were used (output of 54% in UV-B, 280-315 nm, and 46% in UV-A, 315-400 nm). The minimal edema/erythemal dose (MED) was determined to be 500 J/m^2 UV for SKH-1 hairless mice under these lamps. The sub-sunburn group (n=20) received 40 days 70 J/m^2 UV a day which is equal to 0.14 MED/day. The sunburn group (n=21) received the same dose unfractionated in a single exposure: 2.8 kJ/m^2 = 5.6 MED at day 1, a just tolerable dose without wounding the skin. Based on an extrapolation by using an earlier quantitative dose-response model of ours [30] we calculated that virtually no tumors are to be expected from such an initial total dose alone (0.006 tumors > 2 mm per mouse after 2 years; this model makes no distinction between delivering the dose in a single day or 40 days). In earlier studies it was indeed found that a single high UV exposure alone did not give rise to tumors [29] unless the exposure was high enough to cause ulcerations where a small number of benign papillomas occurred preferentially at the edges of scars and a few rare carcinomas after the most extreme doses [31].

The UV overdose causes apoptosis in the basal layer [32; Chapter 2], transient strong epidermal hyperplasia with increased proliferation in the basal layer, which makes it impossible for CPD-retaining epidermal cells to persist [25, 27]. Additional mice in each group (n=4 at each time point) were used to assess CPDs and p53 mutant foci in the course of the TPA treatment (see below). See for a schematic overview of the experimental outline including the time points of UV exposure and of taking samples Supplementary Figure S3.1.

3.2.3. TPA application

From day 47 onward both groups of mice received TPA treatment twice a week for a period of 20 weeks to promote tumor development; the TPA also induced proliferation of quiescent stem cells. TPA (12-O-tetradecanoylphorbol-13-acetate, Sigma-Aldrich, Zwijndrecht, The Netherlands) was dissolved in acetone to a concentration of 100 µg/ml. Each time, about 100 µl TPA was applied to an area of dorsal skin of approximately 6 cm^2 using a fine brush. By 20 weeks of TPA treatment some mice had started to scratch and wound themselves. At that point, TPA treatment was discontinued for all mice. Scratching had occurred equally in both groups affecting a minor dorsal area (<10%) of skin in about 15% of the mice.

3.2.4. Tumor assessment and pathology

For the tumor assessment, mice were inspected every other week. Tumors were scored on maps to record location, size and tumor type. The first tumor was scored when present for at least two successive inspections. The experiment was terminated after 280 days, when most mice in the sub-sunburn group developed a substantial tumor load. Only mice free of tumors (> 4 mm) were maintained up to 350 days to complete Kaplan-Meier plots of tumor-free survival.

With macroscopic tumor assessment two types of tumors were distinguished: papillomas (exophytically growing tumors, protruding from the skin, often pedunculated) and "non-papilloma" tumors (endophytically growing tumors, gradually sloping at the edges) [33]. A small number of tumors arising in scratch-scarred skin was not taken into account and censored. Mice were taken out of the experiment either when in poor health (very rarely) or their tumor load was getting too high (> 0.5 cm^3; also rarely) or at the end of the experiment. Tumors were isolated from the sacrificed animals as described below. At the end of the experiment tumors ≥ 3 mm across were renumbered and a random selection without further information was submitted for pathology.

3.2.5. Tissue preparation

Mice were sacrificed using CO_2 asphyxiation. For anti-CPD and anti-p53 immunohistochemical stainings dorsal skin was obtained using a template. One piece of 5x16 mm was directly frozen in liquid nitrogen, another piece of 5x16 mm was fixed overnight in PBS-buffered 4% formaldehyde solution (Addedpharma, Oss, The Netherlands) and embedded in paraffin. Furthermore two skin samples of 7.5x32 mm were obtained to prepare epidermal sheets. To separate the dermis from the epidermis, one sample was treated with 100 µg/ml thermolysin (Sigma-Aldrich) in PBS containing 1 mM $CaCl_2$ (pH 7.8) and incubated overnight at 4°C. The other sample was treated with 20 mM EDTA (Baker, Deventer, The Netherlands) in PBS for 2 hrs at 37°C. After removal of the dermis, epidermal sheets were stored in 70% alcohol until further use. Tumors ≥ 3 mm were isolated and one half was frozen in liquid nitrogen and the other half was fixed in PBS-buffered 4% formaldehyde solution and embedded in paraffin.

3.2.6. Immunohistochemistry

For anti-CPD staining frozen tissue was embedded in Tissue-tek (Sakura Finetek Europe, Zoeterwoude, The Netherlands) and 6 µm thick cryosections were cut. The sections were fixed in acetone for 10 min, and boiled for 5 min in 10 mM citrate buffer (pH 6.0) for antigen retrieval. The sections were slowly cooled down to 37°C and blocked for 20 min with MilliQ water containing 50% methanol and 0.3% H_2O_2. Next, the samples were pre-incubated with 10% normal goat serum (NGS) (Dakocytomation, Heverlee, Belgium) in PBS with 1% BSA for

20 min followed by overnight incubation at 4°C with anti-cyclobutane pyrimidine dimer antibody (1:1000, Kamiya, Seattle, USA) in PBS containing 1% NGS and 1% BSA. Goat anti-mouse (IgG_1)-biotin (Southern Biotechnologies, Birmingham, USA) 1:200 in PBS 1% BSA was incubated 1hr at RT, followed by incubation with avidin-biotin peroxidase complex (Vectastain Elite, Burlingame, USA) for 45 min. AEC (3-Amino-9-ethylcarbazole Sigma-Aldrich) was used to make the CPDs visible. The sections were counterstained with hematoxyline (Klinipath, Duiven, The Netherlands) and mounted in Kaisers' Glycerin.
For p53 patch staining, epidermal sheets obtained using EDTA or thermolysin were used and stained as described previously [17, 34] with some minor modifications (see Supplementary Material).
The protocols for the anti-CM5 staining and the staining for Notch 1 intracellular domain (Nicd) on tumors are also described in the Supplementary Material.
Images were acquired with a Zeiss Axioplan 2 microscope using the 10x and 20x objectives, Axiocam camera and dedicated software. Final pictures were formatted in Adobe Photoshop CS6 or Adobe Illustrator CS6.

3.2.7. PCR and mutation analyses of tumors (p53, Ras and Notch)

Frozen tumors were incubated in RNAlater-ICE (Life Technologies Europe BV, Bleiswijk, The Netherlands) overnight at -20°C; tumor material was isolated the next day and used for DNA isolation. DNA was isolated using the DNeasy Blood and Tissue kit (Qiagen Benelux BV, Venlo, The Netherlands) according to manufactures protocol including RNase A treatment (Qiagen Benelux BV). The DNA concentration was measured using a Nanodrop and about 18 ng was used as template for PCR. The PCR was performed using the Platinum Taq DNA Polymerase kit (Life Technologies Europe BV) in a Bio-Rad C1000 touch thermo cycler (30 cycles three step protocol for *p53* and a touchdown PCR for *Ras* and *Notch*). Conserved domains in *p53*, exon 4-8 were inspected for mutations. Stretches around codons 12 and 61 in *H-, K-* and *N- Ras* were sequenced to check for oncogenic mutations. And for *Notch1* and *Notch2* we looked at the mouse equivalents of mutated exons in human [35, 36] (see also Supplementary Material).
In Supplementary Table S3.1 the sequences and annealing temperature of the primers for the different PCRs are given. PCR products were isolated using the Nucleospin Gel and PCR clean-up kit (Machery-Nagel, via Bioke, Leiden, The Netherlands). Products were either isolated directly from the PCR mixture or from a 1% agarose gel according to manufactures protocol (for *Notch* the isolation was done slightly differently, see Supplementary Material). The PCR products were sequenced in both directions using forward and reverse PCR primers in combination with Sanger sequencing (Macrogen, Amsterdam, The Netherlands). Sequences were analyzed using Mutation Surveyor V4.0.9 software (Softgenetics LCC, State College, USA) and sequences were double checked by visual inspection for mutations that

the program might have missed. Mutations were scored when present in both the forward and reverse sequence, and when the wild type signal was correspondingly reduced.

3.2.8. Data processing and statistical analyses

Tumor development was scored in two ways: a) tumor-free survival (Kaplan-Meier plots) and b) tumor yield (average number of tumors per survivor). Statistical significant differences in tumor-free survival were determined by the Mantel-Cox test (in Graphpad Prism 6). Differences in tumor yields were analyzed with univariate two way ANOVA (testing for group and gender differences) and with a t-test for independent samples, not assuming equal variances for final differences between groups (in IBM SPSS Statistics 20). Statistical significance was set at $p \leq 0.05$. Means were given with standard error of the mean (SEM) unless otherwise stated. Graphs were generated in Graphpad Prism 6 and formatted in Adobe Illustrator CS6.

3.3. Results

3.3.1. CPDs accumulated in isolated epidermal basal cells and in fibroblasts after low dose UV

As observed in our previous experiment [27], mice in the 'sub-sunburn group' that received the low dose fractions of UV spread over 40 days did not show any immediate observable effects, whereas mice in the 'sunburn group' that received the unfractionated high dose of UV showed severe sunburn which resolved in 2 weeks. From day 47 onward both groups of mice received dorsal TPA treatment twice a week for 20 weeks. TPA treatment induced epidermal cell proliferation shown by epidermal hyperplasia (Figure 3.1C + 3.1D) and, as we have shown earlier, an increase in $Ki67^+$ epidermal cells, but not in (CPD-retaining) fibroblasts in the upper dermis [27]. Mice from both groups showed scaling of the skin after TPA treatment. We observed CPD-retaining cells in the sub-sunburn group (Figure 3.1A). Most of the epidermal CPD-retaining cells were located in the basal layer, i.e., CRBCs, (1.7% of basal cells heavily stained for CPDs). Upon TPA treatment CRBCs were lost and more CPD-containing cells were found suprabasally (Figure 3.1C, arrows). CPD-retaining cells were also observed in the dermis of these mice (Figure 3.1A + 3.1C) but these cells showed no apparent reaction to TPA, no cell morphology of proliferation/mitosis or apoptosis (conform our earlier experiment where we stained for Ki67 and activated caspase-3 [27]; these fibroblasts do eventually lose the CPDs apparently by slow repair). We did not observe any CPD-retaining cells in mice that received a single UV overexposure (Figure 3.1B + 3.1D).

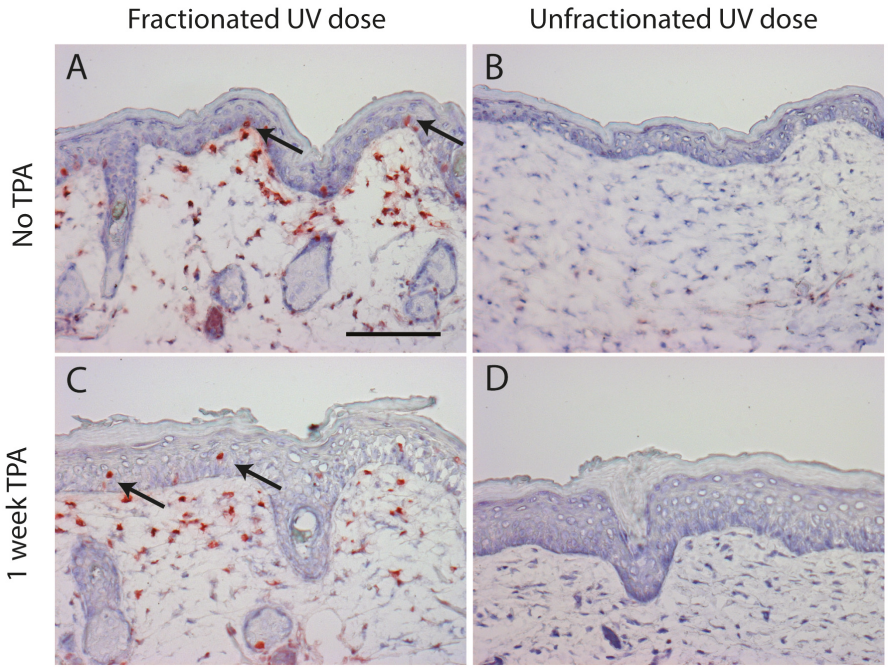


Figure 3.1: CPD retaining cells are only present after a fractionated sub-sunburn UV dose in epidermis (arrows) and in upper dermis (non-dividing fibroblasts). Mouse skin after fractionated sub-sunburn UV dose before TPA treatment, day 47 (A) and after TPA treatment, day 54 (C) and correspondingly after the unfractionated sunburn UV dose (B) and (D). Scale bar 100µm.

3.3.2.Fractionated sub-sunburn UV exposure followed by TPA-induced sparse p53 patches

Skin samples were taken after 8 weeks of TPA treatment to check for (mutant) p53-overexpressing foci ('p53 patches'). Immunohistochemical staining was performed on epidermal sheets using both the CM-5 antibody (detecting wild type and mutant p53) and the PAb240 antibody (detecting only mutant p53). No p53 patches were observed in the sunburn group using either of the antibodies. In the sub-sunburn group we found $CM5^{+}$ patches at a frequency of 3.8 patches/cm^2 (SEM 1.6), yielding about 1 patch per 5000 CRBCs. Using the PAb240 antibody we found 60% fewer patches expressing mutant-p53 (see Supplementary Figure S3.2).

3.3.3. Tumor appearance and pathology

Upon TPA treatment tumors occurred in both groups but after discontinuation of TPA application tumors persisted to grow only in the sub-sunburn group and regressed in the sunburn group.

The histopathological analyses largely confirmed our initial macroscopic observations. The sessile based, endophytically growing tumors, which we provisionally qualified as "non-papilloma" tumors (30% cutaneous horns), were apparently all grades of hyperkeratotic

tumors ranging from benign actinic keratosis (AK)-like lesions (18/41 benign) through Bowenoid tumors (carcinomas in situ, 17/41) up to malignant squamous cell carcinomas, SCCs, and 1 basal cell carcinoma, BCC (5/41 malignant); see Table 3.1 for a comparison with tumor pathology from an older study [37] with chronic, life-long daily UV exposure in which clearly more progression to SCC was observed. In the remainder of this article we will refer to these tumors as AK/SCCs [33]. Only one out of these 41 tumors was not AK/SCC but diagnosed as an inverted papilloma. Exophytically growing tumors (n=7) were confirmed to be papillomas (of which 2 long persisting pedunculated, cauliflower-shaped classical papillomas contained a focus suspect of Bowenoid changes).

Table 3.1: Pathology of tumors (> 3mm) in the present study compared with an earlier study with chronic UV exposure (1 MED or 0.03 MED/day)*

Treatment:	SCC (%)	Bowen (%)	AK (%)
1 MED/d chronic (n=68)[1]	73	3	17
0.14 MED/d 40 d + TPA 20 wks (n= 32)	9 [2,3]	50 [4]	34
5.6 MED 1d + TPA 20 wks (n=9)	11 [3]	11	78 [5]
0.03 MED/d chronic (n=47)[1]	71	9	4

*a small percentage of frank papillomas not included; in the present study the mice were either exposed to a single UV exposure of 5.6 MED or a fractionated dose into 0.14 MED/d over a period of 40 days, and after a week subjected to 2 TPA applications per week for a period of 20 weeks.
[1] De Gruijl et al. [37],[2] one BCC excluded, [3] all SCCs from mice sacrificed at the end of the experiment (day 280), [4] 2 Bowenoid tumors and 1 AK from mouse sacrificed early (day 224), because of swollen lymph node,[5] 5 of 7 AKs from mouse sacrificed early (day 224), because of tumor load and ulceration.

3.3.4. Tumor-free survival for AK/SCC was significantly shorter after fractionated UV exposure

The percentage of tumor-free mice with time is shown in Figure 3.2 for different threshold sizes of AK/SCCs and for papillomas. For AK/SCC tumors ≥ 2 mm there was a clear difference between the sunburn and the sub-sunburn group (p=0.0006); all mice in the sub-sunburn group developed a tumor ≥ 2 mm whereas some mice in the sunburn group remained tumor free. Also, for the tumors ≥ 4 mm there was a clear difference between the two groups (p=0.03). More mice in the sub-sunburn group developed AK/SCCs ≥ 4mm. For the papillomas (very small in number) we did not find any significant differences.
Gender differences in UV carcinogenesis have been reported [38], but we found no significant differences in tumor-free survivals between males and females (Supplementary Figure S3.3)

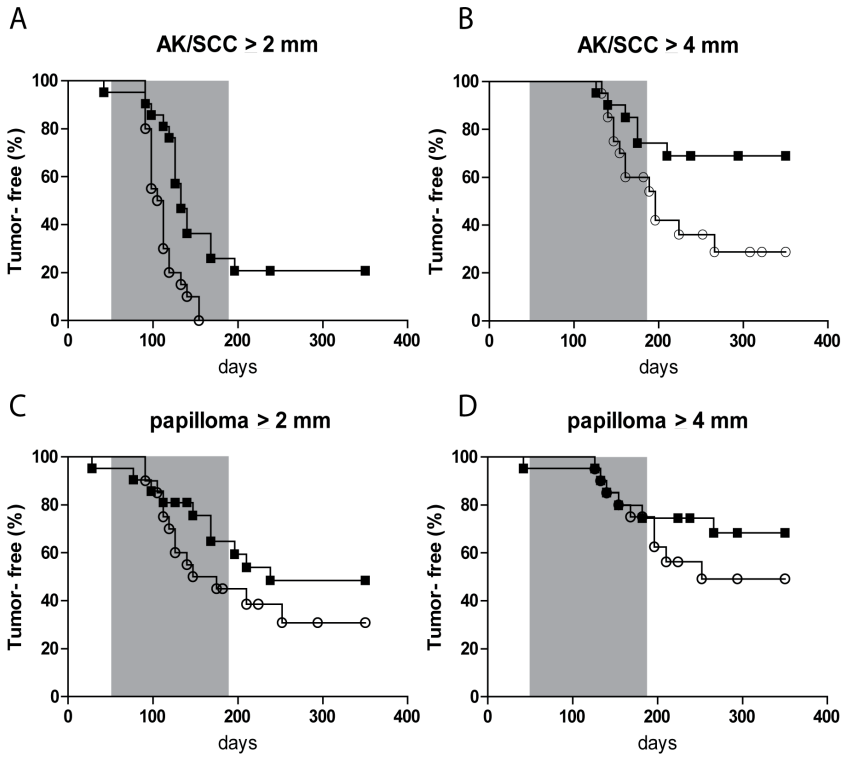


Figure 3.2: Kaplan-Meier plot of tumor- free fraction of mice for AK/SCC drops significantly faster after fractionated sub-sunburn UV exposure. The tumor-free fraction for AK/SCCs ≥ 2 mm (A) and ≥ 4 mm (B) and papillomas ≥ 2 mm (C) and ≥ 4 mm (D) for mice in the sub-sunburn group (o) or in the sunburn group (■). The grey area in the graphs represent the period in which TPA was applied.

3.3.5. Tumor yields showed non-regressing carcinomas only after fractionated UV exposure

After discontinuation of the TPA treatment AK/SCCs ≥ 2 mm went into regression, as reflected in Figure 3.3A by a drop in tumor yield. Almost all tumors in the sunburn group went into complete regression, while most of the tumors in the sub-sunburn group persisted. For the tumors ≥ 4 mm we observed an even more distinct difference at day 280. In the sunburn group virtually no AK/SCC grew out to this size, while in the sub-sunburn group these tumors persisted and grew after discontinuation of the TPA regimen (0.06 vs 2.50 AK/SCC ≥ 4 mm, p=0.03; again, no gender differences, see Supplementary Figure S3.4).

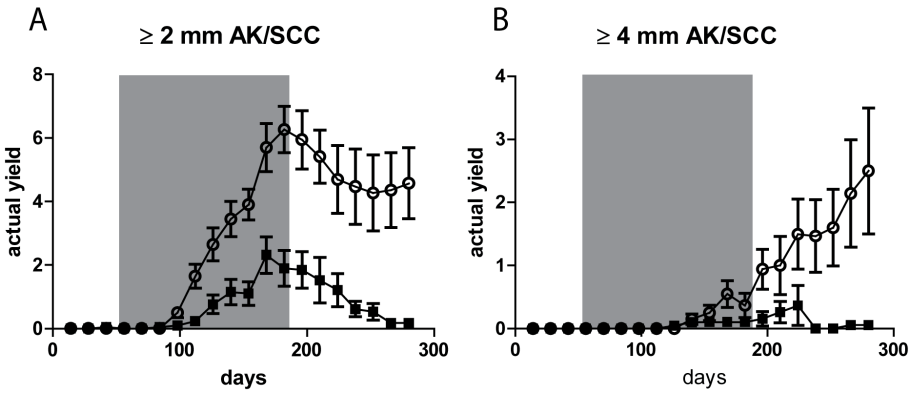


Figure 3.3: Tumor yields (average number of tumors per mouse) showed non-regressing carcinomas only after fractionated sub-sunburn UV exposure. The yield of AK/SCCs ≥ 2 mm (A) and ≥ 4 mm (B) for mice irradiated with the fractionated sub-sunburn UV dose (o) or with the unfractionated sunburn dose of UV (5.6 MED) (■). The grey area in the graphs represent the period in which TPA was applied. Error bars show SEMs. Virtually all AK/SCCs go into regression in the sunburn group after cessation of TPA applications.

3.3.6. No difference in yields of papillomas after different UV treatments

Next to AK/SCC tumors we also observed papillomas (growing exophytically) in small numbers. Figure 3.4 shows the actual yield for papillomas ≥ 2 mm and ≥ 4 mm, respectively. At both thresholds there was no clear difference between the two groups (n.s.). The yield of papillomas was 4-6 fold lower than that of AK/SCCs, with a maximum of 1/mouse for the ≥ 2 mm tumors and a maximum of 0.6/mouse for the ≥ 4 mm tumors, (for AK/SCCs 6 and 2.5/mouse, respectively). In contrast to AK/SCCs papillomas did not appear to regress in the sunburn group after discontinuation of the TPA regimen. We did not find significant differences between male and female mice in papilloma yields (see Supplementary Figure S3.4).

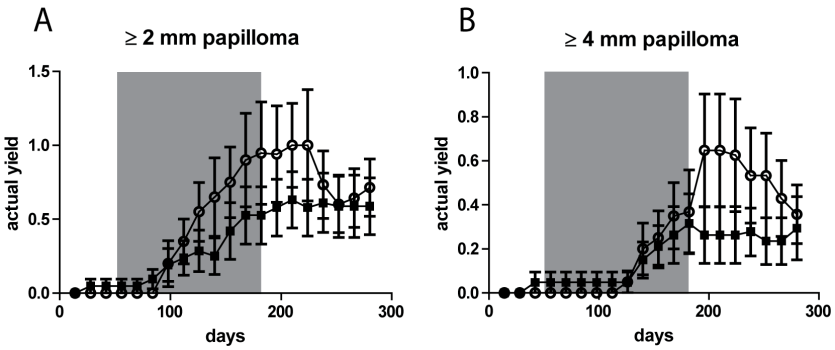


Figure 3.4: No significant difference in tumor yields (average number of tumors per mouse) for papillomas between the fractionated sub-sunburn and unfractionated sunburn UV dose groups. The yield for papillomas ≥ 2 mm (A) and ≥ 4 mm (B) for mice irradiated with the fractionated sub-sunburn UV dose (o) or with the unfractionated sunburn dose of UV (5.6 MED) (■). The grey area in the graphs represent the period in which TPA was applied. Error bars show SEMs.

3.3.7. Lack of p53, Ras and Notch mutations in AK/SCCs

Samples of tumors (22 AK/SCCs and 3 papillomas), mainly from the sub-sunburn group (17/25), were analyzed for mutations in *p*53 and *Ras* genes (*H-, K-* and *N-Ras*). No mutations were found in *p*53 (exons 4-8). Staining with CM5 showed only sparse cells in the tumor masses overexpressing p53 (except for 1 AK/SCC out of 34 that was abundantly positive but without *p53* mutation). Considering the absence of *p53* mutations this could concern reactive wild-type p53 expression (data not shown). We found two papillomas mutated in *H-Ras* codon 12 (G>A), (1 from each group). Furthermore we found one mutation in *H-Ras* codon 13 (G>T) in an AK/SCC from the sub-sunburn group. No mutations were found in *N-* and *K-Ras.*

In follow-up of this paucity of mutations in *p53* and *RAS*, we decided to investigate *Notch* (frequently mutated in human SCC, [35, 36]). First, tumors were stained using an antibody against cleaved Notch1, i.e. recognizing the Notch 1 intracellular domain (Nicd) which relocates to the nucleus up on activation. Nicd expression is affected by mutations in *Notch1* [36]. Our staining (method given in Supplementary Material) showed highly variable Nicd expression in the tumors, and was not conclusive on possible mutations. Next, we sequenced 10 tumors (6 from the sub-sunburn group, 4 from the sunburn group) for mutations in *Notch1* and *Notch2* (focusing on domains most often affected in human cutaneous SCCs [35, 36]; see Supplementary Material). None were found.

3.4. Discussion

In this study we showed that there is a difference in tumor initiation by a single UV overexposure compared to the same total dose delivered in very small sub-sunburn dose fractions: only in the latter case tumors grew persistently after 20 weeks of TPA treatment. In absence of epidermal hyperplasia during exposure, both UV regimens should have produced the same initial DNA damage (CPDs), but spreading this damage over small daily aliquots was apparently linked to the ultimate yield of persistent (in situ) SCCs. In contrast to the single sunburn UV exposure, the fractionated sub-sunburn UV dose resulted in CPD-retaining skin cells which persisted over a week after the last UV exposure. These stationary, non-dividing cells lagging behind in repair of CPDs had apparently accumulated part of the undetectably small daily aliquots of CPDs. Besides fibroblasts in the upper dermis, sparse basal cells in the epidermis showed retention of CPDs; in an earlier study we demonstrated the latter cells (CPD-retaining basal cells, CRBCs) to be quiescent stem cells (QSCs)[26]. TPA induced division of these CPD-retaining epidermal cells, but evoked no discernable response in the CPD-retaining fibroblasts (see Figure 3.1 and our earlier study [27]). Forcing the CRBCs with their high CPD loads to proliferate is likely to increase the risk of mutations and thus have a special bearing on epidermal UV carcinogenesis. In a natural situation the forced proliferation may be evoked by an irritant or a mild sunburn inducing (transient) hyperplasia [25].

With regard to AK/SCC, our data show that a severe sunburn from a single overdose appears to be less hazardous than spreading the same dose over multiple small exposures. This finding appears to be in line with the older finding that single weekly exposures are less effective in inducing SCCs than daily doses mounting up to the same weekly dose [39]. This could be related to the extent to which quiescent stem cells are activated in the hyperplastic response and the speed at which CPDs are removed in the epidermal turnover.

The daily UV dose fractions in our experiment were low enough not to induce any proliferation of quiescent stem cells and hyperplasia, as can be seen in Figure 3.1A. The undetectably small aliquots of CPDs induced daily were being lost mostly in epidermal turnover. This DNA damage only accumulated in long residing (quiescent stem) cells if the repair lagged behind – which it apparently did for CPDs but not for 6-4 photoproducts [26]. In literature there are several markers described for the long-residing non-dividing QSCs, e.g. Wif-1 [40], Lrig1 [41] and Dll1 [42]. We checked for double staining with anti-CPD to see if they would co-localize (see Supplementary Table S3.2 on antibodies used). However, these markers either did not label interfollicular basal cells at all in mice (Lrig1^{+}, Dll1) or did not double stain (Wif1, which was predominantly expressed suprabasally in TPA driven hyperplasia; data not shown). Thus, we could not identify a specific phenotypic marker of these cells which could be exploited to eliminate these cells specifically (e.g. by induction of

a transgene for diphtheria toxin). Such an eliminatory intervention could serve to proof the suspected causal role of CPD-loaded QSCs in raising persistent SCCs.

The retention of UV-induced DNA damage in quiescent stem cells is reminiscent of the retention of chemical DNA adducts in quiescent cells as the tumor-initiating step in a two-stage regimen of chemical skin carcinogenesis (i.e. tumor initiation by a genotoxic agent followed by "tumor promotion" by repeated applications of a cell proliferation inducing agent, such as TPA) [43]. This regimen gives rise to PCR-detectable oncogenic *H-ras* mutations one week after tumor initiation, months before the occurrence of skin tumors carrying such mutations [44].

Only in the sub-sunburn group, corresponding with induction of CPD-retaining cells, we found clear, but rare, p53-overexpressing and p53-mutant clusters of cells ("p53 patches") long before onset of tumors, albeit in very low numbers. This is somewhat in contrast with earlier results [27] where no p53-mutant patches could be detected, but high numbers of small wild-type p53 expressing patches were found, speculated to reflect a reaction of TPA-driven cells to proliferative stress from DNA damage. This discrepancy is most likely attributable to a difference in techniques (detection in epidermal sheets or cross sections) and sensitivity (difference in antigen retrieval), despite using the same antibodies.

Only in the sub-sunburn group we found CRBCs and p53 patches. As the regimen of 1/7 MED/day for 40 days is unlikely to induce p53-mutant patches [17], this suggests that some CRBCs attained *p53* mutations after TPA-induced proliferation and grew out to p53 patches.

But the p53 patches were very sparse (3.8/cm^2 on average), and none of the ensuing persistent (in situ) skin carcinomas carried any *p53* mutations. Very much in contrast to what we found earlier with life-long chronic exposure of SKH-1 hairless mice which gave rise to multitudes of p53 patches and subsequently carcinomas with abundant *p53* mutations with the "UV signature" (>70% of tumors) [13], also at low daily doses [18]. This lack of *p53* mutations could conceivably hamper progression to malignancy (high percentage of in situ SCCs/Bowenoid tumors and low percentage of SCCs in present experiment in comparison to earlier experiments with chronic, life-long daily UV exposure, Table 3.1) [37].

Of human SCCs, 50 – 70 % have been reported to carry UV-related *P53* mutations [10, 45, 46], and similar percentages in AKs [45]. But in some studies much lower percentages have been reported in SCCs (e.g. 15% [47]) and in "low grade" AKs (7% [48]). *NOTCH* genes proved to be even more abundantly UV-mutated than *P53* [35, 36]. The lack of *p53* mutations in the current experiment is evidently due to early termination of the UV regimen, which might also explain the lack of mutations in *Notch*. This apparently also resulted in only a few *p53* mutant clones (p53 patches). Considering the overall high percentages of human SCCs with UV signature mutations in *P53* and *NOTCH*, one is led to infer that most of these tumors are induced by life-long, or at least decades of, chronic UV exposure. Even in temperate climate

with low ambient UV, high frequencies of UV-related *P53* and *NOTCH* mutations were found in sun-exposed adult skin [49, 50].

We have earlier shown that in contrast to chronic UV-B exposure, chronic UV-A exposure of SKH-1 hairless mice induced SCCs of which a large majority (85%) lacked *p53* mutations [51]. Like low level UV-B, UV-A exposure appears to be much less effective in stimulating cell proliferation and hyperplasia than higher level UV-B [52], and it may therefore also be targeted more at QSCs and deeper residing fibroblasts.

The AK/SCCs initiated by low level daily UV-B exposure (40 days) – associated with CPD-retaining skin cells – and promoted to grow out by repeated applications of TPA – specifically stimulating CRBCs - differ from earlier SCCs induced by life-long chronic UV-B exposure in that they harbor no *p53* and *Notch* mutations, and they differ from chemically initiated and TPA-promoted tumors in that they harbor virtually no oncogenic (*H-*) *Ras* mutations. Thus, there appears to be another as yet unknown tumor initiator/driver which may also be involved in the earliest stages of skin carcinogenesis by life-long chronic UV exposure.

Histopathology (Table 3.1) was mainly based on tumor samples from mice sacrificed at the end of the experiment and from a few mice sacrificed earlier. Hence, most of the samples were from persistently growing tumors from the sub-sunburn group, mostly (in situ) SCCs and precursor AKs. As most of the tumors regressed in the sunburn group, few tumors could be analyzed of which most from a mouse sacrificed early, 5 out of 7 AKs (see footnote Table 3.1). The low percentage of SCCs and high percentage of Bowenoid tumors (in situ SCCs) in the sub-sunburn group in comparison with earlier experiments with chronic exposures (Table 3.1) suggests that tumor progression stagnated in the 'in situ' stage without further UV exposure, despite TPA-driven outgrowth of the tumor. As virtually all of the suspected AK/SCCs, i.e., endophytically growing tumors, regressed upon discontinuation of the TPA regimen in the sunburn group, we have very little information on the histopathology of these regressing tumors. AKs are, however, known to regress (e.g. if no longer subjected to sun or UV exposure) [53, 54]. The AK/SCC-like tumors ≥ 3 mm that regressed are not likely to have been truly malignant SCCs. Besides AKs, they may also have been benign keratoacanthomas which are hard to distinguish from SCCs but, unlike SCCs, are known to regress spontaneously in man [55].

Acute overexposure and especially chronic exposure to (solar) UV radiation are associated with the development of squamous cell carcinomas. The present study shows that a single sunburn dose differs in initiating epidermal tumors from an equal dose fractionated into sub-sunburn exposures: the latter results in non-regressing tumors whereas the tumors from the single exposure went into regression upon cessation of tumor promotion by TPA treatment. Interestingly, the initiation of non-regressing tumors was associated with DNA damage-retaining QSCs in the epidermis which were forced to divide by TPA treatment. Surprisingly, none of the persistent skin tumors showed mutations in the common driver

genes, i.e. no mutations in *p53*, *Notch* and *Ras*. We infer that none of these common driver mutations were involved in the UV-driven tumor initiation. Although the as yet unknown tumor-initiating mutations may have been forced to occur by TPA-induced proliferation of DNA damage-retaining cells, they may also constitute the earliest tumor initiation events in skin carcinogenesis by life-long chronic UV exposure.

Acknowledgements

We thank D.C.F. Salvatori and J.A. Bruijn for histopathological assessment of skin tumors, J.J. Out- Luiting, W.H. Zoutman and M.M. Plug for technical assistance and the technicians of the animal facility for animal care.

References

1. Birch-Johansen F, Jensen A, Mortensen L, Olesen AB and Kjær SK. Trends in the incidence of nonmelanoma skin cancer in Denmark 1978–2007: Rapid incidence increase among young Danish women. Int J Cancer. 2010; 127(9):2190-2198.
2. Hollestein LM, de Vries E and Nijsten T. Trends of cutaneous squamous cell carcinoma in the Netherlands: Increased incidence rates, but stable relative survival and mortality 1989–2008. Eur J Cancer. 2012; 48(13):2046-2053.
3. Flohil SC, Seubring I, van Rossum MM, Coebergh J-WW, de Vries E and Nijsten T. Trends in Basal Cell Carcinoma Incidence Rates: A 37-Year Dutch Observational Study. J Invest Dermatol. 2013; 133(4):913-918.
4. Dessinioti C, Antoniou C, Katsambas A and Stratigos AJ. Basal Cell Carcinoma: What's New Under the Sun. Photochem Photobiol. 2010; 86(3):481-491.
5. Weinstock MA. Epidemiology and UV exposure. J Invest Dermatol. 2013; 133(E1):E11-12.
6. Kennedy C, Bajdik CD, Willemze R, De Gruijl FR and Bouwes Bavinck JN. The influence of painful sunburns and lifetime sun exposure on the risk of actinic keratoses, seborrheic warts, melanocytic nevi, atypical nevi, and skin cancer. J Invest Dermatol. 2003; 120(6):1087-1093.
7. Setlow RB and Carrier WL. Pyrimidine dimers in ultraviolet-irradiated DNA's. J Mol Biol. 1966; 17(1):237-254.
8. Mitchell DL. The relative cytotoxicity of (6–4) photoproducts and cyclobutane dimers in mammalian cells. Photochem Photobiol. 1988; 48(1):51-57.
9. Brash DE. UV mutagenic photoproducts in Escherichia coli and human cells: a molecular genetics perspective on human skin cancer. Photochem Photobiol. 1988; 48(1):59-66.
10. Brash DE, Rudolph JA, Simon JA, Lin A, McKenna GJ, Baden HP, Halperin AJ and Pontén J. A role for sunlight in skin cancer: UV-induced p53 mutations in squamous cell carcinoma. Proc Natl Acad Sci U S A. 1991; 88(22):10124-10128.
11. Ziegler A, Leffell DJ, Kunala S, Sharma HW, Gailani M, Simon JA, Halperin AJ, Baden HP, Shapiro PE and Bale AE. Mutation hotspots due to sunlight in the p53 gene of nonmelanoma skin cancers. Proc Natl Acad Sci U S A. 1993; 90(9):4216-4220.
12. de Gruijl FR and Forbes PD. UV-induced skin cancer in a hairless mouse model. Bioessays. 1995; 17(7):651-660.
13. Dumaz N, van Kranen HJ, de Vries A, Berg RJ, Wester PW, van Kreijl CF, Sarasin A, Daya-Grosjean L and de Gruijl FR. The role of UV-B light in skin carcinogenesis through the analysis of p53 mutations in squamous cell carcinomas of hairless mice. Carcinogenesis. 1997; 18(5):897-904.
14. Owens DM, Wei S-JC and Smart RC. A multihit, multistage model of chemical carcinogenesis. Carcinogenesis. 1999; 20(9):1837-1844.
15. van Kranen H, de Gruijl F, de Vries A, Sontag Y, Wester PW, Senden HCM, Rozemuller E and van Kreijl CF. Frequent p53 alterations but low incidence of ras mutations in UV-B-induced skin tumors of hairless mice. Carcinogenesis. 1995; 16(5):1141-1147.
16. Berg RJ, van Kranen HJ, Rebel HG, de Vries A, van Vloten WA, Van Kreijl CF, van der Leun JC and de Gruijl FR. Early p53 alterations in mouse skin carcinogenesis by UVB radiation: immunohistochemical detection of mutant p53 protein in clusters of preneoplastic epidermal cells. Proc Natl Acad Sci U S A. 1996; 93(1):274-278.
17. Rebel H, Mosnier LO, Berg RJW, Vries AW-d, van Steeg H, van Kranen HJ and de Gruijl FR. Early p53-positive Foci as Indicators of Tumor Risk in Ultraviolet-exposed Hairless Mice: Kinetics of Induction, Effects of DNA Repair Deficiency, and p53 Heterozygosity. Cancer Res. 2001; 61(3):977-983.
18. Rebel H, Kram N, Westerman A, Banus S, van Kranen HJ and de Gruijl FR. Relationship between UV-induced mutant p53 patches and skin tumours, analysed by mutation spectra and by induction kinetics in various DNA-repair-deficient mice. Carcinogenesis. 2005; 26(12):2123-2130.

19. Jonason AS, Kunala S, Price GJ, Restifo RJ, Spinelli HM, Persing JA, Leffell DJ, Tarone RE and Brash DE. Frequent clones of p53-mutated keratinocytes in normal human skin. Proc Natl Acad Sci U S A. 1996; 93(24):14025-14029.
20. Ren Z-P, Pontén F, Nistér M and Pontén I. Two distinct p53 immunohistochemical patterns in human squamous-cell skin cancer, precursors and normal epidermis. Int J Cancer. 1996; 69(3):174-179.
21. Hanahan D and Weinberg RA. The Hallmarks of Cancer. Cell. 2000; 100(1):57-70.
22. Tomasetti C and Vogelstein B. Cancer etiology. Variation in cancer risk among tissues can be explained by the number of stem cell divisions. Science. 2015; 347(6217):78-81.
23. Albini A, Cavuto S, Apolone G and Noonan DM. Strategies to Prevent "Bad Luck" in Cancer. J Natl Cancer Inst. 2015; 107(10).
24. Mitchell DL, Greinert R, de Gruijl FR, Guikers KLH, Breitbart EW, Byrom M, Gallmeier MM, Lowery MG and Volkmer B. Effects of Chronic Low-Dose Ultraviolet B Radiation on DNA Damage and Repair in Mouse Skin. Cancer Res. 1999; 59(12):2875-2884.
25. Mitchell DL, Volkmer B, Breitbart EW, Byrom M, Lowery MG and Greinert R. Identification of a Non-Dividing Subpopulation of Mouse and Human Epidermal Cells Exhibiting High Levels of Persistent Ultraviolet Photodamage. 2001; 117(3):590-595.
26. Nijhof JGW, van Pelt C, Mulder AA, Mitchell DL, Mullenders LHF and de Gruijl FR. Epidermal stem and progenitor cells in murine epidermis accumulate UV damage despite NER proficiency. Carcinogenesis. 2006; 28(4):792-800.
27. Nijhof JGW, Mulder AM, Speksnijder EN, Hoogervorst EM, Mullenders LHF and de Gruijl FR. Growth stimulation of UV-induced DNA damage retaining epidermal basal cells gives rise to clusters of p53 overexpressing cells. DNA Repair. 2007; 6(11):1642-1650.
28. Gallagher RP, Lee TK, Bajdik CD and Borugian M. Ultraviolet radiation. Chronic Dis Can. 2010; 29 Suppl 1:51-68.
29. Epstein JH and Roth HL. Experimental ultraviolet light carcinogenesis: a study of croton oil promoting effects. J Invest Dermatol. 1968; 50(5):387-389.
30. de Gruijl FR and van der Leun JC. Development of skin tumors in hairless mice after discontinuation of ultraviolet irradiation. Cancer Res. 1991; 51(3):979-984.
31. Hsu J, Forbes PD, Harber LC and Lakow E. Induction of skin tumors in hairless mice by a single exposure to UV radiation. Photochem Photobiol. 1975; 21(3):185-188.
32. Rebel HG, Bodmann CA, van de Glind GC and de Gruijl FR. UV-induced ablation of the epidermal basal layer including p53-mutant clones resets UV carcinogenesis showing squamous cell carcinomas to originate from interfollicular epidermis. Carcinogenesis. 2012; 33(3):714-720.
33. Kelfkens G, de Gruijl FR and van der Leun JC. Tumorigenesis by short-wave ultraviolet A: papillomas versus squamous cell carcinomas. Carcinogenesis. 1991; 12(8):1377-1382.
34. Remenyik É, Wikonkál NM, Zhang W, Paliwal V and Brash DE. Antigen-specific immunity does not mediate acute regression of UVB-induced p53-mutant clones. Oncogene. 2003; 22(41):6369-6376.
35. Wang NJ, Sanborn Z, Arnett KL, Bayston LJ, Liao W, Proby CM, Leigh IM, Collisson EA, Gordon PB, Jakkula L, Pennypacker S, Zou Y, Sharma M, North JP, Vemula SS, Mauro TM, et al. Loss-of-function mutations in Notch receptors in cutaneous and lung squamous cell carcinoma. Proceedings of the National Academy of Sciences of the United States of America. 2011; 108(43):17761-17766.
36. South AP, Purdie KJ, Watt SA, Haldenby S, den Breems NY, Dimon M, Arron ST, Kluk MJ, Aster JC, McHugh A, Xue DJ, Dayal JH, Robinson KS, Rizvi SM, Proby CM, Harwood CA, et al. NOTCH1 mutations occur early during cutaneous squamous cell carcinogenesis. J Invest Dermatol. 2014; 134(10):2630-2638.
37. de Gruijl F, van der Meer JB and van der Leun JC. Dose-time dependency of tumor formation by chronic UV exposure. Photochem Photobiol. 1983; 37(1):53-62.

38. Widyarini S, Domanski D, Painter N and Reeve VE. Estrogen receptor signaling protects against immune suppression by UV radiation exposure. Proceedings of the National Academy of Sciences of the United States of America. 2006; 103(34):12837-12842.
39. Forbes PD, Blum HF and Davies RE. Photocarcinogenesis in hairless mice: dose-response and the influence of dose-delivery. Photochem Photobiol. 1981; 34(3):361-365.
40. Schlüter H, Stark H-J, Sinha D, Boukamp P and Kaur P. WIF1 is expressed by stem cells of the human interfollicular epidermis and acts to suppress keratinocyte proliferation. J Invest Dermatol. 2013; 133(6):1669-1673.
41. Jensen KB, Collins CA, Nascimento E, Tan DW, Frye M, Itami S and Watt FM. Lrig1 expression defines a distinct multipotent stem cell population in mammalian epidermis. Cell stem cell. 2009; 4(5):427-439.
42. Estrach S, Cordes R, Hozumi K, Gossler A and Watt FM. Role of the Notch ligand Delta1 in embryonic and adult mouse epidermis. J Invest Dermatol. 2007; 128(4):825-832.
43. Morris RJ, Coulter K, Tryson K and Steinberg SR. Evidence That Cutaneous Carcinogen-initiated Epithelial Cells from Mice Are Quiescent Rather Than Actively Cycling. Cancer Res. 1997; 57(16):3436-3443.
44. Nelson MA, Futscher BW, Kinsella T, Wymer J and Bowden GT. Detection of mutant Ha-ras genes in chemically initiated mouse skin epidermis before the development of benign tumors. Proc Natl Acad Sci U S A. 1992; 89(14):6398-6402.
45. Nelson MA, Einspahr JG, Alberts DS, Balfour CA, Wymer JA, Welch KL, Salasche SJ, Bangert JL, Grogan TM and Bozzo PO. Analysis of the p53 gene in human precancerous actinic keratosis lesions and squamous cell cancers. Cancer Lett. 1994; 85(1):23-29.
46. Ren ZP, Ahmadian A, Ponten F, Nister M, Berg C, Lundeberg J, Uhlen M and Ponten J. Benign clonal keratinocyte patches with p53 mutations show no genetic link to synchronous squamous cell precancer or cancer in human skin. Am J Pathol. 1997; 150(5):1791-1803.
47. Moles JP, Moyret C, Guillot B, Jeanteur P, Guilhou JJ, Theillet C and Basset-Seguin N. p53 gene mutations in human epithelial skin cancers. Oncogene. 1993; 8(3):583-588.
48. Nindl I, Gottschling M, Krawtchenko N, Lehmann MD, Rowert-Huber J, Eberle J, Stockfleth E and Forschner T. Low prevalence of p53, p16(INK4a) and Ha-ras tumour-specific mutations in low-graded actinic keratosis. Br J Dermatol. 2007; 156 Suppl 3:34-39.
49. Stahl PL, Stranneheim H, Asplund A, Berglund L, Ponten F and Lundeberg J. Sun-induced nonsynonymous p53 mutations are extensively accumulated and tolerated in normal appearing human skin. J Invest Dermatol. 2011; 131(2):504-508.
50. Martincorena I, Roshan A, Gerstung M, Ellis P, Van Loo P, McLaren S, Wedge DC, Fullam A, Alexandrov LB, Tubio JM, Stebbings L, Menzies A, Widaa S, Stratton MR, Jones PH and Campbell PJ. Tumor evolution. High burden and pervasive positive selection of somatic mutations in normal human skin. Science. 2015; 348(6237):880-886.
51. van Kranen HJ, de Laat A, van de Ven J, Wester PW, de Vries A, Berg RJW, van Kreijl CF and de Gruijl FR. Low Incidence of p53 Mutations in UVA (365-nm)-induced Skin Tumors in Hairless Mice. Cancer Res. 1997; 57(7):1238-1240.
52. Gambichler T, Rotterdam S, Tigges C, Altmeyer P and Bechara FG. Impact of ultraviolet radiation on the expression of marker proteins of gap and adhesion junctions in human epidermis. Photodermatol Photoimmunol Photomed. 2008; 24(6):318-321.
53. Criscione VD, Weinstock MA, Naylor MF, Luque C, Eide MJ, Bingham SF and for the Department of Veteran Affairs Topical Tretinoin Chemoprevention Trial G. Actinic keratoses. Cancer. 2009; 115(11):2523-2530.
54. Hancox JG, Sheridan SC, Feldman SR and Fleischer AB. Seasonal variation of dermatologic disease in the USA: a study of office visits from 1990 to 1998. Int J Dermatol. 2004; 43(1):6-11.
55. Mandrell JC and Santa Cruz D. Keratoacanthoma: hyperplasia, benign neoplasm, or a type of squamous cell carcinoma? Semin Diagn Pathol. 2009; 26(3):150-163.

Supplementary information

S3.1. Methods

S3.1.1. P53 patch staining on epidermal sheets

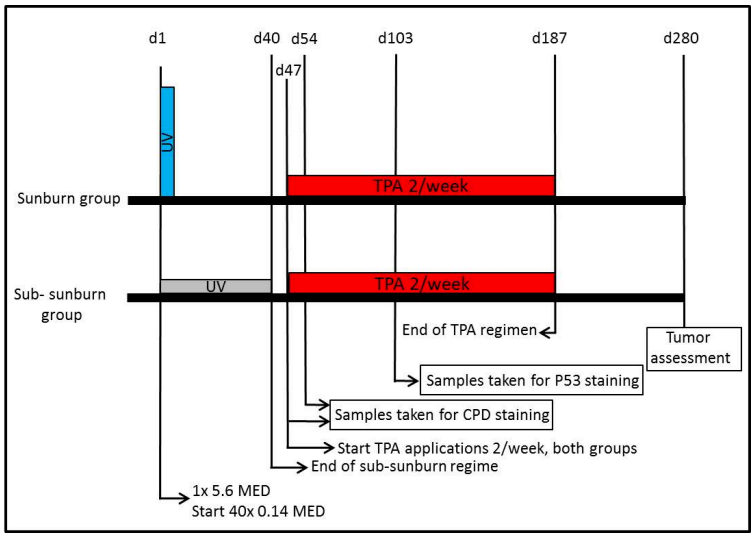
Thermolysin sheets (see materials and method) were fixed with PBS-buffered 4% formaldehyde solution for 10 min and EDTA sheets were fixed for 20 min in aceton. For both antigen retrieval was performed by boiling 5 min at 110 ^{o}C in 10 mM citrate buffer (pH 6.0). Endogenous peroxidases were blocked by incubating the sheets in methanol containing 1.5% H_2O_2 for 20 min. The sheets were pre-incubated for 10 min with 5% normal serum/0.2% BSA/0.1% saponine (Sigma-Aldrich) in PBS; goat serum for CM5 and rabbit serum (Dakocytomation) for Pab240 staining. PBS containing 0.5% BSA and 0.1% saponine was used to dilute the primary antibodies, either Pab240 (mutant specific, mouse monoclonal anti-p53 antibody, Neomarkers, Duiven, the Netherlands) 1:25 for thermolysin sheets or CM5 (rabbit polyclonal anti-p53 antibody, Monosan (Sanbio), Uden, The Netherlands) 1:250 for EDTA sheets. The primary antibodies were incubated overnight at 4^{o}C. Secondary antibodies, rabbit anti mouse (IgG_1)-biotin (Southern Biotechnologies, Birmingham, USA) 1:200 and goat anti rabbit (IgG)-biotin (Vector Laboratories, Peterborough, UK) 1:300 diluted in PBS/BSA/saponine were incubated for 45 min. Sheets were subsequently incubated with avidin-biotin peroxidase complex (Vectastain Elite, Burlingame, USA) for 45 min and stained with 3,3'-diaminobenzidine (DAB, Sigma-Aldrich). Sheets were mounted with the basal side up in Kaiser's glycerin.

S3.1.2. Anti-CM5 and Notch staining on tumors

Anti-CM5 and Notch staining on tumors was performed on paraffin embedded samples that were sectioned at 5 µm thickness. For both stainings, antigen retrieval was performed by boiling the samples 5 min at 110^{o}C in 10mM citrate buffer (pH 6.0). For the anti-CM5 staining the samples were incubated with blocking solution (methanol containing 1.5% H_2O_2) and subsequently with anti-p53 (1:2000, CM-5, Monosan (Sanbio), PSX1021) in 5% NGS in PBS/1% BSA overnight at 4^{o}C. The secondary antibody, goat-anti-rabbit-IgG-biotin (1:300, Vector, BA1000) in PBS/1% BSA was incubated for 1 hr at RT. The avidin-biotin peroxidase complex combined with DAB was used for visualization in the same way as for the p53 patch staining. Samples were embedded in Kaisers Glycerin.
For the Notch staining samples were incubated 10 min with avidin block and 10 min with biotin block (Biotin blocking system X0590, Dako cytomation) and blocked with 2% NGS, in PBS/1% BSA. Subsequently, they were incubated with anti-cleaved Notch1 antibody (Val1744, D3B8, Rabbit mAb, Cell signaling) overnight at 4^{o}C. Goat-anti-Rabbit-IgG-biotin (1:300) was incubated for 1 hr at RT, followed by 1 hr incubation with streptavidin-biotinylated horseradish peroxidase complex (1:100, RPN1051V, Amersham) at RT. DAB was used for visualization (3,3' Diaminobenzidine (D5905, Sigma) and samples were embedded in Depex.

S3.1.3. Bead purification of Notch pcr products

Pcr products were purified using AMPure XP beads (A63881, Beckman-Coulter) using a protocol similar to that of the manufacturer. In short 25 µl H_2O and 50 µl of AMPure XP beads was added to 25 µl of pcr product, mixed by pipetting and incubated for 5-8 min at RT. The samples were placed on a Dynal MPC®-96S magnet (120-27, Invitrogen), and the supernatant was removed. The samples were washed twice with 200 µl 80% ethanol, the supernatant was removed and the pellets were dried for approximately 2 min in a heath block at 37^{o}C. 15 µl of 10 mM Tris-HCl buffer pH 7.5 (diluted from 1M Tris-HCl buffer, 15567-027, Life technologies) was added to the samples; samples were vortexed until all samples were homogenous and incubated for 30 s-2 min at RT. The plate was placed on the magnet again to separate the beads from the solution and the eluate was transferred to a new plate.



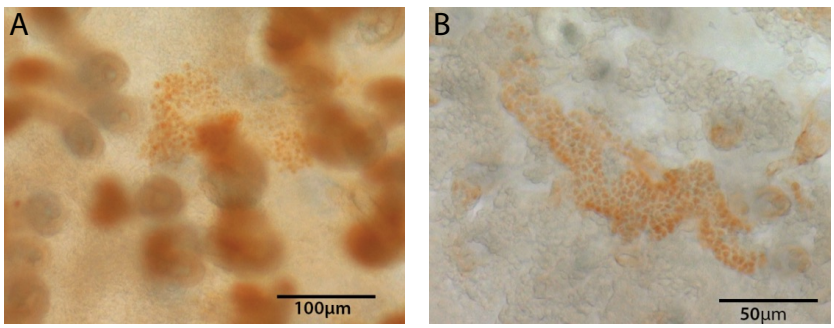
Supplementary Figure S3.1: Experimental outline. Time line of the experiments including time points of sample collection for analyses, d = day. The sunburn group received their single UV overexposure (5.6 MED) on day 1 instead of day 40 to avoid interference of the UV induced hyperplasia with hyperplasia from TPA, and to maximize the time for possible fixation of mutations.

Supplementary Table S3.1: Primer sequences and PCR protocols for amplification of *p53*, *Ras* and *Notch* DNA.

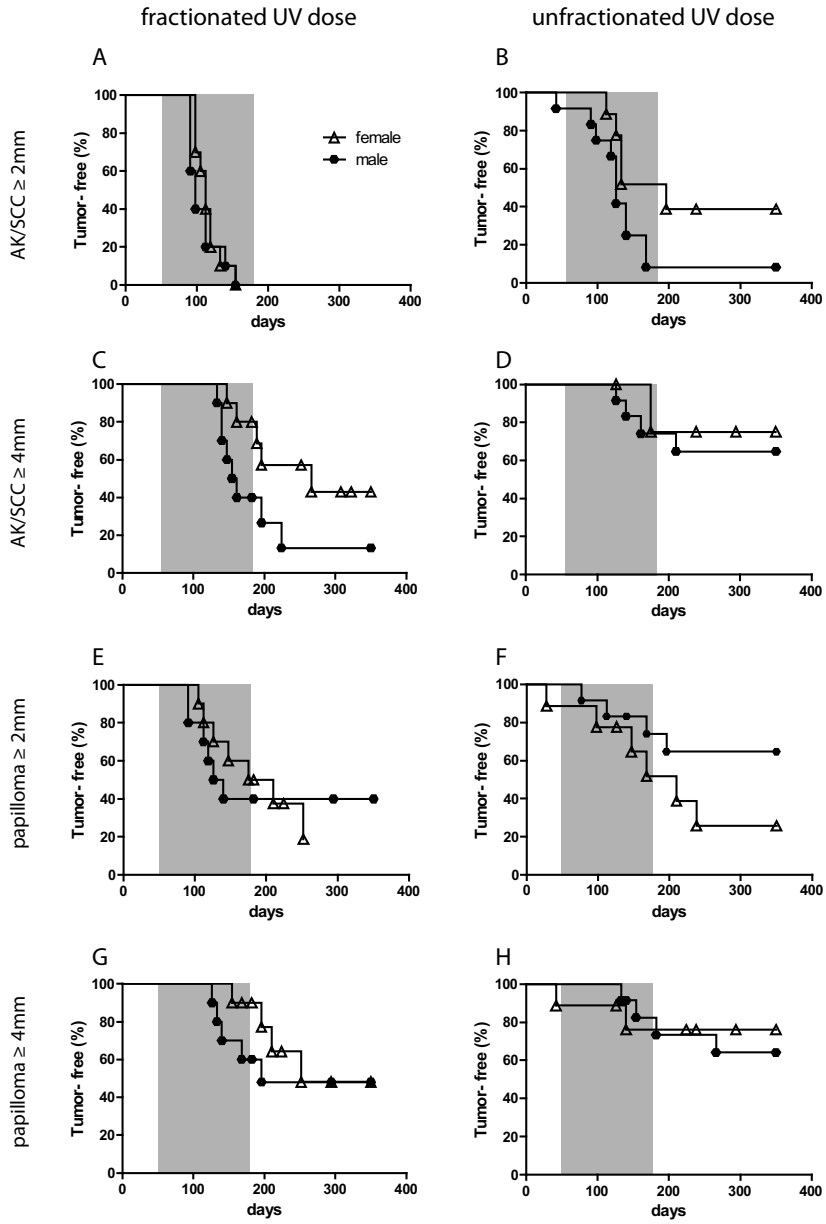
Gene	Forward primer	Reverse primer	PCR protocol*
P53 exon 4	CCCCTGTCATCTTTTGTCCC	TCAGGGCAAAACTAAACTCT	AT 55°C; 32 cycles
P53 exon 5	AGTTCCCCACCTTGACACCT	AGAGCAAGAATAAGTCAGAA	AT 55°C; 32 cycles
P53 exon 6	ACTGGCAGCCTCCCATCTCCC	GTCAACTGTCTCTAAGACGCA	AT 55°C; 32 cycles
P53 exon 7	GTAGGGAGCGACTTCACCTG	CAGAAGCTGGGGAAGAAACA	AT 55°C; 32 cycles
P53 exon 8	CTTGTGCTGGTCCTTTTCTTG	AGGAGAGAGCAAGAGGTGACT	AT 55°C; 32 cycles
Hras codon 12	AGTGTGCTTCTCATTGGCAG	GCAGGTAGGCAGAGCTCACC	TD 65°C>58°C +30x AT 60°C
Hras codon 61	CCCACTAAGCCGTGTTGTTT	TGGTGTTGTTGATGGCAAAT	TD 57°C>50°C +30x AT 52°C
Kras codon 12	TGTAAGGCCTGCTGAAAATG	GCACGCAGACTGTAGAGCAG	TD 65°C>58°C +30x AT 60°C
Kras codon 61	CCAGACTGTGTTTCTCCCTT	TGCCAACTTTCTTATTCAAC	TD 57°C>50°C +30x AT 52°C
Nras codon 12	GACTGAGTACAAACTGGTGG	CTCTATGGTGGGATCATATT	TD 65°C>58°C +30x AT 60°C
Nras codon 61	GGTGAGACCTGCCTGCTGGA	ATACACAGAGGAACCCTTCG	TD 65°C>58°C +30x AT 60°C
Notch1 Exon 2	GCTTTAATCTCCGTCCACCA	GGGCTCTGCTCTGACAAAAG	TD 65°C>58°C +30x AT 60°C
Notch1 Exon 3	CTGTGGCCATGAGAGATGAG	CTAAGGGTCCCAACCGTGA	TD 65°C>58°C +30x AT 60°C
Notch1 Exon 4	AAATCTGCCCTGGGTTCAC	GGACATGGACAACCAGGCTA	TD 65°C>58°C +30x AT 60°C
Notch1 Exon 5	TGTCCAGAGCAGAACATTGC	GCGGTGTGCAGTTTTGTTAG	TD 65°C>58°C +30x AT 60°C
Notch1 Exon 6	CAGAGCAGGGAGCTCATCTT	GTGGTGAGCCAACCAAGTTT	TD 65°C>58°C +30x AT 60°C
Notch1 Exon 9	CCCGTATGAGGGAGGGTTAT	CCTCAAAGGAGTCTGGGAAG	TD 65°C>58°C +30x AT 60°C
Notch1 Exon 12	AGTGGGTGGAAAAGGGTGAG	TGACACCCAGCTTGTGACAT	TD 65°C>58°C +30x AT 60°C
Notch1 Exon 13	GCTCTAGGAGGGGTAGGCTCT	GCCCAAGGCTACAGCTAGTC	TD 65°C>58°C +30x AT 60°C
Notch1 Exon 16	CCAGGCTCACTGGGTTCTAT	CTGACTTCCCATCCACCATC	TD 65°C>58°C +30x AT 60°C
Notch1 Exon 17	AGGGGAGAAGCACTGGAGAT	AGGCACCGAAACATAGGATG	TD 65°C>58°C +30x AT 60°C
Notch1 Exon 19	CCAGGTAGGCATGGAGTTGT	CTGGCCCTCTGAAGGTAGTG	TD 65°C>58°C +30x AT 60°C
Notch1 Exon 21	ATGGGCAGTAGTCCCGAGAG	GCAACACTCACGCTGATACC	TD 65°C>58°C +30x AT 60°C
Notch1 Exon 25	ACCTTTCACAGGCCACAGAC	CTGAGCCCTGGGACTCTAAA	TD 65°C>58°C +30x AT 60°C
Notch1 Exon 26	ATGTCTATCCCTGCCCATTG	CCTCCAGGGTTAAGCTGGTT	TD 65°C>58°C +30x AT 60°C
Notch1 Exon 27	GGGAGTCAGAGCTGGTGTGT	GGGATTTGAACCCTTGTCCT	TD 65°C>58°C +30x AT 60°C
Notch1 Exon 30	CCAAGTGATGAGGCTCTGCT	GGGAATGTGTGCATGTGTCT	TD 65°C>58°C +30x AT 60°C

Notch1 Exon 31	CCAGGGCTATGGTTGAATGT	CAAAATGCAGTGTGGAGGTG	TD 65°C>58°C +30x AT 60°C
Notch1 Exon 34.1	GCAGCACCTGCTTCCCTA	CTGCCATCTCAGGCTTGG	TD 65°C>58°C +30x AT 60°C
Notch1 Exon 34.2	AGTCACCCCATGGCTACTTG	CGGTTGTACATCTGCCTGAC	TD 65°C>58°C +30x AT 60°C
Notch1 Exon 34.3	CCTTGTCCCCGATTATTTACC	AAAAATGGAAATTCTTGTCCTCT	TD 65°C>58°C +30x AT 60°C
Notch1 Exon 7-8	GAAAAGCAGCACCCACTCAC	CCCTGCTGCCTGCTCTTAG	TD 65°C>58°C +30x AT 60°C
Notch1 Exon 10-11	AGCAACCAAGGGGTTAGGAT	GCATGACATGTGGTCAGCTT	TD 65°C>58°C +30x AT 60°C
Notch1 Exon 14-15	ATGTGGCCTTGTCCTCAGAC	TCAGCGAGGAACAGAACCTT	TD 65°C>58°C +30x AT 60°C
Notch1 Exon 23-24	AGGACAGAGCACAGTCAGCA	AAGAGTCGGTCAGGGTTCAG	TD 65°C>58°C +30x AT 60°C
Notch1 Exon 28-29	GATGGAGGAGAGTGGGTGAG	AGCAGAGCCTCATCACTTGG	TD 65°C>58°C +30x AT 60°C
Notch1 Exon 32-33	CAGGCTTGCATTTAGATCACC	TGCTGTTGTCCCAGACACTC	TD 65°C>58°C +30x AT 60°C
Notch2 Exon 2	GTGCAGGGGTGCTAAGAAAG	GCCAGCAACACTTCACAGAA	TD 65°C>58°C +30x AT 60°C
Notch2 Exon 3	CATCGTTTTCTGGTCTTTGGA	TGCACAGTACAGGTCACCAC	TD 65°C>58°C +30x AT 60°C
Notch2 Exon 4	GACAGAGCTGCTGAGTGTGG	TCTGGGAAGTACACCCTCCA	TD 65°C>58°C +30x AT 60°C
Notch2 Exon 5	TGCTGGGATATGCACTGAAA	CCCACTTTGCTAAGAGTTTCG	TD 65°C>58°C +30x AT 60°C
Notch2 Exon 6	GCTGTTAGGGTGCCAGTCAT	CTGCATTCCAGAATGGTCCT	TD 65°C>58°C +30x AT 60°C
Notch2 Exon 7	TGGTTCTGCTTTTGACAAGAAA	ACTTTCTGAGCCGACACGAC	TD 65°C>58°C +30x AT 60°C
Notch2 Exon 8	TGTCTTTGTGGGAACTCTGG	TCAGTGCATGGAGTCAGTGAG	TD 65°C>58°C +30x AT 60°C
Notch2 Exon 9	TGCACATTTTTGCTTCCTTG	GGGTTTTGGAGAGCACAGG	TD 65°C>58°C +30x AT 60°C
Notch2 Exon 10	ACCCCTTGGCATACACTCTG	CAGCTAGGGGAAGACAGTCG	TD 65°C>58°C +30x AT 60°C
Notch2 Exon 11	GGTGTAGACTCAGCGTGCTC	CACCAGACACAGAGCAGGAA	TD 65°C>58°C +30x AT 60°C
Notch2 Exon 12	AAGTGCTGACATTCCTGTGG	GAGCAGACTGCAAACCTTCC	TD 65°C>58°C +30x AT 60°C
Notch2 Exon 13	TAACCCCGTCCCTTGAGAAT	CCAACTGGGCCAATCAGTAA	TD 65°C>58°C +30x AT 60°C
Notch2 Exon 14	GGAAAGGTGAAACTGGCTTT	GGGTGTACCACAAGGGAAGA	TD 65°C>58°C +30x AT 60°C
Notch2 Exon 15	CACCAGGAGAGCTGGTGAGT	CTTGGAGACCACGAGTGACA	TD 65°C>58°C +30x AT 60°C
Notch2 Exon 16	AGTCTTGGGACGCCATCTTT	TTCCAGCTAGTCGCTCCCTA	TD 65°C>58°C +30x AT 60°C
Notch2 Exon 18	GGGTCATCTGCCTTCACAGT	GGTTCATCCTTGCCCTACAA	TD 65°C>58°C +30x AT 60°C
Notch2 Exon 19	CAGGGCCTCAGCTCACAC	CTACTGTGGGGAGCCAGGT	TD 65°C>58°C +30x AT 60°C
Notch2 Exon 22	GCTTAGTGGGATGGAAGCAA	TAGAGGGAATGTCCCTGGTG	TD 65°C>58°C +30x AT 60°C
Notch2 Exon 23	CGGGTTCAGTGGATTTTTGT	CCTAAGCTGGTCTTGGCTTG	TD 65°C>58°C +30x AT 60°C
Notch2 Exon 24	TCTGAGGCTGCTTCCTATCC	GGCTCAATCTCAGCTCCCTA	TD 65°C>58°C +30x AT 60°C
Notch2 Exon 25	GCCCTCACCTGTTGACTGAT	CCGAGCAGTTAGGAGCAAGA	TD 65°C>58°C +30x AT 60°C
Notch2 Exon 26	GAGGCTGCAGTGTGTTCTGA	TCAAAGTGCCCAGCTGTATG	TD 65°C>58°C +30x AT 60°C
Notch2 Exon 29	TTTGCCCAGCTGTAACCTCT	GGCTCCAGGAAAGACACACA	TD 65°C>58°C +30x AT 60°C
Notch2 Exon 30	CTGGAGGGCTCAGGTTAATG	ACCAGCCAGAACCATGGAG	TD 65°C>58°C +30x AT 60°C
Notch2 Exon 31	GGGTTAATTTGAATGTGTTTGC	CCACTGAGCCACCTCATCTT	TD 65°C>58°C +30x AT 60°C
Notch2 Exon 32	CAGGGACACCTCATTTGGAG	TCCTCTCAGAAGGGTAGCAAG	TD 65°C>58°C +30x AT 60°C
Notch2 Exon 33	TGACCTCATGCTGCTCTCTG	AGAGAGACACTGCTGTGAGCATA	TD 65°C>58°C +30x AT 60°C
Notch2 Exon 34.1	GAGGAAGCACTTAGGAAAAGCA	ATGTGGTGGTGGGATAGCAG	TD 65°C>58°C +30x AT 60°C
Notch2 Exon 34.2	GACTCTATCCCCCGTCGATT	TGGCACAATGGTCTGAGCTA	TD 65°C>58°C +30x AT 60°C
Notch2 Exon 34.3	CTTATCCCAAAAGGCAGCAT	CTGCGTCCTCCCCTAAAACT	TD 65°C>58°C +30x AT 60°C
Notch2 Exon 20-21	GAAGGCGTCCCTTTCTTTCT	CGGATGAACTCAGTAGCCAGT	TD 65°C>58°C +30x AT 60°C
Notch2 Exon 27-28	CAGACCTGACCCTTCGTTTC	ATGCCCATCTGCTCATCTCT	TD 65°C>58°C +30x AT 60°C

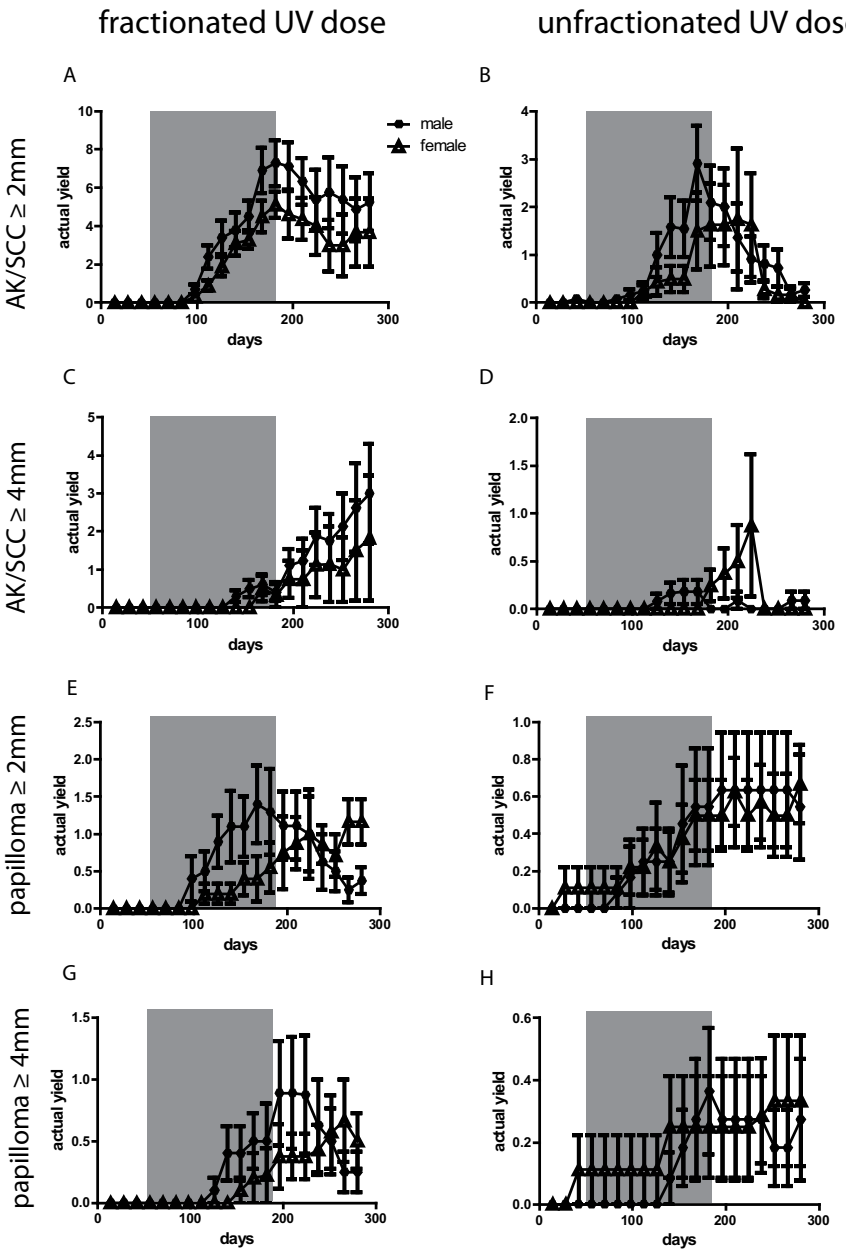
AT= Annealing temperature; TD= Touch down, lowering Annealing temperature over 7 cycles



Supplementary Figure S3.2: P53 patches developed after 40 days subsunburn UV and 8 weeks TPA application. Patch detected using the CM-5 antibody (A) or the Pab240 antibody (B).



Supplementary Figure S3.3: Gender differences in tumor-free survival. (Δ) female and (•) male. Result for fractionated UV in left column and unfractionated in right column, and for AK/SCC in top 4 panels and for papillomas in bottom 4 panels; for tumor sizes > 2 mm in A, B, E, F and > 4 mm in C D, G, H. The grey area in the graphs represent the period in which TPA was applied. Only AK/SCC ≥ 4 mm fractionated dose (C) shows borderline gender difference (p=0.06)



Supplementary Figure S3.4: Gender differences in tumor yields. (Δ) female and (•) male. Result for fractionated UV in left column and unfractionated in right column, and for AK/SCC in top 4 panels and for papillomas in bottom 4 panels; for tumor sizes > 2 mm in A, B, E, F and > 4 mm in C D, G, H. The grey area in the graphs represent the period in which TPA was applied. Error bars show SEMs; no significant differences.

Supplementary Table S3.2: Antibodies used for immunohistochemical staining of quiescent stem cells.

Target	Product number and company
Wif-1	EPR9385, Epitomics
Lrig1	AF3688, R&D
Dll-1	Ab10554, Abcam

Chapter 4

Lgr5^{+} stem cells and their progeny in mouse epidermis under regimens of exogenous skin carcinogenesis, and their absence in ensuing skin tumors

G.C. van de Glind, J.J. Out-Luiting, H.G. Rebel, C.P. Tensen, F.R. de Gruijl

Oncotarget. 2016 Aug 9;7(32):52085-52094

Abstract

Actively proliferating Lgr5$^+$ skin stem cells are found deep in the hair follicle (HF). These cells renew the HF and drive its expansion in anagen phase. Their long residence and continuous mitotic activity make them prime candidates to transform into skin tumor-initiating cells. This was investigated by subjecting Lgr5-EGFP-Ires-CreERT2/R26R-LacZ mice (haired and hairless) to chemical and UV carcinogenic regimens. In the course of these regimens Lgr5$^+$ cells (EGFP$^+$) remained exclusively located in HFs, and in deep-seated cysts of hairless skin. In haired mice, progeny of Lgr5$^+$ stem cells (LacZ$^+$ after a pulse of tamoxifen) appeared in the interfollicular epidermis upon UV-induced sunburn and in TPA-induced hyperplasia. In hairless mice the progeny remained located in deep-seated cysts and in HF remnants. Progeny in hairless skin was only detected interfollicularly at a late stage, in between outgrowing tumors. Lgr5$^+$ stem cells were virtually absent in the ultimate tumors, and no tumor appeared to be a (clonal) expansion of Lgr5$^+$ cells (52 tumors with tamoxifen at the start of carcinogenesis, 42 tumors with tamoxifen late during tumor outgrowth). In contrast to CD34/K15$^+$ quiescent bulge stem cells, actively proliferating Lgr5$^+$ stem cells do therefore not appear to be tumor drivers in experimental skin carcinogenesis.

4.1. Introduction

The skin protects our body against environmental insults. In order to remain vital and functional, the outermost layer, the epidermis, constantly renews itself from dedicated adult stem cells. Classically, these stem cells were thought to be rarely dividing 'quiescent stem cells' [1]. However, a novel class of continuously dividing stem cells, $Lgr5^+$, was found to drive epithelial turnover. These cells were first described for the intestine [2] and later also for the skin [3]. In the skin these $Lgr5^+$ stem cells are located in the lower part of the bulge and in the bulb of the hair follicle (HF), depending on the hair cycle phase. These stem cells renew the cells in the HF [3]. Upon wounding progeny of the $Lgr5^+$ stem cells migrate to the interfollicular epidermis (IFE), to replace damaged cells [4]. Lgr5 is a Leucine-rich repeat-containing G-protein-coupled receptor located on the cell membrane. Upon binding R-spondin Lgr5 enhances Wnt-signaling, with the *Lgr5* gene as one of the transcriptional targets [3].

By their very nature adult stem cells are long residing and divide to renew surrounding tissue. Consequently they are expected to run an increased risk of accumulating mutations, and thus become tumor stem cells or tumor initiating cells [5, 6]. We were therefore interested in how $Lgr5^+$ stem cells react to exogenic carcinogenic stimuli and whether they become initiating cells of skin carcinogenesis.

In studies on skin carcinogenesis mainly two experimental models are used. In one established model hairless mice are chronically UV-exposed to induce squamous cell carcinomas (SCCs). These tumors carry the typical UV-signature mutations in *p53* [7]. In the other classical 'two-stage' model tumors are initiated in the shaven skin of haired mice by a single application of a genotoxic agent, e.g. 7,12-Dimethylbenz[a]anthracene (DMBA). Tumor development is subsequently stimulated by repeated applications of a 'tumor promoter', a hyperplasia inducing irritant. Originally croton oil was used as a tumor-promoter, and later on its active ingredient, 12-*O*-Tetradecanoylphorbol-13-acetate (TPA) [8]. Besides hyperplasia of the IFE, TPA induces anagen in HFs of haired mice [9, 10], which would implicate $Lgr5^+$ stem cells.

Using the second model, mostly frank papillomas with *H-Ras* mutations develop [11, 12], and more rarely SCCs. We showed that the UV-induced SCCs originate from the IFE [13; Chapter 2]. Whereas an earlier study showed that chemically induced SCCs originate from the HFs [14]. Chemically induced skin tumors contain $CD34^+$ stem cells [15]. These cells are normally located in the bulge of HFs in haired mice (but not in hairless mice) [16]. The development of chemically induced skin tumors is impaired in CD34-null epidermis [17]. But despite the absence of $CD34^+$ bulge cells, hairless mice are susceptible to chemically induced skin tumors [18].

In this study we investigated $Lgr5^+$ stem cells and their progeny ("Lgr5 progeny" for short) under exogenous carcinogenic stimuli. We aimed to establish whether these cells drive the

outgrowth of skin tumors. To this end, we used Lgr5-EGFP-Ires-CreERT2 mice carrying a Rosa26-LacZ reporter in a haired as well as in a hairless background. We studied $Lgr5^+$ cells ($EGFP^+$) and their progeny ($LacZ^+$) in skin samples (cross sections, whole mounts and epidermal sheets): a) taken after a single UV overexposure, with massive apoptosis in the epidermal basal layer while overlying epidermis remained intact (i.e. no wounding), b) from sub-acute chronic UV and chemically induced hyperplasia and c) from UV and chemically induced tumors. A schematic overview including the time line of the experiments can be found in Supplementary Figure S4.1.

4.2. Materials and methods

4.2.1 Mice

Lgr5-EGFP-Ires-CreERT2 and RosaSOR-LacZ mice (Jackson Laboratories, Bar Harbor, USA) were crossed to incorporate the LacZ reporter for lineage tracing upon administering tamoxifen [3]. These Lgr5-EGFP-Ires-CreERT2/R26R-LacZ mice were also backcrossed into a hairless background using Crl:SKH1-HR hairless mice (Charles River, Sulzfeld, Germany).
Both male and female mice entered the experiments at 6-10 weeks of age (for each time point in the hyperplasia and ablation experiments n=4). They were kept individually in Macrolon type 1 cages at 25 ± 2^{o}C and about 50% humidity in a 12 hours light-12 hours dark cycle during experiments. The room in which the mice were kept and experiments were performed was illuminated by fluorescent tubes that did not emit any UV radiation. Standard chow and tap water were available ad libitum. As legally required, all mouse experiments were performed with the approval of the Leiden University Medical Centers' ethics committee for animal experiments (approval number DEC 10229) and executed according to EU regulations on animal experiments (Directive 2010/63/EU).

4.2.2. Experimental outline

A schematic overview of the experiments including time points of administering tamoxifen and of taking samples is presented in Supplementary Figure S4.1.

4.2.3. Cre activation by Tamoxifen

Mice received three i.p. injections of tamoxifen (5 mg/injection, T5648 Sigma-Aldrich, Zwijndrecht, The Netherlands) over three days to activate lineage tracing (LacZ-expressing cells) immediately prior to the start of the ablation and hyperplasia experiments. In the tumorigenesis experiments mice were divided into two groups: one group received tamoxifen injections at the start of the experiment and the other group received tamoxifen injections when two tumors ≥ 4 mm developed. The mice in this last group were sacrificed 2-3 weeks after activation of lineage tracing.

4.2.4. UV radiation

Philips TL-12/40W tubes were mounted over the cages and switched on and off automatically to deliver intended doses (output of 54% in UV-B, 280-315 nm, and 46% in UV-A, 315-400 nm). Under these lamps the minimal edema/erythemal dose (MED) was determined to be 900 and 500 J/m^2 UV for haired and hairless mice, respectively. To induce hyperplasia, mice were irradiated daily with 1 MED for 4-8 weeks. This same dose was used in the UV carcinogenesis experiments, where mice were daily irradiated until they had at least two ≥ 4 mm tumors. UV carcinogenesis was only performed with hairless mice (n=10, 5 early induction of lineage tracing and 5 late induction) as shaven haired mice (C57BL6) in our laboratory started wounding themselves by severe scratching after months of chronically UV exposure, before developing any skin tumors [19].
For the overexposure experiments we used a higher dose that was just tolerable (no wounds) but largely ablated the basal layer of the epidermis (for haired mice 3.6 MED and for hairless mice 5 MED; note that this amounts to approximately 3 kJ/m^2 UV for both mouse strains).

4.2.5. DMBA and TPA applications

For the chemocarcinogenesis experiments mice (haired: n=5 early induction of lineage tracing and n=5 late induction; hairless n=4 early induction and n=4 late induction) received a DMBA application (100 µg, 7,12-Dimethylbenz[a]anthracene, D3254, Sigma-Aldrich), on day 1. From day 8 onward they received TPA treatment (12-O-tetradecanoylphorbol-13-acetate, P8139, Sigma-Aldrich) twice a week until at least two ≥ 4 mm tumors developed. With each application, 10 µg TPA in acetone was applied on approximately 6 cm^2 of dorsal skin using a fine brush. Haired mice were priorly shaven to remove hair covering the dorsal skin. For the chemically induced hyperplasia experiments mice received TPA applications twice a week for 6 weeks.

4.2.6. Tissue preparation

Mice were sacrificed by CO_2 asphyxiation. Dorsal and ventral skin was isolated and prepared using different methods. Samples for the caspase-3, β-galactosidase, CD34 and Sox2 stainings were embedded in Tissue-tek, snap frozen in liquid nitrogen and stored at -80°C until sectioning and staining. Samples for the anti-EGFP staining were fixed overnight in PBS-buffered 4% formaldehyde solution (Addedpharma, Oss,The Netherlands) and embedded in paraffin. Whole mount biopsies were cut into pieces of 5x5 mm and incubated in 20 mM EDTA (Baker, Deventer, The Netherlands) in PBS O/N at 37°C. The next day, they were washed with PBS, fixed in PBS-buffered 4% formaldehyde solution for 5 min and incubated O/N with X-gal solution (1 mg/ml X-gal, 5 mM ferrothiocyanide, 5 mM ferrithiocyanide, 2 mM $MgCl_2$ in PBS). After incubation they were embedded in Kaisers glycerin.

Tumors were either snap frozen in liquid nitrogen or fixed in PBS-buffered 4% formaldehyde solution and embedded in paraffin.

4.2.7. Immunohistochemistry

Active caspase-3 Staining. Cryosections were cut at 6 µm thickness and fixed in acetone containing 0.3% H_2O_2. The sections were blocked with 2% Normal Human Serum (NHS) for 20 minutes. After blocking, the sections were incubated overnight at 4°C with anti-active caspase-3 (1:100, ab 2302, 3509322, Abcam, Cambridge, UK). The next day the sections were incubated for one hour with Goat-anti-Rabbit (IgG)-biotin (1:300, Vector Laboratories, Inc Burlingame, USA) followed by streptavidin (1:100, RPN1051v, GE Healthcare UK Limited) for 45 minutes. The staining was visualized with 20 mg 3,3'-Diaminobenzidine (D5905, Sigma-Aldrich, Zwijndrecht, The Netherlands) in 100 ml of PBS and 100 µl of H_2O_2. Sections were counterstained with haematoxylin and mounted in Kaisers' glycerin.

EGFP staining. Paraffin samples were cut at 5µm thickness and incubated at 60°C O/N. The next day, they were dehydrated and antigen retrieval was performed with antigen unmasking solution (H-3300, Vector Laboratories, Inc Burlingame, USA) in a pressure cooker for 5 min. Non-specific binding was blocked with PBS/0.1% Tween for 2 h followed by incubation with anti-EGFP (1:200, ab139070, Abcam, Cambridge, UK) at 4^{o}C O/N. The sections were incubated with secondary antibody Alexa Goat anti-chicken 488 (1: 250, Life technologies, Bleiswijk, The Netherlands) and nuclei were stained with DAPI for 5 min (1:3000, D1306, Invitrogen, Bleiswijk, The Netherlands). The sections were mounted with Vectashield mounting medium for fluorescence (H-1000, Vector Laboratories, Inc. Burlingame, USA).

ß-galactosidase staining. Cryosections were cut at 6 µm thickness and fixed with PBS-buffered 4% PFA (ROL 164810, AddedPharma, Oss, The Netherlands) for 10 min at RT. Sections were washed with PBS and with Rinse solution (2 mM $MgCl_2$, 0,01% NP40 in PBS) and incubated O/N at 37^{o}C with β-galactosidase staining solution (5 mM $K_3Fe(CN)_6$, 5 mM $K_4Fe(CN)_6 \bullet 3H_2O$, 1 mg/ml X-gal in Rinse solution). Sections were washed with rinse solution and counterstained with haematoxylin and eosin. Sections were dehydrated and embedded in Depex (18243.01, Serva Electrophoresis GmbH, Heidelberg, Germany).

CD34 staining. Cryosections embedded in Tissue-tek (Sakura Finetek Europe, Zoeterwoude, The Netherlands) were cut at 6 µm and dried on Superfrost Plus glass slides. The sections were fixed in acetone for 10 min and blocked with 2% normal goat serum (NGS, Dakocytomation, Heverlee, Belgium) and 1% BSA in PBS. Followed by incubation of anti-CD34 antibody (1:50, purified anti-mouse-CD34 14-0341-82, eBioscience, Vienna, Austria) in 2% goat serum and 1% BSA in PBS over night at 4°C. Goat-anti-Rabbit-Cy3 antibody

(1:500, 111-165-003, Jackson Immunoresearch Laboratories, Inc, West Grove, USA) in 1 % BSA in PBS was incubated for 1 hr at RT. Nuclei were labelled with DAPI (1:3000, D1306, Invitrogen, Bleiswijk, The Netherlands) for 2 min and sections were embedded with Vectashield (H-1000, Vector Laboratories, Burlingame, USA).

Sox2 staining. Frozen sections were cut at a thickness of 6 µm and fixed in paraformaldehyde in PBS for 30 min. The sections were incubated with blocking solution (1% BSA and 2% NGS in PBS) for 1 hr at RT. Subsequently, the sections were incubated with Rabbit anti-Sox2 antibody (1:500, Epitomics 2683-1, Abcam Cambridge, UK) overnight at 4°C. The following steps were the same as described above for the CD34 staining. So Goat-anti-Rabbit-Cy3 was used to visualize Sox2 and DAPI to visualize the nuclei, sections were embedded using Vectashield.
Negative controls were stained without first antibody to check for background signal.
Images were acquired using a Zeiss Axioplan 2 microscope with the 10x and 20x objectives, Axiocam camera and dedicated software for immunohistochemistry. For fluorescent pictures a Leica DM 5000B Microscope was used with 5x, 10x and 20x objectives and a Leica DFC300 FX Camera with dedicated software. Final pictures were formatted in Adobe Photoshop CS6 or Adobe Illustrator CS6 and representative cases are presented in Results.

4.3. Results

4.3.1. Lgr5 expressed in skin of hairless mice

Adult hairless SKH-1 mice do not have normal cycling HFs; their follicles seem to be frozen in catagen. The hair follicle remnants are connected by a hardly discernible string of cells to deep-seated cysts (putative outgrowths of bulbs) [13; Chapter 2]. Given these abnormal HFs, we were interested if hairless mice expressed Lgr5. In haired mice Lgr5 is normally expressed in the bulge and bulb regions of HFs (see Supplementary Figure S4.2). In hairless mice we found EGFP-expressing $Lgr5^+$ stem cells in the deep-seated cysts where, after tamoxifen-induced activation of Cre, their $LacZ^+$ progeny built up (see Supplementary Figure S4.2). Furthermore, we observed $Lgr5^+$ cells and their progeny cells higher up at the bottom of the hair follicle remnant (just below sebaceous glands), and in the string of cells running down to the cyst (Supplementary Figure S4.2 D).

4.3.2. $Lgr5^+$ stem cell progeny contributed to the repopulation of an ablated interfollicular basal layer in haired mice

We used a tolerable overdose of UV (3.6 MED for haired and 5 MED for hairless mice, see Materials and Methods) to ablate the epidermal basal layer [13; Chapter 2]. With this dose the basal layer became massively apoptotic (see Supplementary Figure S4.3), but the

overlaying cell layers stayed intact and thus no wounds occurred. We found the Lgr5$^+$ stem cells at successive time points after overexposure to be confined to the HFs, as in homeostasis: at the bottom (bulge or bulb regions) of HFs in haired mice (Figure 4.1). In hairless mice Lgr5$^+$ cells remained in the cysts and higher up at the bottom of hair follicle remnants (see Supplementary Figure S4.4 and data not shown). To trace Lgr5 progeny, tamoxifen was administered prior to UV overexposure. The progeny of Lgr5$^+$ stem cells in hairless mice remained restricted to the cysts and hair follicle remnants (see Supplementary Figure S4.4 and data not shown). However, in haired mice we observed Lgr5 progeny in the IFE: after 3 days progeny was limited to the rims of hair follicles and then clearly migrated into the IFE by 1 week after overexposure (see Figure 4.1I). But after two months progeny was almost completely lost from the IFE. In the controls without an ablating UV dose we did not find any Lgr5 progeny in the IFE (Figure 4.1F and Supplementary Figure S4.4E).

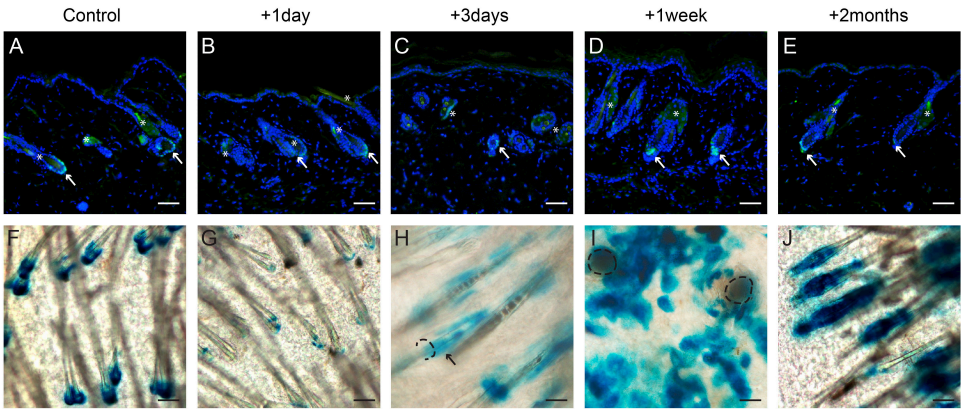


Figure 4.1: Lgr5$^+$ stem cells remain in their homeostatic location, but Lgr5 progeny repopulated the epidermal basal layer after UV overexposure in haired mice. Paraffin sections of control mice and mice that received an UV overexposure were stained with an anti-EGFP antibody (A-E); whole mounts (F-J) were stained for LacZ expression (representative pictures are shown). A+F show Lgr5$^+$ stem cells and their progeny in control mice without any UV exposure (homeostasis). B-E show the location of Lgr5$^+$ stem cells at different time points after UV overexposure; no differences were observed compared to the control mice (see arrows). G-J show the Lgr5 progeny at different time points after overexposure. One week after overexposure progeny clearly migrated out of the hair follicle into the epidermal basal layer (I), this was not observed in control mice. Hair follicle orifice (in H+I) contoured; and arrow in H points at rim staining. scale bar = 100 µm (in A-G and J), scale bar = 50 µm (H+I).

4.3.3. Progeny of Lgr5$^+$ stem cells migrated into the IFE after chemically induced hyperplasia.

Epidermal hyperplasia was induced in haired and hairless mice either by chronic subacute UV exposure or by TPA applications (see materials and Methods). Tamoxifen was administered prior to hyperplasia inducing regimen. The Lgr5$^+$ stem cells remained in their homeostatic location in haired and hairless mice (see Figure 4.2B + 4.2C for haired and

Supplementary Figure S4.4C + S4.4D for hairless mice). However, in haired mice the progeny of Lgr5^{+} stem cells migrated into the IFE in TPA-induced hyperplasia (see Figure 4.2F). This was not the case in UV-induced hyperplasia (Figure 4.2E), nor in hyperplasia in hairless mice up to 8 weeks of TPA or UV exposure (see Supplementary Figure S4.4G + S4.4H).

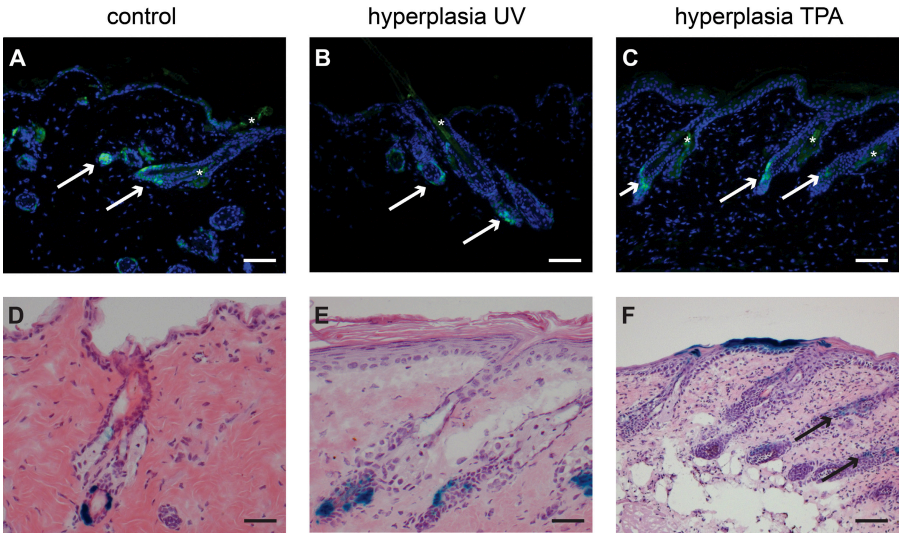


Figure 4.2: Lgr5 progeny migrates out of the hair follicle into the IFE after hyperplasia induced by TPA in haired mice**.** Paraffin sections of haired mice were stained with an anti-EGFP antibody (A-C) and frozen sections (D-F) were stained for LacZ expression (representative pictures are shown). B and C show the location of EGFP-expressing Lgr5^{+} stem cells after hyperplasia induced by UV (B) or chemically by TPA (C), the location is the same as in untreated control mice (A). After UV induced hyperplasia (E) the Lgr5 progeny was found in the same location as in de control mice (D). However, after TPA induced hyperplasia Lgr5 progeny migrated out of the hair follicle into the epidermal basal layer (F). scale bar = 100 µm (in A-C and F), scale bar = 50 µm (D+E) .

4.3.4. Interfollicular inter-tumoral Lgr5 progeny was present in both haired and hairless mice

We also investigated the uninvolved hyperplastic skin adjacent to tumors. In the haired mice subjected to chemocarcinogenesis (TPA treatment for > 6 months), we observed interfollicular Lgr5 progeny similar to what we found earlier in the chemically induced hyperplasia experiments (Figure 4.3A). Surprisingly, we detected interfollicular Lgr5 progeny in hairless mice as well at this stage between both chemo (Supplementary Figure S4.5) and UV tumors (Figure 4.3D).

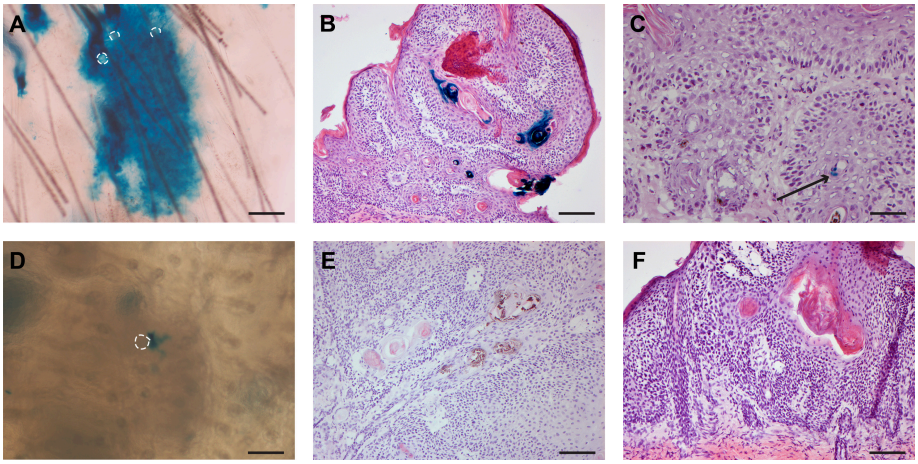


Figure 4.3: Progeny of Lgr5⁺ stem cells is (largely) absent in skin tumors; in hairless mice progeny of Lgr5⁺ stem cells migrated into the IFE only after prolonged treatment (over 6 months) with carcinogenic stimuli. Whole mount skin samples of haired mice after chemocarcinogenesis (A) and of hairless mice after UV-carcinogenesis (D) were stained for LacZ and showed interfollicular Lgr5 stem cell progeny. Hair follicle orifices contoured (dotted lines). Tumors were induced by chemocarcinogenesis (B+C) in haired mice or UV carcinogenesis (E+F) in hairless mice, respectively. LacZ lineage tracing was induced at the start of the experiment (B+E) or when tumors were formed (C+F), and tumor sections were stained for LacZ expression. Sparse inclusions of Lgr5 progeny in terminally differentiated parts were only observed in haired mice after chemocarcinogenesis when tracing was induced at the start of the experiment (B, some positivity seen near and in keratin pearls in 7/29 tumors). Scale bar in D = 50 µm, all other scale bars represent 100 µm.

4.3.5. Lgr5⁺ stem cells were not the tumor-driving cells in skin tumors

Our main interest in this study was to investigate the role of Lgr5⁺ stem cells in tumor formation in the skin. Therefore we subjected mice either to UV-induced skin carcinogenesis (only in hairless mice; see Materials and Methods) or chemically induced carcinogenesis using DMBA and TPA (both in hairless and haired mice); see Supplementary Table S4.2. Each group was divided into two; one group received tamoxifen injections to initiate lineage tracing at the beginning of the experiments and the other group received the injections when tumors (> 4 mm) had formed. Giving the injections at the beginning of the experiments enabled us to study clonal expansion of the Lgr5 progeny into the tumor. If so, the progeny should make up the complete tumor mass, resulting in entirely blue tumors after staining for LacZ. Injecting after the first tumors had occurred and subsequent tracing for 2-3 weeks would reveal whether Lgr5⁺ stem cells in the tumor were fueling the growth. Under the chemocarcinogenic regimen mainly (exophytically growing) papillomas developed in contrast to UV carcinogenesis where mainly (endophytically growing) SCCs developed. However, independent of tumor type we did not find any EGFP-positive cells in the tumor masses (n=32 tumors). Most Lgr5⁺ stem cells that we observed were located in

hair follicle-like structures below or neighboring the tumor mass and none in the tumor mass itself (data not shown). Correspondingly, progeny did not significantly contribute to the tumor mass; some sporadic minor $LacZ^+$ patches in terminally differentiated parts of the tumors were most likely inclusions. In the haired mice subjected to chemocarcinogenesis and traced from the beginning of the experiment, we detected some rare $LacZ^+$ keratin 'pearls' and sparse $LacZ^+$ cells in the outer most differentiated layer of the tumor (16 out of 29; see Figure 4.3B). Progeny was clearly present in neighboring HFs, but the bulk of the tumor mass was negative. In the group where the tracing was initiated when tumors had already formed, almost no Lgr5 progeny was found at all in the tumors (n=11, see Figure 4.3C). And again we did observe progeny in neighboring HFs. Tumors that developed in hairless mice did not show substantial Lgr5 stem cell progeny either, irrespective of the carcinogenic regimen (n= 54, see Figure 4.3E + 4.3F and Supplementary Figure S4.5).
A lack of Lgr5 expression in tumors could be due to promoter hypermethylation. Previously, LGR5 promoter hypermethylation was shown in colorectal cancer [20]. We therefore checked our skin tumors for hypermethylation of the relevant promoters, i.e of *Lgr5* and *Rosa*. We found no indication of hypermethylation of these promoters (see Supplementary Figure S4.6 for the methylation-specific melting curves and Supplementary Table S4.1 for used primers).

4.3.6. Stem cell markers CD34 and Sox2 are expressed in UV-induced skin tumors

Stem cell markers, CD34 and Sox2, are known to be expressed in chemically induced skin tumors. We were interested whether these markers were also expressed in UV-induced tumors. CD34 is expressed in the bulge region of the HF but is not expressed in the hair follicle remnants of hairless mice [16], while Sox 2 is expressed in the dermal papilla [21].
As depicted in Figure 4.4, CD34 was expressed in the proliferative compartment of chemically induced tumors in haired mice (15/21 tumors positive, Figure 4.4A). Surprisingly, the tumors induced in hairless mice also showed CD34 positivity but in the differentiated compartments and more granularly distributed than in the haired mice (Figure 4.4C) (8/10 positive of chemically induced tumors, data not shown; and 6/14 of UV-induced tumors). $Sox2^+$ cells were found in chemically and UV-induced tumors from both haired and hairless mice (Figure 4.4B + 4.4D; haired chem. 7/8 positive; hairless chem. 8/10 and hairless UV 10/11). However, Sox2 expression was apparently not restricted to stem cells as it was also observed in differentiated compartments of tumors (Figure 4.4B).

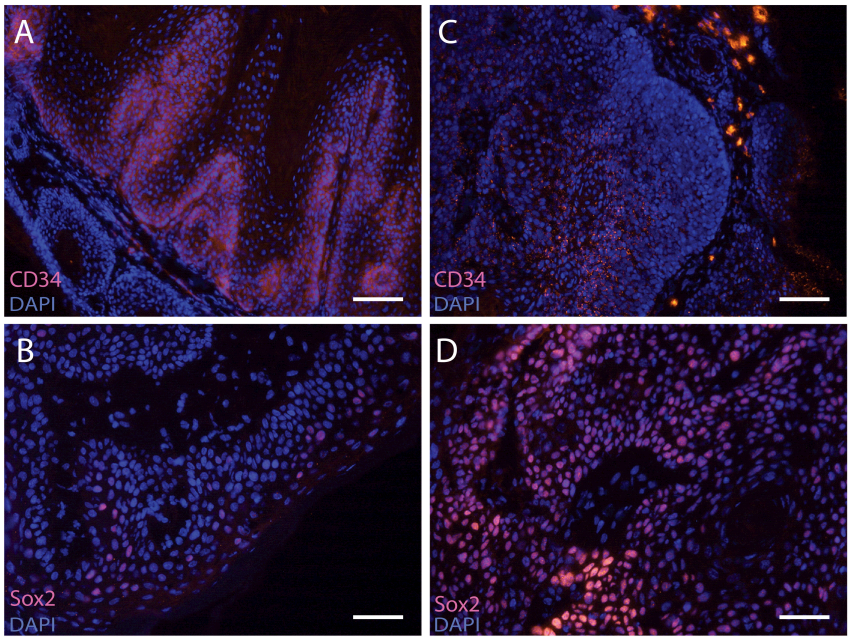


Figure 4.4: CD34 and Sox2 expression in skin tumors. Sections of tumors were stained with anti-CD34 (A+C) or anti-Sox2 (B+D). Both chemically induced tumors in haired mice (A+B) ($CD34^+$ 15 of 21 tumors and $Sox2^+$ 7 of 8 tumors) as well as UV-induced tumors in hairless mice (C+D) showed CD34 (6 of 14 tumors) and Sox2 expression (10 of 11 tumors). The CD34 expression in hairless mice was located in the differentiated compartments and more granular (C) compared to the haired mice. Scale bar = 100 µm.

4.4. Discussion

In this study we showed that Lgr5$^+$ stem cells remain in the hair follicle upon challenges with carcinogenic agents, but their progeny could end up in the IFE. The Lgr5$^+$ stem cells did not appear to become tumor-initiating cells in skin carcinogenesis by exogenous agents. With lineage tracing from the start of the skin carcinogenic regimen no tumors showed up completely stained blue from LacZ activity, which would have indicated a (clonal) expansion of Lgr5 progeny. A schematic depiction of the locations of Lgr5$^+$ stem cells and their progeny in the different experiments is given in Supplementary Figure S4.7.

Overall, the Lgr5$^+$ stem cells were mainly located at the bottom of the cycling HFs in haired mice: in the lower bulge region in telogen and in the bulb in anagen. As shown by Jaks et al. [3] the Lgr5$^+$ cells only partially overlapped with CD34$^+$ bulge cells in telogen, but not in anagen when Lgr5$^+$ cells were present in the bulb. We infer that the Lgr5$^+$ cells are more bulb-related than bulge-related stem cells as they migrate up and down in the hair cycle at the bottom of the HF. Furthermore, we are the first to show that hairless mice, lacking normal cycling HFs and CD34$^+$ bulge cells, do harbor Lgr5$^+$ stem cells in their skin. These cells and their progeny are located in cysts that appear to be expanded bulb remnants. At the point where a string of cells connected a cyst to a hair follicle remnant (just below the sebaceous glands) we also observed some Lgr5 expressing cells (see Supplementary Figure S4.4B and [13; Chapter 2]).

In haired mice the progeny of Lgr5$^+$ stem cells migrated to the interfollicular epidermis after UV-induced ablation of the epidermal basal layer and during chemically driven epidermal hyperplasia, but not during UV-driven hyperplasia up to 8 weeks. In the hairless mice however, no Lgr5 progeny appeared in the IFE in these experiments. Apparently, the location and activity of the Lgr5$^+$ stem cells in haired mice, enables these cells to contribute to the IFE if adequately stimulated. TPA can enter the orifices of HFs and easily reach the Lgr5$^+$ stem cells. This also explains the strong follicular hyperplasia not observed with sub-acute UV exposure. UV radiation cannot penetrate deeply into the HF thus leaving the Lgr5$^+$ stem cells unaffected. In hairless mice most of the Lgr5$^+$ cells reside in the deep-seated cysts which make them poorly accessible for both TPA and UV. The effect of UV on Lgr5$^+$ cells is most likely indirect, stemming from stress factors released higher up in the skin (most strongly after a severe sunburn). Not only are the deep-seated Lgr5$^+$ cells inaccessible, but their progeny has to pass through a narrow corridor over a large distance in order to reach the surface and migrate into the IFE. This combination of factors may explain why Lgr5 progeny emerged in the IFE of hairless mice only after prolonged carcinogenic stress, i.e. at a very late stage in between the tumors (see Figure 4.3A + 4.3D and Supplementary Figure S4.5A).

Previously, Kasper et al. described that after incisional wounding, involving the dermis, the Lgr5 progeny contributed to the repair of the epidermis [4]. They suggested that severe

damage (including a strong or long-lasting inflammatory response) is necessary to induce Lgr5 progeny to migrate into the IFE [4]. Here we show that loss of (only) the epidermal basal layer (in combination with an inflammatory skin reaction) appears to be a sufficient condition for Lgr5 progeny to migrate to the IFE to contribute to its repair.

In the tumors we did not observe any substantial clonal expansion of $Lgr5^+$ stem cells. Instead sparse remnants of progeny were found, most likely inclusions of wild type cells. We reasoned that our results might have been affected by methylation of CpG islands in the *Lgr5* or *Rosa* promoter. But we found no proof of methylation (see Supplementary Figure S4.6). Furthermore, we detected LacZ staining in nearly all of our samples in adjacent skin tissue. This served as an internal positive control, demonstrating that progeny was properly detected.

Kasper et al. [4] found Lgr5 stem cell progeny in interfollicular foci of basaloid hyperproliferation. They induced these lesions by activating the Hedgehog pathway in basal cells (K5tTA/TREGLI1) and by wounding. Without wounding and subsequent recruitment of Lgr5 progeny to the IFE, no Lgr5 progeny was found in the lesions. Progeny of $Lgr5^+$ stem cells was observed in BCC-like tumors only when these tumors were initiated from $Lgr5^+$ stem cells (Lgr5-creER^{T2}/Ptch$^{fl/fl}$) [4]. Da Silva-Diz et al. found some Lgr5 progeny in papillomas induced by HPV proteins expressed in basal cells [22]. In our chemocarcinogenesis experiments Lgr5 progeny was recruited to the IFE (see Figure 4.2F), but did not contribute to any significant extent to the ultimate tumor masses.

Liu et al. found up-regulation of LGR5 using Western Blots of human SCCs [23]. They used a polyclonal antibody that might have cross reacted with other (LGR) proteins, and they did not confirm their results with qPCR [23]. Furthermore, studies on the gene expression profiles of human SCCs have found no indication for the enrichment of LGR5-expressing cells [24, 25]. Hence, combined with our results we conclude that Lgr5 stem cells do not become tumor-initiating cells of cutaneous SCCs from exogenous carcinogens.

As reported earlier, we found $CD34^+$ cells in the proliferative compartment (bordering the stroma) of chemically induced skin tumors of haired mice. These cells were shown to display the features of tumor-initiating cells [15, 17], and in normal HFs they include the classical quiescent stem cells [1]. Hence, the $CD34^+$ bulge cells appear to be targeted in two-stage chemocarcinogenesis to become tumor-initiating cells. Actually, $K15^+$ bulge cells (overlapping $CD34^+$ cells) were shown by lineage tracing to drive the growth of chemically induced skin tumors [15].

Unexpectedly, we did find CD34 expression in the skin tumors from hairless mice, albeit aberrantly with a granular pattern in the differentiated cells; evidently not marking any tumor stem cells. Another marker expressed in various stem cells, transcription factor Sox2, was also found to be a driver of skin tumors [26]. In our experiments these cells were present to variable degrees in tumors induced chemically and by UV irradiation in hairless

and haired mice; sometimes mainly in differentiating cells clearly not marking stem cells (see Figure 4.4B).

We conclude that the novel class of continuously proliferating stem cells bearing the Lgr5 membrane receptor does not entail tumor-initiating cells in experimental skin carcinogenesis by exogenous agents (DMBA/TPA and UV radiation). In contrast, it has been established earlier that $CD34^+$ quiescent stem cells in the bulge are targets for transformation into tumor-initiating cells in chemocarcinogenesis [15, 17]. We have recently found indication that interfollicular quiescent stem cells may become initiating cells of persistently growing UV-induced skin tumors [27; Chapter 3]. These results suggest that the quiescent stem cells are more vulnerable to cancerous transformation than the actively cycling $Lgr5^+$ stem cells. The reason of this discrepancy between these two types of stem cells could be a difference in DNA repair capacity and apoptotic response, where DNA damage has been shown to accumulate and be retained over long periods of time in quiescent stem cells [14, 28].

Acknowledgements

We thank prof. Hans Clevers and his team for starting us up with the transgenic mice and analyses. Kamin M. Hau performed the first stainings and analyses. Wim H. Zoutman was invaluable in assisting us in the methylation experiments. Maria Kasper (Karolinska Institute, Stockholm, Sweden) is thanked for the protocol of robust LacZ staining on cryosections for lineage tracing without appreciable background, which was crucial to our study. Furthermore, we thank the technicians of the animal facility for animal care.

References

1. Cotsarelis G. Epithelial stem cells: a folliculocentric view. J Invest Dermatol. 2006; 126(7):1459-1468.
2. Barker N, van Es JH, Kuipers J, Kujala P, van den Born M, Cozijnsen M, Haegebarth A, Korving J, Begthel H, Peters PJ and Clevers H. Identification of stem cells in small intestine and colon by marker gene Lgr5. Nature. 2007; 449(7165):1003-1007.
3. Jaks V, Barker N, Kasper M, van Es JH, Snippert HJ, Clevers H and Toftgard R. Lgr5 marks cycling, yet long-lived, hair follicle stem cells. Nat Genet. 2008; 40(11):1291-1299.
4. Kasper M, Jaks V, Are A, Bergstrom A, Schwager A, Svard J, Teglund S, Barker N and Toftgard R. Wounding enhances epidermal tumorigenesis by recruiting hair follicle keratinocytes. Proceedings of the National Academy of Sciences of the United States of America. 2011; 108(10):4099-4104.
5. Tomasetti C and Vogelstein B. Cancer etiology. Variation in cancer risk among tissues can be explained by the number of stem cell divisions. Science. 2015; 347(6217):78-81.
6. Albini A, Cavuto S, Apolone G and Noonan DM. Strategies to Prevent "Bad Luck" in Cancer. J Natl Cancer Inst. 2015; 107(10).
7. Dumaz N, van Kranen HJ, de Vries A, Berg RJ, Wester PW, van Kreijl CF, Sarasin A, Daya-Grosjean L and de Gruijl FR. The role of UV-B light in skin carcinogenesis through the analysis of p53 mutations in squamous cell carcinomas of hairless mice. Carcinogenesis. 1997; 18(5):897-904.
8. Reddy AL and Fialkow PJ. Influence of dose of initiator on two-stage skin carcinogenesis in BALB/c mice with cellular mosaicism. Carcinogenesis. 1988; 9(5):751-754.
9. Cotsarelis G, Sun TT and Lavker RM. Label-retaining cells reside in the bulge area of pilosebaceous unit: implications for follicular stem cells, hair cycle, and skin carcinogenesis. Cell. 1990; 61(7):1329-1337.
10. Wilson C, Cotsarelis G, Wei ZG, Fryer E, Margolis-Fryer J, Ostead M, Tokarek R, Sun TT and Lavker RM. Cells within the bulge region of mouse hair follicle transiently proliferate during early anagen: heterogeneity and functional differences of various hair cycles. Differentiation. 1994; 55(2):127-136.
11. Quintanilla M, Brown K, Ramsden M and Balmain A. Carcinogen-specific mutation and amplification of Ha-ras during mouse skin carcinogenesis. Nature. 1986; 322(6074):78-80.
12. Sutter C, Strickland JE, Welty DJ, Yuspa SH, Winter H and Schweizer J. v-Ha-ras-induced mouse skin papillomas exhibit aberrant expression of keratin K13 as do their 7,12-dimethylbenz[a]anthracene/12-O-tetradecanoylphorbol-13-acetate -induced analogues. Mol Carcinog. 1991; 4(6):467-476.
13. Rebel HG, Bodmann CA, van de Glind GC and de Gruijl FR. UV-induced ablation of the epidermal basal layer including p53-mutant clones resets UV carcinogenesis showing squamous cell carcinomas to originate from interfollicular epidermis. Carcinogenesis. 2012; 33(3):714-720.
14. Morris RJ, Tryson KA and Wu KQ. Evidence that the epidermal targets of carcinogen action are found in the interfollicular epidermis of infundibulum as well as in the hair follicles. Cancer Res. 2000; 60(2):226-229.
15. Malanchi I, Peinado H, Kassen D, Hussenet T, Metzger D, Chambon P, Huber M, Hohl D, Cano A, Birchmeier W and Huelsken J. Cutaneous cancer stem cell maintenance is dependent on beta-catenin signalling. Nature. 2008; 452(7187):650-653.
16. Nijhof JG, Braun KM, Giangreco A, van Pelt C, Kawamoto H, Boyd RL, Willemze R, Mullenders LH, Watt FM, de Gruijl FR and van Ewijk W. The cell-surface marker MTS24 identifies a novel population of follicular keratinocytes with characteristics of progenitor cells. Development. 2006; 133(15):3027-3037.
17. Trempus CS, Morris RJ, Ehinger M, Elmore A, Bortner CD, Ito M, Cotsarelis G, Nijhof JG, Peckham J, Flagler N, Kissling G, Humble MM, King LC, Adams LD, Desai D, Amin S, et al.

CD34 expression by hair follicle stem cells is required for skin tumor development in mice. Cancer Res. 2007; 67(9):4173-4181.
18. Iversen OH. Hairless mouse skin in two-stage chemical carcinogenesis. Virchows Arch B Cell Pathol Incl Mol Pathol. 1982; 38(3):263-272.
19. Rebel H, der Spek CD, Salvatori D, van Leeuwen JP, Robanus-Maandag EC and de Gruijl FR. UV exposure inhibits intestinal tumor growth and progression to malignancy in intestine-specific Apc mutant mice kept on low vitamin D diet. Int J Cancer. 2015; 136(2):271-277.
20. Su S, Hong F, Liang Y, Zhou J, Liang Y, Chen K, Wang X, Wang Z, Wang Z, Chang C, Han W, Gong W, Qin H, Jiang B, Xiong H and Peng L. Lgr5 Methylation in Cancer Stem Cell Differentiation and Prognosis-Prediction in Colorectal Cancer. PLoS One. 2015; 10(11):e0143513.
21. Driskell RR, Giangreco A, Jensen KB, Mulder KW and Watt FM. Sox2-positive dermal papilla cells specify hair follicle type in mammalian epidermis. Development. 2009; 136(16):2815-2823.
22. da Silva-Diz V, Sole-Sanchez S, Valdes-Gutierrez A, Urpi M, Riba-Artes D, Penin RM, Pascual G, Gonzalez-Suarez E, Casanovas O, Vinals F, Paramio JM, Batlle E and Munoz P. Progeny of Lgr5-expressing hair follicle stem cell contributes to papillomavirus-induced tumor development in epidermis. Oncogene. 2013; 32(32):3732-3743.
23. Liu S, Gong Z, Chen M, Liu B, Bian D and Wu K. Lgr5-positive cells are cancer stem cells in skin squamous cell carcinoma. Tumour Biol. 2014; 35(11):11605-11612.
24. Hudson LG, Gale JM, Padilla RS, Pickett G, Alexander BE, Wang J and Kusewitt DF. Microarray analysis of cutaneous squamous cell carcinomas reveals enhanced expression of epidermal differentiation complex genes. Mol Carcinog. 2010; 49(7):619-629.
25. Hameetman L, Commandeur S, Bavinck JN, Wisgerhof HC, de Gruijl FR, Willemze R, Mullenders L, Tensen CP and Vrieling H. Molecular profiling of cutaneous squamous cell carcinomas and actinic keratoses from organ transplant recipients. BMC Cancer. 2013; 13:58.
26. Boumahdi S, Driessens G, Lapouge G, Rorive S, Nassar D, Le Mercier M, Delatte B, Caauwe A, Lenglez S, Nkusi E, Brohee S, Salmon I, Dubois C, del Marmol V, Fuks F, Beck B, et al. SOX2 controls tumour initiation and cancer stem-cell functions in squamous-cell carcinoma. Nature. 2014; 511(7508):246-250.
27. van de Glind G, Rebel H, van Kempen M, Tensen K and de Gruijl F. Fractionation of a tumor-initiating UV dose introduces DNA damage-retaining cells in hairless mouse skin and renders subsequent TPA-promoted tumors non-regressing. Oncotarget. 2016.
28. Mitchell DL, Volkmer B, Breitbart EW, Byrom M, Lowery MG and Greinert R. Identification of a Non-Dividing Subpopulation of Mouse and Human Epidermal Cells Exhibiting High Levels of Persistent Ultraviolet Photodamage. 2001; 117(3):590-595.

Supplementary Material

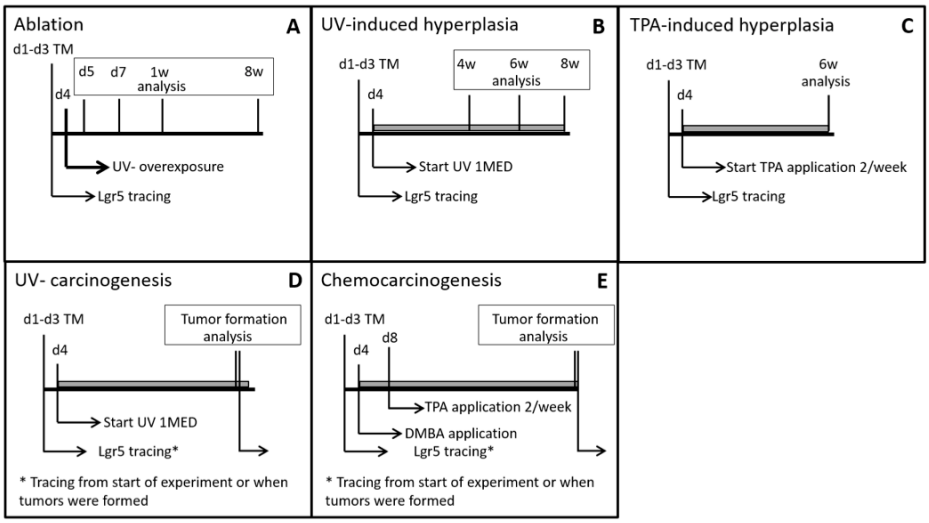
S4.1. Methods

S4.1.1. Methylation assay

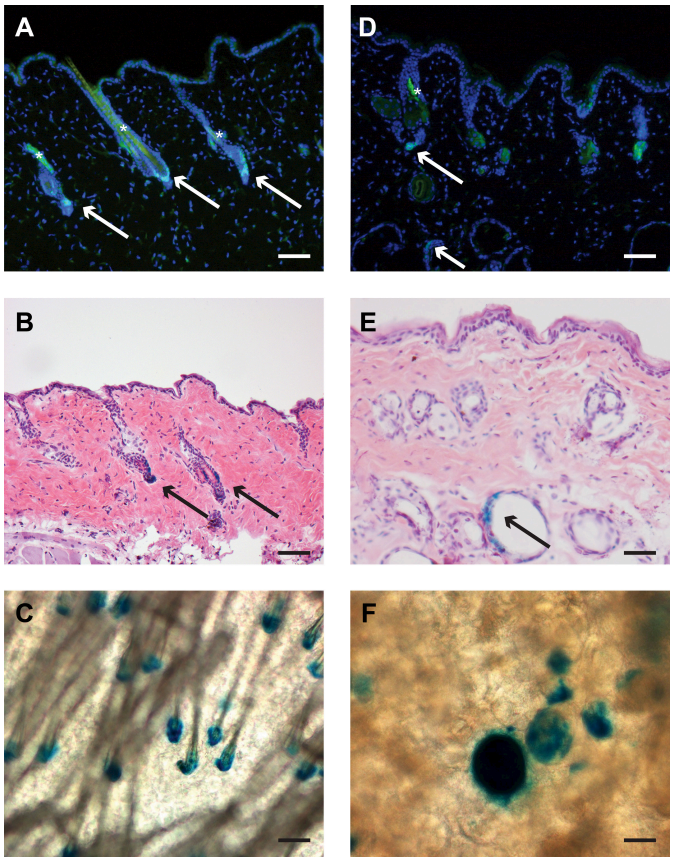
DNA was isolated from frozen tissue using the DNeasy kit (Qiagen) according to manufacturer's protocol. Bisulphite conversion of extracted DNA was performed using the EZ DNA methylation kit (Zymo Research, Orange, CA). Bisulphite primer sequences were designed to amplify the CpG island in the close proximity of the TSS of *Lgr5* and *Rosa*. Primers were developed in such a way that both methylated as well as unmethylated sequences were amplified using the same bisulphite-treated DNA as PCR template (Supplementary Table S1). Amplification was performed with iQ SYBR Green Supermix on a CFX384 Touch Real-Time PCR Detection System (Bio-Rad, Veenendaal, The Netherlands) using a touchdown PCR protocol with the following parameters: denaturing at 95°C for 30 seconds (ramp rate at 2°C per second), followed by 7 cycles of annealing at 65°C to 58°C for 40 seconds (with a 1°C decrement per cycle) and extension at 72°C for 40 seconds. For the following 33 cycles annealing was performed at 60°C. The last extension step at 72°C was extended to 3 minutes. Following amplification, melting curves were acquired during a linear temperature transition from 65 to 90°C with increments of 0.2°C per 10 seconds. Bisulfite primer sets were validated for gene specificity on bisulfite treated methylated CpGenome Universal Methylated Mouse DNA Standard (Millipore, Amsterdam, The Netherlands) and unmethylated WT C57BL/6 mice DNA as reference control sample.

Supplementary Table S4.1: Primers for methylation assay

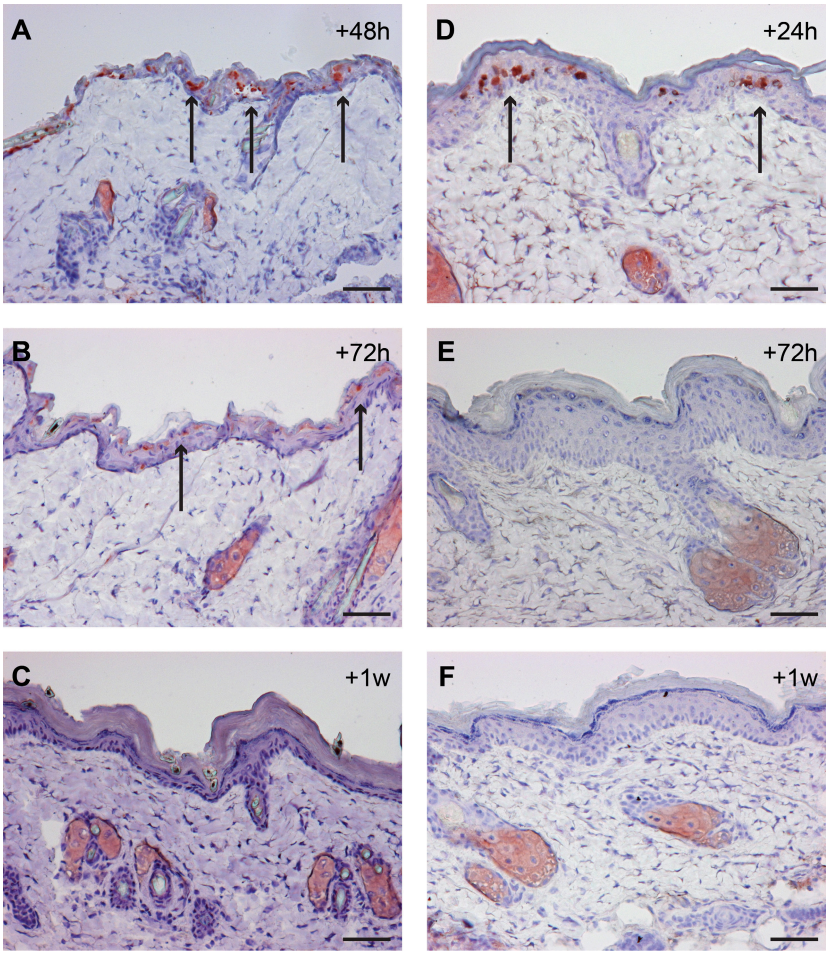
Gene	Primer sequence (5'-> 3')	Amplicon size	Number of CpG's	Relative to TSS	Tm unmethylated amplicon	Tm methylated amplicon
Lgr5	GGGTGTTTGGAAA GTAGGGTT	268 bp	22	-70 to +199	79.40 °C	82.8 °C
	CACCGACTTCTACA ACTCACCAAAC					
Rosa	GGTGTAATGGTGT GTAAAGGTAGTTG	192 bp	8	-684 to -493	78.8 °C	80.6 °C
	CCTAAATCAAAATA AAAATCCAACAAA					



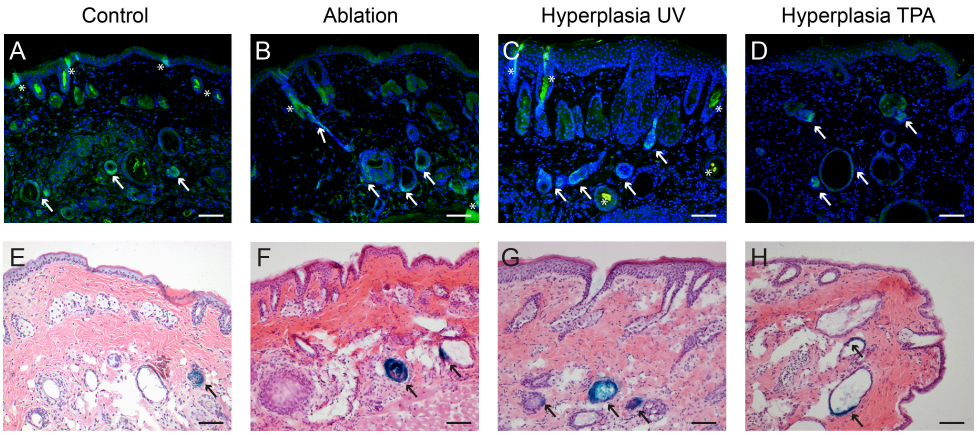
Supplementary Figure S4.1: Experimental outline. Time line of the experiments including time points of sample collection for analyses. TM= tamoxifen injection, d= day, w=week. In experiments A,B and C the lineage tracing started at the beginning of the experiment. In experiment D and E the tracing started either at the start of the experiment or when tumors were formed.



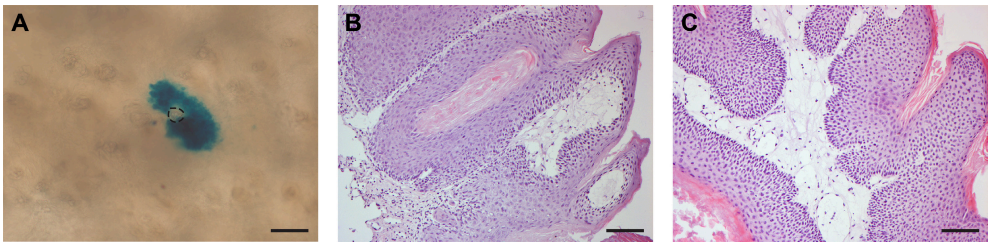
Supplementary Figure S4.2: In homeostasis Lgr5^{+} stem cells and progeny are present in the lower part of the hair follicles and in cysts. Skin sections of Lgr5-EGFP-Ires-CreERT2/R26R-LacZ haired (A-C) and hairless (D-F) mice were stained for EGFP (A+D) or LacZ expression (B, E, F after 8 weeks tracing, C after 4 weeks). Skin whole mounts in top view (C+F). EGFP expression representing Lgr5 stem cells was present in the lower part of the hair follicle in haired mice (A, see arrows) and in the hair follicle remnant and cysts of hairless mice (D, see arrows). LacZ lineage tracing shows the Lgr5^{+} stem cells and their progeny in haired (B+C) and hairless mice (E+F), in the lower part of the hair follicle and in cysts respectively. *= auto fluorescence from hairs. Scale bar in A, B, C, D, F = 100 µm, scale bar in E = 50 µm.



Supplementary Figure S4.3: Anti-caspase-3 staining showing apoptosis after UV overexposure and largely an ablation of the epidermal basal layer in either haired (A-C) or hairless mice (D-F). Anti-caspase-3 staining (red, see arrows) shows apoptotic cells. Pictures show different time points after UV overexposure. In hairless mice the apoptotic cells have already moved out of the epidermis 72h after overexposure (E), but in haired mice they are still present in the upper layer of the epidermis (B). At 1 week after overexposure no apoptotic cells are found anymore in haired or hairless skin (C+F). Scale bars = 50 µm.



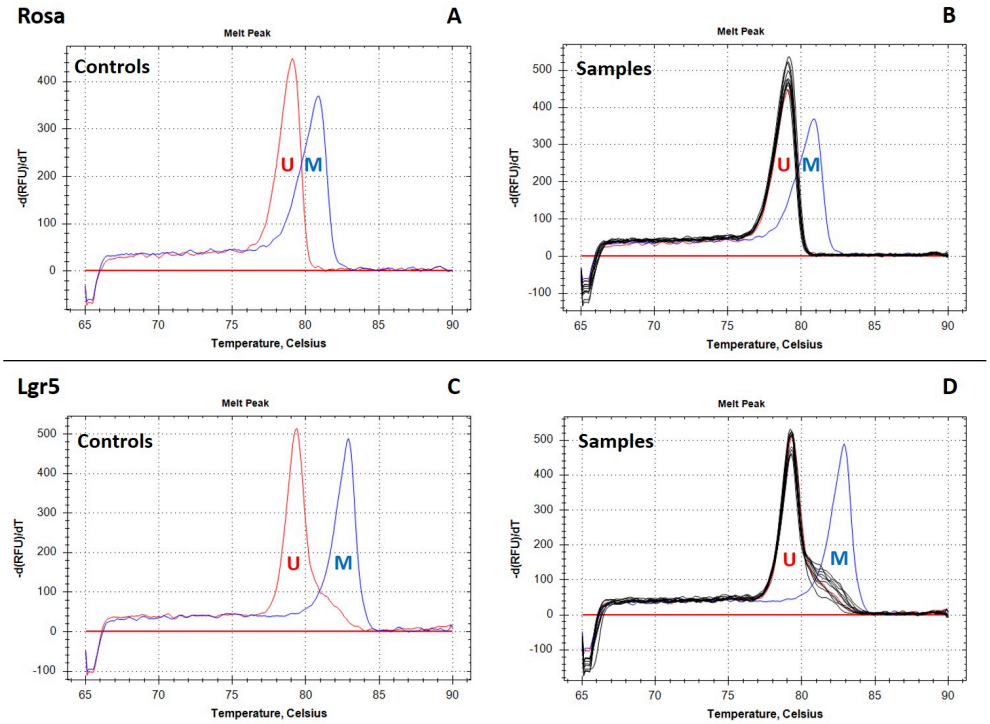
Supplementary Figure S4.4: Lgr5⁺ stem cells and their progeny remain in homeostatic positions in hairless mice over 8 weeks of treatment with either UV or TPA. Anti-EGFP staining was used to localize the Lgr5⁺ stem cells (A-D) and LacZ staining was used to localize their progeny (E-H). Lgr5⁺ stem cells and their progeny were found in the same locations after ablation (B+F), hyperplasia induced by UV (C+G) and hyperplasia induced by TPA (D+H); as in homeostasis (shown in the control mice, A+E). Representative pictures of the different experiments and the different time points are shown. Scale bar represents 100 µm.



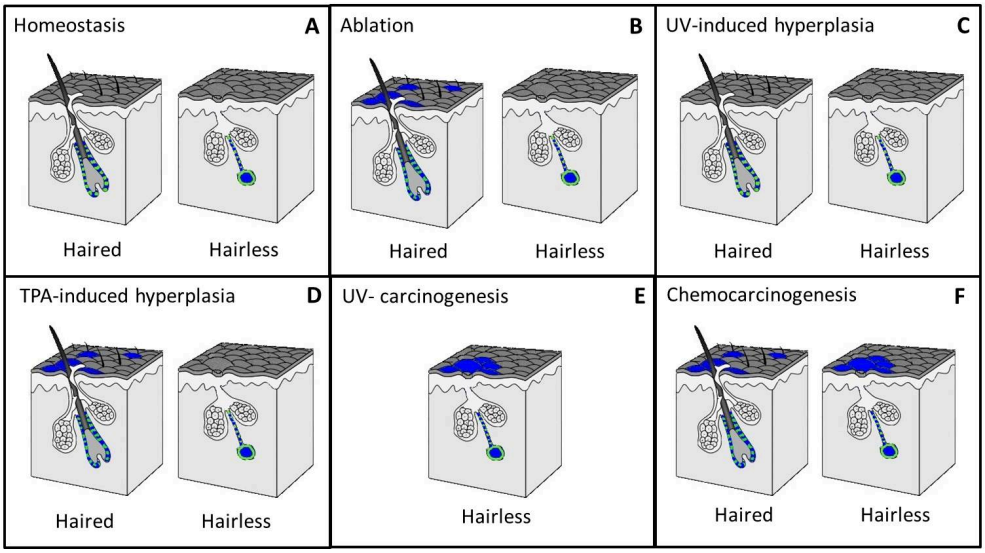
Supplementary Figure S4.5: Lgr5⁺ stem cell progeny is present in inter-tumoral skin but absent in chemically induced tumors in hairless mice. Samples of hairless mice subjected to chemocarcinogenesis were stained for LacZ⁺ cells. Whole mount inter-tumoral skin after chemocarcinogenesis (A) showed islands of Lgr5 progeny in the IFE. Hair follicle orifice contoured (A). Lineage tracing by LacZ activation was induced early, just before tumor initiation (B) or late when tumors were growing out (C). No Lgr5 progeny was found in these tumors. Scale bar = 100 µm.

Supplementary Table S4.2: Number of tumors stained for EGFP and LacZ

Regimen	# stained for EGFP	# stained for lacZ early injected	# stained for lacZ late injected
Haired chemocarcinogenesis	7	29	11
Hairless chemocarcinogenesis	6	11	15
Hairless UV-carcinogenesis	19	12	16



Supplementary Figure S4.6: Methylation-specific melting curve analysis (MS-MCA) shows absence of methylation of CpG sites in the *Lgr5* and *Rosa* promoter. MS-MCA of control samples showed either completely unmethylated (U) or methylated (M) bisulphite-converted DNA amplified with *Rosa* promoter specific primers (A) or *Lgr5* promoter specific primers (C) (see supplementary Table S4.1 for primers and their specific melting temperatures). B and D) combined MS-MCA melting curve profiles for 10 samples and controls plotted jointly in one graph, showing a single peak at the Tm for unmethylated DNA amplified with *Rosa* promoter specific primers (B) or *Lgr5* promoter specific primers (D).



Supplementary Figure S4.7: Schematic representation of the localization of $Lgr5^+$ stem cells (green) and their progeny (blue) in haired and hairless mice. The stem cells remained at the same location after treatment as during homeostasis (A-F). The progeny of $Lgr5^+$ stem cells was found interfollicularly in haired mice after ablation (B), TPA-induced hyperplasia (D) and chemocarcinogenesis (F). In hairless mice progeny of $Lgr5^+$ stem cells was only found in the IFE in between the tumors in the carcinogenesis experiments (E+F)

Chapter 5

Lgr6$^+$ stem cells and their progeny in mouse epidermis under regimens of exogenous skin carcinogenesis, and their absence in ensuing skin tumors

G.C. van de Glind, H.G. Rebel, J.J. Out-Luiting, W.H. Zoutman
C.P. Tensen, F.R. de Gruijl
Oncotarget. 2016 Dec 27;7(52):86740-86754

Abstract

Lgr6$^+$ cells have been identified as a novel class of proliferating (Ki67$^+$) stem cells in mouse epidermis. We investigated their response to UV exposure in *Lgr6-EGFP-Ires-CreERT2/R26R-LacZ* haired and hairless mice and whether they become initiating cells of UV- or chemically induced skin tumors. UV overexposure erased Lgr6$^+$ cells (EGFP$^+$) from the interfollicular epidermis (IFE), but - as after wounding - they apparently repopulated the IFE from the hair follicles. Under sub-sunburn chronic UV exposure, Lgr6$^+$ cells and their progeny (LacZ$^+$ after pulse of tamoxifen) diminished strongly in the IFE. Although the inter-tumoral IFE clearly showed Lgr6 progeny, none of the UV- or chemically induced tumors (n=22 and 41, respectively) appeared to be clonal expansions of Lgr6$^+$ stem cells; i.e. no Lgr6$^+$ cells or progeny in the proliferating tumor bulk. In checking for promoter methylation we found it to occur stochastically for the *EGFP-Cre* cassette. *Lgr6* mRNA measured by qPCR was found to be diminished in skin tumors (also in UV tumors from wt type mice). The ratio of *Lgr6/Ki67* was significantly reduced, pointing at a loss of Lgr6$^+$ cells from the proliferative pool. Our data show that Lgr6$^+$ cells are not major tumor-initiating cells in skin carcinogenesis.

5.1. Introduction

Skin cancer is the most common cancer in white-skinned European ancestral populations; the incidence of non-melanoma (squamous cell carcinoma and basal cell carcinoma) and melanoma skin cancer is rising [1, 2]. UV exposure plays an important role in the etiology of these skin cancers [3, 4]. Cancer is a multistep process (multiple 'hits' or mutations) that eventually results in a malignant cell sprouting into a cancerous growth [5]. Since stem cells are long residing cells, these cells are prime candidates to accumulate oncogenic changes over time. One of the more recently identified stem cell populations in the skin is that of Lgr6$^+$ cells [6]. We therefore posed the question whether these stem cells are targeted in experimental skin carcinogenesis by exogenic agents.

Lgr6$^+$ stem cells are located in the isthmus region of the hair follicle (HF), in the sebaceous gland (SG) and in the interfollicular epidermis (IFE) [6-9]. Snippert et al. identified these stem cells in the skin and found that they are a unique population not expressing CD34 or K15 [6]. The Lgr6$^+$ cells in the IFE, isthmus and SG are able to maintain their respective compartments in the long term [9]. It was recently shown that Lgr6$^+$ cells increase in numbers in the IFE of mice from birth to adulthood (8 weeks of age) [9]. Like its family members Lgr4 and 5, the Lgr6 receptor (leucine-rich repeat-containing G protein-coupled receptor 6) contains a seven transmembrane region and an ectodomain with 13 leucine-rich repeats [10], and after binding R-spondin it can enhance canonical Wnt/β-catenin signaling [11].

We have previously demonstrated that experimental, UV-induced squamous cell carcinomas (SCCs) originate from the IFE [12; Chapter 2]. A recent study of ours [13; Chapter 3] implicated quiescent stem cells in UV-induced tumor initiation. These cells accumulate and retain DNA damage (cyclobutane pyrimidine dimers) during low level chronic UV exposure, which increases the risk of mutagenesis when these cells are forced to divide. Additionally, the continuously actively dividing Lgr6$^+$ stem cells in the IFE are likely UV-targeted candidate cells from which SCCs may originate. To investigate this latter possibility we carried out experiments on how these Lgr6$^+$ stem cells and their progeny respond to UV radiation and whether they drive UV carcinogenesis. Next to UV carcinogenesis, the Lgr6$^+$ stem cells may be targeted in chemical skin carcinogenesis, which we studied in additional experiments.

The established model for UV carcinogenesis is chronic UV exposure of SKH-1 hairless mice [14]. After daily genotoxic challenges from sub-sunburn UV dosages these mice develop SCCs similar to those in humans. These tumors in mice harbor UV-signature mutations in *p53* similar to those in SCCs in humans [15]. The widely used model for chemical skin carcinogenesis is the two-stage model: a single application of a genotoxic agent (e.g. 7,12-Dimethylbenz[a]anthracene, DMBA) initiates tumors and subsequent repeated applications of a (non-genotoxic) irritant (most commonly 12-O-Tetradecanoylphorbol-13- acetate, TPA)

promotes further tumor development (outgrowth) [16]. The tumors that develop are mainly papillomas with *H-Ras* mutations [17, 18] and to a much lesser extent SCCs. We have used both models to investigate the role of $Lgr6^+$ stem cells and their progeny in skin carcinogenesis.

In the present study we used hairless and shaven haired heterozygous transgenic *Lgr6-EGFP-Ires-CreERT2/R26R-LacZ* mice containing a *Rosa26-LacZ* reporter for lineage tracing. Lgr6-expressing cells were $EGFP^+$ and, after administering tamoxifen, the progeny could be detected as $LacZ^+$ cells (i.e. with β-galactosidase activity which cleaves X-gal leaving a blue product). These transgenic mice were subjected to genotoxic UV regimens that are physiologically relevant to humans. One regimen was daily sub-acute exposure for 4-8 weeks inducing epidermal hyperplasia, and the other regimen was a single tolerable UV overexposure that largely ablated the epidermal basal layer by apoptosis but left the overlying layers intact (i.e. no wounding). In the UV carcinogenesis experiments the hyperplasia-inducing UV regimen was prolonged to develop tumors in hairless mice (see Materials and Methods). Haired and hairless mice subjected to chemical carcinogenesis received a single initial DMBA application followed by TPA applications twice a week. We studied skin samples (cross sections, whole mounts and epidermal sheets) and tumor samples to investigate the response of $Lgr6^+$ stem cells and their progeny ("Lgr6 progeny" for short) to the ablative and carcinogenic regimens (see time lines for the different experiments in Supplementary Figure S5.1).

5.2. Materials and methods

5.2.1. Mice

Lgr6-EGFP-Ires-CreERT2 (a kind gift of Prof. Hans Clevers) and Cre reporter *R26R-LacZ* mice (Jackson Laboratories, Bar Harbor, USA) were crossed to incorporate the LacZ reporter under the control of the Rosa (*R26R*) promoter for lineage tracing upon administering tamoxifen [6]. These *Lgr6-EGFP-Ires-CreERT2/R26R-LacZ* mice were also backcrossed into a hairless background using Crl:SKH1-HR hairless albino mice (Charles River, Sulzfeld, Germany).

Both male and female mice entered the experiments at 6-10 weeks of age (for each time point in the hyperplasia and ablation experiments n=4). They were kept individually in Macrolon type 1 cages at 25 ± 2°C and about 50% humidity in a 12 hours light-12 hours dark cycle during experiments. The room in which the mice were kept and experiments were performed was illuminated by fluorescent tubes that did not emit any UV radiation. Standard chow and tap water were available ad libitum. As legally required, all mouse experiments were performed with the approval of the Leiden University Medical Centers's ethics committee (approval number DEC 10229).

5.2.2. Experimental outline

A schematic overview of the experiments including time points of administering tamoxifen and of taking samples is presented in Supplementary Figure S5.1.

5.2.3. Cre activation by Tamoxifen

Mice received three i.p. injections of tamoxifen (5 mg/injection, T5648 Sigma-Aldrich, Zwijndrecht, The Netherlands) over three days to activate lineage tracing (LacZ-producing cells) immediately prior to the start of the ablation and hyperplasia experiments. In the tumorigenesis experiments mice were divided into two groups: one group received tamoxifen injections at the start of the experiment, before the carcinogenic regimen, and the other group received tamoxifen injections when two tumors ≥ 4 mm developed. The mice in this last group were sacrificed 2-3 weeks after activation of lineage tracing.

5.2.4. UV radiation

Philips TL-12/40W tubes were mounted over the cages and switched on and off automatically to deliver intended doses (output of 54% in UV-B, 280-315 nm, and 46% in UV-A, 315-400 nm). Under these lamps the minimal edema/erythemal dose (MED) for a naïve (previously unexposed) skin was determined to be 900 and 500 J/m^2 UV for haired and hairless mice, respectively. To induce hyperplasia, mice were irradiated daily with 1 MED for 4-8 weeks, which induced no sign of sunburn (mice adapt to UV exposure). This same dose was used in the UV carcinogenesis experiments, where mice were daily irradiated until they had at least two ≥ 4 mm tumors. UV carcinogenesis was only performed with hairless mice (n=13, 5 for early induction of lineage tracing and 8 for late induction) as shaven haired mice (C57BL6) in our laboratory started wounding themselves by severe scratching after months of chronically UV exposure, before developing any skin tumors [19]. For the overexposure experiments we used a higher dose that was just tolerable (no wounds) but largely ablated the basal layer of the epidermis (for haired mice 3.6 MED and for hairless mice 5 MED, 3.2 and 2.5 kJ/m^2 UV respectively; i.e. quite similar).

5.2.5. DMBA and TPA applications

For chemical carcinogenesis mice (haired: n=4 for early induction of lineage tracing and n=6 for late induction; hairless n=5 for early induction and n=4 for late induction) received a DMBA application (100 µg, 7,12-Dimethylbenz[a]anthracene, D3254, Sigma-Aldrich), on day 1 and from day 8 onward TPA treatment (12-O-tetradecanoylphorbol-13-acetate, P8139, Sigma-Aldrich) twice a week until at least two ≥ 4 mm tumors developed. With each application, 10 µg TPA in 100 µl acetone was applied on approximately 6 cm^2 of dorsal skin using a fine brush. Haired mice were priorly shaven to remove hair covering the dorsal skin.

5.2.6. Tissue preparation

Mice were sacrificed by CO_2 asphyxiation. Dorsal and ventral skin was excised and segmented for use in different histochemical stainings. Samples for the anti-caspase-3 and β-galactosidase staining were embedded in Tissue-tek, snap frozen in liquid nitrogen and stored at -80°C until sectioning and staining. Samples for the anti-EGFP staining were fixed overnight in PBS-buffered 4% formaldehyde solution (ROL1642810, Addedpharma, Oss,The Netherlands) and embedded in paraffin. Whole mount skin biopsies for LacZ lineage tracing were cut into pieces of 5x5 mm and incubated in 20 mM EDTA (Baker, Deventer, The Netherlands) in PBS O/N at 37°C. The next day, they were washed with PBS, fixed in PBS-buffered 4% formaldehyde solution for 5 min and incubated O/N with X-gal solution (1 mg/ml X-gal, 5 mM ferrothiocyanide, 5 mM ferrithiocyanide, 2 mM $MgCl_2$ in PBS). After incubation they were embedded in Kaisers glycerin. Epidermal sheets for LacZ staining were treated similar to the whole mounts. Skin was excised, fatty tissue was removed, and samples were submerged for 2 hrs in 20 mM EDTA in PBS at 37°C. After incubation the epidermal sheet was pealed from the dermis and was fixed for 5 min in PBS-buffered 4% formaldehyde solution and stained according to the protocol of the whole mount biopsies. Clusters of LacZ positive cells in an epidermal sheet were counted in 10 microscopic frames at 10X objective (2 mm cross section).
Tumors were either snap frozen in liquid nitrogen or fixed in PBS-buffered 4% formaldehyde solution and embedded in paraffin.

5.2.7. Immunohistochemistry

EGFP staining. Paraffin samples were cut at 5 µm thickness and incubated at 60°C O/N. The next day, they were dehydrated and antigen retrieval was performed with antigen unmasking solution (H-3300, Vector Laboratories, Inc Burlingame, USA) in a pressure cooker for 5 min. Non-specific binding was blocked with PBS/0.1% Tween/1% BSA for 2 h followed by incubation with anti-EGFP (1:200, ab139070, Abcam, Cambridge, UK) at 4°C O/N. The sections were incubated with secondary antibody Alexa Goat anti-chicken 488 (1: 250, Life technologies, Bleiswijk, The Netherlands) and nuclei were stained with Dapi for 5 min (1:3000, D1306, Invitrogen, Bleiswijk, The Netherlands). The sections were mounted with Vectashield mounting medium for fluorescence (H-1000, Vector Laboratories, Inc. Burlingame, USA).

ß-galactosidase/LacZ staining. Cryosections were cut at 6 µm thickness and fixed with 4% PFA in PBS (P6418, Sigma Aldrich, Steinheim, Germany) for 10 min at RT. Sections were washed with PBS and with Rinse solution (2 mM $MgCl_2$, 0,01% NP40 in PBS) and incubated O/N at 37°C with β-galactosidase staining solution (5 mM $K_3Fe(CN)_6$, 5 mM $K_4Fe(CN)_6 \bullet 3H_2O$, 1 mg/ml X-gal in Rinse solution). Sections were washed with rinse solution and

counterstained with haematoxylin and eosin. Sections were dehydrated and embedded in Depex (18243.01, Serva Electrophoresis GmbH, Heidelberg, Germany).
Images were acquired using a Zeiss Axioplan 2 microscope with 10x and 20x objectives, Axiocam camera and dedicated software for immunohistochemistry. For fluorescent pictures a Leica DM 5000B Microscope was used with 5x, 10x and 20x objectives and a Leica DFC300 FX Camera with dedicated software. Final pictures were formatted in Adobe Photoshop CS6 or Adobe Illustrator CS6 and representative cases are presented in Results.

5.2.8. CLSM

For confocal microscopy of fluorescent EGFP$^+$ cells epidermal sheets were prepared by incubating skin for 2 hrs in 20 mM EDTA (Baker, Deventer, The Netherlands) in PBS at 37°C. After incubation the epidermis and dermis were separated. The epidermis was fixed for 10 min in 4% paraformaldehyde and embedded in Vectashield containing DAPI (H1200, Vector Laboratories, Burlingame, U.S.A). Pictures were taken using the LSM 700 confocal microscope (Zeiss) with the LCI Plan-Neofluar 25x objective/0.8 Imm Korr DIC M27.
The area of EGFP$^+$ cells was calculated using the CLSM data and ImageJ. We measured the area (number of pixels) of DAPI$^+$ cells (after smoothening the nuclear fluorescence to create a contiguous area of DAPI$^+$ cells) in a z-stack plane and the area of EGFP$^+$ cells in the same plane for multiple samples/frames from 2-3 mice. From those data we calculated the percentage of the total area that was EGFP$^+$.

5.2.9. Methylation specific melting curve analysis (MS-MCA)

DNA was isolated from frozen tissue using the DNeasy kit (Qiagen, Hilden, Germany) according to manufacturer's protocol. Bisulphite conversion was performed on 1 µg DNA using the EZ DNA methylation kit (Zymo Research, Orange, CA). Bisulphite primer sequences were designed to amplify part of the CpG island located in the gene body of *Lgr6,* +245 to +371 bp downstream of the TSS (NM_001033409.3). Primers were developed in such a way that both methylated as well as unmethylated sequences were amplified using the same bisulphite-treated DNA as PCR template (Supplementary Table S5.1). Amplification was performed with iQ SYBR Green Supermix on a CFX384 Touch Real-Time PCR Detection System (Bio-Rad, Veenendaal, The Netherlands) using a touchdown PCR protocol with the following parameters: denaturing at 95°C for 30 seconds (ramp rate at 2°C per second), followed by 7 cycles of annealing at 65°C to 58°C for 40 seconds (with a 1°C decrement per cycle) and extension at 72°C for 40 seconds. For the following 33 cycles annealing was performed at 60°C. The last extension step at 72°C was extended to 3 minutes. Following amplification, melting curves were acquired during a linear temperature transition from 65 to 90°C with increments of 0.2°C per 10 seconds. Bisulfite primer sets were validated for gene specificity on bisulfite treated methylated CpGenome Universal Methylated Mouse

DNA Standard (Millipore, Amsterdam, The Netherlands) and unmethylated wt C57BL/6 mice DNA as reference control sample. The presence of methylated DNA was detected through melting peaks with higher melting curve temperatures compared to unmethylated DNA as obtained from the reference control samples. Melting peaks were detected by CFX manager 3.1 software (Bio-Rad) and average melting temperatures were calculated for these recognized peaks. A promoter was considered methylated if melting temperatures were exceeding half of the maximum temperature difference as determined for the reference control samples.

5.2.10. Quantitative real-time PCR (qPCR)

Total RNA was isolated from frozen skin and tumors using the RNeasy mini kit (74106, Qiagen, Hilden, Germany) including on-column DNase treatment. cDNA was synthesized from 1 µg total RNA using the iScript™ cDNA Synthesis Kit (170-8891, Biorad, Veenendaal, The Netherlands) according to manufacturer's instructions. qPCR for Lgr6 mRNA was performed using the SYBR Green Supermix (Bio-Rad) on the CFX384™ real-time PCR detection system (Biorad). Cycle parameters were as follows: Hot start for 3 minutes at 95°C; denaturation for 15 seconds at 95°C, annealing and extension for 30 seconds at 60°C for 40 cycles. Specificity of the PCR products was confirmed by melting curve analysis. Data was normalized against reference genes Cyc1 and Ddx52 (see Supplementary Table S5.3 for primers used) using the ΔΔCq method [20] and is presented as relative mRNA expression.

5.2.11. Data processing and statistical analyses

Statistical significant differences in $EGFP^+$ areas and in mRNA expression were determined by the Mann-Whitney test (in Graphpad Prism 6). Statistical significance was set at $p \leq 0.05$. Means were given with standard error of the mean (SEM) unless otherwise stated. Graphs were generated in Graphpad Prism 6 and formatted in Adobe Illustrator CS6.

5.3. Results

5.3.1. $Lgr6^+$ stem cells are present in the skin of hairless mice

We first ascertained whether $Lgr6^+$ stem cells were present in the epidermis of (transgenic) hairless mice (see Figure 5.1, also for comparison with haired mice). To this end, haired *Lgr6-EGFP-Ires-CreERT2/R26R-LacZ* mice were backcrossed into a hairless background using albino SKH-1 mice. The progeny was viable and did not show a specific phenotype. As in SKH-1 mice, HFs in hairless *Lgr6-EGFP-Ires-CreERT2/R26R-LacZ* mice appeared to be arrested in catagen. HF remnants were connected to deep-seated cysts in the dermis (presumed bulb remnants) [12; Chapter 2]. Lgr6-expressing stem cells ($EGFP^+$ in Figure 5.1A) were present in the IFE and near the bottom of HF remnants (region of sebaceous glands). Lgr6 progeny ($LacZ^+$) was found in the lower part of the HF remnant (see Figure 5.1 C). We also found Lgr6 stem cell progeny ($LacZ^+$) in the IFE (see Figure 5.1B + 5.1C).

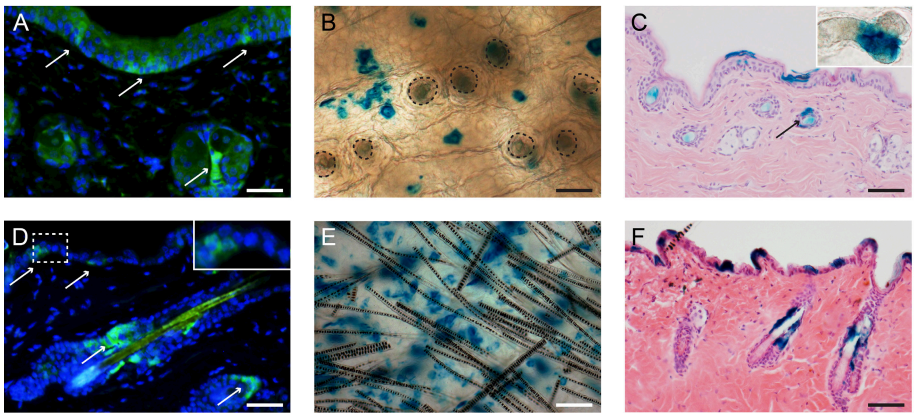


Figure 5.1: In homeostasis Lgr6$^+$ stem cells and their progeny are present in the lower part of the HF remnants and in the IFE of hairless mice (A-C) and in the isthmus and IFE of haired mice (D-F). Skin sections of *Lgr6-EGFP-Ires-CreERT2/R26R-LacZ* mice were stained for EGFP to detect Lgr6$^+$ stem cells (A+D, arrows). Skin whole mounts (B+E; HF orifices contoured in B), cross sections (C+F) and epidermal sheets (insert HF remnant in C) were stained (blue) for LacZ expression (8-9 weeks after tamoxifen) to detect Lgr6 progeny. Scale bar in E = 100 µm, scale bar in B, C, F=75 µm, scale bar in A+D=50 µm

5.3.2. Lgr6$^+$ stem cells and their progeny repopulate the interfollicular epidermis after UV overexposure

We ablated a large part of the epidermal basal layer using a tolerable UV overexposure (3.2 and 2.5 kJ/m^2 UV for haired and hairless mice, respectively; see Material and Methods). This dose induced massive apoptosis in basal cells but left the overlying cell layers intact [12; Chapter 2]. We stained for Lgr6$^+$ stem cells, using an anti-EGFP antibody, in skin samples taken at different time points after UV overexposure; see Figures 5.2 and 5.3E-H for hairless and haired mice, respectively. EGFP-expression was much less prevalent but still weakly present in the apoptotic basal layer of the IFE 1 day after UV overexposure both in haired and hairless mice. However, 3 days after UV overexposure the IFE no longer showed any EGFP$^+$ expression. From 1 week after UV overexposure onward EGFP-expressing Lgr6$^+$ cells reoccurred in the IFE. In the control samples that did not receive a UV overexposure we found EGFP$^+$ cells in the IFE equally at all time points (Figures 5.2 and 5.3A-D). The EGFP$^+$ cells in the isthmus of haired mice and in HF remnants of hairless mice were present at all time points and did not appear to be influenced by the overexposure. Also, Lgr6 progeny (LacZ$^+$) remained present in HF (isthmus) of haired and HF remnants of hairless mice. A lack of progeny in the IFE appeared only in haired mice 1 day after exposure (Fig 5.3M). In haired mice Lgr6 progeny reappeared in the IFE 3 days after UV overexposure (Figure 5.3N) whereas in hairless mice it never fully disappeared, already reappearing early after 1 day (Figure 5.2M). From day 3 onward progeny was more associated with HFs in the overexposed groups than in controls (Figures 5.2 and 5.3). This clearly indicated outgrowth

of the progeny from the HFs to replace the ablated epidermal basal cells. Furthermore, we observed more LacZ$^+$ progeny in the HFs and HF remnants at 3 days and 1 week after UV overexposure all the way up to the rims where HFs are connected to the IFE (Figures 5.2 and 5.3N + 5.3O). This was indicative of increased proliferation in HFs after overexposure. Eight weeks after the ablative dose, the skin was still perturbed with 2.0 (SEM 0.3) LacZ$^+$ clusters of Lgr6 progeny per mm^2 in the IFE versus 3.9 (SEM 0.6) in controls of which 52% (SEM 11%) versus 2.5% (SEM 0.4%) were associated with HFs.

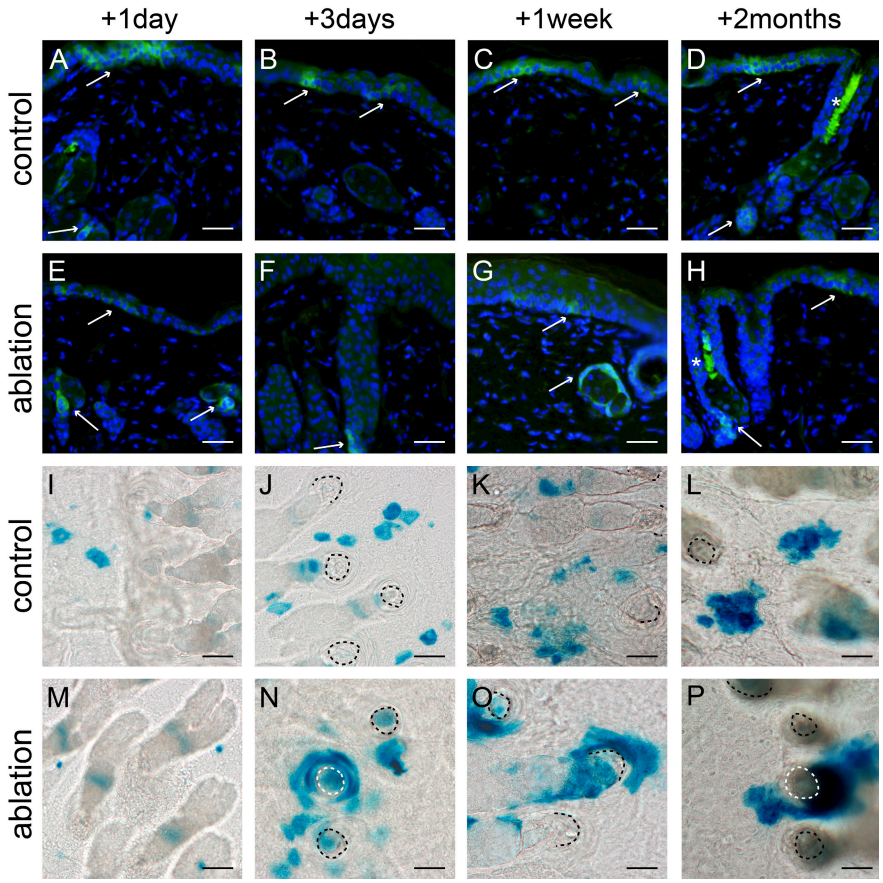


Figure 5.2: Lgr6$^+$ stem cells and their progeny in hairless mice after UV overexposure**.** Anti-EGFP staining was used to localize the Lgr6$^+$ stem cells (A-H) and epidermal sheets were stained for LacZ$^+$ progeny (I-P) at different time points (representative pictures are shown). The control mice (A-D) showed clear EGFP$^+$ cells in the IFE and at the bottom of the HF remnants (A+D see arrows). The LacZ$^+$ Lgr6 progeny spread in the IFE in control skin (I-L). One day after UV overexposure we still observed some EGFP-expression in the IFE (E), this expression was lost after 3 days (F) and reappeared sparsely after 1 week (G). EGFP expression at the bottom of the HF remnants was present at all time points (E-H). After UV overexposure Lgr6 progeny was more prevalent in HF remnants and in the IFE progeny was more associated with the hair follicle remnants (M-P) compared to the controls. Scale bars 50 µm. *= auto fluorescence/ false positivity caused by keratins.

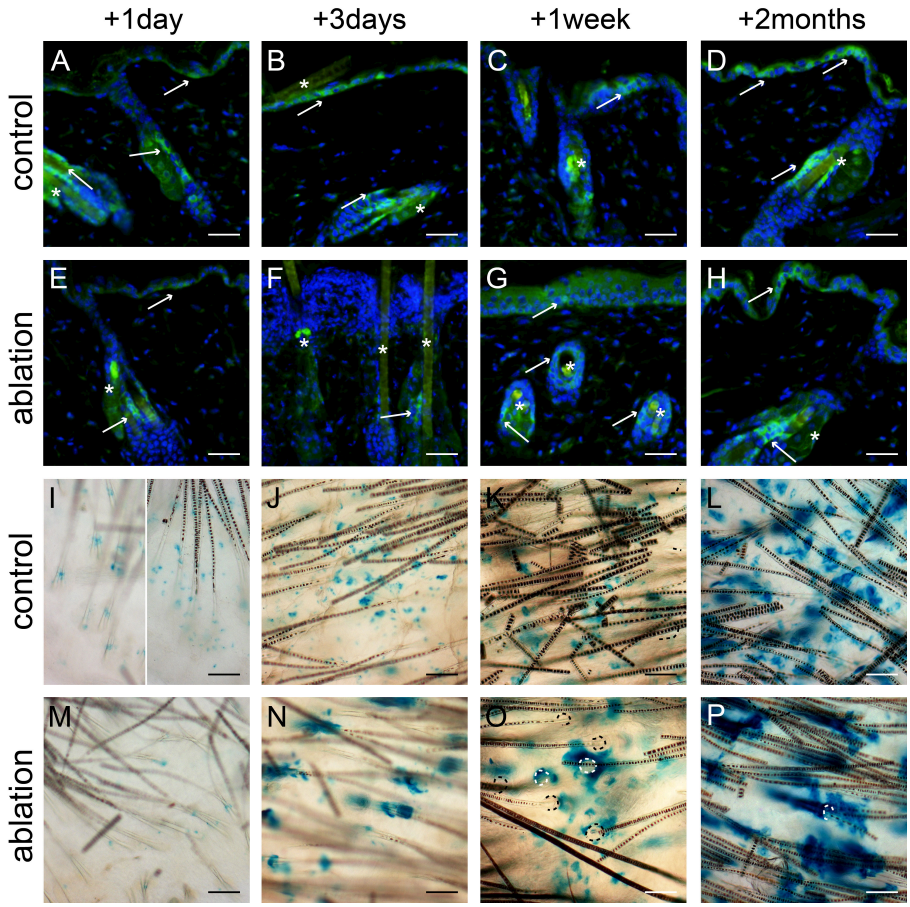


Figure 5.3: Lgr6$^+$ stem cells and their progeny in haired mice after UV overexposure. Anti-EGFP staining was used to localize the Lgr6$^+$ stem cells (A-H) and whole mounts were stained for LacZ$^+$ progeny (I-P) at different time points. We observed some autofluorescence in hairs. The control mice (A-D) showed clear EGFP$^+$ cells in the IFE and in the isthmus (A-D, see arrows). Lgr6 progeny built up in the HFs and islands in the IFE (I-L). One day after UV overexposure we still found some EGFP expression in the IFE (E, in apoptotic basal layer), that expression was lost after 3 days (F, with inflammatory infiltrate in papillary dermis) and reappeared sparsely after 1 week (G). We found EGFP expression in the isthmus at all time points (E-H). One day after UV overexposure we only observed some LacZ$^+$ cells in the HFs and not at all in the IFE (I). From three days after UV overexposure the Lgr6 progeny was found in the IFE, more associated with HFs remnants (N-P) compared to the controls. HF orifices indicated by dotted lines (O+P). Scale bars = 50 µm. *= background autofluorescence in sebaceous glands and from hairs.

5.3.3. Interfollicular Lgr6 expression is reduced after chronic UV exposure.

Mice were subjected to daily sub-acute exposure (1 MED/d) for 4-8 weeks to induce epidermal hyperplasia. These mice were sacrificed at the different time points together with their respective controls that did not receive any UV treatment. Upon UV induction of epidermal hyperplasia Lgr6$^+$ stem cells remained in the isthmus of haired mice and in the HF remnants of hairless mice (see Figure 5.4, hairless data not shown). However, their number was reduced in the IFE (see Figure 5.4 for haired and Figure 5.5 for hairless mice). The difference was most strikingly observable in epidermal sheets from hairless mice. In the control samples there were clear large 'islands' of Lgr6$^+$ cells (Figure 5.5A), whereas we only saw some isolated single Lgr6$^+$ cells or small clusters of Lgr6$^+$ cells in the sheets of UV-hyperplastic epidermis (Figure 5.5D). We measured the EGFP$^+$ area (by number of pixels) within the area populated by epidermal cells (high density of DAPI$^+$ nuclei), and found a significant difference in EGFP$^+$ fractions by area between the control and hyperplastic skin at week 7-8 ($p=0.036$, Figure 5.5G). The reduction of EGFP expression was not a UV-bleaching effect, since this reduction persisted after 6 days without UV exposure.

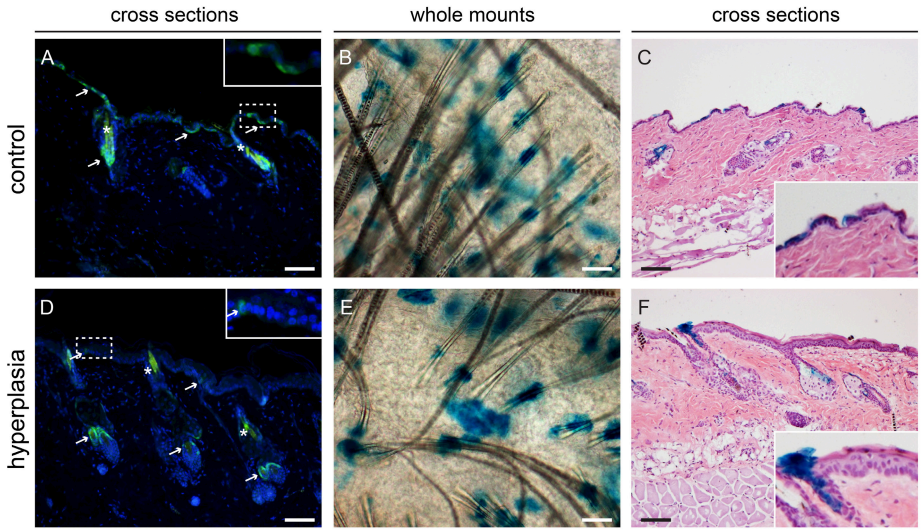


Figure 5.4: Lgr6$^+$ stem cells and their progeny in haired mice after chronic UV exposure. Samples were isolated at the 8-week time point. Anti-EGFP staining was used to localize the Lgr6$^+$ stem cells (in cross sections, A+D) and LacZ$^+$ cells as progeny (stained blue in whole mounts in top view, B+E and in cross sections C+F). We observed some auto-fluorescence in hairs (*). In control samples we observed patches of EGFP$^+$ cells in the IFE (A), in hyperplastic skin only a few EGFP$^+$ cells were found in the IFE (D). Inserts in A and B are magnifications of dashed frames of the IFE. Lgr6 progeny was found in the isthmus and in islands in the IFE in both control and hyperplastic skin (B, C, E, F). Scale bars = 100 µm.

Corresponding observations were made for the progeny of Lgr6$^+$ stem cells. In UV-exposed hairless mice LacZ$^+$ cell clusters also diminished strongly in the IFE: after 8 weeks from 8.6 (SEM 2.7) LacZ$^+$ clusters per mm^2 in unexposed controls down to 0.09 (SEM 0.08) in the UV-exposed animals. Most of the clusters in the IFE of controls were not associated with HFs, only 0.10 (SEM 0.05) clusters/mm^2 were. Virtually all clusters not connected to HFs had disappeared from the UV-irradiated IFE (< 0.01/mm^2), leaving only a low and highly variable number of clusters evidently sprouting from HF remnants (Figure 5.5B vs 5.5E). The LacZ$^+$ clusters associated with HF remnants in the hyperplastic IFE tended to be larger than the clusters in unexposed controls. A reduction in LacZ$^+$ clusters was also observed in (shaven) haired mice (Figure 5.4B vs 5.4E note that many LacZ$^+$ HFs are present next to LacZ$^+$ cell clusters in the IFE; discrimination under the microscope was actually made easier by varying focus depth between superficial IFE and deeper HFs).

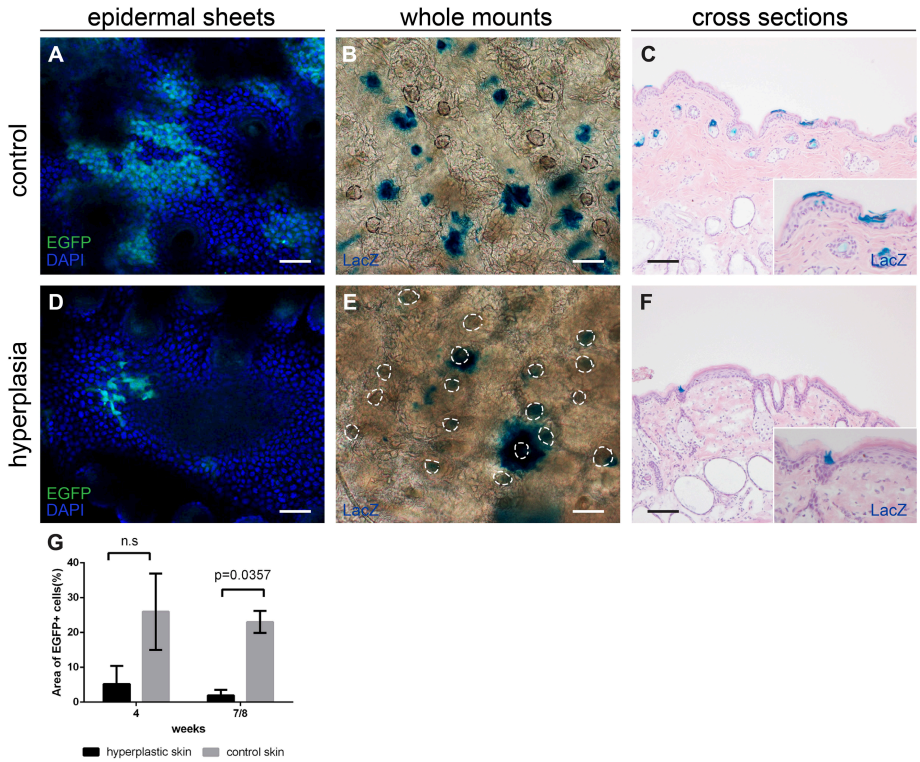


Figure 5.5: Lgr6$^+$ stem cells and their progeny in hairless mice after chronic UV exposure, samples after 8 weeks of exposure. CLSM on epidermal sheets was used to investigate EGFP expression (A+D). Nuclei were stained with DAPI. In control mice clear EGFP$^+$ islands were visible in the IFE (A), in the UV-hyperplastic skin the clusters of EGFP$^+$ cells were smaller and less frequent (D). The area occupied by EGFP$^+$ cells as a percentage of the area of DAPI$^+$ cells was calculated for 4 and 7-8 weeks, graphs represent mean and SEM (G). Whole mounts (B+E) and cross sections (C+F) were stained for LacZ$^+$ progeny. Hyperplastic skin (E+F) showed fewer LacZ$^+$ cell clusters in the IFE and these tended to be larger and more often found associated with HF remnants. Scale bars = 100 µm.

5.3.4. Interfollicular inter-tumoral Lgr6 progeny

In the haired and hairless mice from the carcinogenesis experiments we investigated the uninvolved hyperplastic skin adjacent to the tumors. Lgr6 progeny remained present in the HFs and HF remnants. When lineage tracing was started from the beginning of the experiment (i.e. tamoxifen before carcinogenic regimen) we found clear islands of $LacZ^+$ Lgr6 progeny in the IFE (Figures 5.6A + 5.6D and Figures 5.7A, 5.7D, 5.7F). However, the hairless IFE subjected to UV carcinogenesis (1MED/day > 6 months) showed much less progeny (Figure 5.6A) than that subjected to chemical carcinogenesis (Figure 5.6D), more similar to the earlier UV-induced hyperplasia (Figure 5.5E). In stark contrast to UV carcinogenesis, chemical carcinogenesis resulted in large and much more frequent clusters of Lgr6 progeny in the IFE. Virtually all of this progeny was contiguous with that in HFs (all $LacZ^+$) while growing around other $LacZ^-$ HFs (Figures 5.7A + 5.7D).

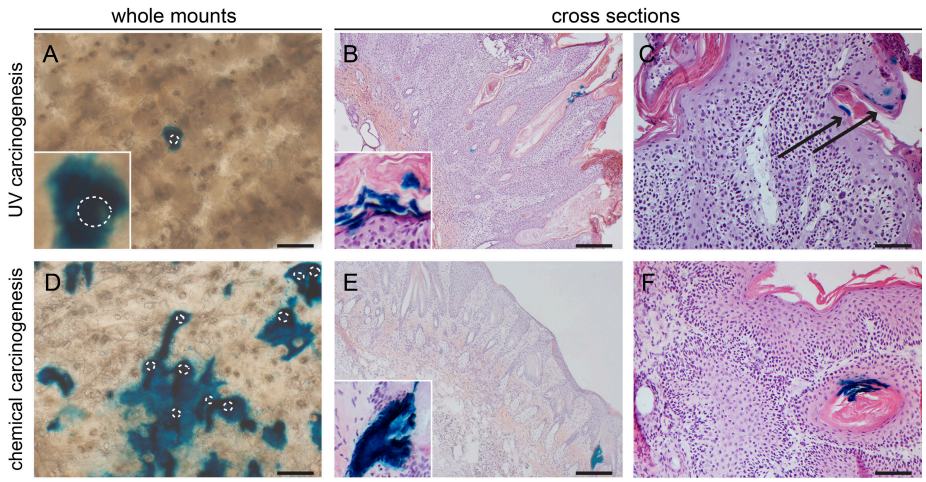


Figure 5.6: Lgr6 progeny in inter-tumoral skin and skin tumors of hairless mice. Samples were stained for $LacZ^+$ cells (UV carcinogenesis A-C; chemical carcinogenesis D-F). Whole mount inter-tumoral skin after UV carcinogenesis (A) showed less Lgr6 progeny in the IFE compared to inter-tumoral skin after chemical carcinogenesis (D). UV-induced tumors showed very sparse labelling in differentiated cells either when lineage tracing was initiated at the beginning of the experiment (B) or when tumors were formed (C); the same holds true for chemically induced tumors (E, F). Some hair follicle-like structures bordering the tumor masses stained $LacZ^+$, with early lineage tracing (E and insert); tumor with late tracing in F. Scale bars = 100 µm (C+F) and 200 µm (A, B, D, E).

5.3.5. Lgr6$^+$ stem cells are not tumor-driving cells

The main interest of our study was the role of Lgr6$^+$ stem cells and their progeny in the formation of skin tumors. Hence, we subjected *Lgr6-EGFP-Ires-CreERT2/R26R-LacZ* hairless mice to UV-induced skin carcinogenesis and *Lgr6-EGFP-Ires-CreERT2/R26R-LacZ* haired and hairless mice to DMBA and TPA-induced (chemical) carcinogenesis (see also Materials and Methods). In each experiment one group received tamoxifen injections to initiate lineage tracing just prior to starting the carcinogenic regimen and the other group received the injections when tumors (> 4 mm) had formed. Giving the injections at the beginning of the experiments would give us the opportunity to study clonal expansion of a lineage of Lgr6$^+$ stem cells into tumors. In this case the Lgr6 progeny would make up the complete tumor mass, staining completely blue from X-gal cleaved by β-galactosidase, coded for by the *LacZ* gene. Injecting in mice with already established tumors and subsequent tracing for 2-3 weeks would enable determining whether Lgr6$^+$ stem cells in the tumor were driving the growth.

Mice that received the UV-carcinogenic regimen mainly developed (endophytically growing) SCCs and precursors (actinic keratoses). These differed from chemically induced tumors which were mainly (exophytically growing) papillomas. We only found some sporadic Lgr6$^+$ cells (EGFP$^+$) in the bulk of 1 tumor (out of 6 tumors from 4 mice) from the UV carcinogenesis group (data not shown). The tumors obtained with the chemical carcinogenic regimen (n=12 tumors from 7 mice) were all negative. Overall, Lgr6 progeny was present very sparsely and most tumors showed no staining at all (60-70 % of chemically-induced tumors and early traced UV tumors, and virtually all late traced UV tumors). In the following paragraphs we give a more detailed description.

In the hairless mice subjected to UV carcinogenesis and traced from the start of the experiment, we observed some signs of progeny in keratin 'pearls' and sparse clusters of a few cells in the outer most differentiated layers of the tumors (9 out of 22 tumors from 4 mice, see Figure 5.6B). Furthermore, some progeny was found in undifferentiated cells in hair follicle-like structures at the edge of the tumors (data not shown). However, the proliferative bulk of the tumors was negative. When we started the lineage tracing when tumors had already formed, only 1 tumor showed LacZ$^+$ cells, and these cells were again very sparse and terminally differentiated (Figure 5.6C). All other tumors were negative (n=43 from 7 mice).

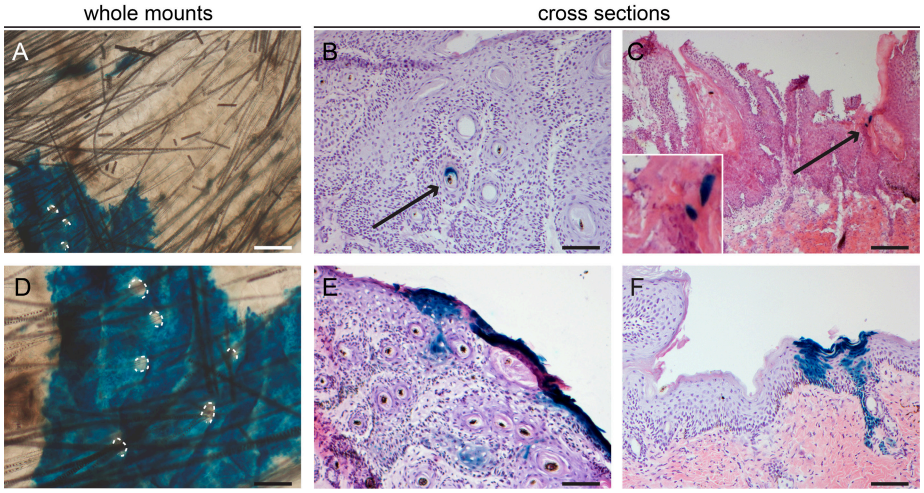


Figure 5.7: Lgr6 progeny in inter-tumoral skin and skin tumors of haired mice. Samples subjected to chemical carcinogenesis were stained for LacZ^{+} cells. Whole mount inter-tumoral skin after chemical carcinogenesis (A+D) showed large islands of Lgr6 progeny in the IFE when lineage tracing was induced at the start of the experiment. Hair follicle orifices contoured in A+D of hair follicles that did not stain. Only after early lineage tracing some tumors showed incidental staining in engulfed hair follicle-like structures (B). We found more abundant staining in uninvolved skin adjacent to the tumors, notice features of proliferating units (F). When lineage tracing was induced when tumors were formed we found some incidental staining in differentiated cells (C and insert). E shows the only tumor (out of 43) in haired mice subjected to chemical carcinogenesis that showed some staining at the outer rim of the tumor with early tracing. Scale bars = 100 µm (B-F) and 200 µm (A).

Haired and hairless mice subjected to chemical carcinogenesis showed similar results. With early initiation of lineage tracing Lgr6 progeny appeared in sparse clusters of a few cells in the outermost differentiated cell layers. Remnants of progeny (blue X-gal staining) were observed in some keratin 'pearls' or hair follicle-like structures in the tumors (most likely inclusions of normal cells). This occurred in 6 out of 20 tumors from 3 haired, and in 6 out of 21 tumors from 5 hairless mice (Figure 5.6E and Figure 5.7). And again, Lgr6 progeny was present in HFs bordering the tumors. In one tumor from a haired mouse subjected to chemical carcinogenesis and traced from the start of the experiment, we found more abundant Lgr6 progeny at the outer rim of the tumor but not in the tumor bulk (see Figure 5.7E). In contrast to UV-induced tumors, chemically induced tumors showed some Lgr6 progeny in sparse clusters of a few differentiated cells up on starting the tracing when the tumors had formed (haired 8 out of 23, hairless 6 out of 19, from 6 and 4 mice respectively; see Figure 5.6F and Figure 5.7C).

5.3.6. The Lgr6 promoter becomes methylated in Lgr6-EGFP-Ires-CreERT2/R26R-LacZ mice but not in wild type mice

Since Lgr6$^+$ stem cells and their progeny were absent in the tumor bulk, we posed the question whether EGFP and LacZ expression could have been silenced by aberrant methylation of the promoters involved. Therefore, we checked the methylation status of these promoters in several skin samples and tumors. After identifying CpG islands, promoter hypermethylation was evaluated for *Lgr6* and *Rosa* (*R26R*) in samples from wild type (wt) SKH-1 and C57Bl/6 mice, *Lgr5-EGFP-Ires-CreERT2/R26R-LacZ* and *Lgr6-EGFP-Ires-CreERT2/R26R-LacZ* mice (see Table 5.1 and Supplementary Table S5.2). Three of the aforementioned strains do not contain the *EGFP-Ires-CreERT2* cassette in the *Lgr6* locus and therefore carry only wt *Lgr6* loci. Independent of treatment, aberrant promoter hypermethylation was only observed in part of the *Lgr6-EGFP-Ires-CreERT2/R26R-LacZ* samples (see Supplementary Figure S5.2). These included untreated skin samples (3 methylated out of 8, see Table 5.1 and Supplementary Figure S5.2). Combined with the unmethylated status of all wt *Lgr6* samples, these results indicate that *de novo* methylation was exclusively evoked by the insertion of the *EGFP-Ires-CreERT2* cassette. This points to a possible monoallelic silencing of the cassette by methylation of its *Lgr6* promoter (we never observed complete promoter hypermethylation indicating that the wt *Lgr6* promoter remained unmethylated, see Supplementary Figure S5.2). No differences were observed between haired and hairless *Lgr6-EGFP-Ires-CreERT2/R26R-LacZ* mice nor between chemical and UV carcinogenesis (hence the condensed form of Table 5.1, a more stratified version in Supplementary Table S5.2). All chemically induced tumors and most of UV-induced tumors from *Lgr6-EGFP-Ires-CreERT2/R26R-LacZ* mice showed monoallelic methylation. Aberrant hypermethylation of the *R26R* promoter was not observed in any of the samples (data not shown).

Table 5.1: Samples tested for aberrant methylation of the Lgr6 promoter by MS-MCA*.

Sample group	# samples tested	# with part of Lgr6 promoters methylated	% samples showing methylation
Skin untreated (wt)	10	0	0
skin untreated (tg)	16	7	44
skin treated with UV 30 days 1 MED (wt)	4	0	0
skin treated with UV 4-8 weeks 1 MED (tg)	14	6	43
inter-tumoral skin (tg)	16	14	88
Tumors (tg)	27	26	96
Tumors (wt)	12	0	0

*Samples were tested from mice with a wt *Lgr6* locus (wt) and from haired and hairless *Lgr6-EGFP-Ires-CreERT2/R26R-LacZ* mice (tg). Samples of these last two groups were lumped together since no differences were observed; the same was true for tumors from the chemical and UV carcinogenesis experiments.

5.3.7. Lgr6 expression is reduced in skin tumors

As the wt *Lgr6* allele appeared not to be subjected to *de novo* promoter hypermethylation, it would be transcribed normally. Hence, we performed qPCR to investigate *Lgr6* mRNA expression in the skin tumors and check whether it was lost or reduced when compared to untreated or hyperplastic skin (the *EGFP-Ires-CreERT2* cassette was inserted in exon 1 of the *Lgr6* gene and blocked transcription of this gene [6]). In UV tumors from *Lgr6-EGFP-Ires-CreERT2/R26R-LacZ* and wt mice, we found a reduction of *Lgr6* expression when compared to untreated and hyperplastic skin (Figure 5.8A), in particular relative to *Ki67* expression (p=0.004, see Supplementary Figure S5.3). Therefore, the qPCR analysis confirmed that $Lgr6^+$ stem cells were lost from the pool of cycling cells ($Ki67^+$) in UV-induced tumors. Although there was a trend towards lower expression of *Lgr6* in chemically induced tumors, the difference was not consistently significant (p=0.07 in haired, Figure 5.8B; p=0.04, in hairless mice, data not shown). In contrast to hairless mice, where *Ki67* expression was rather constant from untreated skin through UV- or TPA-treated skin up to and including tumors, shaven haired skin showed increased *Ki67* expression in UV-, TPA-treated skin and tumors (Supplementary Figure S5.4). *Lgr6* showed a relative decrease with increasing *Ki67*, again indicating a relative loss of $Lgr6^+$ cells from the pool of cycling $Ki67^+$ cells which apparently expanded in response to TPA (*Lgr6/Ki67* was significantly higher in untreated skin than in skin and tumors from TPA-treated haired mice, p=0.04, see Supplementary Figure S5.4).

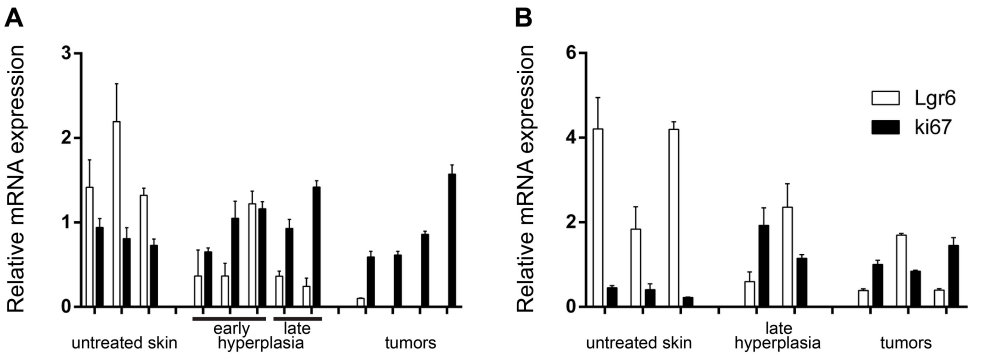


Figure 5.8: Relative mRNA expression of Lgr6 in hairless (A) and haired (B) mice. Gene expression of *Lgr6* and *Ki67* was measured by qPCR and normalized against stably expressed reference genes (see Material and Methods). RNA was isolated from hairless samples taken from untreated skin, hyperplastic skin induced by UV and UV-induced tumors (A). *Lgr6* gene expression was significantly reduced in UV-induced tumors compared to the untreated and hyperplastic skin samples (p=0.004). RNA was also isolated from untreated skin, chemically induced hyperplastic skin and chemically induced tumors from shaven haired mice (B). Reduction of *Lgr6* in chemically induced tumors compared to the untreated and hyperplastic skin was not significant (p=0.07). Error bars are SEMs.

5.4. Discussion

In this study we showed that Lgr6$^+$ stem cells repopulate the IFE after a UV overexposure, and became much less frequent in the IFE after sub-acute chronic UV exposure, as did their progeny. Lgr6$^+$ cells did not appear to become the tumor-initiating cells (TICs) in UV carcinogenesis, nor in two-stage chemical carcinogenesis.

To our knowledge we are the first to report that hairless mice with aberrant hair follicles do express *Lgr6*. As in haired mice, the Lgr6$^+$ stem cells (EGFP$^+$) are abundantly present in the interfollicular epidermis (IFE) and also present in the hair follicles (HFs) (Figure 5.1). In hairless mice most of the HFs are dysfunctional and the Lgr6$^+$ cells reside at the bottom of the HF remnants in the region of the sebaceous glands. The fraction of EGFP$^+$ cells (20-25%), which we established by area in epidermal sheets from hairless mice, was similar to the fraction of basal cells reported by Füllgrabe et al. for haired mice [9].

This baseline abundance of EGFP$^+$ cells in the IFE provided an excellent initial condition for lineage tracing by expression of LacZ after tamoxifen-induced activation of Cre. Both in shaven haired and hairless mice we observed a transient elimination of Lgr6$^+$ stem cells (EGFP$^+$) from the IFE, and a corresponding reduction in their progeny 1 - 3 days after overexposure. As found previously in wounding [6, 9], the IFE was repopulated with Lgr6$^+$ stem cells from the HF and, in contrast with unexposed controls, most of the progeny thereafter was associated with HFs. It was noted that the response in hairless mice appeared to evolve more rapidly than in haired mice, which corresponded to our earlier observations of a more rapid expulsion of apoptotic basal cells and stronger hyperplastic response in the hairless mice (see Supplement of ref [21]; Chapter 4). This appears to parallel the observation under chronic UV exposure (see Supplement to [21]; Chapter 4), that the epidermal hyperplasia was stronger in hairless than in haired mice.

Two months after the UV overexposure Lgr6 stem cell progeny was still observed in the IFE which confirmed that the Lgr6$^+$ cells were indeed genuine stem cells (again similar to what was observed after wounding [6]). In shaven haired and hairless mice, daily sub-acute UV exposure led to a persistent decrease in Lgr6$^+$ stem cells in the IFE (from > 20 to < 5%, Figure 5.5G) whereas the population in the HFs was not affected. The corresponding Lgr6 progeny was even more strongly reduced in the IFE and became exclusively associated with HFs. Evidently, under chronic UV exposure the scarce interfollicular Lgr6 progeny originated mainly from the HF, and in the IFE the Lgr6$^+$ stem cells were most likely outcompeted by other interfollicular stem cells.

Liao and Nguyen [7] observed a juxtaposition of Lgr6$^+$ stem cells and cutaneous nerve endings, and went on to demonstrate a dependency of the former on the latter. As UV has been reported to reduce epidermal nerve endings and dermal nerve fibers [22], this effect may underlie the depletion of Lgr6$^+$ stem cells we observed in the chronically UV-exposed skin. Interestingly, Fullgrabe et al. [9] found Lgr6$^+$ stem cells from haired mice to express

genes for axon guidance. These results would point at a reciprocal relationship between Lgr6$^+$ stem cells and nerve endings, and thus, a UV-induced loss of Lgr6$^+$ stem from the epidermis could lead to a loss of cutaneous nerve endings.

With lineage tracing from the start of the UV carcinogenic regimen, the Lgr6 progeny in the hyperplastic IFE between tumors appeared to be very similar to that observed earlier after 4-8 weeks of daily sub-acute UV exposure. However, the Lgr6 progeny in between chemically induced tumors appeared in large clusters contiguous with multiple HFs per cluster, suggesting that progeny from neighboring HFs had merged into large LacZ$^+$ "islands". Many HFs remained blank (LacZ$^-$) and were surrounded by LacZ$^+$ progeny in the IFE. This would suggest that progeny from interfollicular Lgr6$^+$ stem cells may also have merged with these LacZ$^+$ islands, outcompeting unlabeled progeny from blank HFs. Thus, the TPA tumor-promoting regimen appears to have had a totally different effect on Lgr6$^+$ stem cells and their progeny in the IFE than the UV regimen.

The tumors themselves were devoid of Lgr6$^+$ stem cells (no EGFP detected) and their progeny, except for some LacZ positivity in rare and small patches in terminally differentiated parts of the tumors – most likely inclusions of normal cells in the tumor mass. No tumor was raised from the lineage of the initially abundance of EGFP$^+$ cells, i.e. none of the tumor was a clonal expansion of LacZ$^+$ cells (which should have yielded a blue staining from cleaved X-gal throughout the tumor mass). The absence of Lgr6$^+$ cells as driver cells in the tumor was further confirmed by starting lineage tracing after tumors had developed. Again, no progeny was detected in the tumors (progeny in surrounding skin constituted an internal positive control).

Because of these negative results in the tumors we investigated whether the reporter constructs in the mice were silenced, i.e whether the promoters of the *EGFP-CreERT2* cassette and *LacZ* were hypermethylated. The *Rosa* (*R26R)* promoter of *LacZ* was not methylated. Therefore, once the *LacZ* expression was switched on in Lgr6$^+$ cells it was not affected by methylation and persisted in the progeny. If tumors arose in the lineage of initially abundantly present Lgr6$^+$ stem cells this should have resulted in LacZ$^+$ tumor masses. The *Lgr6* promoter, on the other hand, appeared stochastically methylated in the *Lgr6-EGFP-Ires-CreERT2* mice. As this methylation was never complete and it did not occur in wt mice we inferred that the methylation was directed at the *Lgr6* promoter of the *EGFP-CreERT2* cassette; it is known that insertion of foreign DNA can trigger *de novo* methylation [23]. This methylation could impair expression of the *EGFP-CreERT2* cassette and thus cause a loss of *EGFP* and *CreERT2* expression in Lgr6$^+$ stem cells. As the methylation appeared to increase toward the end of the carcinogenic regimens (up to 100% of the samples with detectable methylation), both in tumors and uninvolved hyperplastic skin, detection of Lgr6$^+$ stem cells and starting up lineage tracing could have been censored. Despite this possible censoring by methylation, starting up lineage tracing did yield positive results in the skin neighboring the tumors but not in the tumor bulk.

To check expression of *Lgr6* mRNA directly we performed qPCR. In hairless mice *Lgr6* expression was reduced in UV-induced tumors (Figure 5.8A) (also from wt mice) and in chemically induced tumors when compared to control and hyperplastic skin, especially relative to *Ki67* expression (Supplementary Figure S5.4). The latter would indicate a loss of $Lgr6^+$ cells from the pool of proliferative ($Ki67^+$) cells. The same tendency was observed for chemically induced tumors in shaven haired mice (Figure 5.8B). But the effect was obscured by an increase in the pool of cycling cells in TPA-treated skin and ensuing tumors, as reflected by an increase in *Ki67* expression. Relative to *Ki67* expression, *Lgr6* was significantly decreased when compared to control skin (Supplementary Figure S5.4). *Lgr6* expression provided no indication of an enrichment for $Lgr6^+$ cells in the skin tumors raised by exogenous carcinogenic agents. In line with our data, Jensen et al. [24] found overexpression of SRSF6 in SCCs, and this overexpression induced epidermal hyperplasia with a reduction in $Lgr6^+$ cells.

Analyses of gene expression profiles of human SCCs have provided no indication of enrichment of Lgr6-expressing cells [25, 26]. This is in apparent agreement with our present results on experimentally (UV-) induced SCCs.

We conclude that the actively proliferating $Lgr6^+$ stem cells are not targeted in UV or chemical carcinogenesis. Instead, quiescent stem cells are more likely to play an important role in skin carcinogenesis. Earlier it has been established in chemical carcinogenesis experiments that $K15^+/CD34^+$ quiescent stem cells in the bulge of the hair follicle are targets for transformation into TICs [27, 28]. We found that proliferating $Lgr5^+$ stem cells in the hair follicle are not targeted in two-stage chemical skin carcinogenesis; like proliferating $Lgr6^+$ stem cells in the present study, they do not appear to become TICs [21; Chapter 4]. Moreover, we recently found that DNA damage-retaining quiescent stem cells in the IFE are linked to the initiation of persistent skin tumors by low level UV exposure [13; Chapter 3]. Overall, these data suggest that the quiescent stem cells are more likely to become TICs by carcinogenic insults than continuously proliferating stem cells, such as $Lgr6^+$ cells.

Acknowledgements

We thank prof. Hans Clevers and his team for starting us up with the transgenic mice and analyses. Oliver Mainwaring performed the first stainings and analyses. Maria Kasper (Karolinska Institute, Stockholm, Sweden) is thanked for the protocol of robust LacZ staining on cryosections for lineage tracing without appreciable background, which was crucial to our study. Furthermore, we thank the technicians of the animal facility for animal care.

References

1. Lomas A, Leonardi-Bee J and Bath-Hextall F. A systematic review of worldwide incidence of nonmelanoma skin cancer. Br J Dermatol. 2012; 166(5):1069-1080.
2. Arnold M, Holterhues C, Hollestein LM, Coebergh JW, Nijsten T, Pukkala E, Holleczek B, Tryggvadottir L, Comber H, Bento MJ, Diba Ch S, Micallef R, Primic-Zakelj M, Izarzugaza MI, Perucha J, Marcos-Gragera R, et al. Trends in incidence and predictions of cutaneous melanoma across Europe up to 2015. J Eur Acad Dermatol Venereol. 2014; 28(9):1170-1178.
3. Dessinioti C, Antoniou C, Katsambas A and Stratigos AJ. Basal Cell Carcinoma: What's New Under the Sun. Photochem Photobiol. 2010; 86(3):481-491.
4. Weinstock MA. Epidemiology and UV exposure. J Invest Dermatol. 2013; 133(E1):E11-12.
5. Hanahan D and Weinberg RA. The Hallmarks of Cancer. Cell. 2000; 100(1):57-70.
6. Snippert HJ, Haegebarth A, Kasper M, Jaks V, van Es JH, Barker N, van de Wetering M, van den Born M, Begthel H, Vries RG, Stange DE, Toftgard R and Clevers H. Lgr6 marks stem cells in the hair follicle that generate all cell lineages of the skin. Science. 2010; 327(5971):1385-1389.
7. Liao XH and Nguyen H. Epidermal expression of Lgr6 is dependent on nerve endings and Schwann cells. Exp Dermatol. 2014; 23(3):195-198.
8. Page ME, Lombard P, Ng F, Gottgens B and Jensen KB. The epidermis comprises autonomous compartments maintained by distinct stem cell populations. Cell stem cell. 2013; 13(4):471-482.
9. Fullgrabe A, Joost S, Are A, Jacob T, Sivan U, Haegebarth A, Linnarsson S, Simons BD, Clevers H, Toftgard R and Kasper M. Dynamics of Lgr6 Progenitor Cells in the Hair Follicle, Sebaceous Gland, and Interfollicular Epidermis. Stem cell reports. 2015.
10. Hsu SY, Kudo M, Chen T, Nakabayashi K, Bhalla A, van der Spek PJ, van Duin M and Hsueh AJ. The three subfamilies of leucine-rich repeat-containing G protein-coupled receptors (LGR): identification of LGR6 and LGR7 and the signaling mechanism for LGR7. Mol Endocrinol. 2000; 14(8):1257-1271.
11. Gong X, Carmon KS, Lin Q, Thomas A, Yi J and Liu Q. LGR6 is a high affinity receptor of R-spondins and potentially functions as a tumor suppressor. PLoS One. 2012; 7(5):e37137.
12. Rebel HG, Bodmann CA, van de Glind GC and de Gruijl FR. UV-induced ablation of the epidermal basal layer including p53-mutant clones resets UV carcinogenesis showing squamous cell carcinomas to originate from interfollicular epidermis. Carcinogenesis. 2012; 33(3):714-720.
13. van de Glind G, Rebel H, van Kempen M, Tensen K and de Gruijl F. Fractionation of a tumor-initiating UV dose introduces DNA damage-retaining cells in hairless mouse skin and renders subsequent TPA-promoted tumors non-regressing. Oncotarget. 2016.
14. de Gruijl FR and Forbes PD. UV-induced skin cancer in a hairless mouse model. Bioessays. 1995; 17(7):651-660.
15. Dumaz N, van Kranen HJ, de Vries A, Berg RJ, Wester PW, van Kreijl CF, Sarasin A, Daya-Grosjean L and de Gruijl FR. The role of UV-B light in skin carcinogenesis through the analysis of p53 mutations in squamous cell carcinomas of hairless mice. Carcinogenesis. 1997; 18(5):897-904.
16. Reddy AL and Fialkow PJ. Influence of dose of initiator on two-stage skin carcinogenesis in BALB/c mice with cellular mosaicism. Carcinogenesis. 1988; 9(5):751-754.
17. Quintanilla M, Brown K, Ramsden M and Balmain A. Carcinogen-specific mutation and amplification of Ha-ras during mouse skin carcinogenesis. Nature. 1986; 322(6074):78-80.
18. Sutter C, Strickland JE, Welty DJ, Yuspa SH, Winter H and Schweizer J. v-Ha-ras-induced mouse skin papillomas exhibit aberrant expression of keratin K13 as do their 7,12-dimethylbenz[a]anthracene/12-O-tetradecanoylphorbol-13-acetate -induced analogues. Mol Carcinog. 1991; 4(6):467-476.

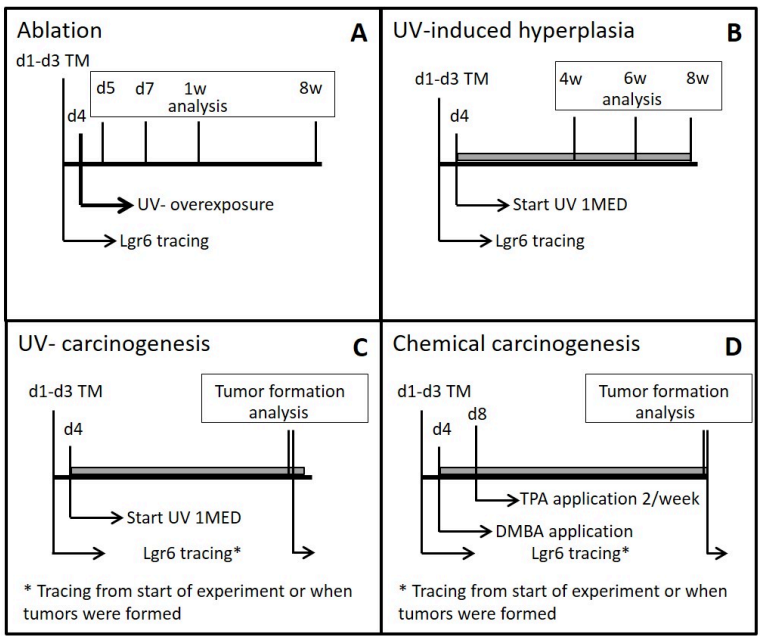
19. Rebel H, der Spek CD, Salvatori D, van Leeuwen JP, Robanus-Maandag EC and de Gruijl FR. UV exposure inhibits intestinal tumor growth and progression to malignancy in intestine-specific Apc mutant mice kept on low vitamin D diet. Int J Cancer. 2015; 136(2):271-277.
20. Livak KJ and Schmittgen TD. Analysis of Relative Gene Expression Data Using Real-Time Quantitative PCR and the 2−ΔΔCT Method. Methods. 2001; 25(4):402-408.
21. van de Glind GC, Out-Luiting JJ, Rebel HG, Tensen CP and de Gruijl FR. Lgr5+ stem cells and their progeny in mouse epidermis under regimens of exogenous skin carcinogenesis, and their absence in ensuing skin tumors. Oncotarget. 2016.
22. Wallengren J and Sundler F. Phototherapy reduces the number of epidermal and CGRP-positive dermal nerve fibres. Acta Derm Venereol. 2004; 84(2):111-115.
23. Doerfler W. Epigenetic consequences of foreign DNA insertions: de novo methylation and global alterations of methylation patterns in recipient genomes. Rev Med Virol. 2011; 21(6):336-346.
24. Jensen MA, Wilkinson JE and Krainer AR. Splicing factor SRSF6 promotes hyperplasia of sensitized skin. Nat Struct Mol Biol. 2014; 21(2):189-197.
25. Hudson LG, Gale JM, Padilla RS, Pickett G, Alexander BE, Wang J and Kusewitt DF. Microarray analysis of cutaneous squamous cell carcinomas reveals enhanced expression of epidermal differentiation complex genes. Mol Carcinog. 2010; 49(7):619-629.
26. Hameetman L, Commandeur S, Bavinck JN, Wisgerhof HC, de Gruijl FR, Willemze R, Mullenders L, Tensen CP and Vrieling H. Molecular profiling of cutaneous squamous cell carcinomas and actinic keratoses from organ transplant recipients. BMC Cancer. 2013; 13:58.
27. Malanchi I, Peinado H, Kassen D, Hussenet T, Metzger D, Chambon P, Huber M, Hohl D, Cano A, Birchmeier W and Huelsken J. Cutaneous cancer stem cell maintenance is dependent on beta-catenin signalling. Nature. 2008; 452(7187):650-653.
28. Trempus CS, Morris RJ, Ehinger M, Elmore A, Bortner CD, Ito M, Cotsarelis G, Nijhof JG, Peckham J, Flagler N, Kissling G, Humble MM, King LC, Adams LD, Desai D, Amin S, et al. CD34 expression by hair follicle stem cells is required for skin tumor development in mice. Cancer Res. 2007; 67(9):4173-4181.

Supplementary Material

S5.1 Methods:

S5.1.1. Active caspase-3 Staining

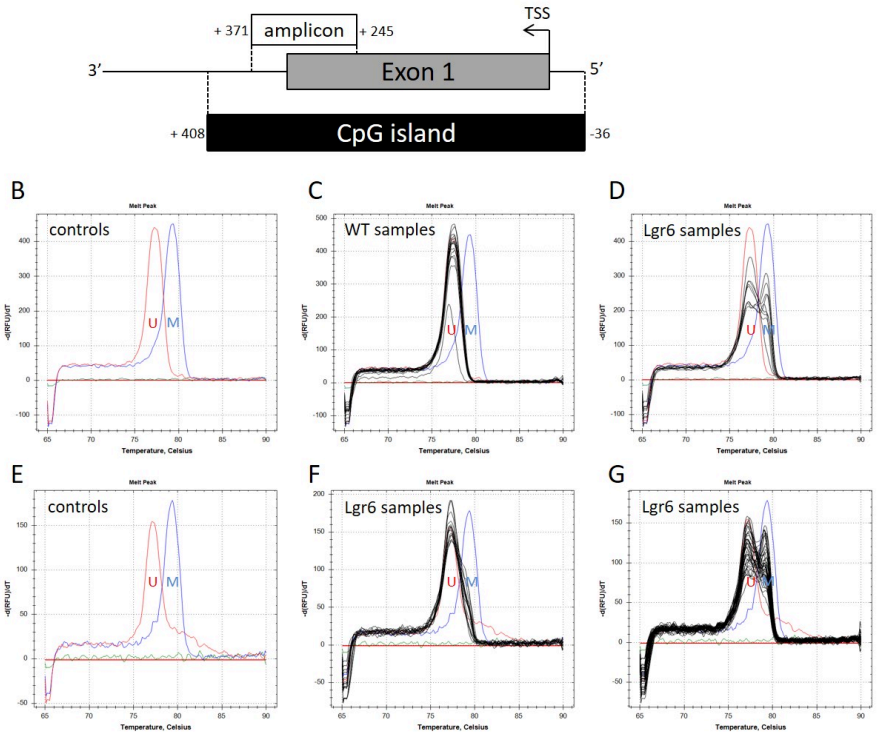
Cryosections were cut at 6 µm thickness and fixed in acetone containing 0.3% H_2O_2. The sections were blocked with 2% Normal Human Serum (NHS) for 20 minutes. After blocking, the sections were incubated overnight at 4°C with anti-active caspase-3 (1:100, ab 2302, 3509322, Abcam, Cambridge, UK). The next day the sections were incubated for one hour with Goat-anti-Rabbit (IgG)-biotin (1:300, Vector Laboratories, Inc Burlingame, USA) followed by streptavidin (1:100, RPN1051v, GE Healthcare UK Limited) for 45 minutes. The staining was visualized with 20 mg 3,3'-Diaminobenzidine (D5905, Sigma-Aldrich, Zwijndrecht, The Netherlands) in 100 ml of PBS and 100 µl of H_2O_2. Sections were counterstained with haematoxylin and mounted in Kaisers' glycerin.



Supplementary Figure S5.1: Experimental outline. Time lines of the experiments including time points of sample collection for analyses. TM= tamoxifen injection, d = day, w = week. In experiments A and B the lineage tracing started at the beginning of the experiment. In experiment C and D the tracing started either at the start of the experiment or when tumors were formed.

Supplementary Table S5.1: Primers for methylation assay

Gene	Primer sequence (5'-> 3')	Amplicon size	Number of CpG's	Relative to TSS	Tm unmethylated amplicon	Tm methylated amplicon
Lgr6	GGTATTAGTAGGTGA GTATTTATAGGTAAG ACTCCCTACCACTACC AAAAAAAC	127 bp	6	-36 to +408	77.4 °C	79.4 °C
Rosa	GGTGTAATGGTGTGTA AAGGTAGTTG CCTAAATCAAAATAAA AATCCAACAAA	192 bp	8	-684 to -493	78.8 °C	80.6 °C



Supplementary Figure S5.2: Methylation-specific melting curve analysis (MS-MCA). A Schematic depiction of the CpG island in relation to the promoter and gene body and amplicon for MS-MCA relative to the transcription start site (TSS) of *Lgr6* (A). MS-MCA on methylation control samples resulting in a melting temperature of 77.4 °C for unmethylated (U) and 79.4 °C for methylated (M) bisulphite converted DNA (B+E). In the first experiment (B-D) samples from *Lgr6* transgenic mice (D) and mice with only wildtype (wt) *Lgr6* loci were tested (C). The wt samples were all unmethylated, however several *Lgr6* samples showed aberrant promoter methylation, demonstrated by the presence of both a methylated as well as an unmethylated fraction. In a second experiment only *Lgr6* samples were tested (E-G), 15 out of 54 were unmethylated (F) and 39 out of 54 showed aberrant methylation (G). See also supplementary table S5.2 for the tested samples.

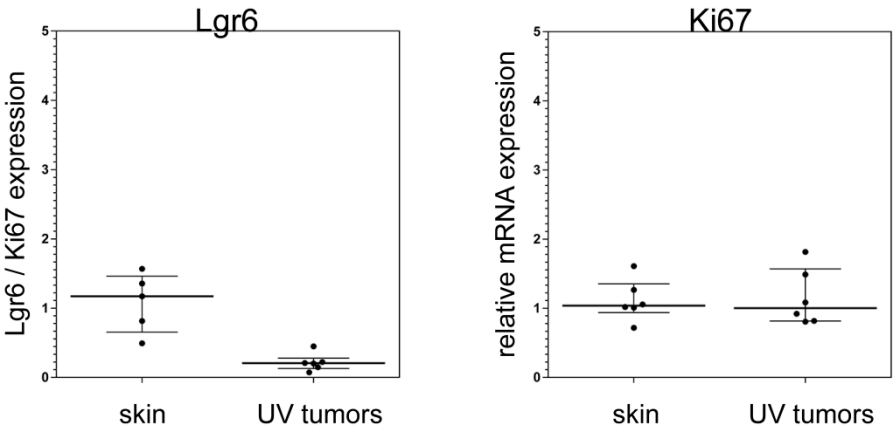
Supplementary Table S5.2: Samples tested for promoter hypermethylation#

Sample group	Tested (n)	Aberrantly methylated Lgr6 promoter (n)	Samples aberrantly methylated (%)
Skin untreated (C57BL/6 mice)	5	0	0
Skin untreated (SKH-1 mice)	2	0	0
Skin untreated (haired *Lgr5* mice)	3	0	0
Skin untreated (haired *Lgr6* mice)	8	3	38
Skin untreated (hairless *Lgr6* mice)	8	4	50
Skin treated with UV 30 days 1 MED (SKH-1 mice)	4	0	0
Skin treated with UV 4-8 weeks 1 MED (*haired Lgr6 mice*)*	8	2	25
Skin treated with UV 4-8 weeks 1 MED (*hairless Lgr6 mice*)*	6	4	67
Skin treated with TPA 6 weeks (haired *Lgr5 mice*)	3	0	0
Inter-tumoral skin UV-carcinogenesis (hairless *Lgr6 mice*)	4	3	75
Inter-tumoral skin chemical carcinogenesis (haired *Lgr6 mice*)	6	6	100
Inter-tumoral skin chemical carcinogenesis (hairless *Lgr6 mice*)	6	5	83
Tumors: UV-carcinogenesis (SKH-1 mice)	6	0	0
Tumors: UV-carcinogenesis (hairless *Lgr6 mice*)	9	8	89
Tumors: chemical carcinogenesis (haired *Lgr5 mice*)	6	0	0
Tumors: chemical carcinogenesis (haired *Lgr6 mice*)	9	9	100
Tumors: chemical carcinogenesis (hairless *Lgr6 mice*)	9	9	100

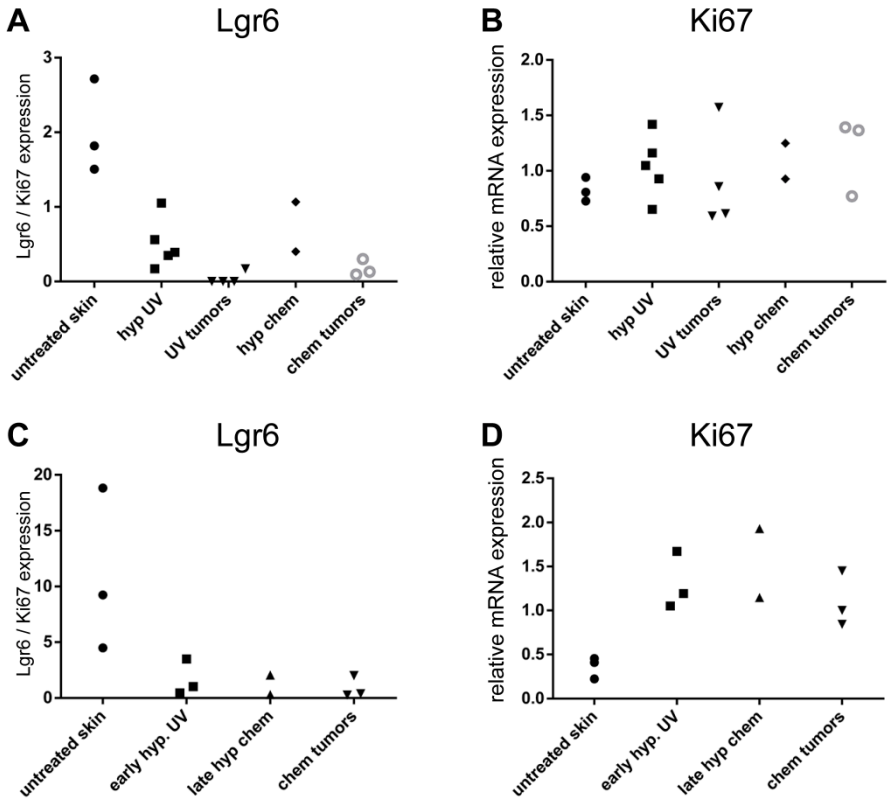
#Lgr5 mice are Lgr5-EGFP-Ires-CreERT2/R26R-LacZ mice, and Lgr6 mice are Lgr6-EGFP-Ires-CreERT2/R26R-LacZ mice.*no significant difference between skin treated with UV of haired and hairless mice ($p = 0.28$; fisher exact test).

Supplementary Table S5.3: Primers used for qPCR.

Gene	Primer sequence (5'-> 3')	Amplicon size	Exonic Location	Accession No.	Amplification efficiency	Correlation (R^2)
Cyc1	GATGTCGCCACCTT CCTTCGC GGACTGACCACTTA TGCCGCTTC	136	6, 7	NM_025567.2	98.6%	0.99
Ddx52	CACAGCAGCAGCG AGATAACAC CTCTTCCAGTCCGA CCTATCCTATG	177	10-11, 11-12	NM_030096	107.0%	0.99
Lgr6	TCAGGGAACCACCT CTCACA CATAGTGCCTCTGC TGGGAT	113	3, 4	NM_001033409	92.0%	0.95
Mki67	CAGAAGAAATGGA AGCCAAAA TGCAGATGCATCAA ACTTGG	110	12, 13	NM_001081117.2	96.5%	0.99



Supplementary Figure S5.3: Normalized *Lgr6* and *Ki67* expressions in wildtype SKH-1 mice. Left panel: ratio of *Lgr6* expression over *Ki67* expression. Right panel: normalized *Ki67* expression (proliferating cells). Relative *Ki67* expression was equal in tumors induced by UV and in skin (untreated and hyperplastic skin) samples. However, *Lgr6* expression was significantly reduced in tumors (p=0.004, Mann-Whitney test). Lines depict median with interquartile range.



Supplementary Figure S5.4: Normalized *Lgr6* and *Ki67* expressions in hairless (A+B) and haired (C+D) *Lgr6* mice. The expression of *Lgr6* in each sample was divided by the corresponding expression of *Ki67* (A+C). Tumors and skin samples showed a similar expression of *Ki67* in hairless mice (B), while in haired mice the *Ki67* expression in untreated skin was reduced compared to the other samples (D). In hairless mice the *Lgr6* expression relative to the *Ki67* expression in UV tumors was lower than in untreated skin, though not statistically significant (p=0.057, Mann-Whitney test). In chemically induced tumors and hyperplasia samples this expression was significantly reduced (p=0.036) compared to untreated skin. In haired mice the ratio of *Lgr6* over *Ki67* expression in untreated skin was higher than in chemically induced late hyperplasia and chemo tumors (p=0.036).

Chapter 6

RNA-seq analysis of Lgr6^{+} stem cells and identification of an Lgr6 isoform

G.C. van de Glind*, A.N. Bastidas Torres*, W.H. Zoutman, S.A.J. van der Zeeuw, S.M. Kielbasa, F.R. de Gruijl, C.P. Tensen

*contributed equally to this study

Exp. Dermatol . 2017 Oct 7. doi: 10.1111/exd.13453.

Abstract

UV carcinogenesis is experimentally studied in hairless mice, a well-established model of squamous cell carcinomas in humans. In this model we studied whether Lgr6$^+$ epidermal stem cells could become tumor-initiating cells (TICs). Here we report on gene expression profiling to further characterize Lgr6$^+$ cells in hairless mice. The cells were isolated by fluorescence-activated cell sorting from the epidermis of transgenic hairless mice bearing an EGFP-Ires-CreERT2 cassette (Tg/Tg and Tg/wt) under control of the Lgr6 promoter (high purity confirmed by ERT2$^+$ vs ERT2$^-$). Lgr6/EGFP$^+$ versus Lgr6/EGFP$^-$ basal ($\alpha6^+$) cells were compared by quantitative RNA deep seq and in-silico pathway analysis. A collection of 682 protein-encoding and non-coding RNAs was differentially expressed between Lgr6/EGFP$^+$ and Lgr6/EGFP$^-$ basal cells (Tg/wt). RNA expression profiling of Lgr6/EGFP$^+$ basal cells revealed stem cell characteristics and correspondence with cancer-related pathways. In addition, we found a set of genes coding for proteins which may serve further robust identification of these cells, also in human skin. We discovered that in presumed *Lgr6* null mice (Tg/Tg) an Lgr6 isoform (delta-Lgr6) is transcribed encoding a protein lacking 74 N-terminal amino acids, but expected to still bind the Lgr6 ligands (R-spondins). The human orthologue (delta-LGR6) was found in a proteome database.

6.1. Introduction

The skin is constantly renewed, and this regeneration is fueled by stem cells. Different stem cell populations have been characterized in the epidermis and its appendages [1]. In the present study we focused on Lgr6$^+$ stem cells which reside in the isthmus of the hair follicle, in the sebaceous gland (SG) and in the interfollicular epidermis (IFE) [2-5]. These stem cells were identified by lineage tracing and found to be a unique population not expressing the markers of the classic quiescent stem cells in the bulge: CD34 and K15 [5]. In homeostasis Lgr6$^+$ stem cells regenerate the upper part of the hair follicle, the SGs and the IFE [2-5]. Furthermore, Lgr6$^+$ stem cells have been shown to contribute to wound healing with persistent progeny and "de novo" hair formation [5].

Lgr6 (Leucine-rich repeat-containing G-protein coupled receptor 6), together with the closely related receptors Lgr4 and Lgr5, belongs to the G protein-coupled receptor (GPCR) superfamily. Lgr6 shares almost 50% amino acid sequence similarity with Lgr4 and Lgr5 [6]. All Lgr subtypes contain an unusual large N-terminal ectodomain composed of leucine-rich repeats which binds the ligands, R-spondins (Rspo), and share similarities with a prototypic receptor first identified in snails [6, 7].

Lgr receptors have been found to enhance the canonical Wnt/β-catenin signaling pathway [8]. Binding of R-spondin to these receptors enhances Wnt/ β-catenin signaling by decreasing endocytosis of the Wnt receptor complex. In the process, Lgr is lost from the membrane, which lowers its detectability. The Lgr protein family and related Wnt signaling appears to be important in organ development and maintenance. However, remarkably, homozygous Lgr6 knock-in mice do not show any phenotype, despite their supposed Lgr6 null alleles [5].

Because of their long residence and proliferative activity, we deemed that Lgr6$^+$ stem cells were likely candidates to become "tumor-initiating cells" (TICs) in UV-induced skin carcinogenesis. UV carcinogenesis has long been experimentally studied in a well-established model of squamous cell carcinomas related to solar UV exposure [9]. This model is based on chronic UV exposure of hairless mice. We found that Lgr6$^+$ stem cells appeared in large clusters in the IFE and in very small clusters in the remnants of hair follicles of hairless mice [10; Chapter 5]. Surprisingly, the number of Lgr6$^+$ cells in the IFE dwindled under chronic UV exposure, as did their progeny. Contrary to our expectation, no evidence was found that Lgr6$^+$ cells turned into TICs [10; Chapter 5].

In parallel to that study we isolated Lgr6/EGFP$^+$ cells from naïve hairless mouse skin to characterize these cells in greater detail. Here, we report on the results of determining their gene expression signature. To this end, *Lgr6-EGFP-Ires-CreERT2/R26R-LacZ* hairless mice were used, which circumvents the low level of *Lgr6* expression. The inserted *EGFP-Ires-CreERT2*-cassette in these mice is under control of the *Lgr6* promoter, and thus *Lgr6* promoter activity will lead to EGFP expression. Lgr6/EGFP$^+$ and Lgr6/EGFP$^-$ epidermal basal

cells (integrin α6$^+$) were isolated from homozygous and heterozygous *Lgr6-EGFP-Ires-CreERT2/R26R-LacZ* transgenic hairless mice by live cell sorting and subjected to quantitative RNA deep sequencing (RNA-seq). Mice of different ages were used to identify genes that are differentially expressed between Lgr6/EGFP$^+$ and Lgr6/EGFP$^-$ epidermal basal cells through life. Results of this study may not only provide further insight into the phenotype and function of *Lgr6*-expressing cells, but may also yield novel robust markers for their identification.

6.2. Materials and Methods

6.2.1. Mice

Lgr6-EGFP-Ires-CreERT2/R26R-LacZ transgenic mice (kindly provided by Prof. Hans Clevers) [5] were backcrossed into a hairless background using Crl:SKH1-HR hairless mice (Charles River, Sulzfeld, Germany). Both homozygous and heterozygous transgenic "Lgr6 mice" were obtained, not showing any phenotypic alterations despite *Lgr6* gene disruption. Male and female mice were used in the experiments (see for details Supplementary Table S6.1). They were kept individually in Macrolon type 1 cages at 25 ± 2°C with a humidity of 50% in a 12 hours light-12 hours dark cycle during experiments. Standard chow and tap water were available *ad libitum*. As legally required, all mouse experiments were performed with the approval of the Leiden University Medical Centers' ethics committee (approval number DEC 10229) and executed according to EU regulations on animal experiments (Directive 2010/63/EU).

6.2.2. Cell suspension preparation, antibody labelling and FACS sorting

Epidermal cell suspensions were obtained by trypsin digestion. A modified version of the protocol described by Jensen et al. [11] was implemented (see Supplementary Material). With this method we mainly isolated Lgr6/EGFP$^+$ cells from interfollicular epidermis where they were abundantly present in large EGFP-fluorescent clusters [10; Chapter 5], whereas only very few Lgr6/EGFP$^+$ cells were visible in the hair follicle remnants. For FACS analysis, cell suspensions were stained with anti-α6-integrin-PE conjugated monoclonal antibodies (CD49f clone GoH3, BD Bioscience, San Jose, CA, USA) for 1 hour at 4°C. Cells were sorted using a FACSAria III cell sorter (BD Bioscience) on the basis of single cell detection (pulse width), viability/integrity (scatter profile) and both EGFP and PE fluorescence. Sorting of PE$^+$/EGFP$^+$ and PE$^+$/ EGFP$^-$ cells (Lgr6/EGFP$^+$ and Lgr6/EGFP$^-$ basal cells, respectively) was accomplished through very strict gating settings as shown in Supplementary Figure S6.1. Sorted cells were collected in sheath fluid on ice. FlowJo software version 7.2.5 (FlowJo, Ashland, OR, USA) was used to obtain FACS plots of raw data. RNA extraction was performed immediately after each sorting procedure.

6.2.3. RNA isolation

Total RNA from sorted cells was extracted by using RNeasy Mini kit (74106, Qiagen, Hilden, Germany), which included on-column DNase digestion. All samples were eluted in 35 µl of RNAse-free water. RNA concentration and purity were determined using a Nanodrop 1000 spectrophotometer (Thermo Fisher Scientific, Wilmington, DE, USA). In addition, integrity of RNA molecules was evaluated by using Agilent RNA 6000 Pico Kit on a 2100 Bioanalyzer (Agilent Technologies, Santa Clara, CA, USA). RNA samples with a RNA integrity number (RIN) above 8 were used for subsequent RNA-seq sample preparations. RNA isolated from female and male cell suspensions of matched ages (4, 12, 23 weeks) were pooled pairwise.

6.2.4. RNA precipitation, library preparation and RNA deep sequencing

For RNA-seq, eight total RNA samples (450 ng) were processed. These samples were composed of 2 individual mice (a male and a female) bearing the same transgene zygosity. Combined RNA samples were concentrated by ethanol-mediated precipitation and resuspended in 10 µl RNAse-free water for library preparation. Eight individual barcoded libraries were made, normalized and pooled to be sequenced in the same run. Library preparation (rRNA depletion by Ribo-zero magnetic kit, Illumina) and paired-end sequencing of 100 bp were performed by the Leiden Genome Technology Center (LGTC). Sequencing was performed on a Illumina HiSeq-2000 (Illumina Inc., San Diego, CA, USA) following the instructions of the manufacturer. On average 100 million reads per sample were generated.

6.2.5. Data processing

RNA-seq data was processed using bioinformatics pipelines of the Sequence Analysis Support Core (SASC) of the Leiden University Medical Center (LUMC) according following method.

Sequencing adapters in the FastQ files were detected using FastQC version 0.10.1 and removed using the cutadapt tool (version 1.4.2). Base quality trimming was performed using the sickle tool (version 1.200). RNA paired-end reads where aligned to *Mus musculus* (murine) reference genome version mm10. (GSNAP version 2014-05-15; novel splicing flag set to true). The resulting alignment file was compressed, indexed, and name-sorted using samtools tool (version 0.1.19-44428cd). The count table was generated using htseq-count (HTSeq suite version 0.6.1p1). The UCSC genePredToGtf generated RefSeq annotation (raw database dump of the refGene table) was used as a GTF reference.

With this method, we were able to identify differentially expressed coding and (long) non coding transcripts.

6.2.6. Detection of differential mRNA and lncRNA expression

Differential gene expression analysis was performed using edgeR [12] and R/Bioconductor (https://www.R-project.org/, http://www.bioconductor.org). The TMM method [13] was used to normalize gene counts. We selected statistically significantly differentially expressed genes based on false discovery rates (FDR) obtained with the Benjamini-Hochberg procedure (correcting for multiple testing).

6.2.7 Visualization

Sequencing results were visualized using the Integrative Genomics Viewer (IGV) [14]. Heatmaps depicting log2 transformed relative differentially expressed genes were created using Gene-E (Broad institute, http://www.broadinstitute.org/cancer/software/GENE-E/ accessed September 9 2016).

6.2.8. Functional gene clustering

Biochemical pathways were analyzed using the web-based annotation tool DAVID v 6.8 (Database for Annotation, Visualization and Integrated Discovery [15]) to cluster statistically significantly differentially regulated genes by their common functionality. Higher and lower expressed genes were subjected to DAVID analysis as two separate entities.

6.3. Results

6.3.1. Lgr6/EGFP$^+$ cells are highly enriched for human ESR1 (ERT2) mRNA and express higher levels of Lgr6 than Lgr6/EGFP$^-$ cells

We used live-cell sorting to isolate "Lgr6/EGFP$^+$" epidermal basal stem cells (Lgr6/EGFP$^+$ & integrin α6$^+$), and "Lgr6/EGFP$^-$" epidermal basal cells (Lgr6/EGFP$^-$ & integrin α6$^+$) from heterozygous (n=6) and homozygous (n=2) *Lgr6-EGFP-Ires-CreERT2/R26R-LacZ* transgenic hairless mice (see Materials and Methods and Supplementary Figure S6.1). Both cell populations were subjected to RNA-seq and subsequent bioinformatical analyses (including normalization and quantification). To evaluate cell purification efficiency we first examined transcription of ERT2 in the *Lgr6-EGFP-Ires-CreERT2/R26R-LacZ* cassette. ERT2 is an engineered form of human *ESR1* with a tamoxifen binding domain regulating nuclear Cre activation [16]. Since it shares homology with murine *Esr1* its reads could be mapped to the mouse reference genome, in contrast to EGFP. We confirmed nearly exclusive expression of *ERT2* (*ESR1*) in Lgr6/EGFP$^+$ cells (Figure 6.1 and Supplementary Table S6.2A). Next, we compared *Lgr6* expression and noted that, although sorted Lgr6/EGFP$^-$ cells were not completely devoid of *Lgr6* transcripts, the Lgr6/EGFP$^+$ stem cell population showed significantly higher expression (see Supplementary Figure S6.2 and Supplementary Table S6.2A). Furthermore, we verified the *Lgr6* expression by qPCR (see Supplementary Figure S6.3a).

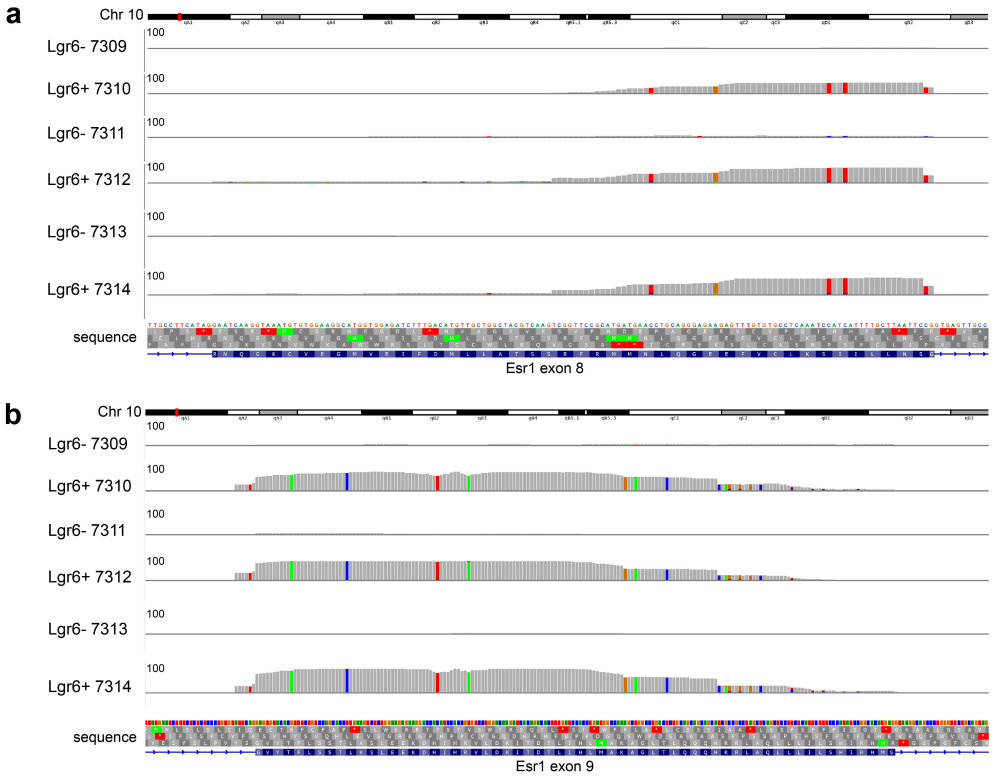


Figure 6.1: RNA-seq reads mapped to Exon 8 (chr10: 4969159-4969292; a) and 9 (chr10:4997830-4998013; b) of the *Esr1* gene for all heterozygous transgenic samples. Screenshot from IG viewer of the base counts for both exons are shown (y-axis = 100), for Lgr6/EGFP^{+} stem cells (even numbered samples) and for epidermal basal cells (Lgr6/EGFP^{-}, odd numbered samples). Colored bars in the cumulative counts mark bases deviant from the reference mouse sequence but in accordance with the human sequence. Lgr6/EGFP^{+} stem cells clearly express human *ESR1* (present as *ERT2* in the *EGFP-Ires-CreERT2* cassette) while Lgr6/EGFP^{-} cells show very low counts mainly from (endogenous) *Esr1*.

6.3.2. Differential expression of coding and non-coding transcripts between Lgr6/EGFP^{+} and Lgr6/EGFP^{-} basal cells from heterozygous mice

Analyzed transcriptome data were ranked by FDR, log fold change (log FC) and normalized relative expression. This separated higher expressed (log FC > 0) from lower expressed (log FC < 0) genes in Lgr6/EGFP^{+} stem cells compared to Lgr6/EGFP^{-} cells. By using a FDR cut-off value of 0.05 we found 291 genes higher and 391 lower expressed in Lgr6/EGFP^{+} cells (the top 35 higher and lower expressed genes are shown in Figure 6.2A and Supplementary Table S6.1A + S6.1B). Within the statistically significantly differentially expressed transcripts in Lgr6/EGFP^{+} cells we found a large number of non-coding RNAs with reduced expression (e.g. 15 of the top 35 attenuated RNAs). Two prominently lower

expressed non-coding RNAs located in the same gene locus are *Snord15a* and *Snord15b* (see Figure 6.2A, and Supplementary Figure S6.4). Among the protein-coding RNAs most strongly reduced were *Sostdc1* and *Fst* (Figure 6.2A, arrow heads). We also identified several more highly expressed protein-coding genes (Figure 6.2A). From these most differentially expressed (e.g. *Igfbp3*, *Adam8*, *Nat8l*, *Skint7*, *Crispld2*, *Adamts14*, *Ngfr*, *Slc2a12*), we identified Ngfr (low affinity nerve growth factor receptor) and Slc2a12 (glucose transporter 12), as promising surface markers of Lgr6$^+$ stem cells (Supplementary Table S6.3).

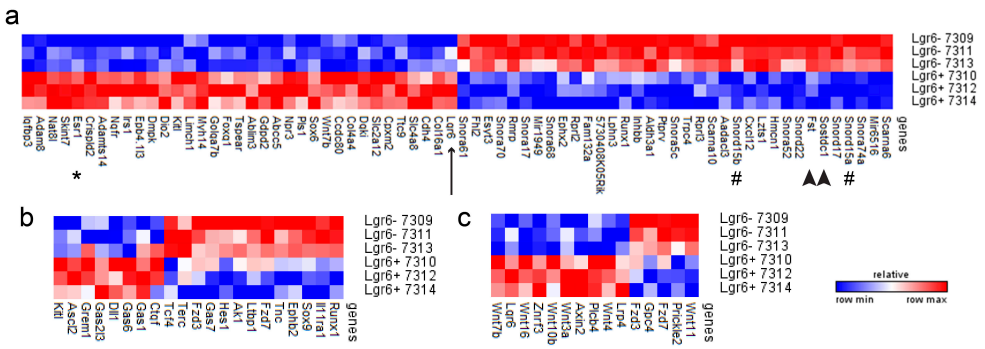


Figure 6.2: Heatmaps showing differentially expressed genes between Lgr6/EGFP$^+$ and Lgr6/EGFP$^-$ cells from tg/wt mice. (a) showing the top 35 higher and lower expressed genes (ranked on FDR) (*= *Esr1*, arrow = *Lgr6*, # = *Snord15a* and *b*, arrow heads = *Fst* and *Sostdc1*). (b) shows stem cell-related genes and (c) genes from the Wnt pathway.

6.3.3. Stem cell and cancer-related genes are higher expressed in Lgr6/EGFP$^+$ cells

Lgr6$^+$ cells are one of several stem cell populations localized in the skin [5]. Therefore, we looked for expression of previously identified stem cell-related genes in the Lgr6/EGFP$^+$ population from heterozygous mice [17-21]. Quantitative analysis of RNA-seq data showed higher expression of several stem cell-related genes (e.g. *Kitl*, *Gas* family members, *Ctgf*) (see Figure 6.2B). Furthermore, several bulge stem cell markers (e.g. *Tcf4*, *Fzd3*, *Runx1*, *Sox9*, *Tnc*) were lower expressed in Lgr6/EGFP$^+$ cells.

Gene-annotation enrichment analysis using DAVID and KEGG pathway mapping [15] supported stem cell characteristics of Lgr6/EGFP$^+$ cells showing increased expression of 11 genes involved in regulating pluripotency of stem cells and decreased expression of > 50 genes controlling metabolic pathways (Supplementary Table S6.4). Also, highly significant increased expression of pathways related to cancer, particularly basal cell carcinoma, including the hedgehog pathway was observed (Supplementary Table S6.4).

6.3.4. Wnt pathway genes are transcribed in Lgr6/EGFP⁺ cells from heterozygous mice

As Lgr6 receptor activation enhances canonical Wnt/β-catenin signaling [22], we checked expression levels of Wnt pathway genes (annotated according to the KEGG Wnt Pathway (http://www.genome.jp/kegg/ accessed April 22nd 2016) as well as genes previously described by de Lau et al. and Fearon and Spence [23, 24]. Several of these 'Wnt genes' (e.g. Wnt7b, Lgr6, Znrf3, Axin2) showed increased expression in Lgr6/EGFP⁺ stem cells (see Figure 6.2C; Axin2 expression verified by qPCR, Supplementary Figure S6.3b). However, other Wnt genes (for example Wnt11 and the Wnt pathway inhibitor Apcdd1) were reduced in expression in Lgr6/EGFP⁺ stem cells (Figure 6.2C). Of the four types of Rspos that have been described as ligands for Lgr6 [22, 25], only expression of Rspo3 was observed in Lgr6/EGFP⁺ and Lgr6/EGFP⁻ cells.

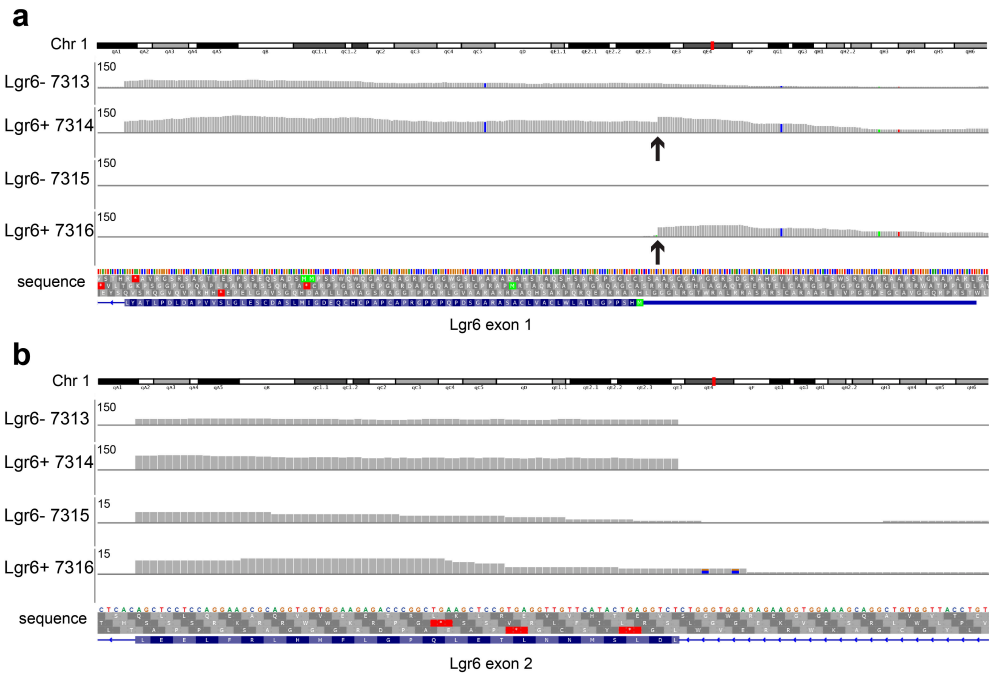


Figure 6.3: *Lgr6* expression of exon 1 and exon 2 in a heterozygous (tg/wt) and a homozygous sample (tg/tg). Screenshot from IG viewer of the base counts for *Lgr6* exon 1 (a) and exon 2 (b) are depicted for epidermal basal cells (Lgr6/EGFP⁻, odd samples) and for Lgr6/EGFP⁺ stem cells (even samples). RNA transcription progresses from right to left (Lgr6 is located on the reverse DNA strand). Samples 7313 and 7314 are heterozygous and 7315 and 7316 are homozygous transgenic. The arrow (a) shows the position were the cassette (*EGFP-Ires-CreERT2*) is inserted. This results in no transcription of exon 1 in the homozygous sample. In the homozygous sample transcription starts in close proximity to exon 2 (b).

6.3.5. Homozygous transgenic Lgr6-EGFP-Ires-CreERT2/R26R-LacZ mice express delta-Lgr6

Detailed inspection of the RNA-seq results obtained from homozygous knock-in mice, shows that these mice do transcribe *Lgr6*. However, transcription is initiated in close proximity to exon 2 (see Figure 6.3) and ends in exon 18 resulting in an mRNA encoding an isoform of Lgr6. In-silico translation of the resulting open reading frame gives rise to a N-terminal truncated protein (delta-Lgr6) lacking 74 amino acids compared to Lgr6. Expression of this truncated form of Lgr6 was confirmed by qPCR (see Supplementary Figure S6.5 and Supplementary Table S6.5 for used primers).

Since Lgr6 (mouse) and LGR6 (human) display a high degree of amino acid sequence homology in their N-terminal region, we used the human proteome database (proteomicsDB) to search for a human delta-LGR6 homologue. A perfectly matching tryptic peptide (minus the N-terminal methionine) was found in dataset PRDB000032 [26], indicating that the human delta-LGR6 homologue is expressed (see Figure 6.4) and post translationally modified by removing the N-terminal methionine.


```
exon 1
 5'-.............................ATGCCCAGCCCGCCGGGGCTCCGGGCGCTA     30
    .............................-M--P--S--P--P--G--L--R--A--L-     10
exon 1
 31 TGGCTTTGCGCCGCGCTGTGCGCTTCCCGGAGGGCCGGCGGCGCCCCCCAGCCCGGCCCG     90
 11 -W--L--C--A--A--L--C--A--S--R--R--A--G--G--A--P--Q--P--G--P-     30
exon 1
 91 GGGCCCACCGCCTGCCCGGCCCCCTGCCACTGCCAGGAGGACGGCATCATGCTGTCTGCC    150
 31 -G--P--T--A--C--P--A--P--C--H--C--Q--E--D--G--I--M--L--S--A-     50
exon 1
151 GACTGCTCTGAGCTCGGGCTGTCCGCCGTTCCGGGGGACCTGGACCCCCTGACGGCTTAC    210
 51 -D--C--S--E--L--G--L--S--A--V--P--G--D--L--D--P--L--T--A--Y-     70
exon 1| exon 2
211 CTGGACCTCAGCATGAACAACCTCACAGAGCTTCAGCCTGGCCTCTTCCACCACCTGCGC-3' 270
 71 -L--D--L--S--M--N--N--L--T--E--L--Q--P--G--L--F--H--H--L--R-     90
```

Figure 6.4: Sequence of human delta-*LGR6* starting at exon 2. The nucleotide (upper line) and amino acid sequence (bottom line) of *LGR6* and delta-*LGR6* (in bold, starting at the in-frame Methionine (M) at position 75 in *LGR6*) are given. The tryptic peptide corresponding to the N-terminal part of the delta-LGR6 protein (without N-terminal Methionine) identified in the human proteome database (proteomics DB) is underlined.

6.4. Discussion

In this study we characterized *Lgr6*-expressing cells in skin of hairless mice using a combination of live cell sorting (Lgr6/EGFP$^+$ vs Lgr6/EGFP$^-$ epidermal basal cells) and RNA-seq. We identified a collection of differentially expressed protein-coding and non-coding RNAs in Lgr6/EGFP$^+$ stem cells when compared to Lgr6/EGFP$^-$ basal epidermal cells. In addition, we found that in *Lgr6-EGFP-Ires-CreERT2/R26R-LacZ* homozygous mice, presumed *Lgr6-null*, an Lgr6-encoding mRNA is transcribed starting from exon 2 of the *Lgr6* gene resulting in a delta-Lgr6 isoform lacking 74 N-terminal amino acids.

Live cell sorting on fluorescence of EGFP expressed from a cassette under transcriptional control of the *Lgr6* promoter resulted in a cell population highly purified for expression of *ERT2* mRNA from the same cassette. As expected, *Lgr6* was amongst the statistically significantly higher expressed genes in the Lgr6/EGFP$^+$ cells. However, the Lgr6/EGFP$^-$ fraction of cells showed some expression of *Lgr6* mRNA. This might be explained by *Lgr6* promoter hypermethylation in some cells. We found this mono-allelic, *de novo*, methylation to occur stochastically [10; Chapter 5] leaving the wildtype (wt) *Lgr6* allele (without insertion of the cassette) unaffected. Thus, silencing EGFP expression from the cassette without silencing of the wt *Lgr6* allele would result in *Lgr6* mRNA expression in an EGFP-negative cell.

Among the differentially expressed genes we found many non-coding (nc) RNAs that were lower expressed. Two lower expressed ncRNAs are located in the *Rps3* locus; *Snord15a* and *Snord15b*. Rps3 plays a role in repair of UV-damaged DNA, by cleaving the phosphodiester bond between pyrimidine dimers [27, 28]. *Rps3* itself was not significantly differentially expressed between Lgr6/EGFP$^+$ and Lgr6/EGFP$^-$ cells (FDR 0.14), suggesting no difference in related DNA repair capacities between these cell populations. However, the functional impact of these SnoRNAs as well as the other differentially expressed ncRNAs is unknown.

Most prominently lower expressed protein-coding genes in Lgr6/EGFP$^+$ cells compared to Lgr6/EGFP$^-$ cells were *Sostdc1* and *Fst*. *Sostdc1* is a negative regulator of BMP signaling, while *Fst* has been recognized as a regulator of epidermal homeostasis, wound repair and hair growth [29, 30]. Furthermore, Fst is a bulge marker [31] and its decreased expression is in line with the finding that Lgr6 stem cells are not bulge stem cells but a unique population also not expressing CD34 and K15 [5]. Our RNA seq data showed lower expression of several bulge stem cell markers and higher expression of stem cell related genes in Lgr6/EGFP$^+$ cells. Among the top of higher expressed protein-coding genes in Lgr6/EGFP$^+$ cells, Ngfr (low affinity nerve growth factor receptor) and Slc2a12 (glucose transporter 12) were identified as promising markers of Lgr6$^+$ stem cells. These proteins are membrane bound and are expressed in a fraction of epidermal basal cells (see Supplementary Table S6.3). However, further research is evidently needed to verify *LGR6* expression in human skin cells carrying these alternative markers. Regarding R-spondin

expression, only *Rspo3* mRNA rose above detection level (equally expressed in Lgr6/EGFP$^+$ and Lgr6/EGFP$^-$ cells) suggesting that this protein is key for Lgr6 activation in the (murine) skin. Lgr6/EGFP$^+$ basal cells appear to show significant collective increased expression of genes coding for proteins involved in cancer. Despite this incriminating feature we found no evidence of Lgr6$^+$ basal stem cell becoming tumor-initiating cells in UV-driven or chemically induced skin carcinogenesis [10; Chapter 5]. The lowered expression of genes coding for proteins involved in metabolism would appear to be a sound feature for a long lived stem cell in keeping its integrity. Decreased expression of oxidative phosphorylation could spare mitochondria and lower the leakage of reactive oxygen species. The KEGG pathway analysis did, however, not identify a mirror increase of expression of genes coding for proteins catalysing glycolysis, a putative feature of stem cells [32]. But the balance between oxidative phosphorylation and glycolysis may depend on the nutrients available [33].

In our homozygous *Lgr6-EGFP-Ires-CreERT2/R26R-LacZ* mice we identified delta-Lgr6, a truncated isoform of Lgr6, which has several implications. Firstly, it could underlie the remarkable finding of Snippert et al. [5] and our own observation with hairless mice that homozygous EGFP-Ires-CreERT2 knock in mice, erroneously assumed *Lgr6 null*, are healthy and fertile. Based on sequence homology with LGR4, critical R-spondin binding residues in the ectodomain of LGR6 are identified and located in a stretch of amino acids ranging from residue 121-263 [34]. This domain is completely preserved in delta-LGR6/Lgr6 implicating that this isoform is able to bind R-spondins. Thus, delta-Lgr6 could be functional, explaining the lack of a phenotype in homozygous knock-in mice (Tg/Tg). The biological implications of truncated delta-LGR6 need to be explored by performing functional assays. Furthermore, expression of delta-Lgr6 provides an (additional) explanation for the presence of Lgr6 transcripts in Lgr6/EGFP$^-$ cells. Lgr6/EGFP$^+$ cells were isolated assuming transcription initiation in exon 1 and hence forcing expression of the inserted EGFP cassette. Cells solely expressing delta-Lgr6 (and not the full length variant) may be part of the Lgr6/EGFP$^-$ fraction. Thirdly, the identification of a human homologous protein, corresponding to the N-terminal of delta-LGR6, indicates that this isoform is expressed in human tissues as well. In this context, it sheds a new light on the earlier suggestions that *LGR6* is a tumor suppressor gene [22], with a promoter hypermethylated in 30-50% of colorectal samples tested [35], but also an oncogene in gastric carcinoma [36]. We envision a scenario in which methylation of the promoter region upstream of exon 1 results in silencing of the full length transcript (and hence losing its tumor suppressor function), but not affecting expression of the delta-LGR6 isoform. The functional implications of the isoform of *Lgr6* requires further investigation.

After initial presentation of this work (Bastidas et al. 2015) [37], Füllgrabe et al. [2] reported an in depth analysis of Lgr6$^+$ cells in the hair follicle, SG and IFE of haired transgenic *Lgr6-EGFP-Ires-CreERT2* knock-in mice. They claim that there is no distinct Lgr6-associated gene

expression signature and only found differential expression in the hair follicle and not in the IFE (which particularly held for Lgr6 itself). Our data pertain mainly to IFE Lgr6/EGFP$^+$ basal cells, as Lgr6/EGFP$^+$ cells are most numerous in the IFE of hairless mice and epidermal cells were scraped off the dermis. We suspect that the contradiction between the data is due to deficiencies in their experimental set up. They started from samples of 1 ng RNA whereas we used 450 ng RNA input for RNA-seq. We attained on average 100 million reads per sample (100x more than Füllgrabe et al.) allowing reliable quantification of low abundant transcripts [38] and rigorous statistical testing. Hence, they are likely to have missed many of the differentially expressed genes we have found. Furthermore, they obtained some data that appears contradictory to earlier findings of the group. In their real-time PCR data they find Lgr5 expressed in HF Lgr6$^+$ cells [2], however Lgr6$^+$ and Lgr5$^+$ cells were earlier established as two distinct cell populations [5].

We conclude that Lgr6/EGFP$^+$ basal epidermal keratinocytes (mainly of interfollicular origin) display a distinct RNA expression pattern, which harbors known hallmarks of stem cells like increased expression of genes encoding signalling proteins regulating pluripotency and decreased expression of genes controlling metabolic activity [39]. The pattern is also typified by differential expression of a large collection of non-coding RNAs and a set of protein-encoding RNAs hitherto not recognized as being co-expressed with *Lgr6* (e.g. *Igfbp3*, *Adam8*, *Nat8l*, *Skint7*, *Crispld2*, *Adamts14*, *Ngfr*, *Slc2a12*). This RNA expression profile of Lgr6/EGFP$^+$ cells serves as a starting point for future functional characterization and identification of these cells by robust markers, also in human skin.

Acknowledgements

We thank prof. Hans Clevers and his team for starting us up with the transgenic mice and Heggert Rebel for assistance in performing the experiments. Paul Hensbergen suggested and supported searching the proteomicsDB database. Yavuz Ariyurek carried out the RNA-seq. Furthermore, we thank the technicians of the LUMC animal facility for breeding our mouse strains.

Accession Numbers

RNA-seq data available at http://www.ebi.ac.uk/ena/data/view/PRJEB15002.

References

1. Jaks V, Kasper M and Toftgard R. The hair follicle-a stem cell zoo. Exp Cell Res. 2010; 316(8):1422-1428.
2. Füllgrabe A, Joost S, Are A, Jacob T, Sivan U, Haegebarth A, Linnarsson S, Simons B D, Clevers H, Toftgård R and Kasper M. Dynamics of Lgr6(+) Progenitor Cells in the Hair Follicle, Sebaceous Gland, and Interfollicular Epidermis. Stem cell reports. 2015; 5(5):843-855.
3. Liao XH and Nguyen H. Epidermal expression of Lgr6 is dependent on nerve endings and Schwann cells. Exp Dermatol. 2014; 23(3):195-198.
4. Page ME, Lombard P, Ng F, Gottgens B and Jensen KB. The epidermis comprises autonomous compartments maintained by distinct stem cell populations. Cell stem cell. 2013; 13(4):471-482.
5. Snippert HJ, Haegebarth A, Kasper M, Jaks V, van Es JH, Barker N, van de Wetering M, van den Born M, Begthel H, Vries RG, Stange DE, Toftgard R and Clevers H. Lgr6 marks stem cells in the hair follicle that generate all cell lineages of the skin. Science. 2010; 327(5971):1385-1389.
6. Hsu SY, Kudo M, Chen T, Nakabayashi K, Bhalla A, van der Spek PJ, van Duin M and Hsueh AJ. The three subfamilies of leucine-rich repeat-containing G protein-coupled receptors (LGR): identification of LGR6 and LGR7 and the signaling mechanism for LGR7. Mol Endocrinol. 2000; 14(8):1257-1271.
7. Tensen CP, Van Kesteren ER, Planta RJ, Cox KJ, Burke JF, van Heerikhuizen H and Vreugdenhil E. A G protein-coupled receptor with low density lipoprotein-binding motifs suggests a role for lipoproteins in G-linked signal transduction. Proceedings of the National Academy of Sciences of the United States of America. 1994; 91(11):4816-4820.
8. de Lau W, Peng WC, Gros P and Clevers H. The R-spondin/Lgr5/Rnf43 module: regulator of Wnt signal strength. Genes Dev. 2014; 28(4):305-316.
9. Chitsazzadeh V, Coarfa C, Drummond JA, Nguyen T, Joseph A, Chilukuri S, Charpiot E, Adelmann CH, Ching G, Nguyen TN, Nicholas C, Thomas VD, Migden M, MacFarlane D, Thompson E, Shen J, et al. Cross-species identification of genomic drivers of squamous cell carcinoma development across preneoplastic intermediates. Nature communications. 2016; 7:12601.
10. van de Glind GC, Rebel HG, Out-Luiting JJ, Zoutman W, Tensen CP and de Gruijl FR. Lgr6+ stem cells and their progeny in mouse epidermis under regimens of exogenous skin carcinogenesis, and their absence in ensuing skin tumors. Oncotarget. 2016; 7(52):86740-86754.
11. Jensen KB, Driskell RR and Watt FM. Assaying proliferation and differentiation capacity of stem cells using disaggregated adult mouse epidermis. Nat Protoc. 2010; 5(5):898-911.
12. Robinson MD, McCarthy DJ and Smyth GK. edgeR: a Bioconductor package for differential expression analysis of digital gene expression data. Bioinformatics. 2010; 26(1):139-140.
13. Robinson MD and Oshlack A. A scaling normalization method for differential expression analysis of RNA-seq data. Genome Biol. 2010; 11(3):R25.
14. Robinson JT, Thorvaldsdottir H, Winckler W, Guttman M, Lander ES, Getz G and Mesirov JP. Integrative genomics viewer. Nat Biotechnol. 2011; 29(1):24-26.
15. Huang da W, Sherman BT and Lempicki RA. Systematic and integrative analysis of large gene lists using DAVID bioinformatics resources. Nat Protoc. 2009; 4(1):44-57.
16. Feil R, Wagner J, Metzger D and Chambon P. Regulation of Cre recombinase activity by mutated estrogen receptor ligand-binding domains. Biochem Biophys Res Commun. 1997; 237(3):752-757.
17. Ambler CA and Maatta A. Epidermal stem cells: location, potential and contribution to cancer. J Pathol. 2009; 217(2):206-216.

18. Beck B and Blanpain C. Mechanisms regulating epidermal stem cells. EMBO J. 2012; 31(9):2067-2075.
19. Blanpain C and Fuchs E. Epidermal stem cells of the skin. Annu Rev Cell Dev Biol. 2006; 22:339-373.
20. Saldanha SN, Royston KJ, Udayakumar N and Tollefsbol TO. Epigenetic Regulation of Epidermal Stem Cell Biomarkers and Their Role in Wound Healing. International journal of molecular sciences. 2016; 17(1).
21. Tumbar T, Guasch G, Greco V, Blanpain C, Lowry WE, Rendl M and Fuchs E. Defining the epithelial stem cell niche in skin. Science. 2004; 303(5656):359-363.
22. Gong X, Carmon KS, Lin Q, Thomas A, Yi J and Liu Q. LGR6 is a high affinity receptor of R-spondins and potentially functions as a tumor suppressor. PLoS One. 2012; 7(5):e37137.
23. de Lau WB, Snel B and Clevers HC. The R-spondin protein family. Genome Biol. 2012; 13(3):242.
24. Fearon ER and Spence JR. Cancer biology: a new RING to Wnt signaling. Curr Biol. 2012; 22(19):R849-851.
25. de Lau W, Barker N, Low TY, Koo BK, Li VS, Teunissen H, Kujala P, Haegebarth A, Peters PJ, van de Wetering M, Stange DE, van Es JE, Guardavaccaro D, Schasfoort RB, Mohri Y, Nishimori K, et al. Lgr5 homologues associate with Wnt receptors and mediate R-spondin signalling. Nature. 2011; 476(7360):293-297.
26. Munoz J, Low TY, Kok YJ, Chin A, Frese CK, Ding V, Choo A and Heck AJ. The quantitative proteomes of human-induced pluripotent stem cells and embryonic stem cells. Mol Syst Biol. 2011; 7:550.
27. Kim J, Chubatsu LS, Admon A, Stahl J, Fellous R and Linn S. Implication of mammalian ribosomal protein S3 in the processing of DNA damage. J Biol Chem. 1995; 270(23):13620-13629.
28. Seong KM, Jung SO, Kim HD, Kim HJ, Jung YJ, Choi SY and Kim J. Yeast ribosomal protein S3 possesses a beta-lyase activity on damaged DNA. FEBS Lett. 2012; 586(4):356-361.
29. Antsiferova M, Klatte JE, Bodo E, Paus R, Jorcano JL, Matzuk MM, Werner S and Kogel H. Keratinocyte-derived follistatin regulates epidermal homeostasis and wound repair. Lab Invest. 2009; 89(2):131-141.
30. Chen CC, Murray PJ, Jiang TX, Plikus MV, Chang YT, Lee OK, Widelitz RB and Chuong CM. Regenerative hair waves in aging mice and extra-follicular modulators follistatin, dkk1, and sfrp4. J Invest Dermatol. 2014; 134(8):2086-2096.
31. Ohyama M, Terunuma A, Tock CL, Radonovich MF, Pise-Masison CA, Hopping SB, Brady JN, Udey MC and Vogel JC. Characterization and isolation of stem cell-enriched human hair follicle bulge cells. J Clin Invest. 2006; 116(1):249-260.
32. Hamalainen RH. Mitochondria and mtDNA integrity in stem cell function and differentiation. Curr Opin Genet Dev. 2016; 38:83-89.
33. Zhang H, Badur MG, Divakaruni AS, Parker SJ, Jager C, Hiller K, Murphy AN and Metallo CM. Distinct Metabolic States Can Support Self-Renewal and Lipogenesis in Human Pluripotent Stem Cells under Different Culture Conditions. Cell reports. 2016; 16(6):1536-1547.
34. Xu JG, Huang C, Yang Z, Jin M, Fu P, Zhang N, Luo J, Li D, Liu M, Zhou Y and Zhu Y. Crystal structure of LGR4-Rspo1 complex: insights into the divergent mechanisms of ligand recognition by leucine-rich repeat G-protein-coupled receptors (LGRs). J Biol Chem. 2015; 290(4):2455-2465.
35. Mokarram P, Kumar K, Brim H, Naghibalhossaini F, Saberi-firoozi M, Nouraie M, Green R, Lee E, Smoot DT and Ashktorab H. Distinct high-profile methylated genes in colorectal cancer. PLoS One. 2009; 4(9):e7012.

36. Steffen JS, Simon E, Warneke V, Balschun K, Ebert M and Rocken C. LGR4 and LGR6 are differentially expressed and of putative tumor biological significance in gastric carcinoma. Virchows Arch. 2012; 461(4):355-365.
37. Zhao Q PP, Arias-Mendoza F, Stoyanova R, Brown T. An interactive software for 3D chemical shift imaging data analysis and real time spectral localization and quantification. Proc Int Soc Magn Reson Med 2005; 13:2465.
38. Sims D, Sudbery I, Ilott NE, Heger A and Ponting CP. Sequencing depth and coverage: key considerations in genomic analyses. Nat Rev Genet. 2014; 15(2):121-132.
39. Cheung TH and Rando TA. Molecular regulation of stem cell quiescence. Nat Rev Mol Cell Biol. 2013; 14(6):329-340.

Supplementary Material

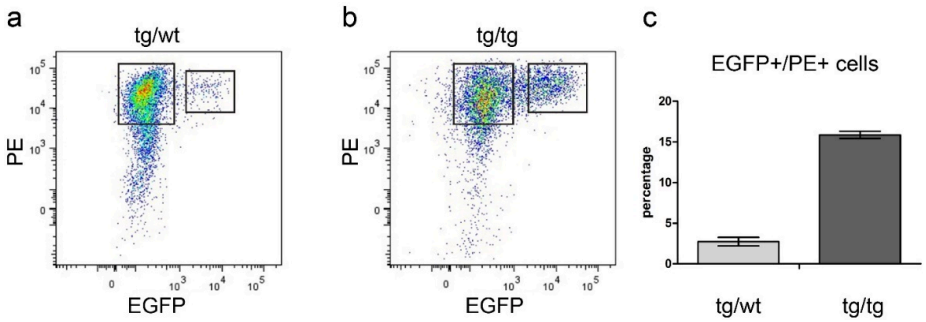
S6.1. Methods

S6.1.1. Cell suspension preparation

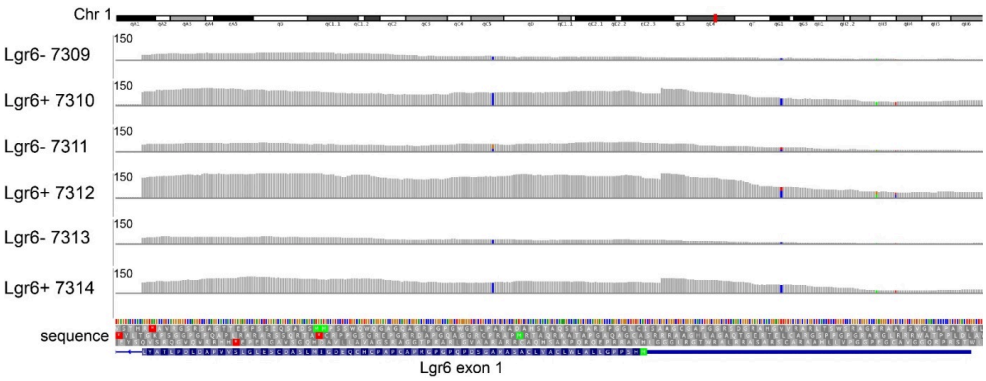
Mice were sacrificed by CO_2 asphyxiation, and back and belly skin was removed. The skin sample was incubated epidermal side up in 25 ml PBS containing trypsin (0.25%; T4799, Sigma-Aldrich, St. Louis, MO, USA) + D-glucose (0.1%; G5400, Sigma-Aldrich) over night at 4°C and at 37°C for 15 min. The epidermis was scraped off of the dermis and minced. The epidermis was digested using 8 ml PBS containing trypsin (0.25%) + D-glucose (0.1%) and repeated pipetting. 16 ml PBS with 5% BSA (A9647, Sigma-Aldrich), DNAse I (200 Kunitz units/ml; DN25, Sigma-Aldrich) and $MgCl_2.6H_2O$ (5 mM; M2393, Sigma-Aldrich) was added and the suspension was put through a 70 µm cell strainer. The strained cell suspension was incubated for 30 minutes at RT. Cells were spinned down and resuspended in 300 µl of supernatant. 8 ml PBS with BSA (1%), DNAse I (50 Kunitz units/ml) and $MgCl_2.6H_2O$ (5 mM) was added, spinned down and again resuspended in 300 µl of the supernatant. The volume was brought to 2 ml with PBS containing BSA (0.2%), DNAse I (50 Kunitz units/ml) and $MgCl_2.6H_2O$ (5 mM). Back and belly cell suspensions of the same animal were combined and cell viability and cell numbers were determined.

S6.1.2. Reverse transcription and qPCR

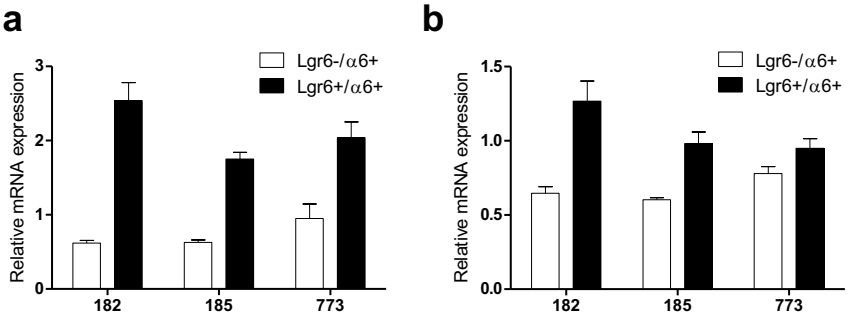
Total RNA was isolated from frozen skin using the RNeasy mini kit (74106, Qiagen, Hilden, Germany) including on-column DNase treatment. cDNA was synthesized from 1 µg total RNA using the iScript™ cDNA Synthesis Kit (170-8891, Biorad, Veenendaal, The Netherlands) according to manufacturer's instructions. qPCR for the different exons of Lgr6 was performed using the SYBR Green Supermix (Bio-Rad) on the CFX384™ real-time PCR detection system (Biorad). Cycle parameters were as follows: Hot start for 3 minutes at 95°C; denaturation for 15 seconds at 95°C, annealing and extension for 30 seconds at 60°C for 40 cycles. Specificity of the PCR products was confirmed by melting curve analysis. Data was normalized against reference genes Cyc1 and Ddx52 (see supplementary Table S6.5 for primers used) using the ΔΔCq method (Livak and Schmittgen, 2001) and is presented as relative mRNA expression (see supplementary figure S4).



Supplementary Figure S6.1: FACS sorting of Lgr6/EGFP⁺ cells from murine skin. The FACS plots show three main distinguishable areas: apparent Lgr6⁺ epidermal stem cells (PE⁺/EGFP⁺), cells that are negative for both markers (PE⁻/EGFP⁻) and basal layer epidermal cells (PE⁺/EGFP⁻); the latter group constituting the largest fraction of cells in suspension. a**)** FACS sorting of a heterozygous Lgr6⁺ knock-in mouse and b) a homozygous Lgr6⁺ knock-in mouse c**)** EGFP⁺/PE⁺ cells constitute on average 2.5% and 15% of all cells in suspension in heterozygous and homozygous knock-in animals, respectively. Error Bars: Standard Error, Tg/wt (n=11), Tg/Tg (n=4).



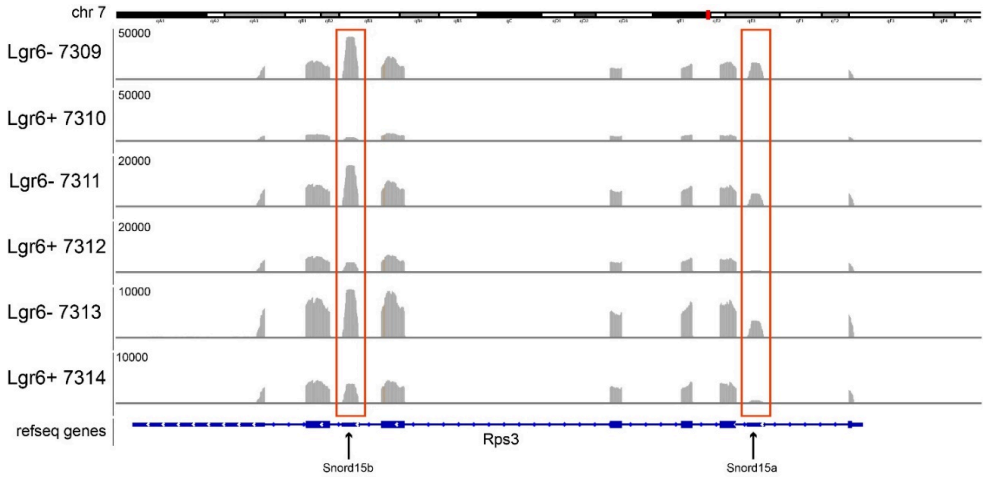
Supplementary Figure S6.2: IGV visualization of reads aligned to Exon 1 of the Lgr6 gene for all heterozygous transgenic samples. Read count for Lgr6 exon 1 is shown (y-axis = 150) for epidermal basal cells (Lgr6/EGFP^{-}, odd sample numbers) and Lgr6/EGFP^{+} stem cells (even sample numbers). Lgr6/EGFP^{+} stem cells express higher counts (also after normalization), however the Lgr6/EGFP^{-} samples are not completely negative for Lgr6.



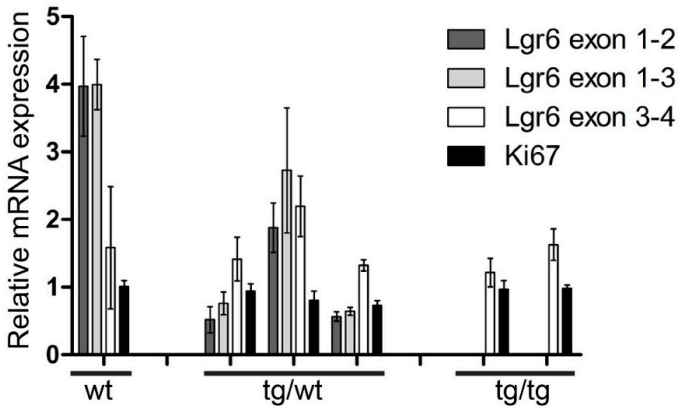
Supplementary Figure S6.3: Relative mRNA expression of stem-cell markers in *Lgr6/EGFP*$^{+}$ and Lgr6/EGFP^{-} cells. Gene expression of *Lgr6* (a) and *Axin2* (b) was measured in sorted *Lgr6/EGFP*$^{+}$ (black bars) and *Lgr6/EGFP*$^{-}$ basal layer cells (white bars) from 3 heterozygous (Tg/wt) *Lgr6-EGFP-Ires-CreERT2/R26R-LacZ* hairless mice by qPCR and normalized against stably expressed reference genes (see Methods above and Supplementary table S3 for used primers). a) *Lgr6* expression (ANOVA p<0.0001) b) *Axin2* expression (ANOVA p<0.0001). Whiskers depict SEMs.

Supplementary Table S6.1: Sample information Lgr6-EGFP-Ires-CreERT2/R26R-LacZ mice for RNA-seq

Mouse code	Gender	Genotype	Age (days)	sample IDs
701	M	Tg/wt	28	7309/ 7310
721	F	Tg/wt	31	
720	M	Tg/wt	31	7311/ 7312
722	F	Tg/wt	31	
565	M	Tg/wt	95	7313/ 7314
774	F	Tg/wt	90	
508	M	Tg/Tg	147	7315/ 7316
550	F	Tg/Tg	176	



Supplementary Figure S6.4: IGV screenshot of (m)RNA expression corresponding to the region encoding the *Rps3* gene (including *Snord15a* and *Snord15b*) for all heterozygous transgenic samples. The counts for the *Rps3* gene, *Snord15a* and *Snord15b* are represented (on y-axis, with max values), for the epidermal basal cells (Lgr6/EGFP^{-}, odd sample numbers) and for the Lgr6/EGFP^{+} stem cells (even sample numbers). The Lgr6/EGFP^{+} cells show lower counts for *Rps3* compared to the Lgr6/EGFP^{-} cells. *Snord15a* and *Snord15b* are even more prominently downregulated in Lgr6/EGFP^{+} cells (see red boxes and arrows).



Supplementary Figure S6.5: Relative mRNA expression of *Lgr6* in hairless mice. Gene expression of *Lgr6* and *Ki67* was measured by qPCR and normalized against stably expressed reference genes (see Methods above and Supplementary table S5 for used primers). RNA was isolated from SKH-1 mice (wt), heterozygous *Lgr6-EGFP-Ires-CreERT2/R26R-LacZ* mice (Tg/wt) and homozygous *Lgr6-EGFP-Ires-CreERT2/R26R-LacZ* mice (Tg/Tg). *Lgr6* gene expression was measured using different primer pairs. The primer pairs for exon 1-2 and exon 1-3 detect expression of the wt *Lgr6* allele, the primers for exon 3-4 detect expression of the wt allele and the alternative transcript. In homozygous *Lgr6-EGFP-Ires-CreERT2/R26R-LacZ* mice expression of exon 1-2 and exon 1-3 is not detected at all, however expression of *Lgr6* exon 3-4 was found. Error bars are SEMs.

Supplementary Table S6.2: The top 35 higher (A) and lower (B) expressed genes in Lgr6/EGFP^{+} basal epidermal keratinocytes (FDR <0.05).

A. higher expressed cells in Lgr6/EGFP^{+} cells

genes	logFC	logCPM	LR	PValue	FDR	S7309	S7311	S7313	S7310	S7312	S7314
Igfbp3	1.7449	9.5469	72.978	1.31E-17	1.71E-14	324.10z	403.13	304	1305.4	1300.2	850.83
Adam8	1.2265	7.0886	68.619	1.19E-16	1.31E-13	83.817	77.296	83.216	214.35	196.17	161.29
Nat8l	1.4536	5.0829	64.432	9.99E-16	9.08E-13	14.311	21.148	19.067	42.709	52.784	53.034
Esr1	2.2224	3.6625	62.661	2.46E-15	2.07E-12	3.1384	4.1264	6.3258	16.389	24.489	21.389
Skint7	1.1538	6.8996	62.646	2.47E-15	2.07E-12	64.024	82.012	76.177	154.93	165.88	172.95
Crispld2	1.1386	5.1898	61.572	4.27E-15	3.3E-12	21.258	22.99	24.145	53.043	48.977	48.125
Adamts14	1.1792	7.0443	59.966	9.65E-15	6.5E-12	69.045	84.665	89.007	165.02	203.61	180.23
Ngfr	1.4180	5.2511	49.561	1.92E-12	7.87E-10	19.207	23.948	18.977	55.546	70.264	40.148
Irs1	1.7518	4.7576	48.582	3.17E-12	1.23E-09	9.7082	17.463	9.9788	36.169	54.602	34.1
Epb4.1l3	1.2735	4.9235	48.021	4.22E-12	1.55E-09	16.655	19.6	16.928	45.292	49.583	33.574
Dmpk	1.6867	4.0894	46.435	9.47E-12	3.3E-09	6.4861	9.7265	8.0187	23.009	34.526	20.074
Dio2	1.3821	5.0598	45.085	1.89E-11	6.16E-09	15.525	16.211	23.878	40.045	44.304	59.872
Kitl	1.9530	3.5622	40.66	1.81E-10	5.11E-08	3.4313	5.7475	5.4349	25.432	18.431	12.097
Limch1	1.1370	6.2392	39.96	2.59E-10	7.12E-08	54.023	35.443	51.943	121.34	89.214	100.72
Myh14	0.87376	6.1916	39.737	2.91E-10	7.78E-08	57.705	48.632	48.023	92.684	92.33	98.53
Golga7b	1.8483	4.9568	36.684	1.39E-09	3.45E-07	9.7919	18.79	11.939	41.094	74.244	30.243
Foxq1	1.2222	5.1409	36.576	1.47E-09	3.57E-07	18.705	24.169	20.581	38.511	65.332	44.005
Tspear	1.6016	3.9072	36.229	1.75E-09	4.16E-07	6.0676	9.3581	6.8604	19.942	30.805	16.655
Ablim3	1.2686	3.9722	35.692	2.31E-09	5.25E-07	9.2479	8.6949	9.5333	19.861	19.037	27.35
Gdpd2	0.89909	6.4363	33.716	6.38E-09	1.33E-06	55.069	62.633	63.615	93.733	131.53	112.56
Abcc5	0.82111	8.1548	32.282	1.33E-08	2.63E-06	195.84	205.51	216.59	334.32	376.41	380.79
Npr3	1.5884	3.2504	32.221	1.38E-08	2.66E-06	4.5193	6.1896	3.3857	15.501	16.095	10.957
Pls1	1.3763	3.7188	31.88	1.64E-08	3.14E-06	6.5279	7.2949	8.1078	20.91	22.325	13.412
Sox6	0.9710	6.9617	31.497	2E-08	3.76E-06	70.008	82.159	100.59	142.17	154.98	197.59
Wnt7b	0.7848	7.1348	31.014	2.56E-08	4.78E-06	109.09	103.31	96.937	198.37	173.24	161.64
Ccdc80	1.4790	3.7009	30.74	2.95E-08	5.45E-06	8.3691	6.4843	5.4349	23.817	20.248	13.061
Col4a4	4.0657	0.2678	30.705	3E-08	5.5E-06	0.16738	0.073686	0.08910	4.1175	1.298	0.96426
Dgki	1.4240	3.5359	30.476	3.38E-08	6.11E-06	4.8123	8.1054	5.9694	17.439	19.383	13.5
Slc2a12	0.7383	7.0304	29.801	4.79E-08	8.19E-06	95.869	104.93	92.927	170.19	165.19	154.63
Cpxm2	0.7707	6.2835	29.56	5.42E-08	9.2E-06	61.681	53.496	57.2	109.96	91.032	93.358
Ttc9	1.1428	4.0059	28.475	9.49E-08	1.54E-05	9.8756	12.011	7.9296	21.314	25.354	19.373
Slc4a8	1.0628	4.2989	28.005	1.21E-07	1.93E-05	11.173	12.084	14.968	22.283	25.44	31.733
Cdh4	1.2123	4.0320	27.818	1.33E-07	2.08E-05	8.7039	9.2844	11.583	16.389	25.354	26.473
Col16a1	0.8571	8.9276	27.778	1.36E-07	2.11E-05	298.69	346.84	393.72	607.85	691.91	582.15
Lgr6	1.1048	6.6914	27.321	1.72E-07	2.61E-05	45.11	85.254	66.555	117.07	171.94	133.86

LogFC = Log Fold change, LogCPM = Log count per million bases, LR = Log Ratio, FDR = BH corrected P-value, values in columns S7309-S7314 depict TMM normalized relative expression.

B. lower expressed genes in Lgr6/EGFP^{+} cells

genes	logFC	logCPM	LR	PValue	FDR	S7309	S7311	S7313	S7310	S7312	S7314
Scarna6	-2.4245	5.9473	239.01	6.46E-54	1.35E-49	103.94	118.12	88.651	17.842	19.47	20.6
Mir6516	-2.8528	6.6951	199.44	2.76E-45	2.88E-41	229.77	187.24	127.23	24.543	26.392	24.457
Snora74a	-2.7083	6.2649	172.5	2.1E-39	1.46E-35	168.22	134.48	95.689	22.121	16.96	21.915
Snord15a	-3.0501	6.9805	149.66	2.06E-34	1.08E-30	333.68	189.67	150.57	29.226	26.133	26.035
Snord17	-2.4889	7.1345	136.44	1.6E-31	6.69E-28	249.19	284.65	180.24	36.977	34.44	55.839
Sostdc1	-1.7485	7.3240	114.82	8.63E-27	3.01E-23	281.66	232.77	225.24	86.79	65.245	68.112
Fst	-2.2292	5.1724	110.96	6.02E-26	1.8E-22	65.321	59.022	52.656	16.228	13.326	8.1524
Snord22	-3.2174	6.9402	110.12	9.23E-26	2.41E-22	323.89	231.52	107.63	20.265	23.969	27.087
Snora52	-2.702	5.0710	91.082	1.38E-21	3.2E-18	78.21	64.401	30.293	9.5267	8.3071	8.766
Hmcn1	-1.8156	8.6459	87.524	8.33E-21	1.74E-17	711.67	596.71	562.11	190.45	130.23	210.73
Lzts1	-1.6469	4.3742	84.378	4.09E-20	7.76E-17	32.012	29.179	32.075	8.6387	10.211	10.957
Cxcl12	-2.4579	3.4937	83.055	7.98E-20	1.39E-16	20.295	17.021	18.532	4.1175	2.0768	3.9447
Snord15b	-1.9953	8.6561	79.067	6.01E-19	9.65E-16	883.2	614.91	435.32	144.84	167.44	172.78
Aadacl3	-1.4765	5.5179	77.642	1.23E-18	1.84E-15	69.966	68.38	62.813	19.053	24.056	29.278
Scarna10	-2.0741	8.3224	77.048	1.67E-18	2.32E-15	454.44	663.1	433.36	161.39	124.09	82.751
Rprl3	-1.9896	7.6373	71.701	2.5E-17	3.08E-14	312.34	374.91	265.77	71.935	113.88	54.174
Trpc4	-2.2411	3.8988	69.096	9.38E-17	1.09E-13	29.543	25.2	17.641	6.9432	4.1535	4.2077
Snora5c	-2.9615	4.0084	67.249	2.39E-16	2.5E-13	41.009	29.843	12.652	4.279	3.2017	3.2434
Ptprv	-1.4416	5.3521	66.088	4.31E-16	4.29E-13	62.392	64.917	50.785	26.966	18.604	19.986
Aldh3a1	-1.5708	6.1532	64.904	7.86E-16	7.46E-13	116.92	85.107	116.45	46.665	27.69	32.785
Inhbb	-2.4236	4.3925	61.954	3.52E-15	2.82E-12	40.381	39.569	24.769	10.253	5.6246	3.5941
Runx1	-1.7567	4.8999	60.82	6.25E-15	4.66E-12	52.098	47.454	37.42	16.47	8.7397	15.34
Lphn3	-1.9446	5.9612	60.665	6.77E-15	4.87E-12	125.08	100.95	69.228	36.573	21.72	18.409
5730408K05Rik	-1.4932	5.8456	60.201	8.56E-15	5.96E-12	85.365	103.82	64.327	34.716	32.19	23.142
Fam132a	-1.7062	6.6756	59.371	1.31E-14	8.52E-12	164.66	153.27	150.48	66.768	46.9	29.804
Rprl2	-2.5996	2.9395	58.763	1.78E-14	1.13E-11	11.8	16.727	9.7115	1.7762	3.0286	1.4902
Ephx2	-2.3102	3.7890	58.162	2.41E-14	1.48E-11	27.702	22.548	17.285	6.2973	4.9323	2.3668
Snora68	-2.7941	3.2160	57.121	4.1E-14	2.45E-11	19.04	20.411	7.5732	2.3413	2.3364	2.1038
Mir1949	-2.7708	3.2810	56.087	6.93E-14	4.02E-11	23.141	17.832	8.0187	2.745	2.2498	2.1915
Snora17	-2.1567	3.7075	55.668	8.58E-14	4.84E-11	25.944	23.727	12.83	5.3285	3.8074	4.9089
Rmrp	-1.8943	13.3828	55.521	9.25E-14	5.08E-11	14861	19178	16428	5477.7	4995.4	3102.3
Snora70	-2.1428	3.9993	54.941	1.24E-13	6.65E-11	32.305	28.958	15.414	5.8937	4.3266	7.1881
Esyt3	-1.3876	4.3316	54.809	1.33E-13	6.83E-11	31.677	27.779	26.907	11.868	9.0859	12.097
Fhl2	-1.4977	4.4592	54.79	1.34E-13	6.83E-11	38.205	28.516	29.58	13.321	9.1724	11.659
Snora61	-1.9231	4.4797	52.168	5.1E-13	2.53E-10	35.778	48.19	20.67	8.5579	10.384	8.6783

LogFC = Log Fold change, LogCPM = Log count per million bases, LR = Log Ratio, FDR = BH corrected P-value, values in columns S7309-S7314 depict TMM normalized relative expression.

Supplementary Table S6.3: Potential markers of LGR6^{+} stem cells*

Gene	Protein membrane bound	Protein expressed in fraction of epidermal basal cells	Note on protein expression in epidermis
Igfbp3	no	?	Unknown (some RNA expression)
Adam8	yes	no	largely negative, incidental positive basal cell?
Nat8l	yes	?	Unknown (low RNA in skin)
Skint7	yes	?	in mouse; selection and upkeep of intraepithelial γδ T cells
Crispld2	no	no	medium strong mainly in basal layer
Adamts14	no	?	Unknown (some RNA expression)
Ngfr	yes	yes	positive in small patches and isolated basal cells; antibodies CAB000143 and 001995
Slc2a12	yes	yes	positive in small patches and isolated basal cells; antibody HPA031593

*Selection of 8 protein-coding genes with highly increased expression in Lgr6/EGFP^{+} basal cells screened for membrane-bound protein (genecard.org) and partial or sparse presence in epidermal basal layer (proteinatlas.org).

Supplementary Table S6.4: KEGG_Pathway analysis of higher expressed genes (A)* and lower expressed genes (B)# in Lgr6/EGFP+ basal epidermal keratinocytes.

A. Higher expressed genes

Term	Genes	Count	%	P-Value	Benjamini Hochberg corrected
Pathways in cancer	FGFR2, WNT16, FGFR3, PDGFB, WNT3A, ADCY6, FGF13, LAMB3, WNT4, PLCB4, AXIN2, MMP1B, BMP4, COL4A4, COL4A3, BMP2, WNT10B, COL4A2, TGFBR1, ITGA2, KITL, COL4A6, WNT7B, LAMA3, LAMC2, LAMC1, PTCH2	27	9,4	1,70E-10	2,90E-08
Amoebiasis	COL4A4, GNA14, COL4A3, IL1R1, COL4A2, COL4A6, LAMB3, PLCB4, LAMA3, SERPINB2, HSPB1, LAMC2, LAMC1	13	4,5	1,90E-07	1,60E-05
Hedgehog signaling pathway	BMP4, WNT16, WNT10B, BMP2, WNT7B, WNT4, WNT3A, GAS1, PTCH2	9	3,1	5,40E-07	3,10E-05
Basal cell carcinoma	BMP4, WNT16, WNT10B, BMP2, WNT7B, WNT4, WNT3A, PTCH2, AXIN2	9	3,1	1,60E-06	6,80E-05
Small cell lung cancer	COL4A4, COL4A3, COL4A2, LAMB3, LAMA3, ITGA2, LAMC2, LAMC1, COL4A6	9	3,1	3,90E-05	1,30E-03
Signaling pathways regulating pluripotency of stem cells	FGFR2, BMP4, WNT16, WNT10B, BMP2, WNT7B, WNT4, FGFR3, WNT3A, LIFR, AXIN2	11	3,8	4,60E-05	1,30E-03
ECM-receptor interaction	COL4A4, COL4A3, COL4A2, LAMB3, LAMA3, ITGA2, LAMC2, LAMC1, COL4A6	9	3,1	5,50E-05	1,30E-03
PI3K-Akt signaling pathway	FGFR2, COL4A4, COL4A3, COL4A2, FGFR3, PDGFB, OSMR, ITGA2, FGF13, KITL, IRS1, COL4A6, LAMB3, LAMA3, LAMC2, NGFR, LAMC1	17	5,9	8,10E-05	1,70E-03
Cytokine-cytokine receptor interaction	IL12RB2, IL1R1, CXCL14, PDGFB, OSMR, CCR4, IL20RA, TGFBR1, LIFR, EDAR, NGFR, KITL, IL22RA2	13	4,5	3,40E-04	6,40E-03
Hippo signaling pathway	BMP4, WNT16, WNT10B, BMP2, WNT7B, WNT4, CTGF, TGFBR1, WNT3A, AXIN2	10	3,5	4,60E-04	7,90E-03

* 119 of 291 upregulated genes were categorized in a pathway

B. Lower expressed genes

Term	Genes	Count	%	P-Value	Benjamini Hochberg corrected
Metabolic pathways	LDHB, ATP5E, GCNT2, OLAH, ACOT1, ITPKB, ADH7, ATP6V1B2, PSPH, CMBL, FDFT1, ALDH3A1, ISYNA1, UQCR10, CERS2, COX6B1, ATP5O, COX6B2, HADH, SARDH, BDH1, IMPDH1, DCTPP1, NDUFA4, EBP, AK1, COX8A, GALT, EPHX2, ALDH3B2, CBR3, NDUFA12, GNS, NME4, CYP17A1, ADO, CYP27A1, DGAT2, NME1, LIPG, AOX4	41	10,6	3,30E-05	6,00E-03
Metabolism of xenobiotics by cytochrome P450	GSTM1, ALDH3B2, ADH7, CBR3, GSTM5, GSTP1, ALDH3A1	7	1,8	9,70E-05	8,90E-03
Drug metabolism - cytochrome P450	GSTM1, ALDH3B2, AOX4, ADH7, GSTM5, GSTP1, ALDH3A1	7	1,8	1,40E-04	8,60E-03
Oxidative phosphorylation	NDUFA4, ATP5E, UQCR10, COX8A, COX6B1, ATP5O, ATP6V1B2, COX6B2, NDUFA12	9	2,3	2,30E-03	1,00E-01
Alzheimer's disease	NDUFA4, ATP5E, UQCR10, COX8A, GRIN1, COX6B1, ATP5O, COX6B2, CAPN2, NDUFA12	10	2,6	2,90E-03	1,00E-01

131 of 391 down regulated genes were categorized in a pathway

Supplementary Table S6.5: Primers used for qPCR.

Gene	Primer sequence (5'-> 3')	Amplicon size	Exonic Location	Accession No.	Amplification efficiency	Correlation (R^2)
Cyc1	GATGTCGCCACCTTC CTTCGC GGACTGACCACTTAT GCCGCTTC	136	6, 7	NM_025567.2	98.6%	0.99
Ddx52	CACAGCAGCAGCGA GATAACAC CTCTTCCAGTCCGAC CTATCCTATG	177	10-11, 11-12	NM_030096	107.0%	0.99
Lgr6 ex1-2	GCTGTCCGCTGACTG CTC AGCTCCGTGAGGTT GTTCAT	102	1, 2	NM_001033409	95.0%	0.97
Lgr6 ex1-3	GGACCCCCTGACGG CTTA TGTGAGAGGTGGTT CCCTGA	120	1, 3	NM_001033409	95.0%	0.97
Lgr6 ex3-4	TCAGGGAACCACCTC TCACA CATAGTGCCTCTGCT GGGAT	113	3, 4	NM_001033409	92.0%	0.95
Mki67	CAGAAGAAATGGAA GCCAAAA TGCAGATGCATCAAA CTTGG	110	12, 13	NM_001081117.2	96.5%	0.99
Axin2 ex2-3	CACGTAGGTTCCGGC TATGT TACGCTACTGTCCGT CATGG	108	2, 3	NM_015732	100.0%	0.98

Chapter 7

Summary And General Discussion

Summary and General Discussion

The incidence of skin carcinomas has been strongly rising over the last decades to levels posing a large burden on health care, specifically dermatological practices. Ultraviolet (UV) radiation from sun exposure is the main exogenous risk factor. The principal premise underlying the present study is that stem cells are the primary targets of UV irradiation in generating skin carcinomas. These cells reside life-long in the skin and are therefore most likely to accumulate (UV-induced) mutations converting them to cancer stem cells, CSCs (or tumor initiating cells, TICs) from which malignancies arise. Although chemotherapies may appear successful, these CSCs/TICs may be particularly resistant and give rise to relapse of the tumors.

The aim of this study was to identify the main (stem) cell pool that drives skin carcinogenesis. Phenotypic identification of these cells opens up the possibility of targeting them for selective elimination and thus intervene therapeutically or preventively by eradicating the very core of the cancer or a benign precursor lesion. To this end we studied different (stem) cell pools in the skin: (1) cells in the interfollicular epidermis, IFE, (2) classic quiescent stem cells (QSCs) and (3) the novel actively cycling Lgr5$^+$ and Lgr6$^+$ stem cells (SCs).

7.1. Interfollicular basal cells

Chronic UV radiation induces mutant p53 clones, 'p53 patches', in the IFE. These p53 patches appear causally related to subsequent SCCs harboring similar p53 mutations [1-3]. In **Chapter 2** we subjected skin laden with p53-mutant clones to UV overexposure and assessed the effect on subsequent tumor development. After overexposure the entire basal layer in the IFE went into caspase-3 driven apoptosis, including p53-patches. The IFE was repopulated from the hair follicles (HFs). The subsequent tumor development by continued daily UV exposure was delayed by the UV overexposure by 27 days. This time lapse matches the period of daily exposures to induce the p53 patches prior to the overexposure. These data indicate that the mutant p53 patches and UV-induced SCCs originate from the IFE. The data in **Chapter 2** are in contrast to earlier experiments with two-stage chemically induced SCCs, that showed that these SCCs originate from the HFs [4, 5].

UV overexposure apparently resets tumorigenesis. On the other hand, it caused 20% of SCCs induced by subsequent UV carcinogenesis to be of the spindle-cell type. These SCCs are more aggressive, and therefore overexposure is not a suitable preventive intervention. More so, because overexposure is a prominent risk factor for melanoma (most likely attributable to the strong growth stimulus in renewing the overexposed epidermis, which may promote outgrowth of remaining mutated melanocytes).

7.2. Quiescent stem cells

The classical stem cells were identified as label-retaining cells (LRCs). These cells seem to be in a 'quiescent' state, i.e. rarely dividing [6]. Previously our group showed that these cells, present in the epidermal basal layer, accumulate DNA damage in the form of cyclobutane pyrimidine dimers (CPDs) under chronic low level UV exposure [7]. The CPD-retaining basal cells (CRBCs) disappeared when UV exposure caused significant hyperplasia [8] or when

they were forced to proliferate by application of 12- O -Tetradecanoylphorbol-13-acetate (TPA) [8, 9]. In **Chapter 3** we set out to investigate if and what type of tumor would develop if these CRBCs were forced to divide by application of TPA. We found a clear difference in tumor development between the group that received a single UV overexposure and the group that received the same dose in very small sub sunburn fractions over 40 days. The latter group developed persistent (in situ) skin carcinomas while the tumors in the first group regressed after discontinuation of TPA applications (**Chapter 3**). These data show that a single overdose causing a severe sunburn, appears to be less hazardous than receiving the same dose in multiple small exposures (**Chapter 3**). This is in line with the data in **Chapter 2**, where we found that an overexposure resets tumorigenesis.

Only in the group that received the sub sunburn UV doses we found CRBCs and later on clear but rare p53 mutant patches. We forced the CRBCs to proliferate which likely increased the risk of mutations. However, the (in situ) skin carcinomas that developed did not carry mutations in the common driver genes: e.g. p53, H/K/N- Ras and Notch 1/2. This is very much in contrast to what is found after life-long chronic UV exposure, where high percentages of tumors carry UV signature mutations in p53 [3, 10]. This lack in p53 mutations could have hampered the progression to malignancy, and is evidently due to the early termination of UV exposures. Considering these data and the fact that human SCCs contain high percentages of UV signature mutations in P53 and NOTCH, one is led to infer that these tumors are induced by life-long chronic UV exposure. The absence of mutations in p53, Notch and Ras hints at the existence of other, as yet unknown, tumor-initiating driver mutations. In our experiments these unknown mutations may have arisen by forcing DNA-damage retaining cells to proliferate. However such a mutation may also constitute the earliest tumor initiation event in skin carcinogenesis by life-long chronic UV exposure. Our data suggest that P53, H/K/N-Ras and Notch 1/2 are not involved in UV-driven tumor initiation, nevertheless they might be important in the progression of the tumor from the 'in situ' to the malignant state.

The data in **Chapter 3** indicate that forcing CPD-loaded QSCs to divide gives rise to persisting, mainly 'in situ', skin carcinomas. However, since we could not find a specific phenotypic marker to selectively eliminate these CPD-loaded QSCs we could not establish causality.

7.3. Actively cycling stem cells

More recently two types of actively cycling stem cells were identified, the $Lgr5^+$ and $Lgr6^+$ cells, these cells were not label retaining cells in contrast to the classic QSCs. In haired mice, the $Lgr5^+$ cells reside in lower part of the HF and the $Lgr6^+$ cells higher up in the isthmus, sebaceous glands and the IFE [11-15]. We investigated the response of these proliferating stem cells and their progeny to carcinogenic stimuli, both chemical and UV, to see if these cells drive skin carcinogenesis.

7.3.1. $Lgr5^+$ and $Lgr6^+$ stem cells in hairless mice

We used both haired and hairless mice in our experiments. The established model of UV carcinogenesis is based on hairless mice [16, 17]. These mice do, however, not have normal cycling hair follicles and do not express CD34 in the bulge, a marker of classic follicular stem

cells [11, 12]. Their follicles seem to be frozen in catagen, and the hair follicle remnants are connected to deep-seated cysts (**Chapter 2**). Since all previous research on Lgr5 and Lgr6 was performed in haired mice, we first had to determine if hairless mice expressed Lgr5 and Lgr6. We found that hairless mice express Lgr5 mainly in the deep-seated cysts, some Lgr5 expressing cells were found at the point where the hair follicle remnant is connected to the cyst by a string of cells (**Chapter 4**). Lgr6 was expressed abundantly in the IFE and at the bottom of the hair follicle remnant in the region of the sebaceous glands (**Chapter 5**).

7.3.2. Response of Lgr5$^+$ and Lgr6$^+$ stem cells and their progeny to carcinogenic stimuli

The Lgr5$^+$ and Lgr6$^+$ SCs did not react the same to carcinogenic stimuli. The Lgr5$^+$ SCs never migrated into the IFE upon carcinogenic stimuli. In the Lgr5 haired mice, progeny was found in the IFE only after chemically induced hyperplasia and not after UV-induced hyperplasia (**Chapter 4**). Presumably, UV radiation could not penetrate deep enough into the HF to stimulate the Lgr5$^+$ stem cells. The TPA used in the chemical treatment could easily enter the HF orifices and reach the Lgr5$^+$ stem cells, also explaining the strong follicular hyperplasia that we did not observe when UV exposure was used to induce hyperplasia. In hairless mice, Lgr5$^+$ cells did not appear to react at all to either repeated chemical or UV stimuli inducing epidermal hyperplasia.

After UV-induced hyperplasia we found the Lgr6$^+$ stem cells and their progeny strongly diminished in the IFE, both in haired and hairless mice. The progeny we observed was almost exclusively associated with HFs (**Chapter 5**). These data suggest that under chronic UV exposure the interfollicular Lgr6$^+$ stem cells were outcompeted by other stem cells, and that the scarcely found progeny mainly originated from the HFs.

After UV-induced ablation of the epidermal basal layer of haired mice, Lgr5 progeny was found in the IFE contributing to repair of the ablated basal layer. The Lgr6$^+$ stem cells were erased from the IFE in haired and hairless mice. The Lgr6 progeny repopulated the IFE from the HFs, and most progeny was found associated to the HFs after the overexposure (**Chapter 5**).

In hairless mice no Lgr5 progeny was found in the IFE in the hyperplasia and ablation experiments. Evidently, the Lgr5$^+$ stem cells in the deep-seated cysts are not easily accessible by UV and TPA. Furthermore, their progeny has to pass through a narrow channel and cover a large distance to reach the HF orifice and migrate into the IFE. However, after prolonged carcinogenic stress, i.e. in the tumorigenesis experiments, we did find Lgr5 progeny emerging in the IFE between the tumors even in hairless mice. In the hyperplastic IFE between UV induced tumors the Lgr6 progeny appeared to be similarly scarce as we found in the hyperplasia experiment. In the IFE between chemically induced tumors however, the Lgr6 progeny was abundantly present in large clusters contiguous with multiple HFs per cluster (**Chapter 5**). These data suggest that progeny from neighboring HFs merged into large 'islands' of LacZ$^+$ cells. Furthermore, progeny from interfollicular Lgr6$^+$ stem cells may have also merged with these islands, since we also found LacZ$^-$ HFs surrounded by LacZ$^+$ progeny in the IFE. This shows that TPA tumor-promoting and UV regimens, have completely different effects on Lgr6$^+$ stem cells and their progeny (**Chapter 5**).

In our tumorigenesis experiments we did not observe any tumors with substantial clonal expansion of Lgr5$^+$ or Lgr6$^+$ stem cells. Only sparse remnants of progeny were observed in terminally differentiated parts of the tumors, and these were most likely inclusions of wild type cells. Our results in **Chapter 4** and **5** suggest that Lgr5$^+$ SCs and Lgr6$^+$ SCs are not tumor-initiating cells in cutaneous SCCs from exogenous carcinogens (DMBA/TPA and UV radiation). This is also supported by studies on gene expression profiles of human SCCs where no enrichment of LGR5-expressing or LGR6-expressing cells was found [18, 19].

7.3.3. Molecular aspects of Lgr5$^+$ and Lgr6$^+$ stem cells in the skin

We investigated whether absence of Lgr5$^+$ and Lgr6$^+$ stem cells in the ultimate tumors, could be affected by DNA methylation of CpG islands in the Lgr5, Lgr6 or Rosa promoter, that would cause a loss of LacZ tracing. DNA in the Rosa promoter was not methylated (**Chapter 4**). This implies that once the LacZ expression was switched on in stem cells it would persist in their progeny. Moreover, if the initially abundantly present Lgr6$^+$ stem cells would be the tumor drivers, we would have observed LacZ$^+$ tumor masses. Next to the Rosa promoter, the Lgr5 promoter was also not methylated, and our internal controls, skin adjacent to tumors, did clearly show Lgr5 progeny (**Chapter 4**).

We did find the Lgr6 promoter stochastically methylated in our Lgr6-EGFP-Ires-CreERT2 mice ("Lgr6 mice" for short) but not in wt mice. The methylation appeared to be directed at the Lgr6 promoter of the EGFP-CreERT2 cassette, and this could impair the expression of the cassette. Our data indicated that DNA methylation increased toward the end of the carcinogenesis regimens, e.g. more samples became methylated (**Chapter 5**). This could have impaired our LacZ tracing. Nevertheless, when lineage tracing was induced at the start of the carcinogenic regimen, we did find LacZ$^+$ cells in skin adjacent to the tumors but not in the tumor mass (**Chapter 5**). We performed qPCR to directly confirm Lgr6 mRNA expression. We found a decreased Lgr6 expression in UV- induced tumors from hairless mice (both transgenic and wild type) and chemically induced tumors from hairless and haired mice. This decreased expression was more pronounced relative to Ki67 expression (of cycling cells). Our data indicated a loss of Lgr6$^+$ cells from the pool of proliferative (Ki67$^+$) cells, and definitely not an enrichment of Lgr6$^+$ cells in these tumors. This finding agrees with gene expression profiles of human SCCs that did not indicate any enrichment of Lgr6-expressing cells [18, 19].

In parallel with the experiments using carcinogenic stimuli, we studied the Lgr6$^+$ cells in hairless mice in more depth (**Chapter 6**). We found 682 protein-encoding and non-coding RNAs to be differentially expressed in Lgr6$^+$ compared to Lgr6$^-$ basal cells. In the Lgr6$^+$ population, we found Lgr6 amongst the statistically significantly upregulated genes. However, we also detected expression in the Lgr6$^-$ population (**Chapter 5**). The RNA expression profiling revealed that the Lgr6$^+$ cells displayed stem cell characteristics and showed upregulation of genes coding for proteins involved in cancer. Nevertheless, as described in **Chapter 5** we did not find the Lgr6$^+$ cells to be TICs in skin carcinogenesis using exogenous agents.

Our data also revealed the expression of a mRNA encoding a truncated isoform of Lgr6 (starting from exon 2). This isoform, delta-Lgr6, encodes a protein lacking the 74 N-terminal amino acids of Lgr6 which leaves the ligand-binding domain intact (inference from reported

experiments with LGR4, [20]). Expression of this isoform may therefore compensate for the absence of the full length receptor in homozygous transgenic Lgr6 mice, explaining why these mice are healthy and fertile (**Chapter 5** and [12]). This delta-Lgr6 could also explain Lgr6 expression in the Lgr6- fraction. Furthermore, since a human homologous protein can be identified in the proteome database indicating expression in human tissues, it could maybe resolve the contradictory findings that LGR6 is a tumor suppressor in colorectal cancer [21, 22] but a oncogene in gastric carcinoma [23]. Further investigation is needed to determine the functional implications of delta-LGR6. We envision that methylation of the promoter region upstream exon 1, silencing of the full length transcript, results in loss of the LGR6 tumor suppressor function, but does not necessarily suppress expression of the delta-LGR6 isoform.

7.4. Concluding remarks and future perspectives

Contrary to our expectation, we found no evidence that the novel class of actively proliferating Lgr5$^+$ and Lgr6$^+$ stem cells entail tumor-initiating cells in skin tumors induced by either chemicals or UV radiation. Instead, QSCs seem to play an important role in skin carcinogenesis. Previously, K15$^+$/CD34$^+$ QSCs in the bulge have been established as targets for transformation into TICs in chemocarcinogenesis [24, 25]. Our results in **Chapter 3** indicate that this is similar in UV carcinogenesis. Our data suggest that interfollicular DNA-damage-retaining QSCs may become TICs of persistent skin tumors induced by low level UV exposure (**Chapter 3**). These DNA damage-loaded QSCs are likely to be primed to mutagenesis upon a proliferative stimulus. Taken together, these results indicate that the continuously proliferating Lgr5$^+$ and Lgr6$^+$ stem cells are less vulnerable to cancerous transformation than the QSCs. The QSCs are still very enigmatic and need to be phenotypically characterized for reliable identification. The only reliable hallmark we have of these cells is their 'label-retaining' feature, e.g. after neonatal incorporation of BrdU in their genome, these cells do rarely divide and thus retain the BrdU. Identifying and isolating these cells intact and living would open up the possibility of in-depth characterization (e.g. transcriptome profiling). To this end, we need robust membrane markers and appropriate antibodies. Sada et al. used H2B-GFP pulse-chase to identify label-retaining cells (LRCs) in the IFE of mice and detected some of these cells in the spinous layer [26]. They found the LRCs to divide on average every 5 days. A division rate much higher than we had expected since QSC were observed to retain BrdU (and DNA damage) for months on end. Evidently, the QSC/LRC in the IFE is still very much shrouded in mystery which needs to be resolved, in particular to study its role in skin carcinogenesis.

Next to differences in rates of proliferation and corresponding DNA damage accumulation and retention, the QSCs and actively proliferating stem cells could differ in cancer proneness owing to differences in DNA repair, cell cycle arrest and apoptotic responses. The actively cycling stem cells may also respond differently from QSCs to genotoxic challenges, such as UV radiation. As we observed in **Chapter 5**, where the Lgr6$^+$ SCs and progeny were virtually erased from the IFE after UV exposure, especially lastingly in the course of chronic UV exposure but also transiently after a single UV overexposure. These results on UV responses of proliferative and quiescent stem cells in the skin show parallels with responses of proliferative (Lgr5$^+$) stem cells and (BMi1$^+$) QSCs in the intestine to ionizing radiation. Lgr5$^+$

stem cells have been reported to be radioresistant owing to recombinational DNA repair when compared to transit amplifying progenitors [27]. However, a direct comparison with Bmi1$^+$ QSCs revealed the Lgr5$^+$ stem cells to be radiosensitive [28], confirming earlier inferences on radioresistance of QSCs. Up on 12 Gray the Bmi1$^+$ QSCs are no longer quiescent and proliferate to repopulate the crypts and villi whereas Lgr5 expressing cells are lost with correspondingly no detectable Lgr5 progeny [28]. A better survival of QSCs after such a genotoxic challenge would suggest them to be more likely TICs than Lgr5$^+$ stem cells.

Other groups did find Lgr5 stem cell progeny in skin tumors generated from oncogenetically transformed basal cells. Kasper et al. induced foci of basaloid hyperproliferation by activating the Hedgehog pathway in basal cells (in K5tTA/TREGLI1 and K5Cre*PR1/Ptchfl/fl mice) and by wounding [29]. They found Lgr5 stem cell progeny in interfollicular foci if they induced a wound (in Lgr5-EGFP-IRES-creERT2/R26R and K5tTA/TREGLI1 mice). Without wounding and recruitment of Lgr5 progeny to the IFE, progeny was only found in lesions associated with HFs [29]. Furthermore, they found Lgr5 progeny in BCC-like tumors initiated from Lgr5$^+$ stem cells (Lgr5-creERT2/Ptchfl/fl) [29]. Da Silva-Diz et al. expressed HPV proteins in basal cells and found Lgr5 progeny in the papillomas that developed [30]. Cammareri et al. found SCC development in mice when either the MAPK pathway was constitutively activated or p53 was mutated in Lgr5$^+$ stem cells together with TgfβR1 deletion in these cells [31]. However, all these experiments started with genetic manipulation of basal cells or more specifically Lgr5$^+$ cells. Therefore, they do not faithfully mimic the natural conditions of carcinogenesis by exogenous agents, e.g., the sporadic SCCs that develop through UV exposure. In these sporadic SCCs P53 and NOTCH are often mutated, but not the RAS genes despite an activated MAPK pathway [31]. Strikingly, we found none of these mutations in tumors initiated by low level UV exposure (**Chapter 3**). Therefore, our data indicate that there are other drivers that initiate SCCs.

As our experiments did not raise any BCCs, our results leave open the possibility that these tumors may arise from either Lgr5$^+$ or Lgr6$^+$ stem cells. Aside from mouse strains that are genetically programmed to develop BCCs, we have no suitable mouse model to emulate de novo development of BCC in humans by exogenous carcinogenic agents. As BCC is by far the most common cancer in fair-skinned people of European descent, this area of research should be pursued more vigorously in order to understand the pathogenesis in more detail to improve prevention and therapeutic intervention.

We performed some preliminary studies on LGR5 and LGR6 expression in human skin samples. Although a lack of reliable antibodies and the low expression of LGR5 and LGR6 greatly hampered this work, we found clear indications of LGR5 and LGR6 mRNA expression in human skin and hair follicles, with cultured human skin equivalents (lacking epidermal appendages) exclusively expressing LGR6. Further characterization of these potential stem cells in human skin combined with interspecies comparisons should greatly contribute to our understanding of homeostasis in human skin and pathological disturbances therein, such as the genesis of skin carcinomas.

References

1. Backvall H, Stromberg S, Gustafsson A, Asplund A, Sivertsson A, Lundeberg J and Ponten F. Mutation spectra of epidermal p53 clones adjacent to basal cell carcinoma and squamous cell carcinoma. Exp Dermatol. 2004; 13(10):643-650.
2. Kramata P, Lu YP, Lou YR, Singh RN, Kwon SM and Conney AH. Patches of mutant p53-immunoreactive epidermal cells induced by chronic UVB Irradiation harbor the same p53 mutations as squamous cell carcinomas in the skin of hairless SKH-1 mice. Cancer Res. 2005; 65(9):3577-3585.
3. Rebel H, Kram N, Westerman A, Banus S, van Kranen HJ and de Gruijl FR. Relationship between UV-induced mutant p53 patches and skin tumours, analysed by mutation spectra and by induction kinetics in various DNA-repair-deficient mice. Carcinogenesis. 2005; 26(12):2123-2130.
4. Morris RJ, Tryson KA and Wu KQ. Evidence that the epidermal targets of carcinogen action are found in the interfollicular epidermis of infundibulum as well as in the hair follicles. Cancer Res. 2000; 60(2):226-229.
5. Lademann J, Knorr F, Richter H, Blume-Peytavi U, Vogt A, Antoniou C, Sterry W and Patzelt A. Hair follicles--an efficient storage and penetration pathway for topically applied substances. Summary of recent results obtained at the Center of Experimental and Applied Cutaneous Physiology, Charite -Universitatsmedizin Berlin, Germany. Skin Pharmacol Physiol. 2008; 21(3):150-155.
6. Morris RJ and Potten CS. Highly persistent label-retaining cells in the hair follicles of mice and their fate following induction of anagen. J Invest Dermatol. 1999; 112(4):470-475.
7. Nijhof JGW, van Pelt C, Mulder AA, Mitchell DL, Mullenders LHF and de Gruijl FR. Epidermal stem and progenitor cells in murine epidermis accumulate UV damage despite NER proficiency. Carcinogenesis. 2006; 28(4):792-800.
8. Mitchell DL, Volkmer B, Breitbart EW, Byrom M, Lowery MG and Greinert R. Identification of a Non-Dividing Subpopulation of Mouse and Human Epidermal Cells Exhibiting High Levels of Persistent Ultraviolet Photodamage. 2001; 117(3):590-595.
9. Nijhof JGW, Mulder AM, Speksnijder EN, Hoogervorst EM, Mullenders LHF and de Gruijl FR. Growth stimulation of UV-induced DNA damage retaining epidermal basal cells gives rise to clusters of p53 overexpressing cells. DNA Repair. 2007; 6(11):1642-1650.
10. Dumaz N, van Kranen HJ, de Vries A, Berg RJ, Wester PW, van Kreijl CF, Sarasin A, Daya-Grosjean L and de Gruijl FR. The role of UV-B light in skin carcinogenesis through the analysis of p53 mutations in squamous cell carcinomas of hairless mice. Carcinogenesis. 1997; 18(5):897-904.
11. Jaks V, Barker N, Kasper M, van Es JH, Snippert HJ, Clevers H and Toftgard R. Lgr5 marks cycling, yet long-lived, hair follicle stem cells. Nat Genet. 2008; 40(11):1291-1299.
12. Snippert HJ, Haegebarth A, Kasper M, Jaks V, van Es JH, Barker N, van de Wetering M, van den Born M, Begthel H, Vries RG, Stange DE, Toftgard R and Clevers H. Lgr6 marks stem cells in the hair follicle that generate all cell lineages of the skin. Science. 2010; 327(5971):1385-1389.
13. Füllgrabe A, Joost S, Are A, Jacob T, Sivan U, Haegebarth A, Linnarsson S, Simons B D, Clevers H, Toftgård R and Kasper M. Dynamics of Lgr6(+) Progenitor Cells in the Hair Follicle, Sebaceous Gland, and Interfollicular Epidermis. Stem cell reports. 2015; 5(5):843-855.
14. Liao XH and Nguyen H. Epidermal expression of Lgr6 is dependent on nerve endings and Schwann cells. Exp Dermatol. 2014; 23(3):195-198.
15. Page ME, Lombard P, Ng F, Gottgens B and Jensen KB. The epidermis comprises autonomous compartments maintained by distinct stem cell populations. Cell stem cell. 2013; 13(4):471-482.
16. de Gruijl FR and Forbes PD. UV-induced skin cancer in a hairless mouse model. Bioessays. 1995; 17(7):651-660.

17. Chitsazzadeh V, Coarfa C, Drummond JA, Nguyen T, Joseph A, Chilukuri S, Charpiot E, Adelmann CH, Ching G, Nguyen TN, Nicholas C, Thomas VD, Migden M, MacFarlane D, Thompson E, Shen J, et al. Cross-species identification of genomic drivers of squamous cell carcinoma development across preneoplastic intermediates. Nature communications. 2016; 7:12601.
18. Hudson LG, Gale JM, Padilla RS, Pickett G, Alexander BE, Wang J and Kusewitt DF. Microarray analysis of cutaneous squamous cell carcinomas reveals enhanced expression of epidermal differentiation complex genes. Mol Carcinog. 2010; 49(7):619-629.
19. Hameetman L, Commandeur S, Bavinck JN, Wisgerhof HC, de Gruijl FR, Willemze R, Mullenders L, Tensen CP and Vrieling H. Molecular profiling of cutaneous squamous cell carcinomas and actinic keratoses from organ transplant recipients. BMC Cancer. 2013; 13:58.
20. Xu JG, Huang C, Yang Z, Jin M, Fu P, Zhang N, Luo J, Li D, Liu M, Zhou Y and Zhu Y. Crystal structure of LGR4-Rspo1 complex: insights into the divergent mechanisms of ligand recognition by leucine-rich repeat G-protein-coupled receptors (LGRs). J Biol Chem. 2015; 290(4):2455-2465.
21. Gong X, Carmon KS, Lin Q, Thomas A, Yi J and Liu Q. LGR6 is a high affinity receptor of R-spondins and potentially functions as a tumor suppressor. PLoS One. 2012; 7(5):e37137.
22. Mokarram P, Kumar K, Brim H, Naghibalhossaini F, Saberi-firoozi M, Nouraie M, Green R, Lee E, Smoot DT and Ashktorab H. Distinct high-profile methylated genes in colorectal cancer. PLoS One. 2009; 4(9):e7012.
23. Steffen JS, Simon E, Warneke V, Balschun K, Ebert M and Rocken C. LGR4 and LGR6 are differentially expressed and of putative tumor biological significance in gastric carcinoma. Virchows Arch. 2012; 461(4):355-365.
24. Malanchi I, Peinado H, Kassen D, Hussenet T, Metzger D, Chambon P, Huber M, Hohl D, Cano A, Birchmeier W and Huelsken J. Cutaneous cancer stem cell maintenance is dependent on beta-catenin signalling. Nature. 2008; 452(7187):650-653.
25. Trempus CS, Morris RJ, Ehinger M, Elmore A, Bortner CD, Ito M, Cotsarelis G, Nijhof JG, Peckham J, Flagler N, Kissling G, Humble MM, King LC, Adams LD, Desai D, Amin S, et al. CD34 expression by hair follicle stem cells is required for skin tumor development in mice. Cancer Res. 2007; 67(9):4173-4181.
26. Sada A, Jacob F, Leung E, Wang S and White BS. Defining the cellular lineage hierarchy in the interfollicular epidermis of adult skin. 2016; 18(6):619-631.
27. Hua G, Thin TH, Feldman R, Haimovitz-Friedman A, Clevers H, Fuks Z and Kolesnick R. Crypt base columnar stem cells in small intestines of mice are radioresistant. Gastroenterology. 2012; 143(5):1266-1276.
28. Yan KS, Chia LA, Li X, Ootani A, Su J, Lee JY, Su N, Luo Y, Heilshorn SC, Amieva MR, Sangiorgi E, Capecchi MR and Kuo CJ. The intestinal stem cell markers Bmi1 and Lgr5 identify two functionally distinct populations. Proceedings of the National Academy of Sciences of the United States of America. 2012; 109(2):466-471.
29. Kasper M, Jaks V, Are A, Bergstrom A, Schwager A, Svard J, Teglund S, Barker N and Toftgard R. Wounding enhances epidermal tumorigenesis by recruiting hair follicle keratinocytes. Proceedings of the National Academy of Sciences of the United States of America. 2011; 108(10):4099-4104.
30. da Silva-Diz V, Sole-Sanchez S, Valdes-Gutierrez A, Urpi M, Riba-Artes D, Penin RM, Pascual G, Gonzalez-Suarez E, Casanovas O, Vinals F, Paramio JM, Batlle E and Munoz P. Progeny of Lgr5-expressing hair follicle stem cell contributes to papillomavirus-induced tumor development in epidermis. Oncogene. 2013; 32(32):3732-3743.
31. Cammareri P, Rose AM and Vincent DF. Inactivation of TGFbeta receptors in stem cells drives cutaneous squamous cell carcinoma. 2016; 7:12493.

Chapter 8

Nederlandse Samenvatting

8.1 De huid en zijn stamcellen

De huid is de buitenste laag van ons lichaam en daarom de eerste verdedigingslinie tegen ziekteverwekkers en andere schadelijke factoren uit de omgeving, zoals ultraviolette (UV) straling van de zon. De huid is opgebouwd uit drie lagen: de epidermis (buitenste laag), de dermis en daaronder de subcutane vetlaag. De epidermis bestaat uit lagen van keratinocyten die worden vernieuwd door stamcellen uit de binnenste laag, de basale laag. Naarmate de cellen naar buiten bewegen, differentiëren ze en uiteindelijk sterven ze af en worden platte schijfjes (corneocyten) die de buitenste laag van de huid vormen, de hoornlaag (oftewel stratum corneum). Beschadigde gedifferentieerde cellen in de buitenste lagen worden zo continu vervangen door nieuwe cellen. De epidermis vormt ook haarfollikels met talgklieren en afzonderlijke zweetklieren (epidermale appendices), die ingebed liggen in de onderliggende huidlaag, de dermis.
De haarfollikel bestaat uit verschillende structuren (zie Hoofdstuk 1, Figuur 1.1). Aan de basis bevindt zich een bol (de bulbus) die de haar vormt en daarboven een verdikking (de 'bulge' in het Engels) waar een klein spiertje (muscullus arrector pili) aangehecht zit.
De continue vervanging van cellen in de epidermis en haarfollikels, vereist een blijvend reservoir van stamcellen. Deze stamcellen zijn aanwezig op verschillende plaatsen in de huid: m.n. in de 'bulge' en interfolliculaire epidermis (IFE), maar ook in de bulbus en bij de talgklieren. De klassieke stamcellen werden in de muis geïdentificeerd als cellen die zich meestal in een 'rustende' toestand bevinden en zich zelden delen. Deze rustende stamcellen zitten in de basale laag van de epidermis en in de 'bulge' van de haarfollikel. Meer recent werd een nieuw soort stamcellen geïdentificeerd, $Lgr5^+$ en $Lgr6^+$ cellen die voortdurend actief delen.

8.2 UV-straling en huidkanker

De incidentie van huidkanker (melanoom, basaalcelcarcinoom en plaveiselcelcarcinoom) is de laatste decennia sterk gestegen naar niveaus die een grote last voor de gezondheidszorg vormen. Een beter begrip van de mechanismes die leiden tot het ontstaan van huidkanker kunnen helpen bij preventie en de behandeling van huidkanker.
UV-straling van de zon speelt een belangrijke rol in het ontstaan van huidkanker. Het kan verregaande effecten hebben als UV-straling wordt geabsorbeerd door DNA. Zo kan het DNA beschadigd worden, vooral doordat naburige pyrimidine-basen in een DNA-streng onderling verbonden raken (dimeriseren), waarbij cyclobutaan-pyrimidine-dimeren (CPDs) of 6-4-fotoproducten (6-4PPs) ontstaan. Bij het kopiëren van DNA voor dochtercellen kan dergelijke schade aanleiding geven tot kenmerkende UV-mutaties, die sterk geassocieerd zijn met het ontstaan van huidkanker. *P53*-tumorsuppressorgenen in humane basaalcelcarcinomen en plaveiselcelcarcinomen dragen overwegend deze UV-mutaties. Daarnaast zijn dergelijke *P53*-mutaties aanwezig in goedaardige actinische keratosen (AK), de voorlopers van kwaadaardige plaveiselcelcarcinomen.

8.3 Experimentele modellen voor huidkanker

In experimenteel huidkankeronderzoek worden twee verschillende benaderingen gebruikt om huidkanker te induceren. Het eerste model is gebaseerd op UV bestraling van haarloze muizen. Wanneer deze muizen dagelijks worden blootgesteld aan UV-straling, zonder zonnebrand te veroorzaken, ontstaan er na verloop van tijd plaveiselcelcarcinomen met UV-mutaties in *p53*. Deze tumoren zijn vergelijkbaar met de plaveiselcelcarcinomen bij de mens. Ook worden in deze UV blootgestelde muizen microscopische clustertjes van cellen (kloons) gevonden met hoge concentraties van het gemuteerde p53-eiwit. Deze kloons ontstaan lang voordat er tumoren verschijnen. Dergelijke 'mutante p53-kloons' zijn ook aangetroffen in de aan de zon blootgestelde menselijke huid.
Het tweede (chemische) model kan worden toegepast op zowel behaarde als haarloze muizen, en bestaat uit een initiatie- en promotie-fase. Eerst wordt de initiator, een DNA-beschadigend (genotoxisch) middel (bijv. Dimethylbenz[a]antraceen, DMBA), eenmalig aangebracht op de huid om de tumor te "initiëren". Daarna wordt herhaaldelijk een promotor opgebracht, een irriterend en celdeling stimulerend middel, meestal een phorbolester (m.n. '12-O-tetradecanoylphorbol-13-acetate', TPA), om de verdere ontwikkeling van tumoren te bevorderen. De tumoren die ontstaan, voornamelijk goedaardige papillomen, dragen gewoonlijk mutaties in het *H-ras*-oncogen. Deze mutaties worden echter niet vaak aangetroffen in plaveiselcelcarincomen bij de mens, en niet in UV-geïnduceerde plaveiselcelcarcinomen in haarloze muizen.

8.4 Dit onderzoek

8.4.1 Doel van het onderzoek

Een kanker ontwikkelt zich in fasen met verschillende (achtereenvolgende) genetische veranderingen in de cellen waaruit de kanker ontstaat, en dit kost meestal veel tijd. Omdat stamcellen zich levenslang in de huid bevinden hebben zij de grootste kans om genmutaties te accumuleren en door te geven aan hun nakomelingcellen waardoor deze stamcellen mogelijk een belangrijke rol hebben in het ontstaan van huidkanker. Stamcellen in de epidermis zijn daarom het uitgangspunt van het onderzoek beschreven in dit proefschrift. Het doel van deze studie was het identificeren van de belangrijkste (stam-) cellen waaruit huidkanker, en met name plaveiselcelcarcinomen, voortkomen. We hebben hiervoor gebruik gemaakt van bovengenoemde muismodellen en verschillende (stam-) cellen in de huid bestudeerd.

8.4.2 Interfolliculaire basale cellen

In **Hoofdstuk 2** onderzochten we of (stam-) cellen uit de haarfollikel of de IFE een rol spelen in UV carcinogenese. We onderwierpen de muizenhuid die vol zat met gemuteerde p53-cellen aan een UV-overdosis (zoals bij een zonverbranding) en keken naar het effect op de daaropvolgende tumorontwikkeling. Door de UV-overdosis ging de gehele basale laag van de IFE, inclusief de p53-kloons, verloren door massale apoptose, d.w.z. dat de cellen op gecontroleerde wijze dood gingen. Dit vertraagde de daaropvolgende tumorontwikkeling: deze leek opnieuw te beginnen. Dit resultaat duidt erop dat de mutante p53-kloons en de

door UV geïnduceerde plaveiselcelcarcinomen afkomstig zijn uit de IFE, en niet uit de haarfollikels die ongemoeid bleven bij de UV-overdosis.

8.4.3 Rustende stamcellen

In **Hoofdstuk 3** hebben we rustende stamcellen in de IFE onderzocht. Uit eerder onderzoek bleek dat deze stamcellen onder chronische lage UV-blootstelling, DNA-schade accumuleerden in de vorm van cyclobutaan-pyrimidine-dimeren (CPDs), terwijl CPDs in omliggende cellen niet meetbaar waren. Deze CPD-houdende basale cellen verdwenen wanneer ze werden gedwongen te delen door het aanbrengen van TPA op de huid, of liever, de geactiveerde stamcellen verdwenen niet maar ze verloren gaandeweg CPDs door herhaalde celdeling. Deling van een cel vol DNA schade verhoogd de kans op mutaties. In **Hoofdstuk 3** hebben we onderzocht of de TPA behandeling van de huid met CPD-houdende basaal cellen leidt tot een verhoogde kans op tumoren. We vonden een duidelijk verschil in tumorontwikkeling tussen de groep die een enkele UV-overdosis (zonnebrand) kreeg en de groep die dezelfde hoeveelheid UV kreeg in zeer kleine sub-zonnebrandfracties gespreid over 40 dagen. In de groep die een enkele UV-overdosis kreeg ontstonden geen basale cellen met aanhoudende CPD schade en gingen de tumoren in regressie na stopzetting van TPA-toediening. We vonden alleen CPD-houdende basale cellen in de groep die de sub-zonnebrand-UV-doses kreeg en deze groep ontwikkelde blijvende 'in situ' carcinomen (d.w.z. tumoren met verdachte cellen die nog niet invasief waren). De resultaten uit **Hoofdstuk 3** duiden erop dat geforceerde deling van rustende stamcellen met DNA schade leidt tot meer mutaties met als gevolg autonoom doorgroeiende huidtumoren, voornamelijk 'in situ' carcinomen. We konden echter geen directe causaliteit tussen de CPD-geladen rustende stamcellen en de autonoom groeiende tumoren aantonen. Daarvoor zouden we de rustende stamcellen selectief moeten elimineren voorafgaand aan de TPA behandeling, waarna de autonoom groeiende tumoren zouden moeten uitblijven. Er zijn geen specifieke eiwitten bekend voor rustende stamcellen. Daardoor ontbreekt de mogelijkheid om zulke eiwitten (of de coderende genen ervan), te gebruiken om deze cellen uit te schakelen.

8.4.4 Actief delende stamcellen

In **Hoofdstuk 4 en 5** onderzochten we de respons van de actief delende $Lgr5^+$ en $Lgr6^+$ stamcellen en hun nageslacht op carcinogene stimuli, zowel chemisch als UV, om te zien of deze cellen een rol spelen bij het ontstaan van huidtumoren.
$Lgr5^+$ cellen (diep in de haarfollikels) werden niet beïnvloed door UV-straling, maar $Lgr6^+$ cellen verdwenen uit de IFE. Bij TPA behandeling daarentegen, bleven de $Lgr6^+$ cellen aanwezig in de IFE en produceerden daar veel nakomelingen. We vonden echter geen tumoren met een substantiële uitgroei van $Lgr5^+$ of $Lgr6^+$ stamcellen. Er werden slechts schaarse overblijfselen van nakomelingen in de tumoren aangetroffen, en dan uitsluitend in de niet-delende (gedifferentieerde) cellagen en verhoornde delen van de tumoren. Onze resultaten in **Hoofdstuk 4 en 5** duiden erop dat $Lgr5^+$ stamcellen en $Lgr6^+$ stamcellen geen tumor-initiërende cellen zijn voor huidtumoren geïnduceerd door UV-straling of door chemicaliën (DMBA + TPA).
Parallel aan deze experimenten, hebben we de expressie van genen in $Lgr6^+$ cellen uit de huid van haarloze muizen bestudeerd door middel van kwantitatieve RNA-sequencing

(**Hoofdstuk 6**). We vonden dat 682 eiwitcoderende en niet-coderende RNA's statistisch significant verschillend tot expressie gebracht werden in Lgr6$^+$ in vergelijking met Lgr6$^-$ basale cellen. Het RNA-expressieprofiel toonde aan dat de Lgr6$^+$ cellen stamceleigenschappen vertoonden en lieten (naast *Lgr6*) een hogere expressie zien van genen die coderen voor eiwitten die bij kanker betrokken zijn. In onze gegevens ontdekten we ook expressie van een mRNA dat codeert voor een verkorte vorm van Lgr6 (beginnend in exon 2). Deze isovorm, delta-Lgr6, codeert voor een eiwit zonder de 74 N-terminale aminozuren van Lgr6. Dit eiwit is waarschijnlijk functioneel (het ligand-bindende domein blijft intact), maar de mogelijke functionele implicaties (van delta-Lgr6 en delta-LGR6 in respectievelijk muis en mens) zijn vooralsnog onbekend.

8.5 Conclusies

In dit onderzoek vonden we geen bewijs dat Lgr5$^+$ en Lgr6$^+$ stamcellen tumor-initiërende cellen zijn voor huidtumoren geïnduceerd door chemicaliën of UV-straling bij muizen. In plaats daarvan lijken rustende stamcellen in de IFE wel een belangrijke rol te spelen in het ontstaan van plaveiselcelcarcinomen van de huid door UV-straling, zoals bij de mens.
Omdat onze experimenten niet gericht waren op het opwekken van basaalcelcarcinomen, laten onze resultaten de mogelijkheid open dat deze tumoren kunnen ontstaan uit Lgr5$^+$ of Lgr6$^+$ stamcellen. De verdere karakterisering van deze potentiële stamcellen in de menselijke huid, in combinatie met vergelijkingen tussen muis en mens, zou in grote mate bij kunnen dragen aan ons begrip van de homeostase in de menselijke huid en pathologische verstoringen daarin, zoals bij het ontstaan van huidcarcinomen.

LIST OF PUBLICATIONS

P.J. Tacken, I.S. Zeelenberg, L.J. Cruz, M.A. van Hout-Kuijer, **G. van de Glind**, R.G. Fokkink, A.J.A. Lambeck, C.G. Figdor. *Targeted delivery of TLR ligands to human and mouse dendritic cells strongly enhances adjuvanticity.* Blood 2011 Dec 22:118(26):6836-44

H.G. Rebel, C.A. Bodmann, **G.C. van de Glind**, F.R. de Gruijl. *UV-induced ablation of the epidermal basal layer including p53-mutant clones resets UV carcinogenesis showing squamous cell carcinomas to originate from interfollicular epidermis*. Carcinogenesis. 2012 vol.33 no.3 pp.714–720

G.C. van de Glind, H.G. Rebel, M.J. van Kempen, C.P. Tensen, F.R. de Gruijl. *Fractionation of a tumor-initiating UV dose introduces DNA damage-retaining cells in hairless mouse skin and renders subsequent TPA-promoted tumors non-regressing.* Oncotarget. 2016 Feb 16;7(7):8067-77

G.C. van de Glind, J.J. Out-Luiting, H.G. Rebel, C.P. Tensen, F.R. de Gruijl. *Lgr5^{+} stem cells and their progeny in mouse epidermis under regimens of exogenous skin carcinogenesis, and their absence in ensuing skin tumors.* Oncotarget. 2016 Aug 9;7(32):52085-52094

G.C. van de Glind, H.G. Rebel, J.J. Out-Luiting, W.H. Zoutman, C.P. Tensen, F.R. de Gruijl. *Lgr6^{+} stem cells and their progeny in mouse epidermis under regimens of exogenous skin carcinogenesis, and their absence in ensuing skin tumors.* Oncotarget. 2016 Dec 27;7(52):86740-86754

G.C. van de Glind*, A.N. Bastidas Torres*, W.H. Zoutman, S.A.J. van der Zeeuw, S.M. Kielbasa, F.R. de Gruijl and C.P. Tensen. *RNA-seq analysis of Lgr6^{+} stem cells and identification of an Lgr6 isoform.* Exp Dermatol. 2017 Oct 7. doi: 10.1111/exd.13453. *Contributed equally to this study

CURRICULUM VITAE

Gerritje Cornelia van de Glind was born in Amersfoort, the Netherlands on July 17th 1986. In 2004 she finished her high school education at Christelijk Lyceum Veenendaal after which she started with the Bachelor Biology at Wageningen University. After obtaining her Bachelor's degree she continued her studies at Wageningen University with a Master in Biotechnology. As part of her study she performed research internships at the department of Tumor Immunology of the NCMLS in Nijmegen and at Genethon in Evry (France). In 2010 she received her Master of Science degree in Biotechnology with a specialization in Molecular and Cellular Biotechnology. In 2011, she started as a PhD-student at the Department of Dermatology of the Leiden University Medical Center under the supervision of Dr. F.R. de Gruijl, Dr. C.P. Tensen and Prof. Dr. R. Willemze. The results of this PhD project are described in this thesis. As of April 2017, she is working as a Regulatory Affairs Manager at Novartis Pharma B.V.

